Nectin cell adhesion molecule 1 (Nectin-1) and the plasma membrane citrate carrier (pmCiC) – potential predictive biomarkers

DISSERTATION ZUR ERLANGUNG DES
DOKTORGRADES DER NATURWISSENSCHAFTEN (DR. RER. NAT.)
DER FAKULTÄT FÜR BIOLOGIE UND VORKLINISCHE MEDIZIN DER
UNIVERSITÄT REGENSBURG

vorgelegt von

Barbara Schwertner, M.Sc.

aus

Nürnberg

im Jahr

2024

Das Promotionsgesuch wurde eingereicht am:

25.10.2024

Die Arbeit wurde angeleitet von:

Prof. Dr. Dr. Michael P. Krahn

Unterschrift:

Publication statement and personal contributions

The thesis is composed of the following articles:

1. **Barbara Schwertner**, Georg Lindner, Camila Toledo Stauner, Elisa Klapproth, Clara Magnus, Anette Rohrhofer, Stefanie Gross, Beatrice Schuler-Thurner, Veronika Öttl, Nicole Feichtgruber, Konstantin Drexler, Katja Evert, Michael P. Krahn, Mark Berneburg, Barbara Schmidt, Philipp Schuster, and Sebastian Haferkamp. Nectin-1 Expression Correlates with the Susceptibility of Malignant Melanoma to Oncolytic Herpes Simplex Virus *In Vitro* and *In Vivo*. Cancers (Basel). 2021 Jun 19; 13(12): 3058. Doi: 10.3390/cancers13123058, (Schwertner *et al.,* 2021)

   Personal contributions: Conceptualization, data curation, formal analysis, investigation, methodology, supervision, validation, visualization, writing—original draft, writing—review and editing

2. **Barbara Schwertner**, George Dahdal, Wolfgang Jagla, Luis Grossmann, Konstantin Drexler, Michael P. Krahn, Katja Evert, Mark Berneburg, Sebastian Haferkamp, Christine Ziegler, Eric K. Parkinson, Grit Zahn, Maria E. Mycielska, and Andreas Gaumann**.** Expression of the plasma membrane carrier (pmCiC) in human cancerous tissues – correlation with tumour aggressiveness. Frontiers in Cell and Developmental Biology (Lausanne). 2024 Jul 03. Doi: 10.3389/fcell.2024.1308135, (Schwertner *et al.,* 2024)

   Personal contributions: Conceptualization, data curation, formal analysis, investigation, methodology, supervision, validation, visualization, writing—original draft, writing—review and editing

3. Konstantin Drexler, **Barbara Schwertner**, Silke Haerteis, Thiha Aung, Mark Berneburg, Edward K. Geissler, Maria E. Mycielska, and Sebastian Haferkamp. The Role of Citrate Homeostasis in Merkel Cell Carcinoma Pathogenesis. Cancers (Basel). 2022 Jul 14; 14(14): 3425. Doi: 10.3390/cancers14143425, (Drexler *et al.,* 2022)

   Personal contributions: methodology, software, writing—review and editing

4. Konstantin Drexler, Katharina M Schmidt, Katrin Jordan, Marianne Federlin, Vladimir M Milenkovic, Gerhard Liebisch, Anna Artati, Christian Schmidl, Gregor Madej, Janina Tokarz, Alexander Cecil, Wolfgang Jagla, Silke Haerteis, Thiha Aung, Christine Wagner, Maria Kolodziejczyk, Stefanie Heinke, Evan H Stanton, **Barbara Schwertner**, Dania Riegel, Christian H Wetzel, Wolfgang Buchalla, Martin Proescholdt, Christoph A Klein, Mark Berneburg, Hans J Schlitt, Thomas Brabletz, Christine Ziegler, Eric K Parkinson, Andreas Gaumann, Edward K Geissler, Jerzy Adamski, Sebastian Haferkamp, and Maria E Mycielska. Cancer-associated cells release citrate to support tumor metastatic progression. Life Sci Alliance. 2021 Mar 23; 4(6): e202000903. Doi: 10.26508/lsa.202000903, (Drexler *et al.,* 2021)

   Personal contributions: investigation, methodology, writing—review and editing

Table of contents

Acknowledgement

An erster Stelle möchte ich mich bei Professor Dr. Dr. Sebastian Haferkamp, meinem Mentor und Zweitgutachter, bedanken. Danke dafür, dass du mich so spontan und unkompliziert in der Dermatologie des Universitätsklinikums Regensburg aufgenommen hast. Deine herzliche positive Einstellung, deine Begeisterung für die Forschung, dein Fachwissen und dein Vertrauen in meine Arbeit waren eine unschätzbare Unterstützung. Ohne deine grenzenlose Geduld und deine motivierenden Worte zum richtigen Zeitpunkt hätte ich diese Dissertation niemals abschließen können. Mein Dank gilt auch Herrn Professor Dr. Mark Berneburg, Direktor der Klinik und Poliklinik für Dermatologie am Universitätsklinikum Regensburg. Ich bin sehr dankbar, dass ich meine Dissertation in Ihrem Labor durchführen durfte.

Besonders herzlich danke ich meinem Doktorvater, Herrn Professor Dr. Dr. Michael Krahn, für die Möglichkeit, diese Dissertation anzufertigen, und für die Betreuung aus der Ferne in den vergangenen Jahren.

Während meiner Zeit am Universitätsklinikums Regensburg hatte ich das Vergnügen, mit der wunderbaren AG Schmidt zusammenzuarbeiten. Ich habe in dieser Zeit unglaublich viel gelernt. Mein herzlicher Dank gilt insbesondere Frau Professor Dr. Barbara Schmidt, Dr. Philipp Schuster und Anette Rohrhofer. Vielen Dank für die zahlreichen Treffen und Telefonate, bei denen immer wieder neue Ideen entstanden sind oder Fragen geklärt werden konnten. Ich hoffe, dass diese Zusammenarbeit noch lange anhält.

Thank you, Dr. Maria Mycielska, for your help during the final years of my dissertation. I am grateful for your introduction to the world of citrate and metabolism, your valuable experience, your enthusiasm for my results, and your patience during my parental leave.

Natürlich möchte ich mich auch beim gesamten Derma-Labor im H4 bedanken. Vielen Dank, dass ihr mich so freundlich aufgenommen und unterstützt habt, wo ihr nur konntet! Ein besonderer Dank geht an Prof. Dr. Tim Maisch, Dr. Anja Eichner, PD Dr. rer. nat. habil. med. Stephanie Arndt, Christine Wagner-Bock, Petra Unger, Dr. Irina Ivanova, Teodora Svilenska, Judith Heider und Camila Toledo Stauner. Besonders möchte ich mich auch bei Susanne Wallner bedanken, meiner langjährigen Laborpartnerin. Danke für deine Hilfe, deine positive Einstellung, die schönen Mittagspausen, die motivierenden Gespräche und unsere wunderbare Zeit im Labor. Jeden Tag aufs Neue von dir im Labor begrüßt zu werden, hat meinen Alltag enorm erleichtert. Außerdem möchte ich mich bei Dr. Konstantin Drexler bedanken. Die Zeit mit dir war wirklich “hervorragend”!

Ebenso wichtig und lehrreich war meine Anfangszeit an der Universität Regensburg am Lehrstuhl für Molekulare und Zelluläre Anatomie. Vielen Dank an alle Kolleginnen und Kollegen dort. Insbesondere möchte ich mich bei Dr. Olga Panichkina, Ina Hallstein und Dr. Daniela Sparrer bedanken. Danke für eure Hilfe, euer Verständnis und eure Freundschaft.

Vielen Dank auch an alle Studierenden, die ich betreuen durfte. Ihr habt stets frischen Wind ins Labor gebracht – das war großartig. Ich weiß eure engagierte Mitarbeit sehr zu schätzen und bedanke mich herzlich dafür.

Besonders danken möchte ich auch Jonathan Pirnay für seine Unterstützung in allen statistischen Fragen.

Ein großer Dank gilt auch meiner Familie: meinen Eltern Hildegard und Helmut Schwertner sowie meinen Geschwistern Konrad Schwertner, Theresia Schiffler und Johanna Krüger. Ihr seid mir eine große Stütze.

Meinem besten Freund und Ehemann Moritz Oeding möchte ich abschließend danken. Danke für dein Verständnis. Was würde ich ohne dich machen?

Abstract

Cancer remains a major global health challenge, with metastatic cancer accounting for a significant proportion of cancer-related deaths. Identifying appropriate treatment approaches is often complex and varies by cancer type. Predicting metastasis and response to treatment is critical to optimising patient care. Biomarkers, which detect changes indicative of disease, play an important role in diagnosis and treatment prediction of cancer. They are already an integral part of cancer care, supporting early detection and the development of personalised therapies. Advancing biomarker research is critical to improving the efficiency of cancer treatment and patient outcomes. The aim of this thesis is to address the critical need for improved methods of cancer treatment decision making by exploring the potential of biomarkers, focusing on two novel candidates, Nectin cell adhesion molecule 1 (Nectin-1) and the plasma membrane citrate carrier (pmCiC).

Malignant melanoma is an aggressive form of skin cancer with a high metastatic rate. Oncolytic virotherapy is a promising approach for the treatment of advanced melanoma, with talimogene laherparepvec (T-VEC) being the first oncolytic virus approved by the United States (US) Food and Drug Administration (FDA). T-VEC selectively targets tumour cells and stimulates an immune response. Although effective, treatment with T-VEC requires multiple injections and can cause local and systemic side effects that can be debilitating. In addition, a proportion of patients do not benefit from treatment. This study identified Nectin-1 as a predictive marker of melanoma response to oncolytic virotherapy and demonstrated a significant correlation between Nectin-1 expression and tumour regression in both melanoma cell lines and patient samples. High levels of Nectin-1 were associated with effective T-VEC-induced melanoma cell killing, suggesting its potential as a biomarker to optimise virotherapy efficacy in various tumours.

In the second part of the present study, we investigated whether pmCiC expression is associated with increased disease aggressiveness of cancer and can serve as a prognostic marker. Citrate, a key metabolite in the citric acid cycle, is crucial for lipid synthesis, epigenetic regulation, and adenosine triphosphate (ATP) production. Cancer cells of various origins use pmCiC to take up extracellular citrate to support their metabolism, including fatty acid synthesis, mitochondrial activity, protein synthesis, and histone acetylation. Extracellular citrate is also linked to a metastatic phenotype in cancer cells. Our investigation of pmCiC expression showed that it increases with tumour stage and is highly expressed at metastatic sites as well as in the tumour microenvironment. This highlights the potential role of extracellular citrate in metastasis and tumour progression. We found a strong correlation between pmCiC expression in both cancer cells and the surrounding stroma with tumour stage. Consequently, pmCiC expression may serve as a prognostic marker, although further research is needed for validation. Our findings also introduce citrate as a critical metabolite in tumour

progression, with citrate synthesis and release by cancer associated fibroblasts being integral to tumour-stroma interactions and metastasis. Blocking citrate uptake by cancer cells reduced cancer spread and stromal transformation, providing a novel therapeutic avenue. Our study sheds light on the complex role of citrate in cancer metabolism and microenvironment interactions. Extracellular citrate emerges as a key player in tumour progression, with potential implications for metastasis and therapeutic interventions.

Further research into Nectin-1 and citrate metabolism may improve oncolytic virotherapy and provide new strategies for cancer treatment and metastasis prevention.

List of abbreviations

3-[4,5-dimethylthiazol-2yl]-2,5-diphenyl-tetrazolium bromide	MTT
3-OS-HS	3-O-sulfated heparan sulfate
aa	amino acid
ACC	acetyl-CoA carboxylase
ACD	adrenocortical dysplasia protein homolog
acetyl-CoA	acetyl coenzyme A
ACLY	ATP-citrate lyase
ACO2	aconitase 2
ACON	aconitase
ADMA	asymmetric dimethylarginine
ADP	adenosine diphosphate
AEC	3-amino-9-ethylcarbazole
AIDS	acquired immune deficiency syndrome
AJCC	american joint committee on cancer
ANKH	progressive ankylosis protein homolog
anti-LAG-3	anti-lymphocyte-activation gene 3
AP	alcalic phosphatase
APC	antigen-presenting cell
Arg	arginine
AST	aspartate aminotransferase
ATP	adenosine triphosphate
AUC	area under the curve
BAP1	breast cancer gene 1-associated protein-1
BBB	blood-brain barrier
BRAF	*viral-rapidly accelerated fibrosarcoma oncogene homolog B1*
BSA	bovine serum albumin
c4-OH-Pro	cis-4-hydroxyproline
C5-DC (C6-OH)	glutarylcarnitine\3-hydroxy-hexanoylcarnitine
Ca	calcium
CAC	cancer-associated cell
CAF	cancer-associated fibroblast
CAM	chorioallantoic membrane
CAS	cancer-associated stroma
Cas9	CRISPR associated protein 9
CCCP	carbonyl cyanide m-chlorophenyl hydrazine
CD	cluster of differentiation
CDK4	cyclin-dependent kinase 4
CDKN2A	cyclin-dependent kinase inhibitor 2A
CDN	cyclic dinucleotide
Cer	ceramides
cGAMP	cyclic guanosine monophosphate-adenosine monophosphate
cGAS	cyclic GMP-AMP synthase
CHO	chinese hamster ovary
cit	citrate
CM	conditioned media

CM F-PC+cit	conditioned media from fibroblasts transformed with the conditioned media from PC-3M cells preincubated with extracellular citrate
CM F-PC−cit	conditioned media from fibroblasts transformed with the conditioned media from PC-3M cells preincubated without extracellular citrate
CM PC-3M+cit	conditioned media from PC-3M cells preincubated with extracellular citrate
CM PC-3M−cit	conditioned media from PC-3M cells preincubated without extracellular citrate
CMV	cytomegalovirus
CO_2	carbon dioxide
CR	complete response
CRISPR	clustered regularly interspaced short palindromic repeats
CS	citrate synthase
CT	computer tomography
CTLA-4	cytotoxic T-lymphocyte-associated protein 4
Cu	copper
DAMP	danger-associated molecular pattern
DC	dendritic ell
DMEM	dulbecco's modified eagle's medium
DNA	deoxyribonucleic acid
DPBS	dulbecco's phosphate-buffered saline
DRR	durable response rate
ds	double-stranded
DSMZ	german collection of microorganisms and cell cultures
E-cadherin	epithelial cadherin
ECAR	extracellular acidification rate
ECL	enhanced chemiluminescence
ECM	extracellular matrix
ecto-CRT	surface-exposed endoplasmic reticulum chaperone calreticulin
EDTA	ethylenediaminetetraacetic acid
EGFR	epidermal growth factor receptor
eIF2α	eukaryotic translation initiation factor 2
EMT	epithelial-mesenchymal transition
ER	endoplasmic reticulum
ERGIC	endoplasmatic reticulum-golgi intermediate compartment
ESI-MS/MS	electrospray ionization tandem mass spectrometry
FA	fatty acid
FACS	fluorescence-activated cell sorting
FAD	flavin adenine dinucleotide (oxidized form)
$FADH_2$	flavin adenine dinucleotide (reduced form)
FAO	fatty acid β-oxidation
FAP	fibroblast activation protein
FASN	fatty acid synthase
FBPase	fructose-1,6-biphosphatase
FBS	fetal bovine serum
FDA	food and drug administration
Fe	iron
FIA-ESI-MS/MS	flow injection-electrospray ionization-tandem mass spectrometry

FUM	fumarate hydratase
g	glycoprotein
GAPDH	glyceraldehyde-3-phosphate dehydrogenase
G-CSF	granulocyte-colony stimulating factor
GDP	guanosine diphosphate
Glut1	glucose transporter 1
GM-CSF	granulocyte-macrophage colony-stimulating factor
GRO	growth-regulated protein
GSSG	glutathione disulfide
GTP	guanosine triphosphate
h	human
H_2O	dihydrogen monoxide
H_2O_2	hydrogen peroxide
HCC	hepatocellular carcinoma
HCl	hydrogen chloride
HexCer	hexosylceramides
HIER	heat induced epitope retrieval
His-Tag Ni-NTA	polyhistidine-tag nickel-nitrilotriacetic acid
HMGB1	high mobility group box 1
HRP	horseradish peroxidase
H-score	histochemical score
HSP	heat-shock protein
HSV-1	herpes virus type 1
HVEM	herpesvirus entry mediator
HVSEM	high-voltage scanning electron microscope
ICI	immune checkpoint inhibitor
ICP	infected cell protein
IDH	isocitrate dehydrogenase
IE	immediate early
IFN	interferon
IFNR	IFN receptor
IFN-α2b	interferon-alpha2b
IgG	immunoglobulin G
IHC	immunohistochemistry
IL	interleukin
IRF	IFN-related factor
IR_L	long inverted repeat region
ISG	interferon-stimulated gene
JAK	janus kinase
K	potassium
Kd	dissociation constant
Ki67	marker of proliferation Kiel 67
KO	knockout
KRAS	*kirsten rat sarcoma viral oncogene homolog*
L	late
LC	liquid chromatography
LC-ESI-MS/MS	liquid chromatography-electrospray ionization-tandem mass spectrometry
LC–MS/MS	liquid chromatography tandem mass spectrometry
LDH	lactate dehydrogenase

l-DOPA	l-3,4- dihydroxyphenylalanine
LLOQ	lower limit of quantification
LOCI	laboratory for optical and computational instrumentation
LOD	limit of detection
LPC	lysophosphatidylcholine
lysoPC	lysophosphatydylcholine
MAPK	mitogen-activated protein kinase
MAS	malate-aspartate shuttle
MCC	merkel cell carcinoma
mCiC	mitochondrial citrate transporter
MCP	monocyte chemoattractant protein
MDH	malate dehydrogenase
ME	malic enzyme
MEK	mitogen-activated protein kinase kinase
MET	mesenchymal-epithelial transition
MHC	major histocompatibility complex
miR-21	micro ribonucleic acid-21
MMP	matrix metalloproteinase
MOI	multiplicity of infection
MS/MS	tandem mass spectrometry
MSI	microsatellite instability
MYD88	myeloid differentiation primary response protein
NA	not available
Na+	sodium ion
NaCl	sodium chloride
NaCT	Sodium ion/citrate cotransporter
NAD^+	nicotinamide adenine dinucleotide (oxidized form)
NaDC	sodium dicarboxylate transporter
NADH	nicotinamide adenine dinucleotide (reduced form)
NADPH	reduced nicotinamide adenine dinucleotide phosphate
N-cadherin	neural cadherin
NCBI	national center for biotechnology information
Nectin-1	nectin cell adhesion molecule 1
NF-κB	nuclear factor kappa B
Nitro-Tyr	nitrotyrosine
NK	natural killer
NRAS	*neuroblastoma rat sarcoma virus oncogene homolog*
OAA	oxaloacetate
OGDC	2-oxoglutarate dehydrogenase complex
OPTiM	oncovex (GM-CSF) pivotal trial in melanoma
ORR	overall response rate
OV	oncolytic virus
OXPHOS	oxidative phosphorylation
p value (or p)	probability value
p.i.	post infection
p63 or TP63	tumor protein 63
pA	polyadenylation tail
PAMP	pathogen-associated molecular pattern
PARP	poly (ADP-ribose) polymerase
PBS	phosphate buffered saline

PC	phosphatidylcholine
PC aa	phosphatidylcholine diacyl
PC ae	phosphatidylcholine acly-alkyl
PCK1	phosphoenolpyruvate carboxykinase
PCR	polymerase chain reaction
PD-1	programmed cell death protein 1
PDGFRα	platelet-derived growth factor receptor alpha
PDGFRβ	platelet-derived growth factor receptor beta
PDH	pyruvate dehydrogenase
PD-L1	programmed cell death-ligand 1
PE	phosphatidylethanolamine
PE P	PE-based plasmalogen
PEA	2-phenylethylamine
PECAM-1	platelet endothelial cell adhesion molecule
PEP	phosphoenolpyruvate
PET	positron emission tomography
PFK	phosphofructokinase
PG	phosphatidylglycerol
PGF	placental growth factor
PI	phosphatidylinositol
PKR	protein kinase R
PLS-DA	partial least squares-discriminant analysis
pmCiC	plasma membrane citrate carrier
POT1	protection of telomeres 1
PP1	protein phosphatase 1
PR	partial response
PS	phosphatidylserine
qPCR	quantitative polymerase chain reaction
RANTES	regulated upon activation, normal T cell expressed and presumably secreted
RIG-1	retinoic acid-inducible gene 1
RIPA	radioimmunoprecipitation assay buffer
RMSEE	root mean squared error of estimation
RNA	ribonucleic acid
ROC	receiver-operating characteristic
ROS	reactive oxygen species
RPMI-1640	roswell park memorial institute medium
RT	room temperature
S100B	S100 calcium-binding protein B
SCS	succinyl-CoA synthetase
SDH	succinate dehydrogenase
SDMA	symmetric dimethylarginine
SDS	sodium dodecyl sulfate
sg	single guide
SLC	solute carrier
SLC25	solute carrier family 25
SM	sphingomyelin
SM (OH) C14:1	hydroxysphingomyelin with acyl residue sum C14:1
SM C26:0	sphingomyelin C26
sMRM	scheduled multiple reaction monitoring measurement

STAT	signal transducer and activator of transcription
STING	stimulator of interferon genes
succinyl-CoA	succinyl coenzyme A
T7EI	T7 endonuclease I
TAA	tumour-associated antigen
TBK1	TANK-binding kinase 1
TCA	tricarboxylic acid
TCID50	50% tissue culture infective dose
TDA	tumour-derived antigen
TERF2IP	telomeric repeat-binding factor 2-interacting protein 1
TERT	telomerase reverse transcriptase
TGFβ	transforming growth factor, beta
TGFβ-RII	transforming growth factor, beta receptor II
TLR	toll-like receptor
TMB	tumour mutational burden
TME	tumour microenvironment
TNF	tumour necrosis factor
TNFRSF	tumour necrosis factor receptor superfamily
TRAF	tumour necrosis factor-associated factor
TRIF	TIR-domain-containing adapter-inducing interferon beta
Tris	tris(hydroxymethyl)aminomethane
TR_L	long terminal repeat
Trp	tryptophan
TR_S	short terminal repeat
TUNEL	terminal deoxynucleotidyl transferase deoxyuridine triphosphate nick end labeling
T-VEC	talimogene laherparepvec
UICC	international union against cancer
U_L	unique long region
ULOQ	upper limit of quantification
UniProt	universal protein database
US	united states
U_S	unique short region
US11	unique short sequence 11
UV	ultraviolet
VEGF	vascular endothelial growth factor
VIP	variables of importance in projection
Zn	zinc
α-AAA	alpha-aminoadipic acid
αKG	alpha-ketoglutarate
αSMA	alpha-smooth muscle actin

Throughout this dissertation, standard abbreviations for units and metric prefixes have been used.

1 General introduction

1.1 Research question and aims of the study

1.1.1 Description of the problem and clinical relevance

Cancer remains one of the leading causes of death worldwide, with metastatic tumours accounting for a significant proportion of cancer-related mortality (Hanly *et al.,* 2022; Neophytou *et al.,* 2021). One of the greatest challenges in cancer treatment is the early and accurate prediction of disease progression and treatment response. Biomarkers play a crucial role in this regard. Biomarkers are biological indicators that provide insights into the presence or progression of a disease and can help tailor personalized therapies (Biomarkers Definitions Working Group, 2001).

This dissertation investigates two promising biomarkers: Nectin cell adhesion molecule 1 (Nectin-1) and the plasma membrane citrate carrier (pmCiC). Nectin-1 may serve as a predictive biomarker for the response of malignant melanoma to oncolytic virotherapy with talimogene laherparepvec (T-VEC), while pmCiC could act as a prognostic biomarker for the aggressiveness of various tumours. Identifying and validating these biomarkers could significantly advance personalized cancer treatment.

1.1.2 Research gap and objectives

Despite significant advancements in cancer research, predicting therapeutic outcomes and determining tumour aggressiveness remain challenging. Existing biomarkers do not always provide the necessary precision and reliability. This dissertation aims to fill this research gap by investigating the roles of Nectin-1 and pmCiC as potential predictive and prognostic biomarkers.

Currently, there is no established predictive biomarker for the response to oncolytic virotherapy in malignant melanoma, nor is there a clear prognostic marker that reliably predicts tumour aggressiveness and metastatic potential. Nectin-1 and pmCiC could potentially fill these gaps.

Objectives of the study:

1. To evaluate Nectin-1 as a predictive biomarker for the efficacy of T-VEC therapy in malignant melanoma.
2. To investigate pmCiC as a prognostic marker for the aggressiveness of various tumour types.
3. To understand how pmCiC expression influences merkel cell carcinoma (MCC) proliferation and to assess the therapeutic effects of targeting citrate metabolism.

4. To explore the impact of extracellular citrate on cancer cell metabolism and the induction of invasive phenotypes, and to assess the therapeutic potential of inhibiting citrate uptake.

1.2 Biomarkers in tumours

Cancer is a leading cause of death worldwide, causing nearly 10 million deaths in 2020, 20 % of them in Europe (Hanly *et al.,* 2022). Despite numerous therapeutic advances in cancer treatment, metastatic cancer still accounts for more than 90% of cancer deaths, making it one of the deadliest diseases (Neophytou *et al.,* 2021). Prevention of metastasis and rapid disease progression is therefore the most important goal of cancer treatment. Unfortunately, determining the most suitable treatment plan is often challenging due to the uncertain nature of the disease and its progression. Of course, this primarily depends on the type of cancer that the patient has been diagnosed with. As a result, questions arise regarding whether an aggressive systemic approach is necessary to prevent and treat metastasis or if a less invasive approach would be sufficient.

Cancer treatments are stressful and debilitating, and patients often suffer greatly from aggressive therapies. For clinical practice and decision making, it would be beneficial to be able to predict whether the cancer has the potential to metastasise and to decide whether aggressive treatment is needed or not. It would also be helpful to know whether a particular cancer therapy is promising or whether a different therapeutic approach should be chosen. Many scientists have discovered new targets for early cancer detection. Small changes at the molecular level can play a critical role in how cancer develops and responds to treatment. Biomarkers have become a useful tool in clinical practice to identify and quantify these changes or abnormalities, thereby aiding in diagnosis, prognosis and prediction of response to treatment.

A biomarker can be defined as a “biological observation that substitutes for and ideally predicts a clinically relevant endpoint or intermediate outcome that is more difficult to observe.” (Aronson & Ferner, 2017). “Difficult to observe” means that there may be difficulties with intermediate outcomes or endpoints because they are, for example, difficult to access or distant in time (Aronson & Ferner, 2017). A clinical endpoint is used to reflect or characterise how a patient or a subject in a study or clinical trial feels, functions or survives. Clinical endpoints are precise measurements or analyses noticed during a study or clinical trial. They demonstrate whether a clinical treatment provides benefits to patients (Biomarkers Definitions Working Group, 2001).

Biomarkers are a widely used tool in research and clinical practice. They have many applications, such as detecting diseases early, diagnosing and characterizing them, and monitoring their progress. They can be used as prognostic indicators and for the development

of individualized therapies. Moreover, specific cell types, e.g. tumour cells, can be identified by biomarkers. Additionally, biomarkers can aid in the prediction and management of negative drug reactions. Biomarkers can also be used in pharmacodynamics and dose-response studies.

The advantage of biomarkers is that they are easy and inexpensive to measure in comparison with clinical endpoints. They can be measured multiple times and analysed over a shorter period. Furthermore, implementing biomarkers circumvents ethical challenges related to assessing clinical endpoints.

Biomarkers are already being used in a variety of ways in the clinical practice of patients with cancer. Some examples include *kirsten rat sarcoma viral oncogene homolog* (*KRAS*) mutations as a prognostic biomarker in pancreatic cancer (Li, Tao *et al.,* 2016), serum microRNA-21 (miR-21) as a diagnostic biomarker in breast cancer (Li, Shichao *et al.,* 2016), the three biomarkers programmed cell death-ligand 1 (PD-L1); microsatellite instability (MSI); tumour mutational burden (TMB) predicting the response to immune checkpoint blockade and select patients for immune checkpoint inhibitor (ICI) therapy (Vaddepally *et al.,* 2020), the serum markers lactate dehydrogenase (LDH) and the calcium-binding, acidic cytoplasmic protein S100B (also known as S-100B or S-100β) in the prognosis and monitoring of melanoma (Eton *et al.,* 1998; Weide *et al.,* 2012; Balch *et al.,* 2009; Gaynor *et al.,* 1980; Gaynor *et al.,* 1981; Nakajima *et al.,* 1982), DNA point mutations in melanoma (e.g. mutations in the mitogen-activated protein kinase (MAPK) pathway, most commonly found in *viral-rapidly accelerated fibrosarcoma oncogene homolog B1* (*BRAF*) and *neuroblastoma rat sarcoma virus oncogene homolog* (*NRAS*), which are also important biomarkers in melanoma that predict response to targeted therapy or are correlated with shorter survival (Burotto *et al.,* 2014; Pracht *et al.,* 2015; Chapman *et al.,* 2011).

Advancing biomarker research is essential for improving early detection, treatment selection, patient outcomes, and the overall efficiency of cancer care. This will ultimately lead to better prognoses and quality of life for patients (Duffy, 2013).

In the following section, the two potential new biomarkers, Nectin-1 and pmCiC, will be introduced and their biological background explained.

1.3 Nectin cell adhesion molecule 1 (Nectin-1) and the plasma membrane citrate carrier (pmCiC) – two potential biomarkers and their applications

1.3.1 Nectin-1 as a predictive biomarker for the therapeutic response to oncolytic herpesviruses in malignant melanoma

1.3.1.1 Malignant melanoma

Malignant melanoma, commonly referred to as melanoma, is a type of skin cancer that arises from melanocytes, the cells responsible for producing melanin pigment and originating from the neural crest. Melanocytes are situated in the basal layer of the skin's epidermis and dermis. Together with neighbouring cells such as keratinocytes, they protect deoxyribonucleic acid (DNA) from damage caused by ultraviolet (UV) light. After undergoing malignant transformation, melanocytes express several signalling molecules and factors that promote migration and metastasis. Melanoma is an aggressive form of cancer that often spreads to the lungs, brain, liver, and soft tissues. The tumour displays microsatellite, satellite, nodal, or distant metastases patterns and has a high probability of local recurrence. In addition to its high metastatic potential, melanoma is characterised by a high degree of immunogenicity (Passarelli *et al.,* 2017; Lugowska *et al.,* 2018; Byrne & Fisher, 2017). The progression of melanoma is linked to the failure of the immune system to activate and the tumour's ability to evade it, known as 'immune escape'. The immune system can no longer distinguish between self and non-self-antigens, which is its primary function.

Skin cancer, including non-melanoma skin cancer and melanoma, is one of the most frequently diagnosed cancers globally (Arnold *et al.,* 2022). For 2020, over 1.5 million new cases and more than 120,000 associated deaths were estimated (Sung *et al.,* 2021). Melanomas account for only 324,635 (21%) of all skin cancer cases, yet they are responsible for 57,043 (nearly 50 %) of the associated deaths (Sung *et al.,* 2021). This underlines the severity of this cancer. If the rates from 2020 remain unchanged, it is estimated that the incidence of melanoma will increase to 510,000 new cases (a roughly 50 % increase) and 96,000 deaths (a 68 % increase) by 2040 (Arnold *et al.,* 2022; Sung *et al.,* 2021). Although new therapies, such as immune checkpoint inhibitors and targeted treatments, are having an impact on reducing mortality rates for metastatic melanoma in a few countries (e.g. the US), it remains a challenging cancer to treat and a significant global health issue, especially in fair-skinned populations of European ancestry (Sung *et al.,* 2021; Erdmann *et al.,* 2013; Arnold *et al.,* 2022; Arnold, M. *et al.,* 2014; Berk-Krauss *et al.,* 2020; Mason *et al.,* 2019).

Melanoma is a complex disease. It results from an interaction between genetic susceptibility and environmental exposures. The most important environmental risk factor for the

development of melanoma is exposure to UV radiation due to its genotoxic effect. There is a positive association between intermittent intense sun exposure and melanoma (Gandini *et al.,* 2005). Artificial UV exposure, such as that from sunbeds, may contribute to the development of melanoma as the amount of UVA present in a typical tanning bed session is significantly higher than the exposure during ordinary outdoor activities or sunbathing (The International Agency for Research on Cancer Working Group on artificial ultraviolet (UV) light and skin cancer, 2007).

The key host risk factors for melanoma include skin type, the number of melanocytic nevi, family history, and genetic susceptibility. Melanocytic nevi are benign accumulations of melanocytes. They may be congenital or acquired. About 25% of melanomas occur in association with a pre-existing nevus (Bevona *et al.,* 2003). Furthermore, there is a positive correlation between the total number of nevi and the risk of melanoma (Holly *et al.,* 1987). A family history of melanoma is a significant risk factor for the disease. The familial clustering of a disease is often an indicator of possible heritable causes. Cyclin-dependent kinase inhibitor 2A (CDKN2A or p16) is the most frequently implicated gene in familial melanoma, accounting for predisposition in approximately 20-40 % of melanoma families (Goldstein *et al.,* 2007). Mutations in cyclin-dependent kinase 4 (CDK4), were less frequent. Other known high penetrance melanoma genes are BRCA1-associated protein-1 (BAP1), protection of telomeres 1 (POT1), adrenocortical dysplasia protein homolog (ACD), telomeric repeat binding factor 2 interacting protein 1 (TERF2IP), and telomerase reverse transcriptase (TERT). Certain physical characteristics, including red hair, fair skin, numerous freckles, light eyes, sun sensitivity, and an inability to tan, increase the risk of developing melanoma by about 50% (Titus-Ernstoff *et al.,* 2005).

The prognosis of melanoma depends highly on the clinical stage, which refers to the extent of tumour burden (Markovic *et al.,* 2007). In Germany, approximately 70 % of all melanomas are detected at an early stage (American Joint Committee on Cancer (AJCC) I). The current relative 5-year survival rate for melanoma of the skin is 95 % for women and 93 % for men (Robert Koch Institute (ed.) and the Association of Population-based Cancer Registries in Germany (ed.), 2022). At AJCC IV, the relative 5-year survival rate is significantly lower with 32% for females and 19% for males (Robert Koch Institute (ed.) and the Association of Population-based Cancer Registries in Germany (ed.), 2022). The patient's clinical stage is also a crucial factor in determining the appropriate therapy.

Defeating melanoma is a major challenge due to its highly aggressive nature and resistance to cytotoxic agents (Soengas & Lowe, 2003). According to German and international guidelines, immunotherapy with checkpoint inhibitors and targeted therapy with BRAF and mitogen-activated protein kinase kinase (MEK) inhibitors are the standard of care for metastatic disease. The use of immunotherapeutic agents has significantly improved the

survival of patients with unresectable metastatic melanoma (Bedikian *et al.,* 2006; Middleton *et al.,* 2000; Korn *et al.,* 2008; Wolchok *et al.,* 2021). It all started with the approval of interferon-α2b (IFN-α2b) therapy and the cytokine interleukin-2 (IL-2) as the first immunotherapy agents. Subsequently, the cytotoxic T-lymphocyte-associated protein 4 (CTLA-4) immune checkpoint inhibitor ipilimumab was approved, followed by the anti-programmed cell death protein 1 (PD-1) monoclonal antibodies pembrolizumab and nivolumab. Later, various combinations or monotherapy of the above agents were approved as systemic therapy for advanced disease or as adjuvant therapy for resectable disease. In 2022, a new agent, the anti-lymphocyte-activation gene 3 (anti-LAG-3) antibody relatlimab, was also approved, but only for use in combination with nivolumab. Since 2015, oncolytic virus therapy with T-VEC, has also been approved for unresectable melanoma.

1.3.1.2 Oncolytic viruses and their mode of action

Oncolytic viruses (OVs) are native or modified and therefore often attenuated live viruses. They are an innovative tool for the detection, infection and destruction of cancer cells with negligible effects on normal human cells and are being used as a new class of drugs in cancer therapy (Guo *et al.,* 2008; Russell & Peng, 2007).

OVs frequently exhibit superior replication capabilities in cancerous cells relative to their healthy counterparts. They have a selective advantage due to abnormalities in stress response, cell signalling, and homeostasis (Hanahan & Weinberg, 2011). In addition, antiviral mechanisms are frequently impaired in cancer cells. For example, protein kinase R (PKR), which contributes to the elimination of intracellular viral infections, may be absent. Healthy cells have different signalling pathways to recognize and defend against viral particles (Figure 1A). The virus-infected cells mostly activate antiviral signalling pathways to stop or restrain viral infection. The antiviral machinery can be activated by viral components that activate Toll-like receptors (TLRs), through the detection of viral nucleic acids by retinoic acid-inducible gene 1 (RIG-1) or by the local release of interferons (IFNs). Components activating TLRs are called pathogen-associated molecular patterns (PAMPs). PAMPs are repeated sequences like components of viral capsids, DNA, ribonucleic acid (RNA), and viral protein products. PAMPs are also common in pathogenic bacteria and are not limited to viruses. TLRs are located on the cell surface or intracellular and are able to recognize PAMPs. TLR signalling leads to activation of antiviral responses and induction of the systemic innate immune system. Identified downstream proteins involved in OV combating are for example TNF-associated factor 3 (TRAF3), IFN-related factor 3 (IRF3) and 7 (IRF7), and RIG-1. These proteins activate the janus kinase-signal transducer and activator of transcription (JAK-STAT) pathway, which plays the essential role in regulating the antiviral machinery in infected cells. The antiviral machinery enhances local IFN release. Through the IFN overflow PKR is activated. PKR senses double-stranded RNA and other viral elements, self-activates and blocks translational machinery,

induces apoptosis and viral clearance (Taniuchi *et al.,* 2016). In cancer cells, IFN signalling and PKR activity may be disrupted, impeding viral clearance (Figure 1B) (Clemens, 2004). Several viruses have the ability to replicate particularly well in tumour cells due to their ability to manipulate aberrant signalling factors in cancer cells and delay host cell apoptosis. After viral replication, most oncolytic viruses trigger cell death. Tumour cells are thereby also directly eliminated. In addition, the tumour cell death sets the base for the initiation of systemic immune responses.

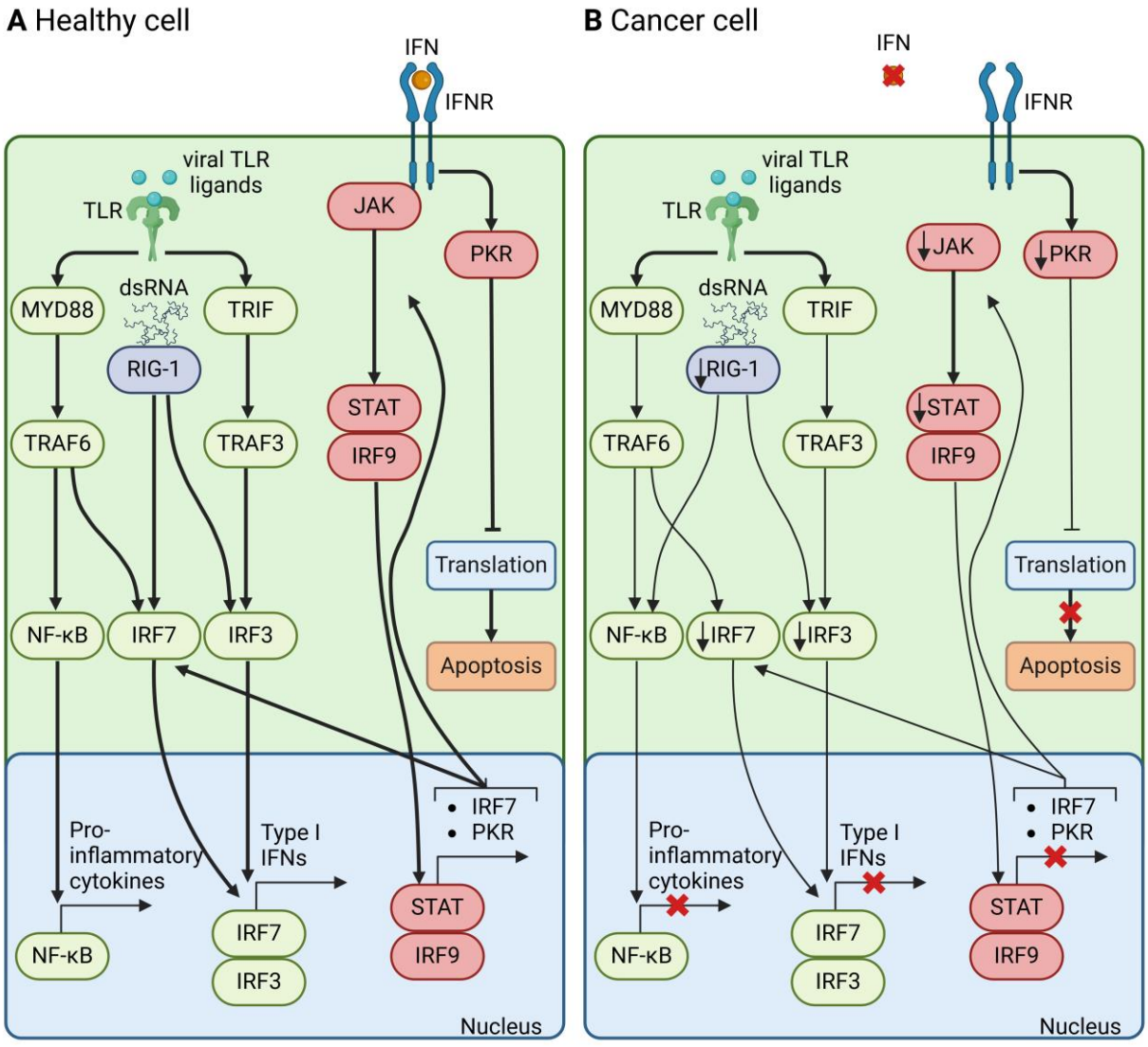

Figure 1: Oncolytic viruses can exploit the pathways of cancer immune defence. (A) Upon viral infection, most normal cells activate an antiviral pathway to contain the virus. This response is triggered by viral pathogen-associated molecular patterns (PAMPs) that bind to toll-like receptors (TLRs) or by the detection of viral nucleic acids by retinoic acid-inducible gene 1 (RIG-1). Once detected, a signalling cascade involving type I interferons (IFNs), Janus kinase (JAK), signal transducer and activator of transcription (STAT), and interferon regulatory factor 9 (IRF9) is initiated. This cascade activates a transcriptional programme that limits viral spread and targets infected cells for apoptosis or necrosis. Local IFN production, triggered by the innate immune response to viral infection, enhances antiviral activity via the IFN receptor (IFNR). Toll-like receptors (TLRs) activate signalling through the proteins myeloid differentiation primary response protein MYD88, TIR-domain-containing adapter-inducing IFNβ (TRIF), IRF7, IRF3 and nuclear factor-κB (NF-κB), leading to the production of pro-inflammatory cytokines and type I IFNs. These IFNs activate the JAK-STAT pathway, which upregulates cell cycle

regulators like protein kinase R (PKR) and IRF7. This response limits viral spread by binding to viral particles, activating type I IFN transcriptional pathways, inducing apoptosis in infected cells, and producing cytokines that alert the immune system to the viral infection. (B) In cancer cells, this process is disrupted. Key components of the innate signalling pathway, such as RIG-1, IRF7, and IRF3, are often downregulated, reducing the detection of viral particles by TLRs and RIG-1. This makes cancer cells more susceptible to viral replication. Additionally, cancer cells may downregulate parts of the type I IFN signalling pathway, weakening the pro-apoptotic and cell cycle regulatory effects of IFNs. Adapted by permission from Springer Nature Customer Service Centre GmbH: Nature Research, Nature Reviews Drug Discovery, Oncolytic viruses: a new class of immunotherapy drugs, (Bommareddy et al., 2017). Created with BioRender.com.

The exact mechanisms by which tumour rejection is mediated are not fully understood. OVs are believed to have a dual effect in destroying cancer. Firstly, they replicate specifically in cancer cells and destroy them directly by cell lysis, and secondly, OVs activate an anti-tumour immune response which provides the indirect killing effect (Figure 2) (Kaufman *et al.,* 2015; Jhawar *et al.,* 2017).

Cell lysis is the result of natural viral replication after infection and is part of the viral life cycle. After lysis of the host cells, virus particles are released and surrounding cells can be infected and destroyed. Thus, the virus reproduces and spreads by itself. In addition, certain OVs are capable of producing cytotoxic proteins during their replication cycle, which also lead to tumour cell death. Virus replication continues until either the immune response is initiated which reduces viral replication, or until there is a deficit of susceptible host cells (Mullen & Tanabe, 2002). The killing effect depends on the virus type and dose, selective tropism, but also on the cancer cell and its susceptibility to the different types of cell death (apoptosis, necrosis, pyroptosis and autophagy). Moreover, availability of targetable receptors, viral replication and cell antiviral response elements are essential for the anti-tumour effect (Alvarez-Breckenridge *et al.,* 2009; Uchida *et al.,* 2013).

The second important effect mechanism of OVs is the enhancement of host immune responses (systemic innate and tumour-specific adaptive). These immune responses not only attack the virus itself, but ideally also target tumour cells (Workenhe *et al.,* 2015). Even non-infected cells can be affected by the immune response when systemic immunity is fully triggered. In this way, even a distant tumour that has not been exposed to the virus can be attacked and regressed. This is a major advantage of oncolytic virotherapy (Andtbacka *et al.,* 2019). Subsequent to oncolytic cell death, tumour cells release tumour-associated antigens (TAAs) that promote an adaptive immune response, thereby mediating tumour regression at distant tumour sites. Furthermore, tumour cells release, surface expose, or secrete viral PAMPs, cellular danger-associated molecular patterns (DAMPs) and cytokines (Bartlett *et al.,* 2013; Inoue & Tani, 2014; Conrad *et al.,* 2013; Zamarin & Postow, 2015). DAMPs are for example ATP (Martins *et al.,* 2009; Garg, Krysko & Verfaillie *et al.,* 2012), high mobility group box 1 (HMGB1) protein (Bell *et al.,* 2006; Fucikova *et al.,* 2011; Scaffidi *et al.,* 2002), surface-exposed endoplasmic reticulum (ER) chaperone calreticulin (ecto-CRT) (Obeid *et al.,* 2007; Garg, Krysko & Verfaillie

et al., 2012), heat-shock proteins (HSP90 and HSP70) (Fucikova *et al.,* 2011; Garg, Krysko, Vandenabeele & Agostinis, 2012; Spisek *et al.,* 2007; Srivastava *et al.,* 1994) and uric acid (Shi *et al.,* 2003). Cytokines are for example, type I IFNs, tumour necrosis factor-α (TNFα), IFNγ, and IL-12 (Pol *et al.,* 2020). PAMPs, DAMPs, and cytokines stimulate antigen-presenting cells (APCs), such as dendritic cells, to mature. APCs activate antigen-specific CD4+ and CD8+ T cell responses. CD8+ T cells migrate to the tumour cells and mediate anti-tumour immunity following antigen recognition.

IFNs and DAMPs can also directly activate natural killer (NK) cells. NK cells are part of the innate immune response and kill cells with reduced major histocompatibility complex (MHC) class I expression. Cancer cells frequently show a downregulated MHCI expression. However, it is important to note that NK cells may also eliminate virally infected cells, which can be counterproductive for OV therapy (Alvarez-Breckenridge *et al.,* 2012).

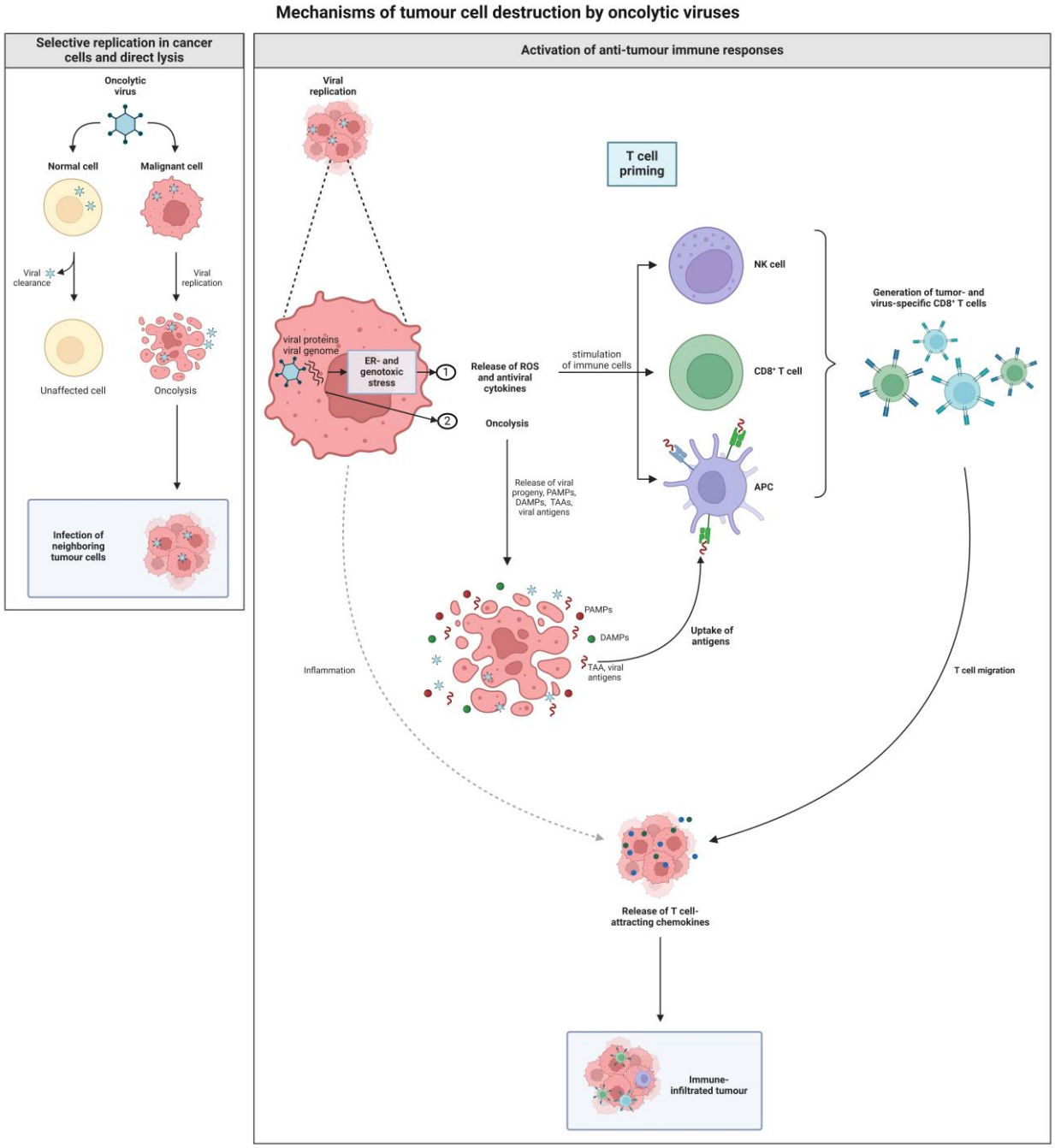

Figure 2: Mechanisms of tumour cell destruction by oncolytic viruses. The therapeutic efficacy of oncolytic viruses is based on a combination of direct destruction of cancer cells and indirect stimulation of anti-tumour immune responses. Oncolytic viruses are designed or naturally inclined to selectively infect and replicate within cancer cells. This selectivity is often due to the unique characteristics of the cancer cell environment, such as specific surface receptors, altered cellular pathways and impaired antiviral responses that are less effective compared to normal cells. Once inside the cancer cell, the oncolytic virus replicates and produces numerous viral progeny. This replication process overwhelms the cell, causing it to rupture (lyse). The lysed cell releases new viral particles that can then infect neighbouring cancer cells, continuing the cycle of infection and destruction. The second mechanism is the activation of anti-tumour immune responses. When cancer cells are infected by an oncolytic virus, they mount an antiviral response involving endoplasmic reticulum (ER) stress and genotoxic stress. This triggers an increase in reactive oxygen species (ROS) and the production of antiviral cytokines. The ROS and cytokines are released by the infected cancer cells and activate immune cells, including antigen-presenting cells (APCs), CD8+ T cells and natural killer (NK) cells. The oncolytic virus then induces oncolysis, resulting in the release of viral progeny, pathogen-associated molecular patterns (PAMPs), danger-associated molecular patterns (DAMPs) and tumour-associated antigens (TAAs). The viral progeny continue to spread the infection. PAMPs (viral particles) and DAMPs (host cell proteins)

activate the immune system by engaging receptors such as Toll-like receptors (TLRs). In this immunostimulatory environment, TAAs are taken up by antigen-presenting cells. Together, these processes lead to the activation of immune responses against virally infected cancer cells and the generation of new immune responses against TAAs on uninfected cancer cells. Created with BioRender.com.

Many virus types have already been proposed or tested as possible OVs and entered into clinical trials, such as herpesviruses, poxviruses, picornaviruses (e.g., coxsackie, polio, and Seneca Valley virus), adenoviruses, paramyxoviruses (e.g., measles virus), parvoviruses, reoviruses, Newcastle reovirus, Newcastle disease virus, rhabdovirus (e.g., vesicular stomatitis virus), and others (reviewed in (Kohlhapp & Kaufman, 2016)). To date, only one replication-competent oncolytic virus, a modified herpes virus type 1 (HSV-1), termed T-VEC (IMLYGIC®, Amgen), has been approved by the FDA for the treatment of advanced melanoma (Andtbacka *et al.,* 2019). This makes T-VEC the first therapeutic agent in oncolytic immunotherapy (Andtbacka *et al.,* 2019).

1.3.1.3 Talimogene laherparepvec (T-VEC)

1.3.1.3.1 Biology

HSV-1 is a prevalent human pathogen, infecting approximately 80% of the human population (David M. Knipe & Peter M. Howley, 2020). It is an enveloped, double-stranded DNA virus that belongs to the subfamily *Alphaherpesvirinae*. Its genome is large, at 152 kb, and the virion size ranges from 150 to 300 nm in diameter (David M. Knipe & Peter M. Howley, 2020). The genome contains approximately 30 kb of genes that are not essential for viral infection. HSV-1 replicates in the nucleus without causing insertional mutagenesis. Due to these characteristics, the virus is attractive for oncolytic virus development.

T-VEC is a genetically modified and thereby attenuated herpes simplex virus type 1 (HSV-1) derived from the JS1 strain and the first oncolytic virus in its class (Liu *et al.,* 2003b). The JS1 strain was isolated from a cold sore and is a minor human pathogen that causes fever blisters. It was found to be superior to standard laboratory strains and other clinical isolates of HSV-1 in killing tumour cells. It was therefore selected for further genetic modification (Liu *et al.,* 2003b). The original strain was modified in several ways to allow virus replication in tumour tissue, tumour cell lysis, and promotion of host anti-tumour immunity (Figure 3).

A

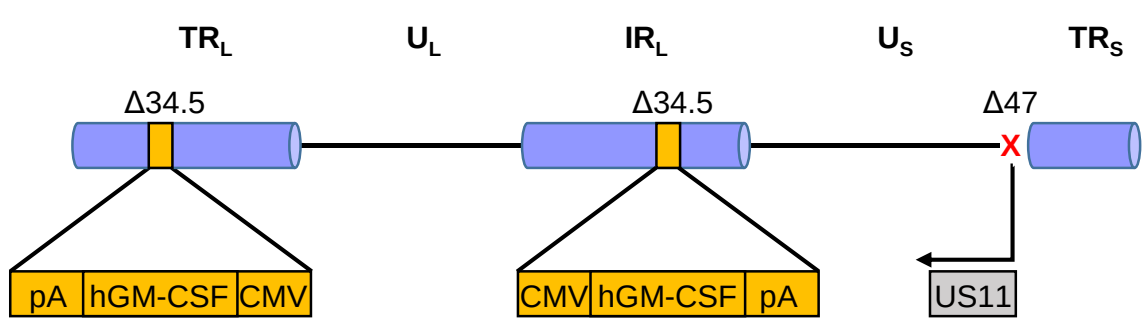

B

Characteristics/modifications	**Purpose**
Usage of JS-1 strain	Improves cell killing in comparison to other clinical isolates.
Deletion of *ICP34.5*	Provides tumor-selective replication and impedes replication in neuronal cells.
Deletion of *ICP47*	Restores antigen presentation and promotes the anti-tumor immune response.
Increased *US11* expression	Increases replication of ICP34.5-deleted virus in cancer cells
Insertion of *hGM-CSF* cDNA	Improves systemic anti-tumor immune responses.
Retention of *thymidine kinase* gene	Maintenance of sensitivity to aciclovir and ganciclovir.

Figure 3: The engineering of JS1 backbone of herpes simplex virus type 1 (HSV-1) to generate talimogene laherparepvec (T-VEC). (A) Schematic of T-VEC genetic modifications. Both viral *ICP34.5* genes have been deleted and exchanged with *hGM-CSF* genes under the control of a CMV promoter. Additionally, *ICP47* was deleted and *US11* thereby placed under the control of the immediate-early ICP47 promoter. (B) Characteristics of T-VEC and their implications. Abbreviations: CMV, cytomegalovirus; hGM-CSF, human granulocyte-macrophage colony-stimulating factor; ICP, infected cell protein; IR_L, long inverted repeat region; pA, polyadenylation tail; TR_L, long terminal repeat; TR_S, short terminal repeat; U_L, unique long region; U_S, unique short region; US11, unique short sequence 11. Adapted by permission from Springer Nature Customer Service Centre GmbH: Springer Nature, American Journal of Clinical Dermatology, Talimogene Laherparepvec (T-VEC) and Other Oncolytic Viruses for the Treatment of Melanoma, (Bommareddy *et al.,* 2017).

After HSV-1 infection, host cells defend themselves through a number of mechanisms. These include the activation of the PKR, which terminates protein translation and blocks further viral replication. PKR is activated by double-stranded RNA in virus-infected cells and mediates among others phosphorylation of the α-subunit of eukaryotic translation initiation factor 2 (eIF2α), which inhibits cellular and viral protein synthesis and can lead to cell death. To interrupt this cascade the unmodified HSV1 expresses two copies of neurovirulence factor infected cell protein (ICP) 34.5. The ICP34.5 protein is required to combat the host's anti-viral response and promote viral replication. This is achieved by ICP34.5 recruiting and activating protein phosphatase 1 (PP1) which dephosphorylates eIF2α, enabling sustained protein synthesis and allowing for viral replication despite PKR activation (He, Gross & Roizman, 1997; Chou *et al.,* 1995). In tumour cells the PKR-eIF pathway is usually disabled. Cell growth and viral replication are therefore usually unhindered. In T-VEC both ICP34.5 copies were deleted. This leads to a selective viral replication in cancer cells, an abortive infection of PKR-active healthy cells, and additionally impedes replication in neuronal cells (Cassady *et al.,* 1998b).

Another gene expressed by HSV-1 is *ICP47*, whose function is to block antigen processing in HSV-infected cells and thus escape the cellular immune system. In T-VEC *ICP47* was deleted which results in the retrieval of the activity of transporter associated with antigen processing (Früh *et al.,* 1995; Goldsmith *et al.,* 1998). This promotes loading of HSV-1 and tumour peptides onto MHC I, which supports recognition and oncolysis of infected tumour tissue by CD8+ T cells.

Deletion of the immediate early (IE) gene *ICP47* also upregulated the coding *unique short sequence 11* (*US11*) by placing it under the control of the *ICP47* promoter. Accordingly, *US11* is regulated in T-VEC as an IE gene and no longer as a late (L) gene as originally in HSV-1 (He & Chou *et al.,* 1997). It was shown, that this modification and the early in infection cycle expression of US11, a RNA-binding protein, in HSV-1 34.5 mutants results in improved tumour cell killing properties (Mohr & Gluzman, 1996; Taneja *et al.,* 2001). US11 protein also inhibits PKR activation in 34.5 mutants (Cassady *et al.,* 1998a; Mulvey *et al.,* 1999).

In addition to the deletion of ICP47, another modification of T-VEC to further support immunogenicity is the insertion of two copies of the coding sequence for human granulocyte-macrophage colony-stimulating factor (hGM-CSF) in place of the two deleted *ICP34.5* genes. Expression of hGM-CSF can promote systemic anti-tumour immune responses through the recruitment of antigen-presenting cells, which induce an effector T-cell response (Kaufman *et al.,* 2010a).

1.3.1.3.2 Mode of action

T-VEC has a dual mode of action (Figure 4). Firstly, it directly infects and kills tumour cells, known as the oncolytic effect. Secondly, it induces local and systemic immune responses, known as the immunotherapy effect (Bommareddy *et al.,* 2017).

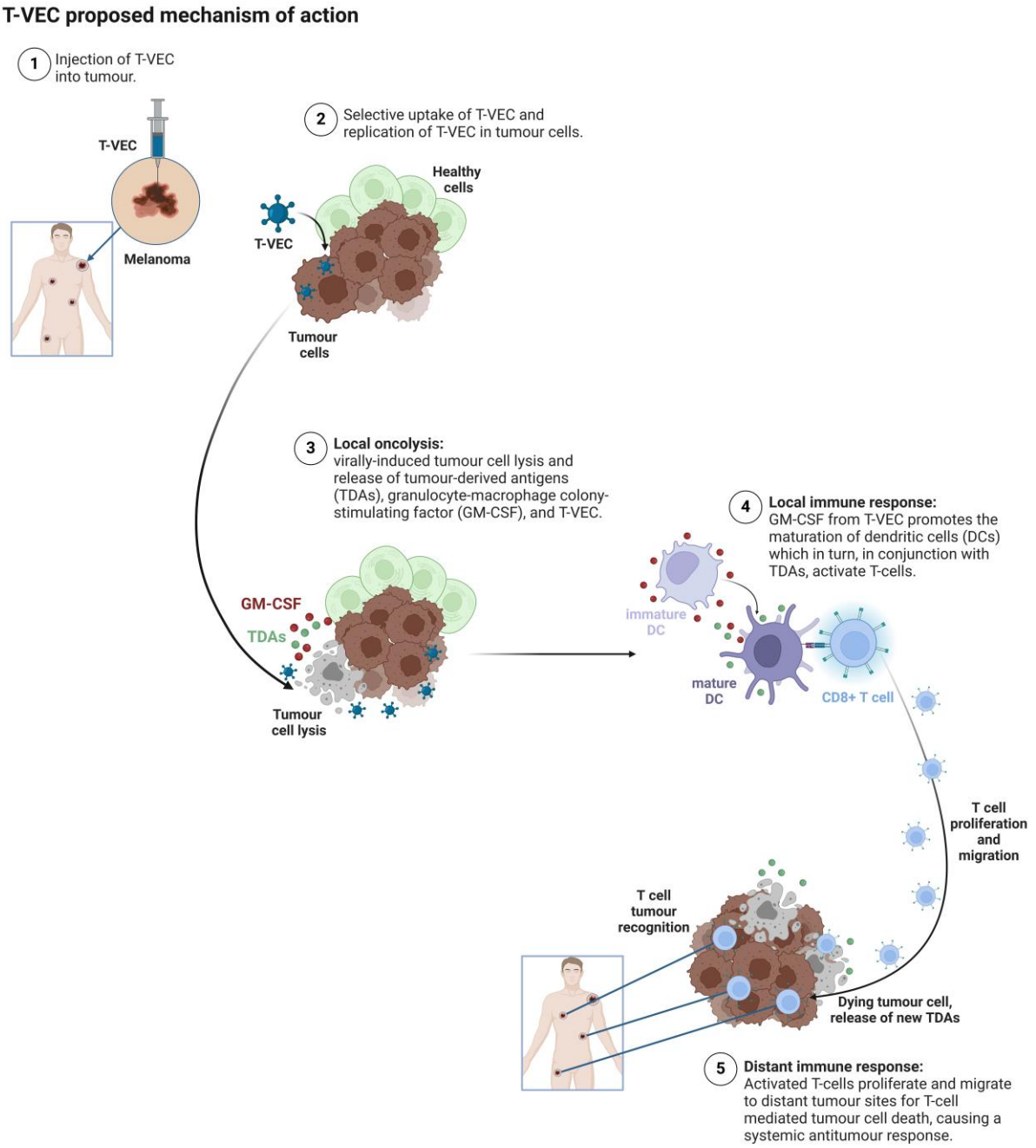

Figure 4: Proposed mechanism of T-VEC oncolysis and immunological response. Abbreviations: T-VEC, talimogene laherparepvec; TDA, tumour-derived antigen; GM-CSF, granulocyte-macrophage colony-stimulating factor; DC, dendritic cell. Created with BioRender.com.

Lysis of the infected tumour cells is induced by replication of T-VEC (Kohlhapp & Kaufman, 2016). This, in turn, leads to the release of soluble tumour-associated antigens, danger signals,

and necrotic tumour cell fragments. These components help to start local immune responses. In addition, the expression of GM-CSF from T-VEC promotes the maturation and migration of dendritic cells. Once activated they move to the regional lymph node where they present antigens to CD4+ T helper cells and CD8+ T effector cells. This triggers a systemic T cell response. Tumour-specific T cells can then travel to distant metastases and initiate immune-mediated killing of the cancer cells. Furthermore, the viral particles released by oncolysis may infect nearby tumour cells, thereby boosting T-VEC's anti-tumour activity. In distant metastases the response rate is lower than in injected lesions. This could be due to local suppression factors in distant metastases or to the insufficient spread of the tumour-specific T-cell reaction. (Bommareddy *et al.,* 2017). Additional research is required to comprehend the precise mechanisms through which T-VEC destroys cancerous cells and stimulates anti-tumour immunity.

1.3.1.3.3 Treatment for metastatic melanoma

The localisation of primary melanoma lesions on the skin and the tendency of melanoma to form regional skin metastases offer the possibility of intra-lesional therapy with minimal surgical risk. T-VEC is an oncolytic virus that is administered by direct injection and is an example of intra-lesional therapy. It is administered through injection into cutaneous, subcutaneous, or nodal melanoma metastases. T-VEC was approved by the FDA on 27th October 2015 for the treatment of unresectable stage IIIB/IVM1a melanoma.

In the Oncovex (GM-CSF) Pivotal Trial in Melanoma (OPTiM) trial, a randomized phase III study, intra-tumoural T-VEC was compared to GM-CSF injection in 436 patients with unresectable stage IIIB to IVM1C melanomas. The study found that 19.3% (n=57) of patients treated with T-VEC had a durable response lasting ≥ 6 months, compared to 1.4% (n=2) in the GM-CSF cohort (Andtbacka *et al.,* 2019). Furthermore, T-VEC treatment resulted in a higher overall response rate (31.5%) compared to GM-CSF treatment (6.4%). Fifty (16.9%) patients and 1 (0.7%) patient in the T-VEC and GM-CSF arms, respectively, achieved complete responses. The median overall survival in the T-VEC arm was 23.3 months (95% CI, 19.5–29.6), compared to 18.9 months with GM-CSF (95% CI, 16.0–23.7). It should be noted that T-VEC was more effective in patients without visceral metastasis (stage IIIB-IVM1a), with a durable response rate of 28.8% and an overall response rate of 46.0%. Adverse events, such as fatigue, chills, pyrexia, nausea, and influenza-like illness, were reported. The toxicity profile was deemed acceptable according to the guidelines. Checkpoint inhibitors significantly enhance the effect of T-VEC, making it an attractive partner in combined cancer immunotherapies (Ribas *et al.,* 2017; Bommareddy *et al.,* 2018).

1.3.1.3.4 Potential predictive biomarkers

The identification of biomarkers that predict successful T-VEC therapy or a response to T-VEC would be a major milestone in the fight against melanoma. Despite the mild side effects, OV

therapy can be stressful for patients and time is of the essence in the fight against cancer. Biomarkers of OV response are therefore urgently needed, but have not yet been well studied. Recent research has shown that mutations in the IFNγ-JAK-STAT signalling pathway can increase sensitivity to treatment with oncolytic viruses (Nguyen *et al.,* 2021). It was previously found that mutations in the IFNγ-JAK-STAT signalling pathway cause resistance to immune checkpoint inhibitors in melanoma (Gao *et al.,* 2016; Shin *et al.,* 2017; Zaretsky *et al.,* 2016). Therefore, Nguyen *et al*. generated cell lines from a melanoma patient who was planned to receive immune checkpoint inhibitors. One cell line was obtained prior to anti-PD-1 therapy, while the other was generated after treatment and relapse. Both cell lines were treated with HSV-1. The cell line from the progressive lesion showed a complete loss of *JAK2* and was seven times more sensitive to a modified HSV-1 (HSV1-dICP0) than the line from the baseline biopsy. Moreover, knockdown of *JAK1/2*, as well as pharmacological inhibition resulted in increased OV sensitivity. In addition, *in vivo* B16-F10 mouse melanoma studies confirmed the *in vitro* findings. In conclusion, it is suggested that OV therapy should be considered in melanomas with mutations in the IFNγ-JAK-STAT signalling pathway and in melanomas that are resistant to immune checkpoint inhibitors. The data suggest that the expression of JAK1 and JAK2 may serve as a biomarker for OV activity.

Furthermore, two proteins, stimulator of interferon genes (STING), and the cyclic GMP-AMP synthase (cGAS), have been proposed as biomarkers for T-VEC response (Bommareddy *et al.,* 2019; Xia *et al.,* 2016). The cGAS-STING pathway is essential in regulating the innate immune system (Sun *et al.,* 2013). The cGAS-STING pathway is crucial for defending against infections caused by viruses, such as HSV-1, microbial pathogens, and other infections. It can be activated by various stimuli, including double-stranded DNA (dsDNA), cyclic dinucleotides (CDNs), ER stress, mitochondrial stress, and energy imbalance in metabolic and immune cells. cGAS mediates STING signalling by synthesizing cyclic guanosine monophosphate-adenosine monophosphate (cGAMP) upon interaction with dsDNA (Decout *et al.,* 2021). STING is activated when cGAMP, which acts as a second messenger, binds to STING dimers located at the ER and changes its conformation. STING traffics to an ER-Golgi intermediate compartment (ERGIC) and then to the Golgi apparatus. Here, it recruits and activates TANK-binding kinase 1 (TBK1), which in turn phosphorylates STING. This phosphorylation enables STING to recruit and phosphorylate interferon regulatory factor 3 (IRF3). The phosphorylated IRF3 dimerises and enters the cell nucleus. Together with NF-κB, which is also activated through STING, and other transcription factors, gene expression of type I IFNs, ISGs, and several other inflammatory mediators, pro-apoptotic genes, and chemokines is induced.

Furthermore, STING was shown substantial for IFNβ-dependent T-cell-responses against tumours (Woo *et al.,* 2014; Woo *et al.,* 2015; Fuertes *et al.,* 2011). Studies showed that in tumour-infiltrating dendritic cells STING is activated (mediated by cGAS) by tumour derived

cytosolic DNA. This leads to production of cytokines (IFNβ) and cytotoxic T lymphocyte production against tumour-associated antigens (Woo *et al.,* 2014; Xia *et al.,* 2016). All things considered; STING-dependent cytokine production has an important role in suppressing cancer development.

Bommareddy *et al*. discovered that STING expression in melanoma cell lines was inversely related to their sensitivity to T-VEC (Bommareddy *et al.,* 2019). They showed that the STING knockout cell lines were more susceptible to T-VEC-induced cell death. However, no correlation was found between T-VEC oncolysis and cGAS expression. In addition, melanoma cells that express low levels of STING and are resistant to PD-1 blockade *in vivo* were found to be sensitive to T-VEC treatment. Xia *et al*. demonstrated that suppression of STING signalling may facilitate immune evasion following DNA damage in melanoma cells (Xia *et al.,* 2016). Loss of STING function resulted in the inability of melanoma cells to produce type I IFN and other cytokines when exposed to cytosolic DNA, rendering these cells highly susceptible to HSV-1. Taken together, these data suggest that STING may serve as predictive biomarker of OV activity.

Expression of viral entry receptors on tumour and stromal cells within the tumour microenvironment could be another potential biomarker. Increased expression of these receptors may indicate greater susceptibility to viral infection. HSV-1 entry into cells involves the interaction of viral glycoproteins with cell surface receptors (Heldwein & Krummenacher, 2008; Connolly *et al.,* 2011). The first step in the entry process may be the attachment of virions to cell surface glycosaminoglycans, principally heparan sulfate proteoglycans, but this is not essential (Nicola, 2016; Shukla & Spear, 2001). However, it may facilitate interaction with cellular receptors and the fusion with a host cell membrane. HSV-1 can enter target cells either by fusion of the viral envelope with the plasma membrane, allowing viral capsids to enter the cytoplasm, or by receptor-mediated endocytosis, in which enveloped virions are internalised into endosomes (Campadelli-Fiume *et al.,* 2012). Depending on the cell type, HSV-1 preferentially uses one of these entry mechanisms or both simultaneously.

HSV-1 consists of a central core with viral DNA, a surrounding envelope composed of glycoproteins and host cell membrane fragments, and a capsid. Viral surface glycoproteins (gB, gC, and gD) bind to host cell entry receptors to mediate virus entry into cells. Fusion with cell membranes is initiated by binding of the viral envelope glycoprotein D (gD) to a receptor (Eisenberg *et al.,* 2012). Most OVs have a natural tropism for certain cell surface proteins. HSV-1 utilises the HVEM, specific Nectins (Nectin-1 and Nectin-2), and 3-O-sulfated heparan sulfate (3-OS-HS) to enter cells (Montgomery *et al.,* 1996; Geraghty *et al.,* 1998; Krummenacher *et al.,* 2004; Shukla *et al.,* 1999; O'Donnell *et al.,* 2010). The Nectin family is a member of the immunoglobulin G (IgG) superfamily of calcium-independent adhesion molecules. They were found in a broad number of tissues, including epithelial tissues and the

chemical synapse of neuronal tissue (Knebel-Mörsdorf, 2016). They are involved in the formation and organisation of adherens and tight junctions (Fukuhara *et al.,* 2002; Samanta & Almo, 2015). HVEM is a member of the TNF receptor superfamily (TNFRSF) and the first identified gD receptor (Montgomery *et al.,* 1996; Croft, 2003). It is expressed in T lymphocytes, B cells, natural killer cells and dendritic cells, where it regulates immune cell activation or inactivation, and in other cell types like neurons, epithelial cells and fibroblasts (Edwards & Longnecker, 2017; Steinberg *et al.,* 2011). Heparan sulfates are present on the cell surface and in the extracellular matrix of most cell types (Lindahl *et al.,* 1998; Annaval *et al.,* 2020). They interact with many ligands to immobilise them, protect them against proteolytic degradation and also have specific regulatory functions. Heparan sulfates play a fundamental role in most biological functions.

It was shown that highly invasive and migratory cancer cells overexpress Nectin-1 which enhances oncolytic herpes virus sensitivity (Yu *et al.,* 2005). It was also shown that Nectin-1 is the major receptor in the epidermis and dermal fibroblasts, while HVEM plays a more subordinate role (Petermann & Thier *et al.,* 2015; Petermann & Rahn *et al.,* 2015). Moreover, a restricted HVEM expression can be replaced by Nectin-1. Nectin-1 is a marker of thyroid cancer, squamous cell carcinoma, and patient-derived paediatric high-grade brain tumour xenografts sensitivity to herpes oncolytic therapy (Huang *et al.,* 2007; Yu *et al.,* 2007; Friedman *et al.,* 2018).

1.3.2 The pmCiC as a prognostic cancer marker

Despite significant advances in cancer research and improved treatment options, metastatic cancer remains the deadliest form of the disease. One of the problems is that cancer cells develop resistance to drugs, which can lead to disease recurrence and metastasis. Tumour cells have high energy requirements compared to normal cells because they need to grow, proliferate and metastasise. These processes demand substantial quantities of biomaterial, which are produced by various anabolic metabolic pathways that generate the necessary energetic and biosynthetic precursors, as well as signalling molecules. As a result, metabolism is often upregulated and deregulated in cancer cells, providing a suitable approach for treatment options. For example, specific inhibitors targeting fatty acid synthase (FASN) (Zaytseva *et al.,* 2018) and isocitrate dehydrogenase (IDH) (Sharma, 2018) have been explored in clinical trials. However, these treatments have often been associated with severe toxic side effects (Tian *et al.,* 2022; Abou-Alfa *et al.,* 2020).

In this thesis, I will focus on citrate, a key metabolite used by cancer cells for fatty acid synthesis (Wang *et al.,* 2016), and the pmCiC (Mycielska *et al.,* 2018). The pmCiC is a plasma membrane-specific variant of the mitochondrial citrate transporter (mCiC), which was found to

provide cancer cells with extracellular citrate (Mycielska *et al.,* 2018) and is expressed in cancer cells of different origin *in vitro* and *in vivo* (Parkinson *et al.,* 2021).

1.3.2.1 Citrate metabolism in non-cancerous cells

1.3.2.1.1 Citric acid cycle

Citrate is an important metabolite generated mainly in the mitochondria, with no exchange with the extracellular space in most benign cells. The only benign cells known to release or take up citrate are prostate and astrocytes, and liver and kidney cells. While prostate epithelial cells utilize pmCiC for citrate release, all other cell types express citrate transporters from a different gene family, known as solute carrier 13 (SLC13).

Citrate is produced as an intermediate in the Krebs cycle (Figure 5), also known as the citric acid cycle or tricarboxylic acid (TCA) cycle (Akram, 2014). The TCA cycle is the major metabolic pathway for the body's energy supply. Carbohydrates, lipids and amino acids are oxidatively catabolized in this cycle. The first substrate and starting point of the TCA cycle is acetyl coenzyme A (acetyl-CoA). Acetyl-CoA can be derived via the glycolytic pathway from glucose, which enters the mitochondria as pyruvic acid and is then oxidatively decarboxylated, from fatty acids that have undergone β-oxidation, from the catabolism of some amino acids (e.g. leucine, tyrosine, isoleucine, lysine, phenylalanine and tryptophan) and from ketone bodies (Akram, 2014). The reaction of oxaloacetate (OAA) and acetyl-CoA to form citrate is catalysed by mitochondrial citrate synthase (CS) (Akram, 2014). The enzyme aconitase 2 (ACO2) catalyses the isomerization of citrate to isocitrate via cis-aconitate. Isocitrate dehydrogenase 3 converts isocitrate to alpha-ketoglutarate (αKG) in a decarboxylation reaction, producing reduced nicotinamide adenine dinucleotide (NADH) cofactor. αKG is then converted to succinyl-CoA in a second oxidative decarboxylation step by the 2-oxoglutarate dehydrogenase complex (OGDC) and NADH is generated. Succinyl-CoA is then converted to succinate by succinyl-CoA synthetase (SCS) and guanosine diphosphate (GDP) is phosphorylated to guanosine triphosphate (GTP). Succinate is converted to fumaric acid by succinate dehydrogenase (SDH). Flavin adenine dinucleotide (FAD) is also converted to reduced flavin adenine dinucleotide ($FADH_2$). The next step is the formation of malate, catalysed by fumarate hydratase (FUM). Finally, malate is dehydrogenated by malate dehydrogenase (MDH) to the substrate of the first step of the TCA cycle, OAA, with recovery of NADH. OAA reacts with acetyl-CoA to form citrate. This completes the cycle.

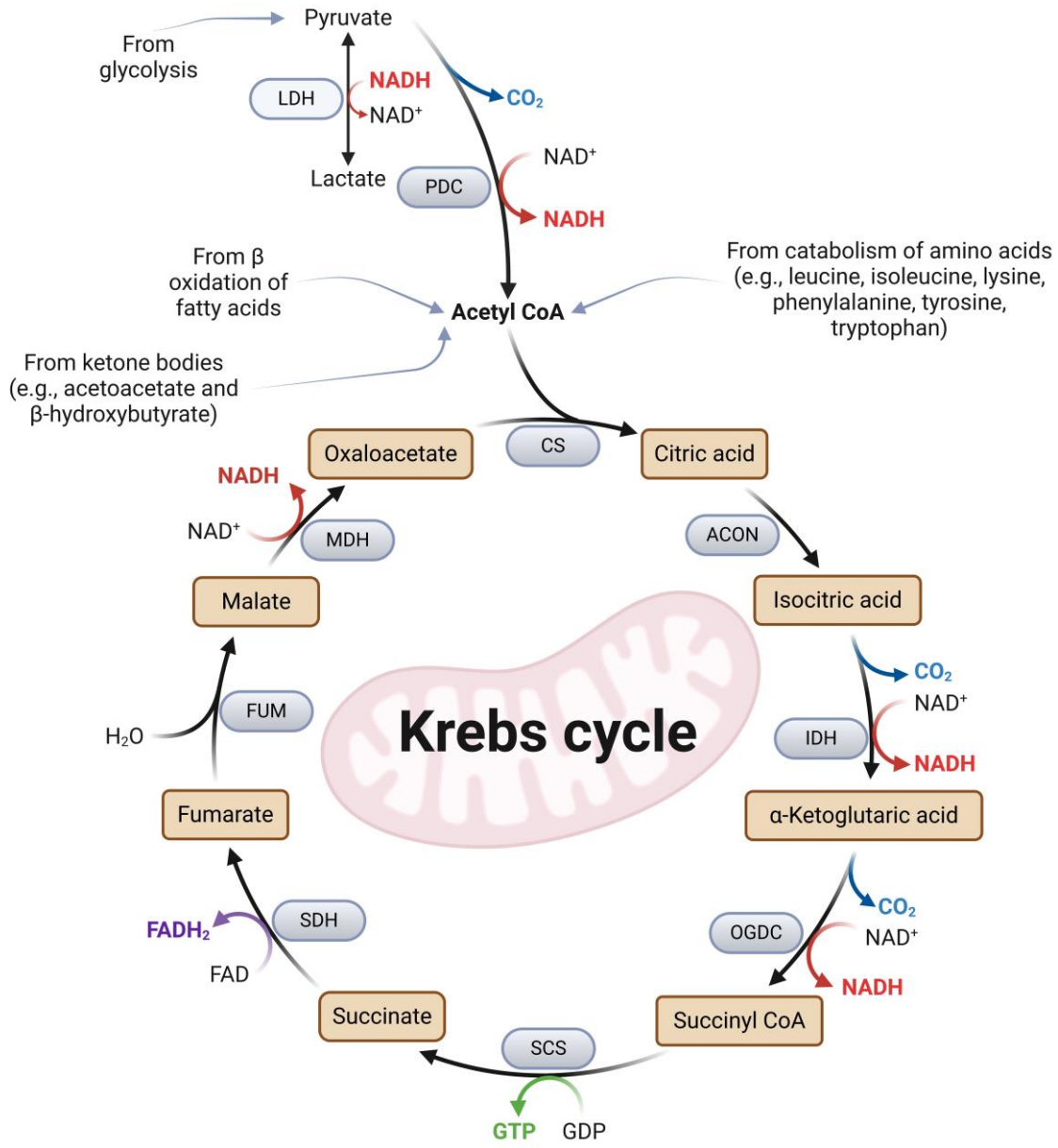

Figure 5: Overview of the Krebs cycle. Abbreviations: LDH, Lactate dehydrogenase; PDC, Pyruvate dehydrogenase complex; CS, Citrate synthase; ACON, Aconitase; IDH, Isocitrate dehydrogenase; OGDC, 2-Oxoglutarate dehydrogenase complex; SCS, Succinyl-CoA synthetase; SDH, Succinate dehydrogenase; FUM, Fumarate hydratase; MDH, Malate dehydrogenase; NADH, Nicotinamide adenine dinucleotide (reduced form); NAD^+, Nicotinamide adenine dinucleotide (oxidized form); CO_2, Carbon dioxide; FAD, Flavin adenine dinucleotide (oxidized form); $FADH_2$, flavin adenine dinucleotide (reduced form). Created with BioRender.com.

As mentioned above, the main function of the TCA cycle is to produce energy. In addition to the ATP or GTP produced directly in the cycle, further energy is generated by feeding reducing equivalents into the electron transfer chain. Complex V, also known as ATP synthase, plays the leading role (Nelson *et al.,* 2021).

In summary, citrate plays an important role in cellular homeostasis by regulating energy synthesis. In high doses, citrate can also directly inhibit the mitochondrial enzyme SDH and

thus directly regulate ATP production (Hillar *et al.,* 1975). Also OAA, derived from citrate, can directly inhibit SDH (Fink *et al.,* 2018).

1.3.2.1.2 Citrate dependent processes

There are three main processes, in which citrate plays an important role, or which are completely dependent on citrate. These are protein acetylation, fatty acid synthesis (FAS) and biosynthesis.

Acetyl-CoA maintains FAS. It provides lipids for storage or membrane formation. Acetyl-CoA serves as substrate for acetylation reactions, in particular it plays a role in the acetylation of histones and ER proteins. Histones are proteins that help package and organise DNA in the nucleus, and acetylation is a key mechanism in regulating gene expression. Acetylation of ER proteins can affect their folding, stability and interactions with other proteins. This has implications for overall protein function and cellular homeostasis.

OAA has many functions in cellular metabolism. It undergoes several transformations with significant effects on energy production, nucleotide synthesis, and redox balance. Aspartate aminotransferase (AST) catalyses the conversion of OAA into aspartate. Aspartate is used as a precursor for the synthesis of nucleotides and polyamines. Moreover, OAA can be transformed into phosphoenolpyruvate (PEP) by phosphoenolpyruvate carboxykinase (PCK1). This is the first rate-limiting step in the process of gluconeogenesis. MDH1 metabolizes OAA to malate. Malate can either be exchanged for citrate and transported back into the mitochondria through mCiC or transported back into the mitochondria through the malate-aspartate shuttle (MAS), allowing the transfer of NADH and H+ ions. This process contributes to ATP production in the mitochondria (Nelson *et al.,* 2021). MDH1 also plays a role in the regeneration of NAD+ from NADH, which is essential for the maintenance of glycolysis, particularly at the level of glyceraldehyde-3-phosphate dehydrogenase (GAPDH). Alternatively, malic enzyme (ME) can convert malate to pyruvate. This reaction generates reduced nicotinamide adenine dinucleotide phosphate (NADPH), which is critical for several cellular processes, including redox balance and FAS (J. Berg, J. Tymoczko, G. Gatto, L. Stryer, 2019).

1.3.2.1.3 Citrate is a regulator of catabolism and anabolism

Citrate plays several roles in cellular metabolism, notably as an intermediate in the Krebs cycle. Citrate can also regulate cellular metabolism by controlling glycolytic activity. Elevated citrate levels inhibit glycolytic ATP production by deactivating phosphofructokinase-1 (PFK1) (SALAS *et al.,* 1965) and phosphofructokinase-2 (PFK2) (Nissler *et al.,* 1995), key enzymes in glycolysis (Nelson *et al.,* 2021), and also by direct or indirect (via OAA) inhibition of the mitochondrial enzyme SDH and indirect inhibition of ATP synthase (Hillar *et al.,* 1975; Fink *et al.,* 2018; Fu *et al.,* 2015). It is noteworthy that citrate coordinates metabolic pathways,

inhibiting gluconeogenesis when glycolysis is active and vice versa. It also suppresses FAS when fatty acid β-oxidation (FAO) is activated and vice versa. In addition, citrate increases the activity of fructose-1,6-biphosphatase (FBPase), a gluconeogenic enzyme (Icard *et al.,* 2018). It activates acetyl-CoA carboxylase (ACC), the primary regulator of FAS, while its downstream product, fatty acid malonyl-CoA, inhibits FAO by reducing the activity of the carnitine cylcarnitine carrier (CAC) (J. Berg, J. Tymoczko, G. Gatto, L. Stryer, 2019; McGarry *et al.,* 1978). CAC is involved in the transfer of fatty acid (FA)-derived acyl-CoA into mitochondria and, like the mCiC transporter, a member of the solute carrier family 25 (SLC25), also called the mitochondrial carrier family (Iacobazzi *et al.,* 2013; McGarry *et al.,* 1978). In addition, citrate senses cellular nutrient status through acetyl-CoA-mediated protein acetylation of histones, metabolic enzymes and transcription factors (Lee *et al.,* 2013).

Therefore, citrate is considered to be the central metabolite in cancer cells and plays an important role in cancer metabolism and its regulation. As discussed above, citrate can either activate or inhibit certain metabolic pathways, making control of intracellular citrate levels critical for cancer cells. During the metastatic process, cancer cells are often deprived of certain substrates as they migrate through different organs, and the possibility of using extracellular citrate as a metabolite and control factor should be considered as playing an important role in maintaining metabolic homeostasis.

1.3.2.2 Citrate metabolism in cancerous cells

1.3.2.2.1 Extracellular citrate is essential to fuel the metabolism of cancer cells

As previously stated, tumour cells require an increased energy supply for the processes of growth, proliferation, and metastasis. Therefore, metabolic activity is increased in cancer cells to meet their need for energy and precursors for macromolecular biosynthesis. It is a well-known fact that cancer cells undergo a metabolic switch from oxidative phosphorylation to glycolysis, a phenomenon known as the 'Warburg effect' (Warburg, 1925; Pascale *et al.,* 2020). Unlike most normal cells, cancer cells produce significant amounts of fatty acids to rebuild their plasma membranes and obtain energy through β-oxidation (Zha *et al.,* 2005). Healthy cells, with the exception of hepatocytes, take up fatty acids from the extracellular space rather than synthesising them. Increased fatty acid synthesis by cancer cells is considered as one of the hallmarks of cancer.

Citrate is the primary substrate for fatty acid synthesis and therefore plays a central role in cancer metabolism. To take part in fatty acid synthesis, citrate is transported from the mitochondria into the cytoplasm through mCiC (mitochondrial citrate carrier) where it is metabolized through ATP-citrate lyase into acetyl-CoA and oxaloacetate. Citrate also plays a crucial role in amino acid synthesis, which is essential for proliferating cells.

Cancer cells can produce excess citrate by utilising the Warburg effect. In this way they synthesise ATP through glycolysis, using mitochondria for citrate synthesis. Use of Warburg effect is also effective in increasing cancer cells resistance to hypoxic conditions to which they are exposed due to rapid growth and metastasis (Icard *et al.,* 2021; Zhang *et al.,* 2021; Damaghi *et al.,* 2021). Another advantage of using Warburg effect is excess production and release of lactate which acidifies the tumour environment and promotes faster growth (Gallo *et al.,* 2015).

1.3.2.2.2 The tumour microenvironment and its impact on tumour development

The term "tumour microenvironment" (TME) is used to describe the surrounding cellular and non-cellular components within and around a tumour mass. The TME consists of proliferating tumour cells and the tumour stroma, which comprises fibroblasts, immune cells, endothelial cells, and other supportive cells. In addition, the TME includes blood vessels, infiltrating inflammatory cells, and a variety of associated tissue cells. The TME is also composed of a network of signalling molecules (cytokines, chemokines, growth factors, and enzymes). These elements are surrounded by collagen and elastin fibres, which make up the extracellular matrix (ECM) (Wang *et al.,* 2017). The TME evolves as the tumour progresses as a result of its interaction with the host. It is formed, and largely influenced by the tumour itself, which controls molecular and cellular processes in the surrounding tissues (Whiteside, 2008). The TME plays a pivotal role in facilitating immune evasion and cancer progression. The interaction between cancer cells and the diverse cell population within the TME influences tumour resistance, progression and metastasis (Kurose *et al.,* 2001).

CAFs represent one of the most abundant stromal components in solid tumours and, as such, constitute a significant component of the TME. They can be distinguished from other cells by expressing several stromal markers, including integrin β1 (CD29), FAP, and α-smooth muscle actin (α-SMA) (Puré & Blomberg, 2018; Costa *et al.,* 2018). After their activation, CAFs secrete signalling molecules that promote the survival of cancer cells and facilitate the recruitment and transformation of additional cell types within the TME (Heneberg, 2016; Räsänen & Vaheri, 2010). Moreover, CAFs facilitate ECM remodelling by releasing collagen and fibronectin, producing matrix metalloproteinases (MMPs) and increasing vascular endothelial growth factor (VEGF) levels (Eck *et al.,* 2009; Murphy & Nagase, 2008; Gonzalez-Avila *et al.,* 2019; Shiga *et al.,* 2015). This results in a reorganisation of the matrix that enables neoplastic cells to migrate in a specific direction in the company of CAFs (Erdogan *et al.,* 2017; Gaggioli *et al.,* 2007).

There is substantial evidence suggesting that human cancer cells can stimulate adjacent stromal cells to generate proteins and metabolites that support tumour growth, advancement, and resistance to drugs (Nazemi & Rainero, 2020). Among the documented metabolites are

nucleotides, lactate, and amino acids like serine and glutamine (Nazemi & Rainero, 2020). However, the involvement of citrate in the communication between tumour cells and the tumour microenvironment remains unexplored in this context.

Citrate is normally produced in the mitochondria of both cancerous and healthy cells through the TCA cycle. However, cancer cells require additional citrate for the synthesis of cytosolic fatty acids, probably through the reverse Krebs cycle or through glutamine reductive carboxylation (Parkinson *et al.,* 2021; Metallo *et al.,* 2011; Wang *et al.,* 2020). Cancer cells may also be able to obtain citrate from various extracellular reservoirs, such as the bloodstream, senescent cells and tumour-surrounding tissue like cancer-associated cells (CACs), which include stromal cells such as CAFs. Blood concentration of citrate is about 200 µM (Mycielska *et al.,* 2015). However, the blood supply to growing tumours is frequently limited and metastatic growth requires the formation of new blood vessels. Senescent fibroblasts, which are known to be part of the cancer environment, have previously been shown to release high levels of citrate due to changes in their metabolism (James *et al.,* 2015; Mycielska *et al.,* 2022). This could be also an additional source of citrate for cancer cells.

Previous research has demonstrated that cancer cells of different origin take up citrate from the extracellular space at concentrations present in the bloodstream (at physiological concentrations) through a plasma membrane-specific variant of the mitochondrial citrate transporter (mCiC) (Mycielska *et al.,* 2018). Experiments have also shown that cancer cells take up more citrate than normal cells. The uptake of extracellular citrate was increased especially under hypoxic and low glucose conditions. Furthermore, the study revealed that cancer cell metabolism gains advantages from extracellular citrate uptake, resulting in diminished mitochondrial activity and subsequently reducing synthesis of ROS. Consequently, this diminishes the necessity for extracellular glucose supply in cancer cells and makes cancer cells more resistant to starvation, tumour progression and cancer proliferation (Mycielska *et al.,* 2018; Petillo *et al.,* 2020).

It can be therefore concluded that extracellular citrate might play a significant role in the process of metastasis by regulating cancer metabolism and supporting necessary transformation of surrounding stroma.

1.3.2.2.3 The plasma membrane citrate carrier and citrate uptake

Citrate transport is maintained by the mCiC and the pmCiC. Both are variants of the *SLC25A1* gene (Mazurek *et al.,* 2010). The sequence of pmCiC is identical to that of mCiC, with only the first exon differing in the first 38 amino acids of the N-terminal domain (Mazurek *et al.,* 2010).

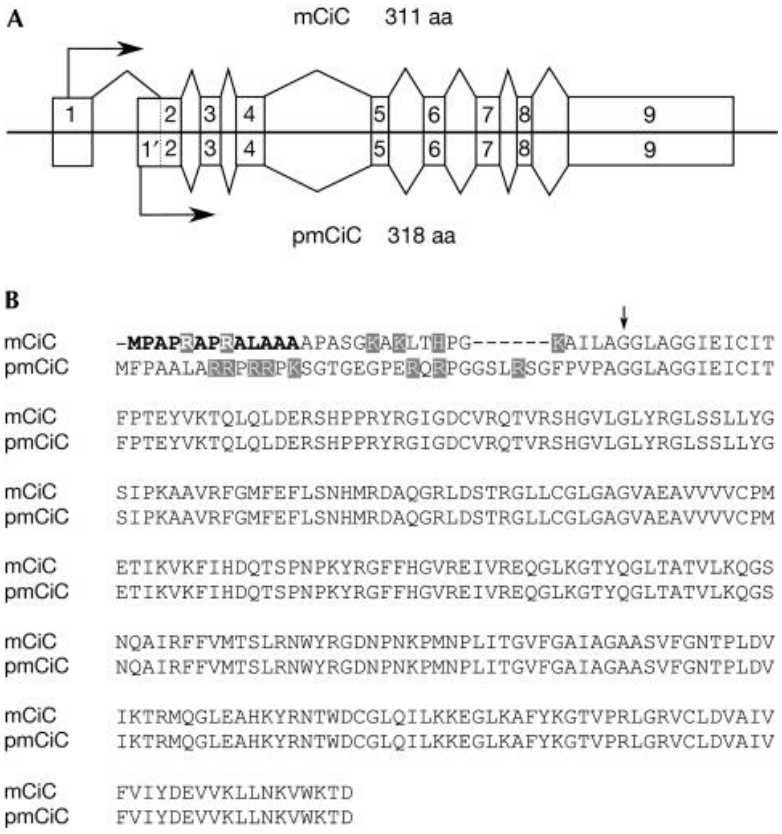

Figure 6: Human citrate transport protein isoforms. Schematic representation of the splicing patterns of mitochondrial (mCiC) and plasma membrane (pmCiC) citrate-transporting proteins. Exons are represented by squares and translation initiation sites by arrows. (B) Alignment of the protein sequences of the isoforms. The 13 amino acid (aa) sequence in the mitochondrial isoform is shown in bold. Positively charged residues in the amino-terminal parts of the proteins are shaded. Abbreviations: mCiC, mitochondrial citrate carrier; pmCiC, plasma membrane isoform of mCiC. Creative Common Attribution License (Mazurek *et al.,* 2010).

The plasma membrane citrate transporter was cloned from prostate secretory epithelial cells (PNT2-C2 cells) that release citrate into prostatic fluid (Mazurek *et al.,* 2010). Citrate concentrations in prostatic fluid can reach 180 mM and are crucial for the viability and mobility of spermatozoa, therefore primary role of prostatic citrate is to act as an energy source for sperm (Medrano *et al.,* 2006). Changes in citrate levels in the prostatic fluid may contribute to reduced fertility (Mycielska *et al.,* 2022). Importantly, citrate levels are significantly decreased in metastatic prostate cancer. Although, the pmCiC is the primary transporter in the prostate gland that releases citrate (Mazurek *et al.,* 2010), another citrate transporter has also been shown to be present in benign prostatic cells - the progressive ankylosis protein homolog (ANKH) also known as SLC62A1. It has been recently discovered that this transporter exports citrate, as well as malate, succinate, and phosphate (Szeri *et al.,* 2020). In addition, citrate uptake in some healthy specialised cells is mediated by transporters that are members of the SLC13 gene family (Akhtar *et al.,* 2023). In hepatocytes and neurons, the Na+/citrate cotransporter (NaCT), encoded by the *SLC13A5* gene, is used (Yodoya *et al.,* 2006; Higuchi *et al.,* 2020). In kidney cells, the sodium dicarboxylate transporter NaDC-3 (encoded by the *SLC13A3* gene) can filter citrate from the blood or from the urine through NaDC-1 (encoded

by the *SLC13A2* gene) (Tobin *et al.,* 2022; Pajor, 2006). This shows that our understanding of plasma membrane transporters and their involvement in transporting Krebs cycle metabolites remains incomplete.

The pmCiC has been mainly associated with cancer cells. Until now, its expression was shown in a variety of human tumours such as adenocarcinomas (prostate, breast, pancreas, lung, colon, hepatocellular carcinoma (HCC) etc.), brain tumours such as glioblastoma, and skin cancer such as melanoma and MCC (Mycielska *et al.,* 2018; Drexler *et al.,* 2021; Parkinson *et al.,* 2021). Cancer cells express pmCiC both in primary tumours and at metastatic sites. An increase in the expression of pmCiC was observed at the front of the invasion and at the sites of metastasis of tumours of different origins. The transporter is overexpressed in human cancer cells in comparison to their non-malignant counterparts *in vivo*. Furthermore, histopathological studies indicate that there is a correlation between the intensity of pmCiC expression and tumour stage (Mycielska *et al.,* 2018). This would suggest that pmCiC expression correlates with cancer progression.

The pmCiC is located at the plasma membrane and the mCiC is located at the mitochondrial inner membrane (Mazurek *et al.,* 2010). Citrate is exported from the mitochondria into the cytosol, in healthy and malignant cells, via mCiC in exchange for malate or another citrate, or it is taken up from the extracellular space via pmCiC (Mycielska *et al.,* 2018; Haferkamp *et al.,* 2020). In the cytosol citrate is converted to acetyl-CoA and OAA by ATP-citrate lyase (ACLY) (Abou-Alfa *et al.,* 2020). In cancer cells, citrate import by pmCiC is Na^+-dependent, whereas in normal prostate epithelial cells, citrate secretion by pmCiC is K^+-dependent (Mycielska *et al.,* 2018; Mazurek *et al.,* 2010; Mycielska *et al.,* 2005). Depending on the cells in which it is expressed, pmCiC appears to change its direction of transport. It is hypothesised that this bidirectional citrate transport may be due to post-translational modifications of the transporter protein, the formation of multimers and/or an altered insertion into the plasma membrane in cancer cells compared to normal cells, but this needs to be clarified in further studies (Mycielska *et al.,* 2018). In normal cells, pmCiC is typically absent or expressed at minimal levels in the plasma membrane. Indeed, expression of pmCiC is upregulated in a large number of cancer tissues, whereby citrate transport into the cell is clearly directed: pmCiC imports citrate from the outside into the cytoplasm, following a citrate/Na gradient.

The uptake of extracellular citrate through pmCiC can be hindered by gluconate (Mycielska *et al.,* 2018; Mycielska *et al.,* 2019). This inhibition can lead to reduced tumour growth and alterations in the metabolic characteristics of tumour tissue (Mycielska *et al.,* 2018). This was shown by pancreatic carcinoma xenograft growth *in vivo*. The subcutaneous human pancreatic (L3.6pl) tumour volume in immunodeficient mice decreased with the application of Na+ gluconate. In addition, this study highlighted the importance of extracellular citrate uptake in lipid biosynthesis and metabolism through metabolite profiling of tumour tissue from the mouse

model, where inhibition of citrate uptake by gluconate showed significant effects (Mycielska *et al.,* 2018). In addition, several recent studies suggest an association between metastatic disease and a reduction in citrate levels in the blood, tissues and urine of cancer patients (Mycielska *et al.,* 2019). This may be due to an increased demand for citrate by cancer cells (Mycielska *et al.,* 2019). Therefore, there is some evidence that gluconate may be useful in the treatment of cancer. Gluconate is a derivative of glucose and exists as a salt of gluconic acid. It is known to chelate divalent metals. Gluconate is considered by the FDA to be a harmless substance (Food and Drug Administration, 1977). In medicine, gluconate is often used as a biologically neutral carrier of Zn^{2+}, Ca^{2+}, Cu^{2+}, Fe^{2+} and K^{+} to treat corresponding ion deficiencies. In addition, gluconate is often combined with other drugs (e.g. chlorhexidine and sodium antimony). Gluconates are not regarded as physiologically active and have not been studied for their own therapeutic benefits.

2 Publications

The following section presents the individual works that have already been published, accompanied by a brief description of their respective contents.

2.1 Nectin-1 expression correlates with the susceptibility of malignant melanoma to oncolytic herpes simplex virus

Summary:

This chapter explores the correlation between Nectin-1 expression and the susceptibility of malignant melanoma to oncolytic HSV therapy, specifically using T-VEC. The research includes both *in vitro* and *in vivo* studies, demonstrating that higher Nectin-1 levels are associated with increased effectiveness of T-VEC-induced melanoma cell death. The chapter discusses the methodology, including cell line analysis, knockout experiments, and patient sample studies, to validate Nectin-1 as a predictive biomarker for T-VEC therapy.

Objective addressed:

Evaluation of Nectin-1 as a predictive biomarker for the efficacy of T-VEC therapy in malignant melanoma.

Nectin-1 expression correlates with the susceptibility of malignant melanoma to oncolytic herpes simplex virus

Barbara Schwertner[1], Georg Lindner[2], Camila Toledo Stauner[1], Elisa Klapproth[2], Clara Magnus[2], Anette Rohrhofer[3], Stefanie Gross[4], Beatrice Schuler-Thurner[4], Veronika Öttl[2], Nicole Feichtgruber[2], Konstantin Drexler[1], Katja Evert[5], Michael P. Krahn[6], Mark Berneburg[1], Barbara Schmidt[2,3], Philipp Schuster[2,†], and Sebastian Haferkamp[1,*,†]

1: Department of Dermatology, University Hospital Regensburg, 93053 Regensburg, Germany

2: Institute of Medical Microbiology and Hygiene, University of Regensburg, 93053 Regensburg, Germany

3: Institute of Clinical Microbiology and Hygiene, University Hospital Regensburg, 93053 Regensburg, Germany

4: Department of Dermatology, University Hospital Erlangen, Friedrich-Alexander-Universität Erlangen-Nürnberg, 91054 Erlangen, Germany

5: Institute of Pathology, University of Regensburg, 93053 Regensburg, Germany

6: Medical Cell Biology, Internal Medicine D, University Hospital Münster, 48149 Münster, Germany

*: Correspondence: Sebastian.Haferkamp@klinik.uni-regensburg.de

†: Authors contributed equally

Manuscript information:

Cancers (Basel). 2021 Jun 19; 13(12): 3058.

Received 28 May 2021

Accepted 16 June 2021

Doi: 10.3390/cancers13123058

2.1.1 Abstract

Simple summary:

Talimogene laherparepvec (T-VEC), a first-in-class oncolytic herpes simplex virus, improves the outcome of patients suffering from unresectable melanoma, in particular in combination with checkpoint inhibitors. However, a certain percentage of patients does not profit from this treatment, which raises the question of potential biomarkers to predict success or failure of oncolytic herpes viruses. For these purposes, we studied the oncolytic activity of T-VEC in a panel of 20 melanoma cell lines and evaluated the clinical response of 35 melanoma metastases to intralesional T-VEC application. Through these studies, we characterized Nectin-1 as a suitable biomarker predicting 86% and 78% of melanoma regression in vitro and in vivo, respectively. In contrast, other molecules involved in the entry (HVEM) and signal transduction (cGAS, STING) of herpes simplex viruses were not predictive. Altogether, our data support the role of Nectin-1 in pretreatment biopsies to guide clinical decision-making in malignant melanoma and supposedly other tumor entities.

Abstract:

Talimogene laherparepvec (T-VEC), an oncolytic herpes simplex virus, is approved for intralesional injection of unresectable stage IIIB/IVM1a melanoma. However, it is still unclear which parameter(s) predict treatment response or failure. Our study aimed at characterizing surface receptors Nectin-1 and the herpes virus entry mediator (HVEM) in addition to intracellular molecules cyclic GMP-AMP synthase (cGAS) and stimulator of interferon genes (STING) as potential bio-markers for oncolytic virus treatment. In 20 melanoma cell lines, oncolytic activity of T-VEC was correlated with the expression of Nectin-1 but not HVEM, as evaluated via flow cytometry and immunohistochemistry. Knockout using CRISPR/Cas9 technology confirmed the superior role of Nectin-1 over HVEM for entry and oncolytic activity of T-VEC. Neither cGAS nor STING as evaluated by Western Blot and immunohistochemistry correlated with T-VEC induced oncolysis. The role of these biomarkers was retrospectively analyzed for the response of 35 cutaneous melanoma metastases of 21 patients to intralesional T-VEC injection, with 21 (60.0%) of these lesions responding with complete (n = 16) or partial regression (n = 5). Nectin-1 expression in pretreatment biopsies significantly predicted treatment outcome, while the expression of HVEM, cGAS, and STING was not prognostic. Altogether, Nectin-1 served as biomarker for T-VEC-induced melanoma regression in vitro and in vivo.

Keywords: malignant melanoma, oncolytic, herpes simplex virus, T-VEC, nectin-1

2.1.2 Introduction

Talimogene laherparepvec (T-VEC) is a genetically modified and thereby attenuated herpes simplex virus type 1 (HSV-1) derived from the JS1 strain (Liu *et al.,* 2003a). Deletion of neurovirulence factor infected cell protein (ICP) 34.5 provides tumor selectivity and impedes replication in neuronal cells (Cassady *et al.,* 1998b), while deletion of ICP47 restores the activity of transporter associated with antigen processing (Goldsmith *et al.,* 1998; Früh *et al.,* 1995). The latter promotes loading of HSV-1 and tumor peptides onto MHC I, which supports recognition and oncolysis of infected tumor tissue by CD8+ T cells. In addition, insertion of the coding sequence for human granulocyte macrophage colony-stimulating factor (GM-CSF) can promote systemic antitumor immune responses through the recruitment of antigen-presenting cells, which induce an effector T-cell response (Kaufman *et al.,* 2010b). T-VEC is approved for the treatment of unresectable stage IIIB/IVM1a melanoma via injection into cutaneous, subcutaneous, or nodal melanoma metastases.

In a randomized phase III trial of intratumoral T-VEC versus GM-CSF injection in unresectable stage III/IV melanoma (OPTiM trial), 19.3% (n = 57) of patients treated with T-VEC had a durable response lasting ≥ 6 months compared to 1.4% (n = 2) in the GM-CSF cohort (Andtbacka *et al.,* 2019). In this trial, an overall response was observed in 31.5%, including 16.9% complete responses of patients receiving T-VEC, and in only 6.4% in the GM-CSF treatment group including one patient achieving a complete response. Importantly, the efficacy of T-VEC was higher in patients without visceral metastasis (stage IIIB–IVM1a) with a durable response rate (DRR) of 28.8% and an overall response rate (ORR) of 46.0%. The effect of T-VEC was significantly enhanced in the presence of checkpoint inhibitors (Ribas *et al.,* 2017), making it an attractive partner in combination cancer immunotherapies (Bommareddy *et al.,* 2018)

Despite the indisputable success of oncolytic herpes viruses in the treatment of malignant melanoma, a certain fraction of patients does not profit from T-VEC administration. Therefore, biomarkers that predict success or failure and guide clinical decision-making in this treatment are urgently needed, in particular in patients with advanced stages of this disease. Several predictive markers have been proposed in in vitro and in vivo models, amongst them the cyclic GMP-AMP synthase (cGAS) with the stimulator of interferon genes (STING) as a recognition pattern of cytosolic HSV DNA in malignant melanoma (Xia *et al.,* 2016). In brain tumor xenografts, the expression of HSV-1 entry receptor Nectin-1 (HVEC, CD111) was associated with tumor regression (Friedman *et al.,* 2018). So far, these markers have not been evaluated systematically for the treatment of malignant melanoma using the oncolytic herpes virus T-VEC.

Our study aimed at characterizing cGAS and STING in addition to Nectin-1 and herpes virus entry mediator (HVEM, CD270), also known as tumor necrosis factor receptor superfamily

member 14, as potential biomarkers for oncolytic HSV-1 treatment. For these purposes, the expression of these markers was correlated with the oncolytic effect of T-VEC in a large collection of 20 melanoma cell lines. Moreover, biomarker expression was correlated with the response of 35 cutaneous melanoma metastases of 21 patients to intralesional treatment with T-VEC. Altogether, Nectin-1 expression correlated with T-VEC induced tumor cell regression in vitro and in vivo, while respective expression of HVEM, STING, and cGAS did not predict response.

2.1.3 Materials and Methods

Cell culture

LOX IMVI, M14, MDA-MB-435, SK-MEL-28, and UACC-257 are part of the NCI60 cancer cell line established by the National Cancer Institute (Bethesda, MD, USA) for drug testing (reviewed in (Shoemaker, 2006)) and were purchased from NCI-Frederick Cancer Center DCTD Tumor/Cell Repository. Melanoma cell lines A375, M26, M19, and FM-88 were contributed by the Department of Dermatology, University Hospital Würzburg, Germany, as reported previously (Houben *et al.,* 2011). Six melanoma cell lines (MEL-JUSO, IGR-1, IGR-37, IGR-39, SK-MEL-3, SK-MEL-30) were purchased from the German Collection of Microorganisms and Cell Cultures (DSMZ), Braunschweig, Germany, while AXBI, LIWE-7, ARST-1, ICNI-5li, and UMBY-1 were contributed by the Department of Dermatology, University Hospital Erlangen, Germany, as reported previously (Thomann *et al.,* 2015). All cells were propagated in DMEM supplemented with 10% heat-inactivated (56 °C, 60 min) fetal calf serum, 90 U/mL streptomycin, 0.3 mg/mL glutamine, and 200 U/mL penicillin (all Pan Biotech, Aidenbach, Germany). All cell lines were tested regularly for mycoplasma using PCR.

Generation of viral stocks

Vero cells were infected at 90% confluency with the replication-competent HSV-1 strain T-VEC (Imlygic®, Amgen, Munich, Germany) and harvested at the peak of virus replication. After three freeze–thaw cycles, supernatants were filtered through 0.45 µm pores and stored at −80 °C. The 50% tissue culture infective dose (TCID50) was determined according to the method of Reed and Muench (REED & MUENCH, 1938).

Infection, cell viability, and toxicity experiments

Melanoma cell lines were plated in 96-well plates with 10,000 cells/well and infected the following day with T-VEC using a multiplicity of infection (MOI) of 1. The MOI was based on titration experiments on SK-MEL-30, IGR-1, and IGR-39 cells, which showed an increased killing of cells with MOI of 1 compared to MOI of 0.1, while MOI of 10 did not further enhance the effect.

The viability of infected cells was compared to mock-infected cells two days post infection (p.i.) using 3-[4,5-dimethylthiazol-2yl]-2,5-diphenyl-tetrazolium bromide (MTT), which was dissolved at 5 mg/mL in DPBS (Biomol, Hamburg). The yellow dye (10 µL) was added to each well and incubated until insoluble violet crystals had formed, which were solubilized overnight using 100 µL of detergent (10% SDS, 10 mM HCl). Absorbance was measured at 595 nm.

The same conditions were applied for the lactate dehydrogenase (LDH) assay except for using DMEM without phenol red, which was supplemented with 5% fetal calf serum. Cell death and cell lysis was colorimetrically quantified two days p.i. using the Cytotoxicity Detection Kit

(Roche, Basel, Switzerland). In short, equal parts of cell free supernatants and reaction mixture, included in the kit, were incubated at room temperature for 20–25 min. Absorbance was measured at 490 nm with a reference wavelength at 630 nm. Toxicity in infected cell cultures was normalized to LDH release of uninfected cells, lysed at the time of infection using a final concentration of 1% Triton X-100 to determine the maximum amount of LDH release.

Caspase-3/7 activity of infected cells was compared to cells treated with a final concentration of 1 µM Staurosporine (Biozol, Eching, Germany) 24 h p.i. using the Caspase-Glo 3/7 Assay (Promega, Fitchburg, WI, USA). The assay was performed according to the manufacturer's recommendations. Luminescence of the cleaved caspase 3/7 substrate was measured after 60 min of incubation at room temperature.

FACS analysis

Melanoma cells were plated into 6-well plates and incubated overnight. After washing with DPBS, cells were dissociated using Gibco Cell Dissociation Buffer (Thermo Fisher Scientific, Schwerte, Germany), resuspended in FACS buffer (DBPS, 1% fetal calf serum, 1 mM EDTA), and incubated with the FcR blocking reagent (Miltenyi Biotec, Bergisch-Gladbach, Germany) at 4 °C for 10 min. Thereafter, cells were stained using anti-CD111-APC (Nectin-1, clone R1.302; Miltenyi Biotech; dilution 1:11) or isotype (clone IS5-21F5; Miltenyi Biotech; dilution 1:50), and anti-CD270-PE (HVEM, clone 122; Biolegend; dilution 1:33) or isotype (clone MOPC21; Acris/OriGene, Herford, Germany; dilution 1:33) at 4 °C for 20 min. After fixation with 4% paraformaldehyde, cells were analyzed using FACS Canto II with FACSDiva software for automatic compensation and measurement of samples (BD Biosciences) and FCS Express 3 software (De Novo Software, Los Angeles, CA, USA). Each cell line was analyzed in at least three independent experiments.

Western blot

Total cellular proteins were extracted on ice using RIPA lysis buffer containing protease inhibitors. Proteins (30 µg/lane) were resolved on Any KD Mini-PROTEAN TGX Precast Polyacrylamide Protein Gels and transferred to nitrocellulose membranes (both Biorad, Feldkirchen, Germany). Western blots were probed with rabbit monoclonal antibodies against cGAS (D1D3G) and STING (D2P2F) (both Cell Signaling, Frankfurt, Germany; dilution 1:1000) or with murine monoclonal antibody against housekeeping β-actin (C4; Santa Cruz, Heidelberg, Germany; dilution 1:1000). The same nitrocellulose membrane was probed with anti-STING, anti-cGAS, and anti-β-actin. For these purposes, it was cut horizontally just below the pre-stained protein ladder band at 55 kDa. The upper part was probed with anti-cGAS and the lower part with anti-STING. After developing, anti-STING was removed using mild stripping buffer (199.8 mM glycin, 3.5 mM SDS, 1% Tween20, pH 2.2) and probed again using anti-β-actin.

Detection was performed using peroxidase AffiniPure donkey anti-rabbit or anti-mouse IgG (H + L) (both Jackson ImmunoResearch, Cambridgeshire, UK; dilution 1:10,000). WesternBright ECL HRP Substrate (Advansta, San Jose, CA, USA) was used as a chemiluminescent substrate to detect the protein targets. Imaging was performed using the ChemiDoc System (Bio-Rad, Hercules, CA, USA).

Biopsies

Between May 2016 and December 2018, a total of 21 patients suffering from malignant melanoma were treated with intralesional T-VEC injection. For diagnostic purposes, 35 biopsies were taken from these patients prior to injection of T-VEC (one, two, three, and four in 14, 2, 3, and 2 patients, respectively). Biopsies were retrospectively analyzed for the expression of Nectin-1, HVEM, cGAS, and STING, as approved by the ethical commission of the Faculty for Medicine, University of Regensburg (Refs. no. 14-101-000 and 21-2300-101). The demographic and clinical characteristics of patients at baseline are detailed in Table 1.

Table 1: Patient demographics and clinical characteristics at baseline.

Characteristics	Patients (n=21)
Sex, n (%)	
Female	11 (53)
Male	10 (48)
Median age, years (range)	72 (56-91)
ECOG performance status, n (%)	
0	19 (86)
1	3 (14)
Disease substage, n (%)	
IIIB	2 (10)
IIIC	19 (90)
LDH, n (%)	
≤ ULN	21 (100)
> ULN	0
Prior anticancer therapy, n (%)	
Interferon	4 (19)
No prior therapy	17 (81)

Immunohistochemistry (IHC)

Melanoma cell lines were embedded in paraffin as described before (Koh, 2013). Patient biopsies were fixed in formalin and embedded in paraffin according to standard procedures.

Paraffin specimens were sectioned in 2-µm-thick slices and IHC was performed using the ZytoChem-Plus HRP Kit (Mouse or Rabbit) (Zytomed/Biozol) according to the manufacturer's recommendations. Sections were dewaxed using xylol (Merck, Darmstadt, Germany) and rehydrated using ethanol. Epitope retrieval was achieved using HIER Citrate Buffer pH6 (Zytomed) heated to 90 °C.

The following primary antibodies were used: Rabbit monoclonal antibody against STING (D2P2F, Cell Signaling; dilution for patient samples 1:50, dilution for cell lines 1:200), murine

monoclonal antibody against Nectin-1 (R1.302.12, Santa Cruz, Heidelberg, Germany; dilution for patient samples 1:50), rabbit polyclonal antibody against Nectin-1 (AB_2736197, Invitrogen/Thermo Fisher; dilution for cell lines 1:100), murine monoclonal antibody against HVEM (CW10, Santa Cruz; dilution 1:500 for patient samples and cell lines), rabbit polyclonal antibody against cGAS (NBP1-86761, Novus Biologicals/Bio-Techne, Wiesbaden Nordenstadt, Germany; dilution for patient samples 1:200), and rabbit monoclonal antibody against cGAS (D1D3G) (Cell Signaling; dilution for cell lines 1:200).

Samples were stained using AEC+ High-Sensitivity Substrate Chromogen Ready-to-Use (Dako/Agilent Technologies, Hamburg, Germany), counterstained using hematoxylin (Carl Roth, Karlsruhe, Germany), and mounted using Aquatex (Merck).

Digital images were generated using the digital microscope and scanner PreciPoint M8 with virtual slide viewing and image processing software ViewPoint Light version 1.0.0.9628 (Precipoint GmbH, Freising, Germany). Optimal staining conditions for immunohistochemistry were evaluated using organ slices provided by the Institute of Pathology, University of Regensburg (Figure S 1). The selection of organs was based on the expression data of the human proteome atlas (Uhlén *et al.,* 2015). The immunohistochemistry was interpreted by six independent individuals and classified into 11 categories based on the respective percentage of stained cells (0%, 1–10%, …, 91–100%).

CRISPR/Cas9 knockout

Nectin-1 and HVEM genes were knocked out using Addgene's lentiviral CRISPR/Cas9 transduction system (Cambridge, MA). Sequences of single guide (sg) RNAs for knockout (KO) of control (5′-GCCAGTTGCTCTGGGGGAACA-3′), Nectin-1 (CD111-1a: 5′-GCAATTGGATAGAGGGTACCC-3′; CD111-2a: 5′-GGGAAACTCGGTTAAAAGGTG-3′), and HVEM (CD270-3a: 5′-GAAGGAGGACGAGTACCCAGT-3′; CD270-4a: 5′-GAGGCCACTTCTGCATCGTCC-3′) were taken from the GECKO library, cloned into the LentiCRISPRv2 puro vector (#52961) and expressed in 293T cells cotransfected with plasmids psPAX2 (#12259) and pMD2.G (#12260), as described previously (Boscheinen *et al.,* 2019).

The efficiency of the CRISPR process was assessed using the T7 endonuclease I mismatch detection assay (Mashal *et al.,* 1995; Vouillot *et al.,* 2015). DNA was extracted from 2.5 × 105 IGR-37, IGR-37 control, IGR-37 Nectin-1-KO, IGR-37 HVEM-KO, and IGR-37 Nectin1/HVEM-KO cell lines using the EZ1 Virus Mini Kit v2.0 in combination with EZ1 Advanced XL system (both Qiagen, Hilden, Germany). Precipitated DNA was amplified using the Expand High Fidelity PCR-System (Roche) with primers Nectin-1-F (5′-TAGGGGCAGGGGCTTATCTC-3′) and Nectin-1-R (5′-AAGCGGTCCATGTGGTAGTT-3′) or HVEM-F (5′-GCAAGGTTGTTCCATGAGCC-3′) and HVEM-R (5′-AGACACCAGCTAAGGGGACT-3′) (all Metabion, Planegg/Steinkirchen, Germany). The cycling conditions were as follows: 95 °C for

5 min, followed by 45 cycles of 95 °C for 30 s, 57 °C for 30 s, and 72 °C for 5 min, and a final 5-min incubation at 72 °C. The PCR products were purified using NucleoFast 96 PCR Plate, 96-well ultrafiltration plates for PCR clean up (Macherey-Nagel, Düren, Germany). 200 ng of the purified PCR products in NEBuffer 2 were heated to 95 °C for 10 min, cooled down to room temperature, and then cleaved with T7 endonuclease I (New England Biolabs) at 37 °C for 15 min. The reaction was stopped by adding EDTA solution (Sigma-Aldrich, St. Louis, MO, USA). The nuclease-treated samples were analyzed on a 1% agarose gel, stained with GelRed Nucleic Acid Gel Stain (Biozol), and photographed under ultraviolet illumination.

HSV-1 DNA qPCR

DNA was extracted from infected cell lines using the EZ1 Virus Mini Kit v2.0 in combination with EZ1 Advanced XL system (Qiagen) according to the manufacturer's recommendations. HSV-1 DNA was quantified using primers HSV1gG1-F (5′-TCCTSGTTCCTMACKGCCTCCC-3′) and HSV1gG1-R (5′-GCAGICAYACGTAACGCACGCT-3′) with TaqMan-HSV1gG1-Probe (VIC-CGTCTGGACCAACCGCCACACAGGT-TAMRA). Values were normalized to housekeeping pyruvate dehydrogenase (PDH) DNA, using TaqMan-PDH-Probe (FAM-CATCTCCTTTTGCTTGGCAAATCTGATCC-TAMRA) with primers PDH-F (5′-TCGATCGGGACTGCTTTCC-3′) and PDH-R (5′-CCCACAACCTAGCACCAAAAGA-3′) (all Metabion).

Statistics

Statistics were performed using GraphPad Prism v. 8.4.2. Details are described in the figure legends. Two-sided p values ≤ 0.05 were considered significant.

2.1.4 Results

2.1.4.1 Melanoma cell lines differ in their susceptibility to herpes virus-induced oncolysis

In the first step, we investigated the susceptibility of melanoma cells to viral oncolysis. After plating a panel of 20 melanoma cell lines into 96-well plates, 10,000 cells/well were infected with the oncolytic HSV-1 strain T-VEC (MOI 1). At two days p.i., cell viability was measured in comparison to uninfected cells using MTT assay measuring metabolically active cells. The oncolytic effect varied considerably between the melanoma cell lines, ranging from 27.89% (IGR-1) to 88.64% (M26) (Figure 7A). Altogether, melanoma cell lines showed a broad range of susceptibility to T-VEC-induced oncolysis in vitro. To validate our MTT viability data, we performed a cell toxicity assay based on LDH release. Both assays showed a significant correlation ($p = 0.015$) using Spearman correlation coefficient analysis (Figure S 2A). To address the question of whether apoptosis is involved in the process of T-VEC-induced cell death, we determined caspase 3/7 activity upon infection with the oncolytic virus. We measured different degrees of caspase 3/7 activity in the 20 cell lines; however, we did not observe a correlation with MTT-based cell viability (Figure S 2B). Based on the MTT viability data, melanoma cell lines were divided equally into responders and non-responders, resulting in cell lines with viability upon T-VEC treatment <60% and >60%, respectively (Figure 7B).

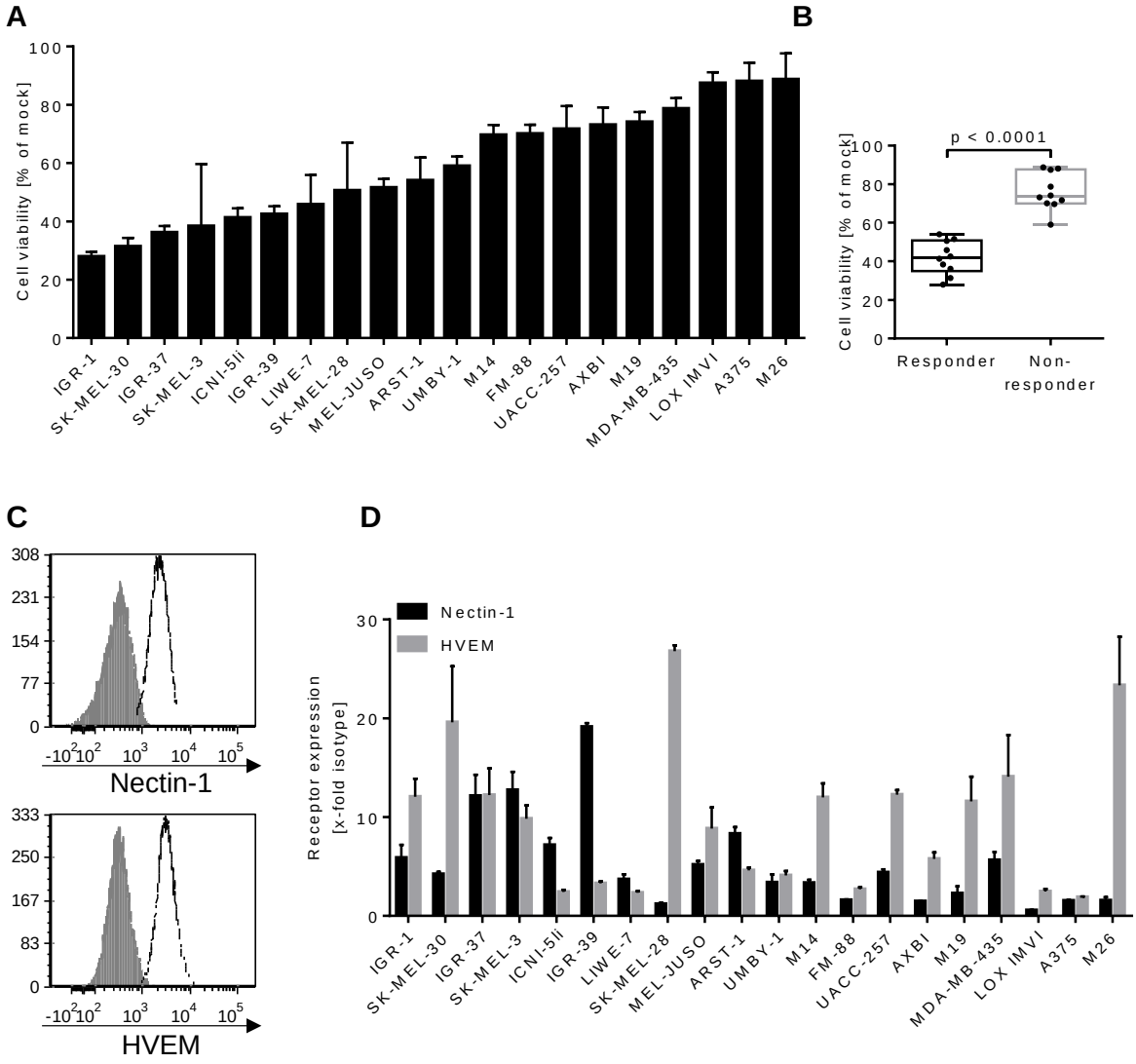
A
B
Cell viability [% of mock]
IGR-1
SK-MEL-30
IGR-37
SK-MEL-3
ICNI-5li
IGR-39
LIWE-7
SK-MEL-28
MEL-JUSO
ARST-1
UMBY-1
M14
FM-88
UACC-257
AXBI
M19
MDA-MB-435
LOX IMVI
A375
M26
p < 0.0001
Responder
Non-responder
C
D
Nectin-1
HVEM
Receptor expression [x-fold isotype]

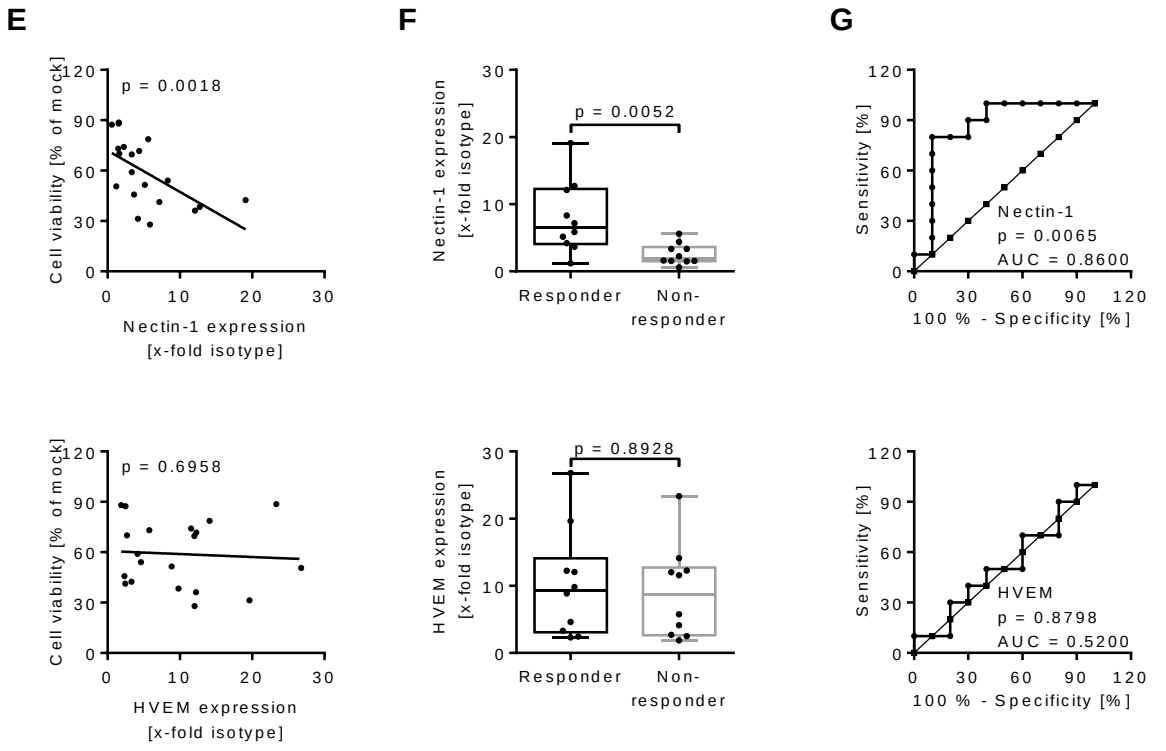
E
F
G
Cell viability [% of mock]
p = 0.0018
Nectin-1 expression [x-fold isotype]
p = 0.0052
Responder
Non-responder
Sensitivity [%]
100 % - Specificity [%]
Nectin-1
p = 0.0065
AUC = 0.8600
p = 0.6958
HVEM expression [x-fold isotype]
p = 0.8928
HVEM
p = 0.8798
AUC = 0.5200

Figure 7: Correlation of the oncolytic activity of herpes simplex virus 1 strain T-VEC with the expression of respective entry receptors on a panel of melanoma cell lines. (A) A total of 20 melanoma cell lines were plated in 96-well plates. Cell viability was measured two days after infection with T-VEC (MOI 1) using MTT assay. Data are expressed as vi-ability of uninfected cells (mock) and show mean and standard error of three separate experiments. (B) Classification of melanoma cell lines as responders and non-responders reflecting viability levels upon T-VEC infection below and above 60%, respectively. Box plots show median and interquartile ranges in addition to minimum and maximum values. (C-D) Expression of Nectin-1 (HVEC, CD111) and herpes virus entry mediator (HVEM, CD270) using flow cytometry with respect to isotype controls on (C) a representative cell line (MEL-JUSO) and (D) all melanoma cell lines. Results represent mean and standard error of three independent experiments. (E) Spearman correlation coefficient, (F) box plot, and (G) ROC curve analyses of all responder and non-responder cell lines with respect to Nectin-1 (upper part) and HVEM expression (lower part) and corresponding susceptibility to T-VEC induced cell death. P values for box plots were calculated using the Mann-Whitney test; ROC curves analyzed the area under the curve (AUC).

2.1.4.2 Oncolytic activity of T-VEC correlates with Nectin-1 expression in vitro

Recently, Nectin-1 was reported to predict the response of brain tumor xenografts to oncolytic HSV-1 infection (Friedman *et al.,* 2018). To identify potential biomarkers for the oncolytic effect induced by T-VEC, we analyzed the expression of Nectin-1 and HVEM with respect to isotype controls on our melanoma cell lines using flow cytometry (Figure 7C). Melanoma cells expressed both receptors to different degrees (Figure 7D). Notably, cell lines with a distinct expression of Nectin-1 (IGR-37, IGR-39, SK-MEL-3) were amongst those with the most pronounced reduction in viability upon T-VEC infection. Spearman correlation coefficient analysis showed that the oncolytic effect induced by T-VEC significantly correlated with the expression of Nectin-1 ($p = 0.0018$), but not HVEM ($p = 0.6958$, n.s.) (Figure 7E). Box plot analysis revealed significantly higher Nectin-1 expression in responder compared to non-responder cell lines ($p = 0.0052$) (Figure 7F). Receiver operating characteristic (ROC) curves showed a significant predictive value of Nectin-1 expression on T-VEC's oncolytic activity ($p = 0.0065$) (Figure 7G). In contrast, the two groups did not differ in HVEM expression levels ($p = 0.8928$, n.s.) (Figure 7F) and ROC analysis failed to detect a predictive value for HVEM expression ($p = 0.8798$, n.s.) (Figure 7G). In conclusion, high Nectin-1 expression was associated with a more pronounced susceptibility to T-VEC mediated oncolysis in malignant melanoma cell lines.

2.1.4.3 Nectin-1 knockout mediates resistance to viral oncolysis

To corroborate the superior effect of Nectin-1 compared to HVEM for the entry of oncolytic HSV-1, both molecules were knocked out from IGR-37 cells by transducing them with lentiviral particles expressing respective sgRNAs. In puromycin-selected bulk cultures, Nectin-1 was knocked out in Nectin-1-KO and Nectin-1-/HVEM-double KO cells, while HVEM was still present in one-third of HVEM-KO and Nectin-1-/HVEM-double KO cells, as evident from flow cytometry (Figure 8A). To also confirm the efficacy of CRISPR knockout at the genomic level, we performed a T7 endonuclease I (T7EI) assay. This analysis corroborated the single knockouts of Nectin-1 and HVEM, while the double knockout still harbored traces of the original sequences (Figure S 3).

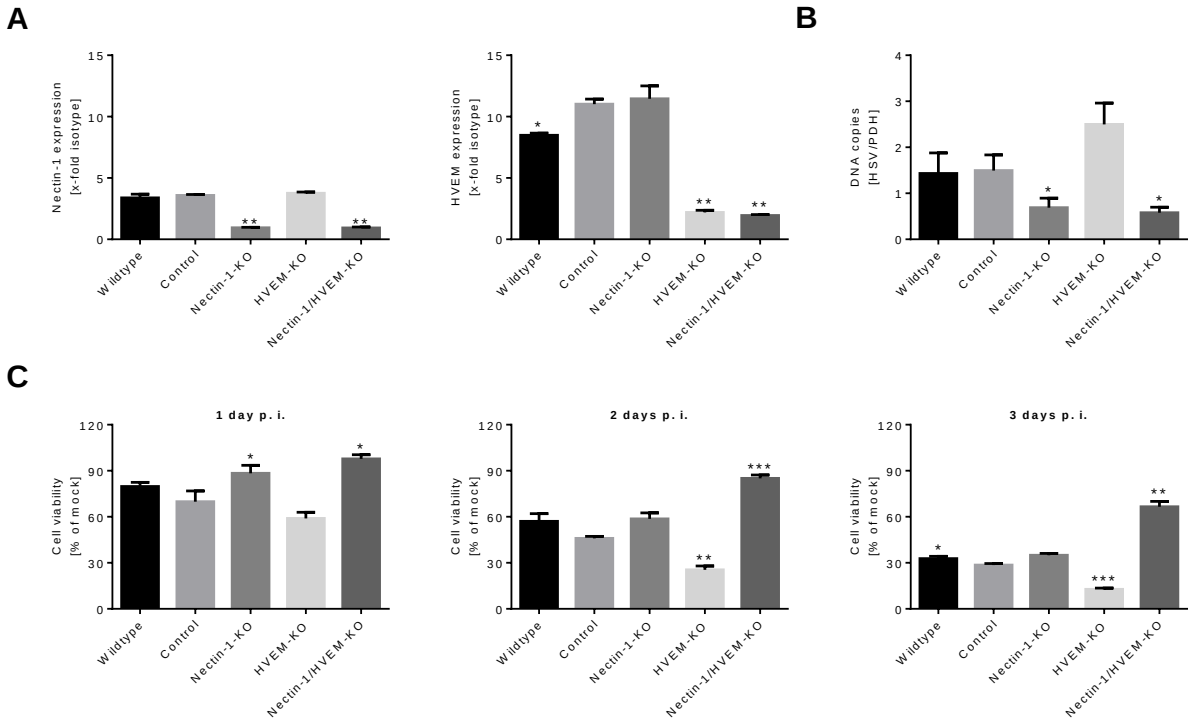

Figure 8: Effect of Nectin-1/HVEM knockout on the entry and oncolytic activity of T-VEC in a melanoma cell line. (A) Expression of Nectin-1 and HVEM after respective knockout(s) (KO) in IGR-37 cells using CRISPR/Cas9 technology. The experiment included cells transduced in parallel with an unrelated sgRNA (control) and untreated IGR-37 cells (wildtype). Flow cytometry data were evaluated with respect to isotype controls and represent mean and standard error of three independent experiments. (B) Amount of HSV-1 DNA in the different cell lines measured 12h after infection with T-VEC (MOI 1) using realtime quantitative PCR. Results were normalized for housekeeping pyruvate dehydrogenase (PDH) DNA and show mean and standard error of five independent experiments. (C) Viability of different cell lines 1, 2, and 3 days post infection (p.i.) with T-VEC. MTT values were normalized for respective values of uninfected cells. Data represent mean and standard error of four independent experiments. Statistics were calculated with respect to control cells using repeated measures one-way ANOVA with Dunnett's correction for multiple comparisons. *p<0.05, **p<0.01, ***p<0.001. Similar data were obtained for the second set of Nectin-1 and HVEM sgRNAs.

The uptake of virions, measured as intracellular HSV-1 DNA at 12 h p.i. using real-time qPCR, was significantly reduced in Nectin-1-KO and Nectin-1-/HVEM-double-KO cells ($p < 0.05$) (Figure 8B), and slightly, although not significantly, increased in HVEM-KO cells. Upon T-VEC

infection, cell viability gradually decreased in HVEM-KO cells, while it was preserved in Nectin-1-KO cells early after infection and Nectin-1-/HVEM-double-KO cells were almost insensitive (Figure 8C). Altogether, entry and oncolytic activity of T-VEC crucially depended on the presence of Nectin-1 on the cell surface, which was more evident with the additional knockout of HVEM.

2.1.4.4 cGAS/STING play a subordinate role for the oncolytic activity of T-VEC

The cGAS-STING pathway reportedly plays an important role in the innate immune defense against herpes viruses via recognition of cytosolic DNA (Ablasser *et al.,* 2013; Sun *et al.,* 2013). The loss of STING function in malignant melanoma predisposed it to oncolytic HSV-1 death (Xia *et al.,* 2016). To evaluate the role of STING and cGAS in our panel of melanoma cell lines, we studied the expression of both molecules using Western blot analysis with respect to the housekeeping protein ß-actin (Figure 9A). In three separate experiments, a broad spectrum of STING and cGAS expression was observed in these cell lines (Figure 9B). In contrast to Nectin-1, neither STING nor cGAS were correlated with the oncolytic activity of T-VEC (Figure 9C). Responder and non-responder cell lines neither differed in the expression of STING nor cGAS (Figure 9D), and ROC curve analyses did not reveal a predictive value for these molecules in our panel of cell lines (Figure 9E).

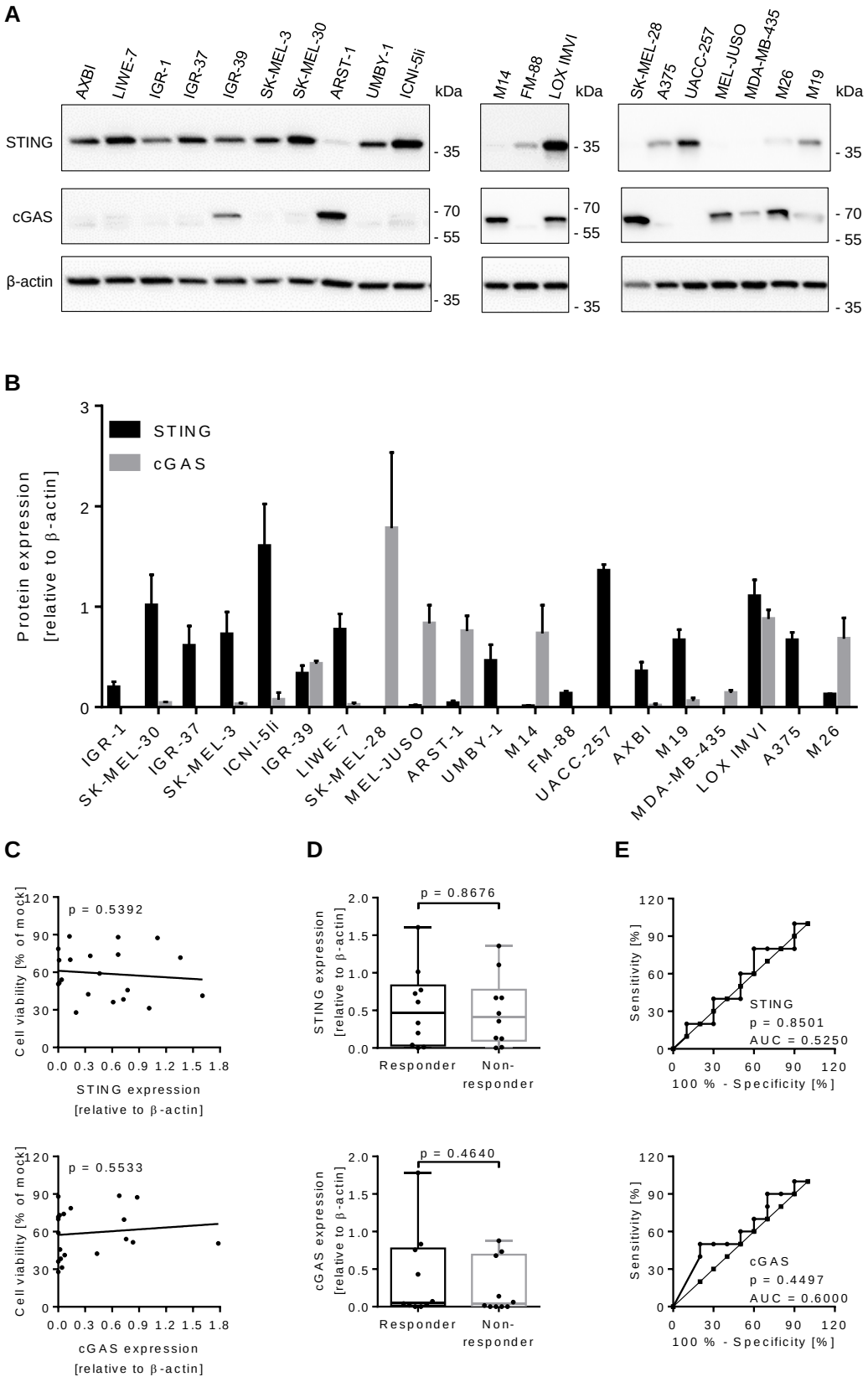

Figure 9: Correlation of the oncolytic activity of T-VEC with the expression of stimulator of interferon genes (STING) and cyclic GMP-AMP synthase (cGAS) in a panel of melanoma cell lines. (A) Western Blot analysis of STING and cGAS with respect to housekeeping protein ß-actin using lysates of 20 melanoma cell lines. (B) Densitometric quantification of STING and cGAS, normalized for ß-actin and shown as the mean and standard error of three independent Western blot experiments. (C)

Spearman correlation coefficient, (D) box plot, and (E) ROC curve analyses of all responder and non-responder cell lines with respect to STING (upper part) and cGAS expression (lower part) and corresponding susceptibility to T-VEC induced cell death. p values for box plots were calculated using the Mann–Whitney test; ROC curves analyzed the area under the curve (AUC).

2.1.4.5 Expression of biomarkers is consistent between different methodological approaches

The results so far showed a predictive value of Nectin-1 expression, as evaluated by flow cytometry, for melanoma cell death upon T-VEC inoculation. In the clinical setting, however, immunohistochemistry rather than flow cytometry is the method of choice to analyze tumor biopsies. To this end, we established Nectin-1, HVEM, STING, and cGAS immunostaining for our panel of 20 melanoma cell lines after embedding them into paraffin. After categorizing the immunohistochemistry staining (Figure S 4A), the inter-individual variability of scoring was assessed (Figure S 4B). Spearman correlation coefficient analysis revealed a significant correlation of Nectin-1 ($p = 0.0063$) and HVEM expression ($p = 0.0117$) in immunohistochemistry and flow cytometry (Figure 10A). STING and cGAS expression in immunohistochemistry and Western blot were also significantly correlated ($p < 0.0001$ and $p = 0.0066$, respectively) (Figure 10B). Nectin-1 expression in immunohistochemistry was significantly correlated with the oncolytic activity of T-VEC ($p = 0.0302$), whereas HVEM, STING, and cGAS failed to show this correlation (Figure 10C). Altogether, data were consistent between flow cytometry, Western blot, and immunohistochemistry.

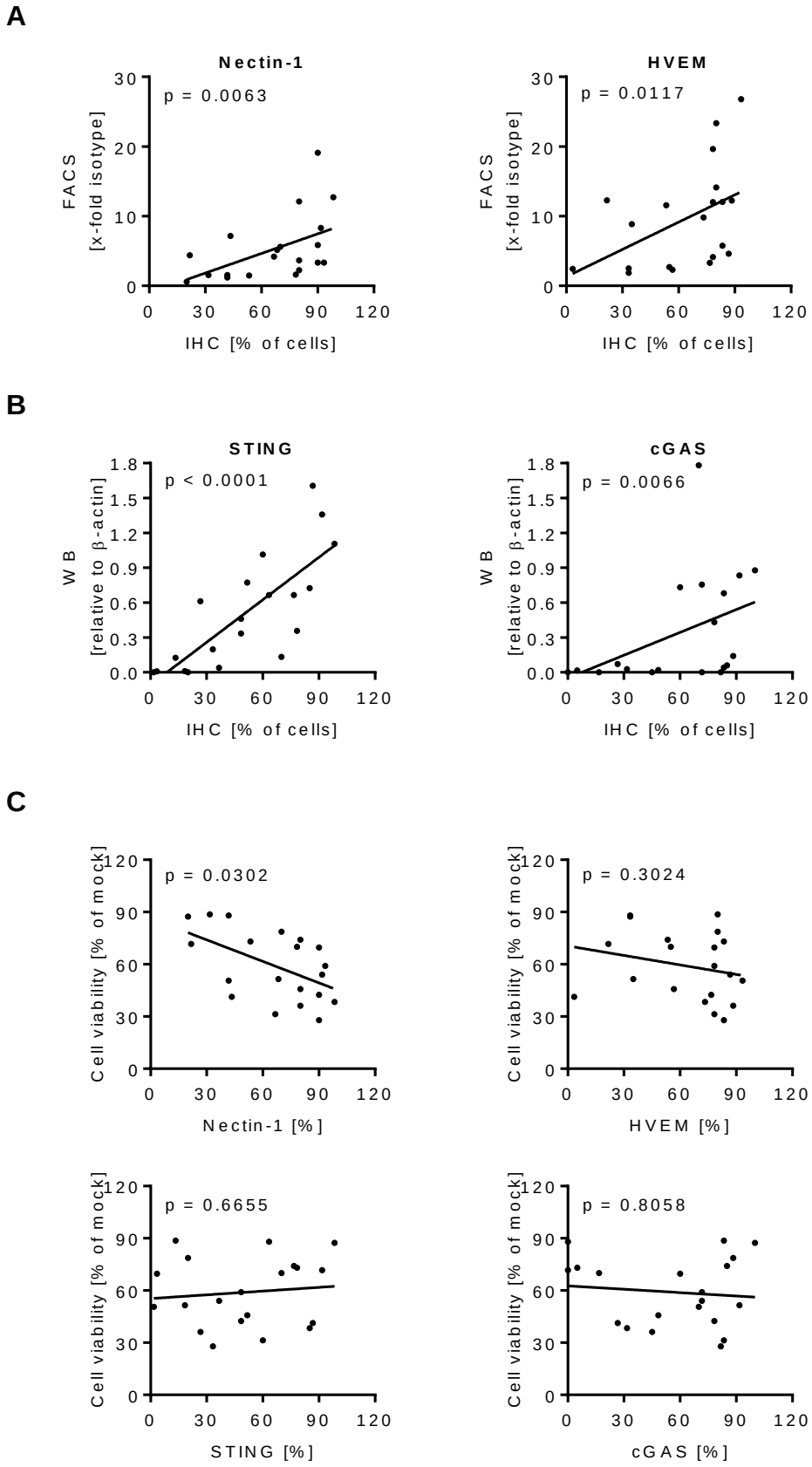

Figure 10: Correlation of biomarkers evaluated by flow cytometry, Western blot, and immunohistochemistry with the oncolytic activity of T-VEC in melanoma cell lines. Spearman correlation coefficient analysis for (A) Nectin-1 and HVEM expression, measured by flow cytometry (FACS) and immunohistochemistry (IHC), (B) STING and cGAS expression, evaluated by Western blot (WB) and immunohistochemistry, and (C) expression of all four biomarkers in immunohistochemistry with the

oncolytic activity of T-VEC in 20 melanoma cell lines. Data shows mean of three independent experiments for each biomarker and MTT assay.

2.1.4.6 60% of melanoma lesions in patients respond to intratumoral T-VEC injection

In order to validate our in vitro findings, we performed a retrospective clinical trial, enrolling 21 patients with biopsies from 35 injectable cutaneous, subcutaneous, or nodal melanoma metastases into our study. Overall, 90% and 10% of the patients had stage IIIB and stage IIIC disease, respectively. A minority of patients (21%) had received prior interferon as adjuvant therapy. Complete baseline characteristics are listed in Table 1. T-VEC was administered intralesionally beginning with a dose of up to 4 mL of 10^6 plaque-forming units/mL followed 3 weeks later with repeated injections of up to 4 mL of 10^8 plaque-forming units/mL every 2 weeks. Injected volume per lesion ranged from 0.1 mL for lesions <0.5 cm to 4.0 mL for lesions >5 cm in longest diameter. Median time to response of lesions responding to injection was 8.6 weeks (range, 5–15 weeks). The clinical response was noted as increase or decrease of the tumor size, calculated as (length x width x thickness)/2 when the optimal anti-tumor effect had been obtained. Before virus inoculation at cycle 1, a diagnostic biopsy was taken from the lesion to be injected. Clinical evaluation and measurement of the lesions were performed at every visit using caliper and ruler, calculating the tumor volume and its change from baseline. The overall response rate (−100% to −30%) was 60.0% (21 of 35 lesions). Complete response (−100%; CR) was achieved in 16 lesions (45.71%) and a partial response (PR), defined as a decrease in size compared to the baseline by at least 30%, in five lesions (14.29%) (Figure 11A). Responder and non-responder lesions differed significantly ($p < 0.0001$) (Figure 11B).

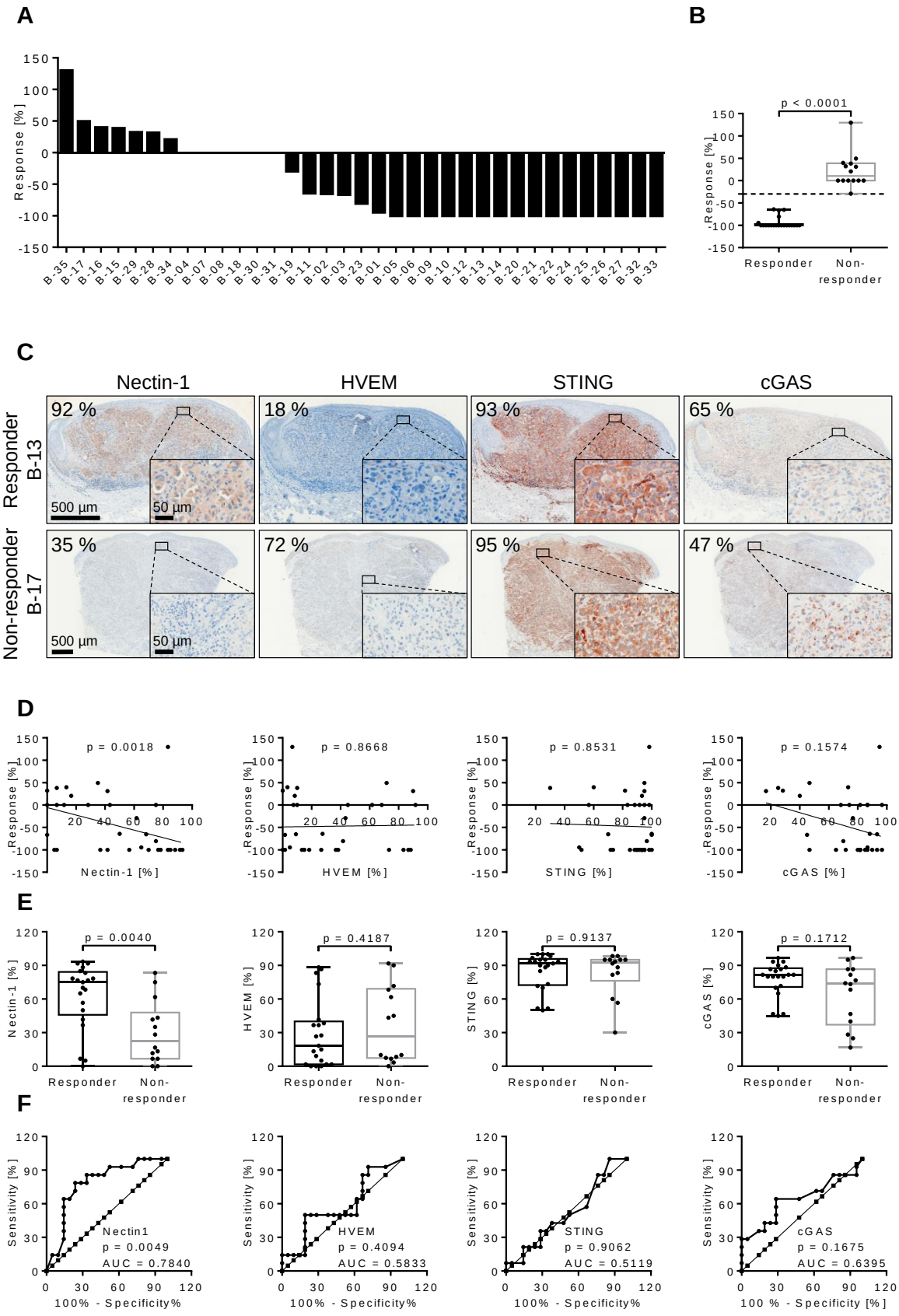

Figure 11: Oncolytic effect of T-VEC upon injection into 35 malignant melanoma lesions. (A) Waterfall plot showing the response rate of each individual lesion as increase or decrease of the tumor volume, calculated as (length × width × thickness)/2 when the maximum anti-tumor effect had been achieved. (B) Based on this criterion, 14 and 21 lesions were respectively categorized as non-responders (+129.89% to −29%) and responders (−30% to −100%). (C) Representative example of Nectin-1, HVEM, STING, and cGAS immunostaining in a melanoma lesion responding (upper panel) or

not responding (lower panel) to intratumoral T-VEC injection. Images provide an overview and details at higher magnification (inserts); corresponding size bars are included. (D) Spearman correlation coefficient analysis of Nectin-1, HVEM, STING, and cGAS immunostaining with the oncolytic activity of T-VEC inoculated into the respective lesion. (E) Box plots (with median, interquartile ranges, minimum, and maximum values) and (F) ROC curve analysis of responder and non-responder lesions with respect to Nectin-1, HVEM, STING, and cGAS immunostaining. p values for box plots were calculated using the Mann–Whitney test; p values for ROC curves analyzed the area under the curve.

2.1.4.7 Oncolytic activity of T-VEC correlates with Nectin-1 expression in vivo

To investigate the possible association between the expression of Nectin-1, HVEM, cGAS, and STING with the response to T-VEC injection in vivo, we analyzed tumor biopsies before treatment with immunohistochemical methods for the expression of these markers. As with the cell lines, six individuals interpreted the immunostaining independently and categorized the respective percentage of stained cells. Figure 11C shows a representative example of Nectin-1, HVEM, STING, and cGAS immunostaining in a responder and a non-responder melanoma lesion. The range of immunostaining for the four biomarkers and the inter-individual variability of scoring is detailed in Figure S 5.

In line with the in vitro data, the Spearman correlation coefficient analysis showed a significant correlation of Nectin-1 expression in immunohistochemistry ($p = 0.0018$) with the response to oncolytic T-VEC treatment in vivo, which was not observed for HVEM, STING, or cGAS (Figure 11D). Correspondingly, expression levels for Nectin-1 were significantly different in responding (CR and PR) versus non-responding tumors (SD and PD) using box plot (Figure 11E) and ROC curve analysis (Figure 11F). Taken together, Nectin-1 expression levels in pretreatment biopsies of cutaneous melanoma metastases significantly predicted the response to T-VEC mediated oncolysis, which paralleled the results obtained with melanoma cell lines.

2.1.5 Discussion

The in vitro data of our study are based on MTT metabolic activity and LDH release of malignant melanoma cell lines 48 h post T-VEC inoculation. The uniform conditions used in our experiments, which allow for a cumulative analysis of cell death over the entire infection period, may not meet the optimal requirements for all 20 melanoma cell lines due to their heterogeneity. In particular, A375 cells have been reported to show a varying response dynamics depending on the time and cell density as well as MOI used for infection (Thomas *et al.,* 2019). Despite these limitations, both the in vitro and in vivo data of our study demonstrated an important predictive role of Nectin-1, a member of the immunoglobulin superfamily, for T-VEC-induced oncolysis of malignant melanoma. Both in cell lines and in melanoma metastases, the degree of Nectin-1 expression significantly correlated with tumor cell regression. Nectin-1 is a known HSV-1 entry receptor (Geraghty *et al.,* 1998), and its relevance for the entry of wildtype HSV-1 into neuronal cells has been shown (Kopp *et al.,* 2009; Karaba *et al.,* 2011). Accordingly, we were able to show that respective knockout cell lines, after inoculation of T-VEC, harbored significantly lower HSV-1 DNA concentrations compared to control cell lines. Our data indicate that Nectin-1 is a key molecule for the entry of oncolytic HSV-1 into malignant melanoma, thus confirming the results obtained in glioblastoma and other malignant tumors using cell lines and a xenograft tumor model (Friedman *et al.,* 2018; Huang *et al.,* 2007; Yu *et al.,* 2007). Along this line, Nectin-1 could be important for the success of oncolytic herpes viruses in other tumor entities (Schuster *et al.,* 2019), which should be evaluated in further studies.

Another well-characterized HSV-1 entry receptor is HVEM (Montgomery *et al.,* 1996), a member of the tumor necrosis factor family, which, similar to Nectin-1, binds to HSV-1 glycoprotein D (Krummenacher *et al.,* 1998). Direct comparison of Nectin-1 and HVEM indicated that the latter was less effective in promoting HSV-1 entry (Krummenacher *et al.,* 2004), which could explain why HVEM was not predictive of T-VEC induced melanoma cell death in our in vitro and in vivo studies. Notably, single HVEM-knockout cells showed an increased amount of intracellular HSV-1 DNA (not significant) and were more sensitive to cell death upon T-VEC inoculation compared to wildtype control. In the absence of HVEM, Nectin-1 seemed to compensate and mediate HSV-1 entry into melanoma cells. This observation is in line with a study that revealed Nectin-1 as the primary receptor for HSV-1 cell entry, whereas HVEM had only a subordinate role (Kopp *et al.,* 2009; Karaba *et al.,* 2011; Petermann & Rahn *et al.,* 2015). In addition, knockout of HVEM could also affect downstream signaling events. In this respect, interaction of glycoprotein D with HVEM was reported to induce TRAF- and RelA-mediated upregulation of pro-survival genes (Sciortino *et al.,* 2008; Cheung *et al.,* 2009), which might be diminished in HVEM-KO cells upon T-VEC infection. Knockout of both Nectin-1 and HVEM efficiently prevented the entry of T-VEC into IGR-37 cells, as indicated by low HSV-1

copy numbers. Hence, double knockout cells were highly resistant to T-VEC-mediated cell death. In this situation, the lack of prosurvival signaling from HVEM may be less relevant, as cell death is not induced in the absence of viral entry. Notably, the reduced viability in the melanoma cell panel upon T-VEC infection did not correlate with the activation of caspase 3/7. These data suggest that T-VEC-induced oncolysis is partially, but not completely, mediated by apoptosis, as has been shown for wildtype HSV-1 infection (Yu & He, 2016). Slight differences in susceptibility of IGR-37 cells to viral oncolysis (Figure 7A and Figure 8C) are attributed to a prolonged cultivation period during the CRISPR process.

The effects of cGAS and STING for viral oncolysis have been analyzed in different studies (Xia *et al.,* 2016; Bommareddy *et al.,* 2019; Queiroz *et al.,* 2019). The pattern recognition receptor cGAS detects cytosolic DNA during viral infection and catalyzes in turn the formation of cyclic-GMP-AMP (cGAMP). Binding of cGAMP to STING results in downstream phosphorylation of transcription factors such as NF-kB and IRF3, which induce the transcription of type I interferons and proinflammatory cytokines as part of an anti-viral defense mechanism (Ma & Damania, 2016). Activation and integrity of the cGAS-STING pathway can therefore affect the efficacy of oncolytic tumor therapy. Indeed, a correlation between STING but not cGAS expression levels and viral oncolysis in melanoma and ovarian cancer cell lines has been reported (Xia *et al.,* 2016; Queiroz *et al.,* 2019). In both studies, a wide range of cGAS/STING expression levels in melanoma cell lines was observed.

Xia et al. demonstrated that oncolytic viral therapy induced pronounced killing in five melanoma cell lines with no or very low STING expression (Xia *et al.,* 2016). Loss of STING was associated with markedly reduced induction of type I interferons as well as increased viral replication. The effect, however, was not limited to STING-negative melanoma, but also occurred in three STING-expressing cell lines (A375, SKMEL2, RPMI7951). Bommareddy et al. showed that CRISPR-mediated STING depletion in the LOX IMVI melanoma cell line resulted in increased killing by the oncolytic virus (Bommareddy *et al.,* 2019).

In our melanoma cell panel, eleven and seven cell lines expressed STING and cGAS, respectively, but only two cell lines were equipped with both molecules (IGR-39, LOX IMVI). This distribution may have contributed to the low impact of STING and cGAS onto the response of our cell lines to T-VEC treatment, because the presence of STING and cGAS is at least the basis for a functioning signaling pathway. In addition, our melanoma panel lacked cell lines harboring different STING levels in combination with high Nectin-1 expression, which would have supported an efficient infection. Thus, Nectin-1 may have played a superior role in this setting and may have masked the more delicate role of STING and cGAS. However, the analysis of different subgroups (Nectin-high and Nectin-low expressing cell lines), did not reveal correlation, most likely due to the low number of cell lines in each group. Taken together, our data indicate that STING affects the oncolytic activity in a subset of melanoma cell lines;

however, additional mechanisms independent of STING may have an impact on T-VEC mediated oncolysis. A further aim of our study was to correlate in vitro data with in vivo findings. For these purposes, we analyzed 35 biopsies of melanoma metastasis before injection with T-VEC. The expression of Nectin-1, HVEM, STING, and cGAS was determined utilizing immunohistochemistry and revealed a significant correlation of Nectin-1 expression with response to therapy. In contrast to the in vitro data, a correlation was also found for cGAS, which was, however, not statistically significant. This may be because environmental factors, e.g., UV exposure and reactive oxygen species (ROS), can potentiate immunorecognition of DNA and thereby trigger the cGAS-STING pathway in vivo (Gehrke *et al.,* 2013). Moreover, protein expression profiles of immortalized melanoma cell lines may not represent the in vivo situation accurately. In fact, melanoma cell lines showed a higher percentage of Nectin-1 and HVEM expression, while cGAS and STING were more prominently expressed in melanoma metastasis (Figure S 6). This abundant expression of both molecules in the biopsies may have contributed to the fact that the STING-cGAS pathway was not a limiting factor in this context. The prediction of the clinical response may profit from combining expression profiles of several biomarkers. For these purposes, a larger panel of cell lines and biopsies from patients treated with T-VEC would be helpful, which will be the focus of future studies.

Biomarkers such as PD-L1 are important tools to guide personalized cancer therapies. Our data demonstrate that baseline expression of Nectin-1 in melanoma metastasis correlates with the response to intralesional T-VEC therapy and can therefore be used as a biomarker. To increase clinical utility, testing of this biomarker should be able to be integrated into routine laboratory workflow. Since IHC is a widely used method for diagnostic purposes and is well established for biomarker assessment, we compared Nectin-1 expression in melanoma cell lines using FACS and IHC. FACS analysis showed superior correlation between Nectin-1 expression and oncolysis compared to IHC. One likely explanation is that FACS measures surface Nectin-1 expression, which is relevant for viral entry, while IHC also stains intracellular protein. However, our IHC staining and scoring protocol was stable and allowed reliable identification of low versus high Nectin-1 expressing tumor biopsies. Importantly, the inter-individual scoring variability between analysts was higher in tissue sections with low Nectin-1 expression. The reproducibility of IHC scoring is known to be more difficult in tumors with faint staining (Brunnström *et al.,* 2017). Overall, our data revealed heterogeneity of Nectin-1 expression in melanoma cell lines as well as in melanoma metastases. Therefore, a robust and reliable protocol for staining and scoring is needed to determine expression levels guiding clinical decision-making. This is especially important since many factors influence IHC results including tissue collection procedures, fixation, section thickness, staining processes, and image analysis.

Altogether, our study revealed Nectin-1 as suitable biomarker for the treatment of melanoma metastases using intratumoral T-VEC application. In seven patients in whom two or more pretreatment biopsies were available, a consistent clinical response occurred across all metastases within an individual patient (Figure S 7), although a notable variation in Nectin-1 expression was observed in one patient (Pat. 17). These data suggest that a single biopsy may be representative for most of the other metastases. In addition, post-treatment biopsies quantifying the intratumoral immune infiltrate may be helpful to predict systemic treatment response via induction of adaptive immunity. What level of Nectin-1 expression is actually required for tumor regression remains an open question. In our study, 35.84% of Nectin-1 positive cells reflected the threshold with the highest likelihood ratio, correctly predicting treatment response and failure in 78.3% and 75.0% of cases, respectively. Further prospective studies are needed to determine the clinical threshold of Nectin-1 expression and additional parameters, which will allow the development of optimized personalized therapies for oncolytic herpes viruses in melanoma and other solid malignancies.

2.1.6 Supplementary materials

Supplementary Figure S 1

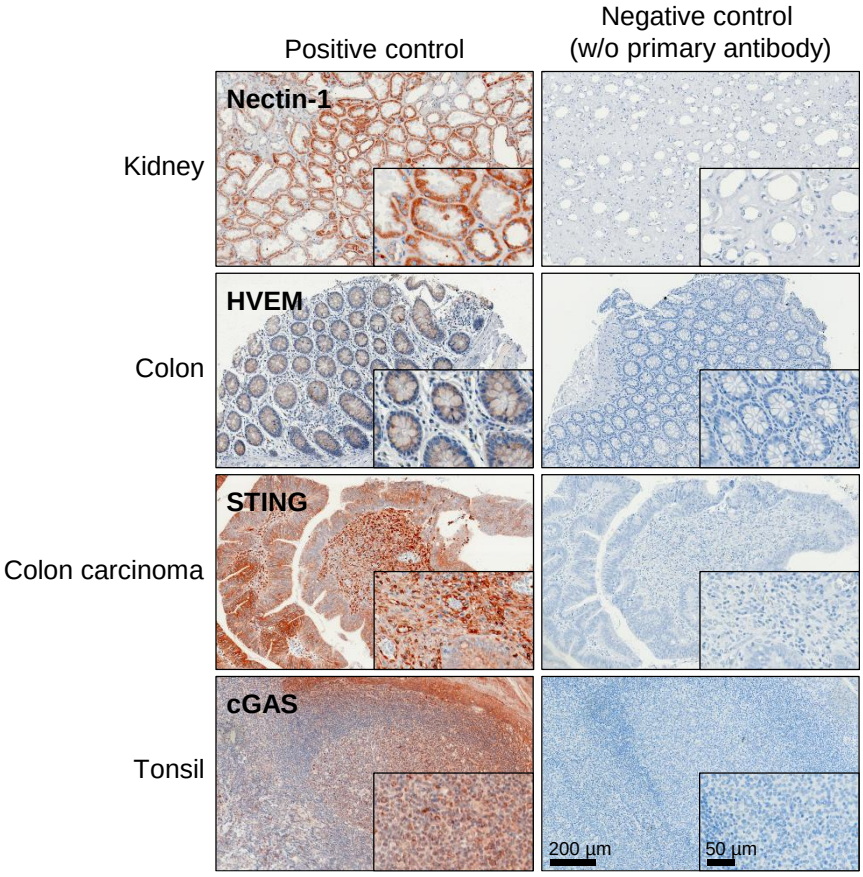

Figure S 1: Optimization of immunohistochemistry staining protocols for Nectin-1, HVEM, STING, and cGAS. Organ slices containing positive control tissues (kidney, colon, colon carcinoma and tonsil) were stained with the respective antibodies and probed with peroxidase-conjugated anti-rabbit or anti-mouse IgG. Negative controls were stained with secondary antibodies only. Images with corresponding size bars show an overview of immunohistochemistry staining and details at higher magnification (insert).

Supplementary Figure S 2

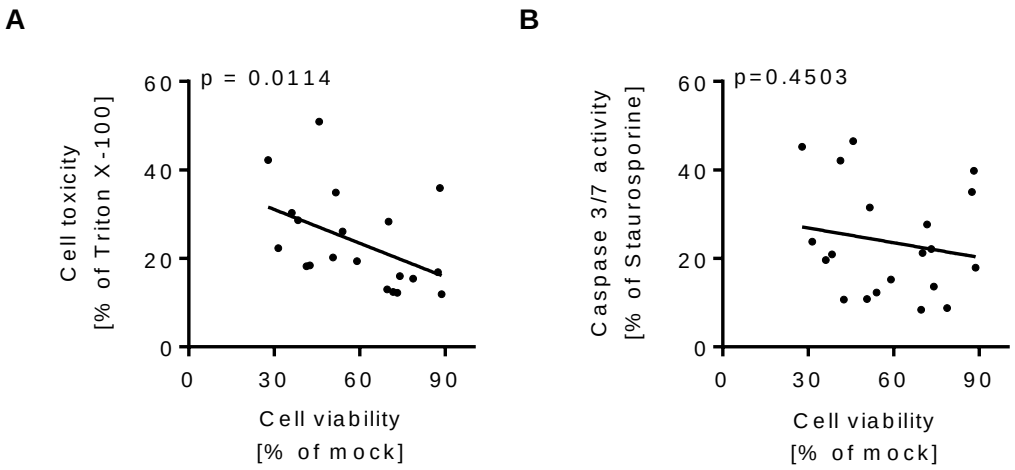

Figure S 2: Correlation analysis of cell viability with toxicity and Caspase 3/7 activity in a panel of 20 melanoma cell lines after T-VEC infection (MOI 1). Cell viability as measured by MTT viability assay was correlated with (A) toxicity as evaluated by the release of lactate dehydrogenase (LDH) in infected cells and (B) caspase 3/7 activity, as described in the Materials and Methods section. Spearman correlation coefficient analysis was performed comparing the mean of two separate experiments for LDH and caspase 3/7 activity assays with the mean of three separate experiments using MTT viability assay.

Supplementary Figure S 3

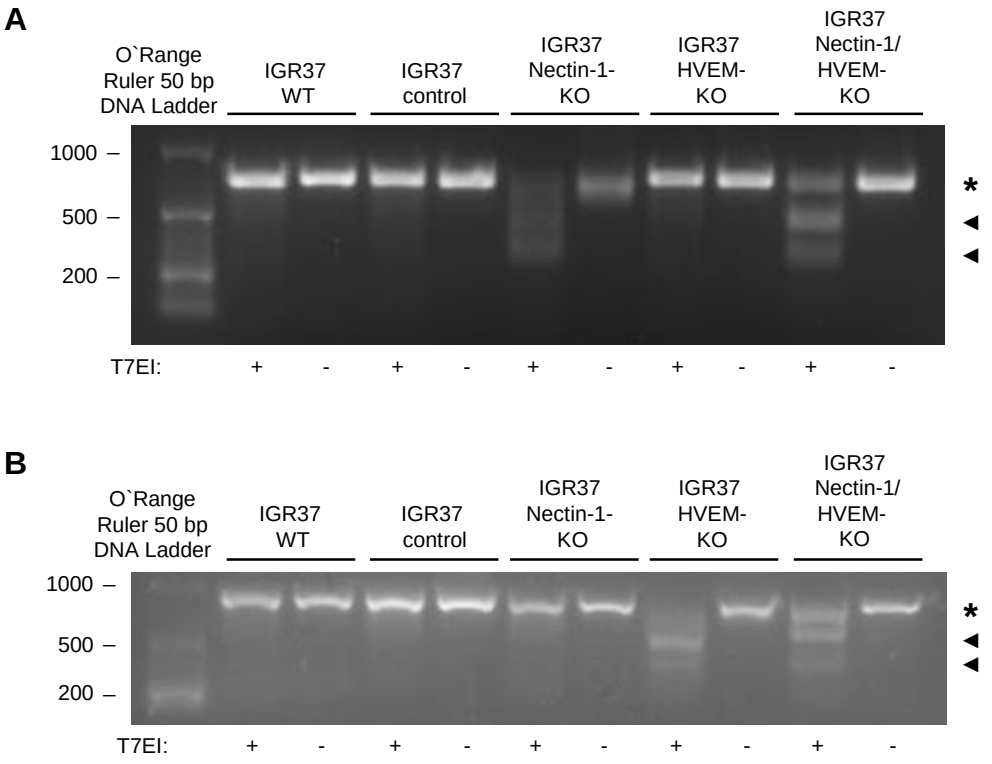

Figure S 3: Evaluation of CRISPR/Cas9 efficiency in different knockout cell lines using T7 endonuclease I (T7EI) assay. Genomic DNA was prepared from the indicated cell lines to amplify the regions flanking the CRISPR sites for either (A) Nectin-1 or (B) HVEM and tested for CRISPR/Cas9-induced mutations by T7EI digestion where indicated. T7EI cleavage products were analyzed by agarose gel electrophoresis. Amplicons are marked by an asterisk, T7E1 cleavage products by arrowheads.

Supplementary Figure S 4

A

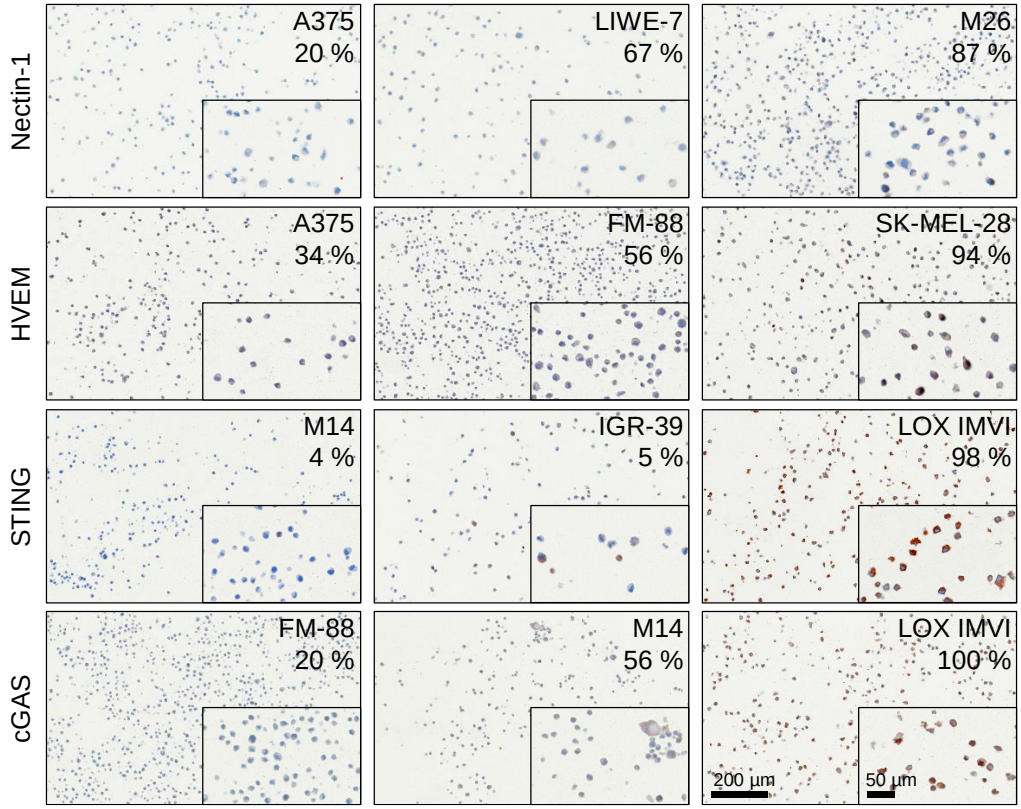

B

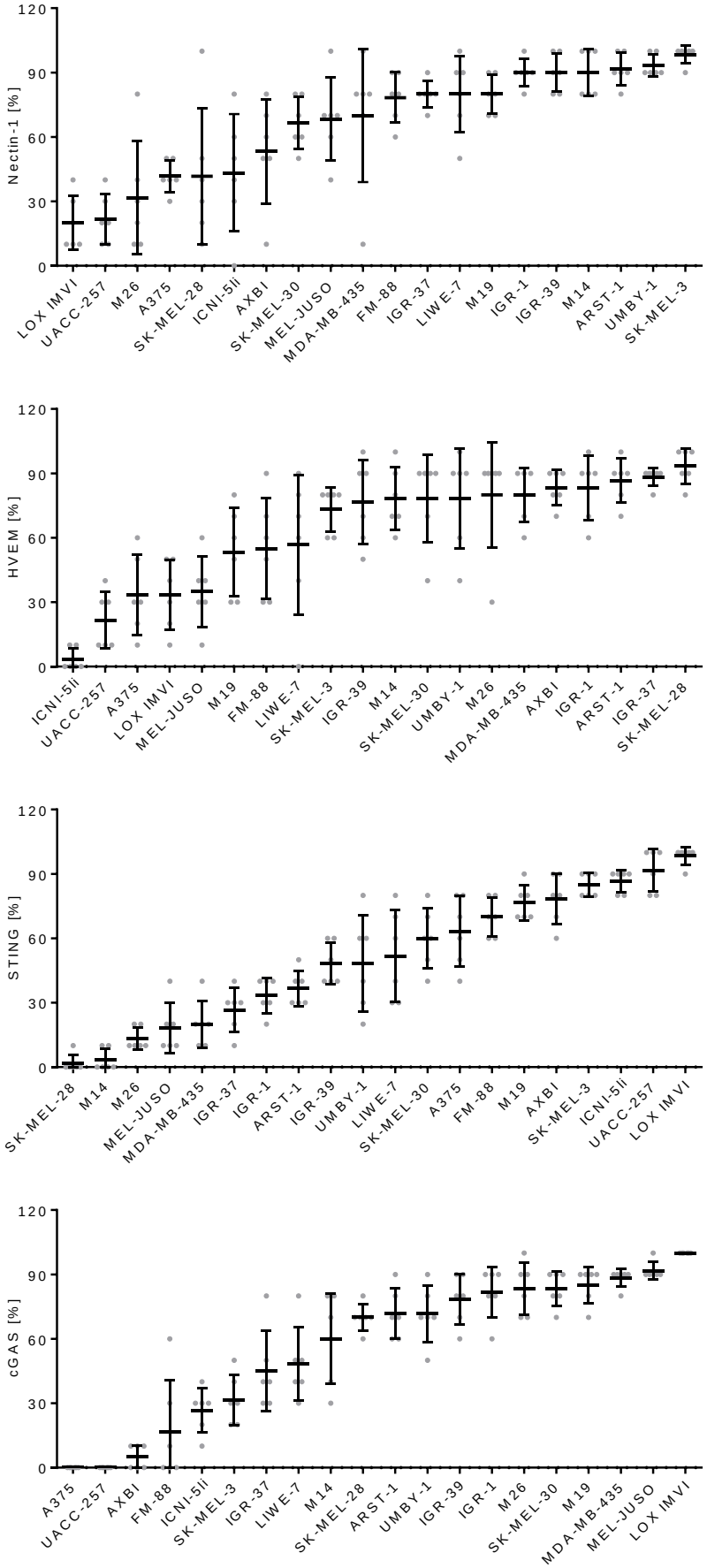
Nectin-1 [%]
120
90
60
30
0
LOX IMVI
UACC-257
M26
A375
SK-MEL-28
ICNI-5ii
AXBI
SK-MEL-30
MEL-JUSO
MDA-MB-435
FM-88
IGR-37
LIWE-7
M19
IGR-1
IGR-39
M14
ARST-1
UMBY-1
SK-MEL-3
HVEM [%]
120
90
60
30
0
ICNI-5ii
UACC-257
A375
LOX IMVI
MEL-JUSO
M19
FM-88
LIWE-7
SK-MEL-3
IGR-39
M14
SK-MEL-30
UMBY-1
M26
MDA-MB-435
AXBI
IGR-1
ARST-1
IGR-37
SK-MEL-28
STING [%]
120
90
60
30
0
SK-MEL-28
M14
M26
MEL-JUSO
MDA-MB-435
IGR-37
IGR-1
ARST-1
IGR-39
UMBY-1
LIWE-7
SK-MEL-30
A375
FM-88
M19
AXBI
SK-MEL-3
ICNI-5ii
UACC-257
LOX IMVI
cGAS [%]
120
90
60
30
0
A375
UACC-257
AXBI
FM-88
ICNI-5ii
SK-MEL-3
IGR-37
LIWE-7
M14
SK-MEL-28
ARST-1
UMBY-1
IGR-39
IGR-1
M26
SK-MEL-30
M19
MDA-MB-435
MEL-JUSO
LOX IMVI

Figure S 4: Evaluation of Nectin-1, HVEM, STING, and cGAS immunohistochemistry in melanoma cell lines. (A) Paraffin-embedded melanoma cell lines were stained with respective antibodies and peroxidase-conjugated anti-rabbit or anti-mouse IgG, as outlined in the Methods section. Images with corresponding size bars show an overview and details at higher magnification (inserts). Six individuals classified the percentage of stained cells into 11 categories (0%, 1-10%, …, 91-100%); the mean value is given. (B) Variability of scoring showing mean and standard deviation plus minimum and maximum for each lesion, ranked with ascending positivity for each marker.

Supplementary Figure S 5

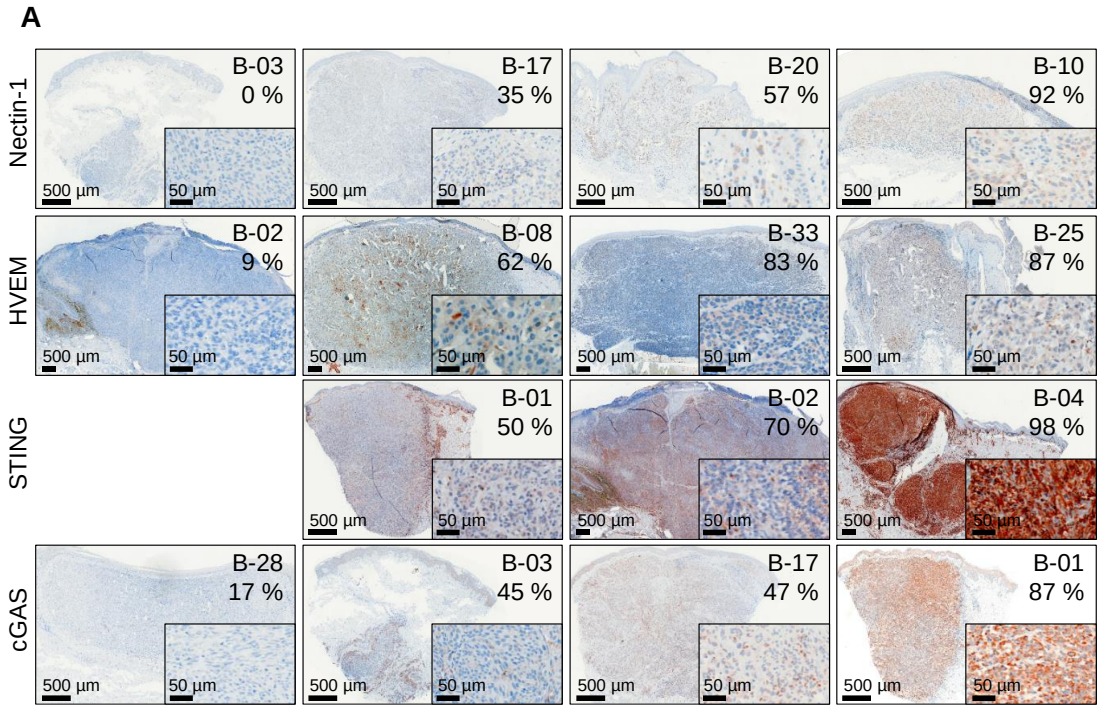

B

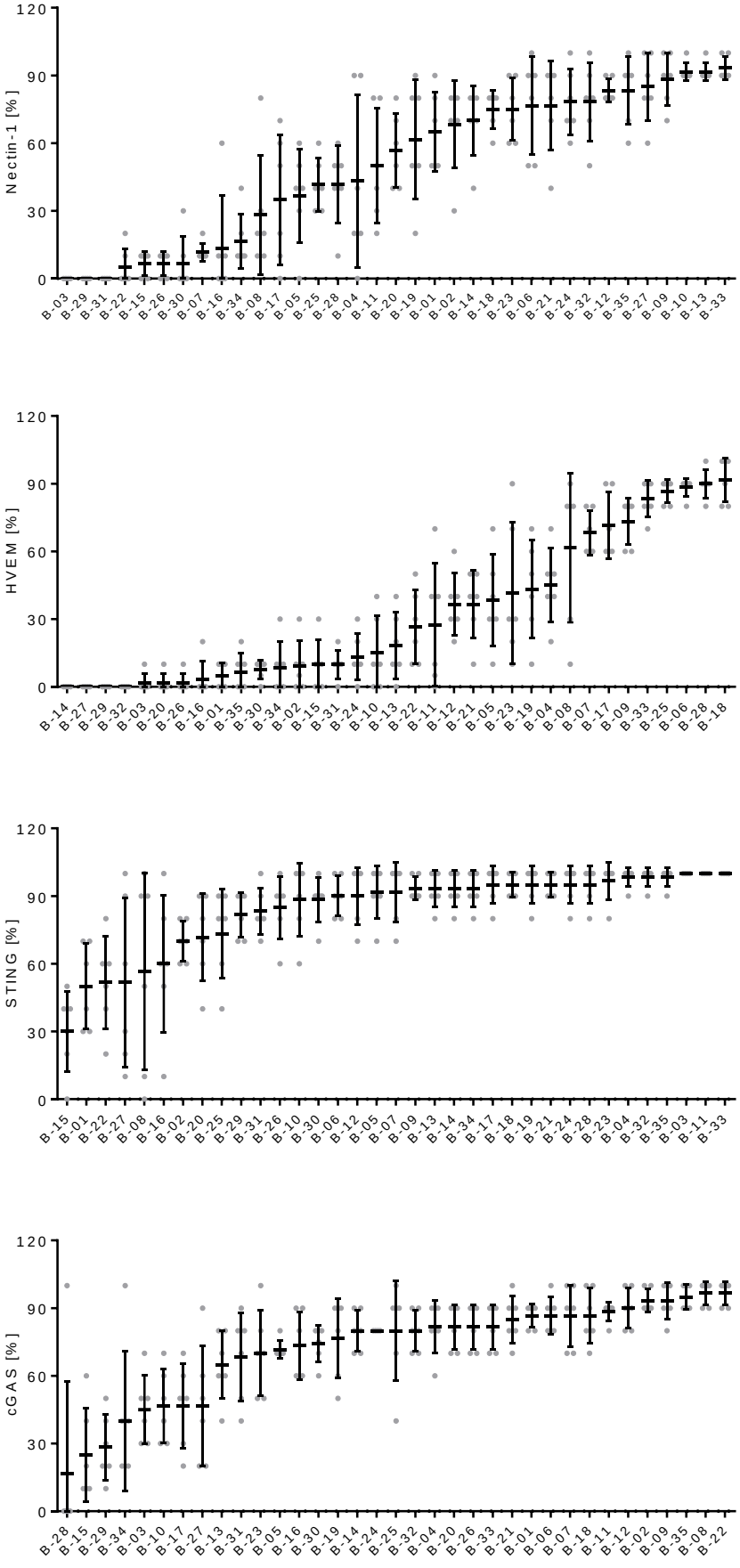
Nectin-1 [%]
120
90
60
30
0
B-03 B-29 B-31 B-22 B-15 B-26 B-30 B-07 B-16 B-34 B-08 B-17 B-05 B-25 B-28 B-04 B-11 B-20 B-19 B-01 B-02 B-14 B-18 B-23 B-06 B-21 B-24 B-32 B-12 B-35 B-27 B-09 B-10 B-13 B-33
HVEM [%]
120
90
60
30
0
B-14 B-27 B-29 B-32 B-03 B-20 B-26 B-16 B-01 B-35 B-30 B-34 B-02 B-15 B-31 B-24 B-10 B-13 B-22 B-11 B-12 B-21 B-05 B-23 B-19 B-04 B-08 B-07 B-17 B-09 B-33 B-25 B-06 B-28 B-18
STING [%]
120
90
60
30
0
B-15 B-01 B-22 B-27 B-08 B-16 B-02 B-20 B-25 B-29 B-31 B-26 B-10 B-30 B-06 B-12 B-05 B-07 B-09 B-13 B-14 B-34 B-17 B-18 B-19 B-21 B-24 B-28 B-23 B-04 B-32 B-35 B-03 B-11 B-33
cGAS [%]
120
90
60
30
0
B-28 B-15 B-29 B-34 B-03 B-10 B-17 B-27 B-13 B-31 B-23 B-05 B-16 B-30 B-19 B-14 B-24 B-25 B-32 B-04 B-20 B-26 B-33 B-21 B-01 B-06 B-07 B-18 B-11 B-12 B-02 B-09 B-35 B-08 B-22

Figure S 5: Evaluation of Nectin-1, HVEM, STING, and cGAS immunohistochemistry in biopsies from melanoma lesions. (A) Range of positivity for the four biomarkers in pretreatment biopsies stained with respective antibodies and peroxidase-conjugated anti-rabbit or anti-mouse IgG, as outlined in the Methods section. Images with corresponding size bars present an overview and details at higher magnification (inserts). (B) Evaluation of the immunostaining by six independent individuals, who categorized the percentage of stained cells for each marker (0%, 1-10%, …, 91-100%). Data show mean and standard deviation plus minimum and maximum for each lesion, ranked with ascending positivity for each marker.

Supplementary Figure S 6

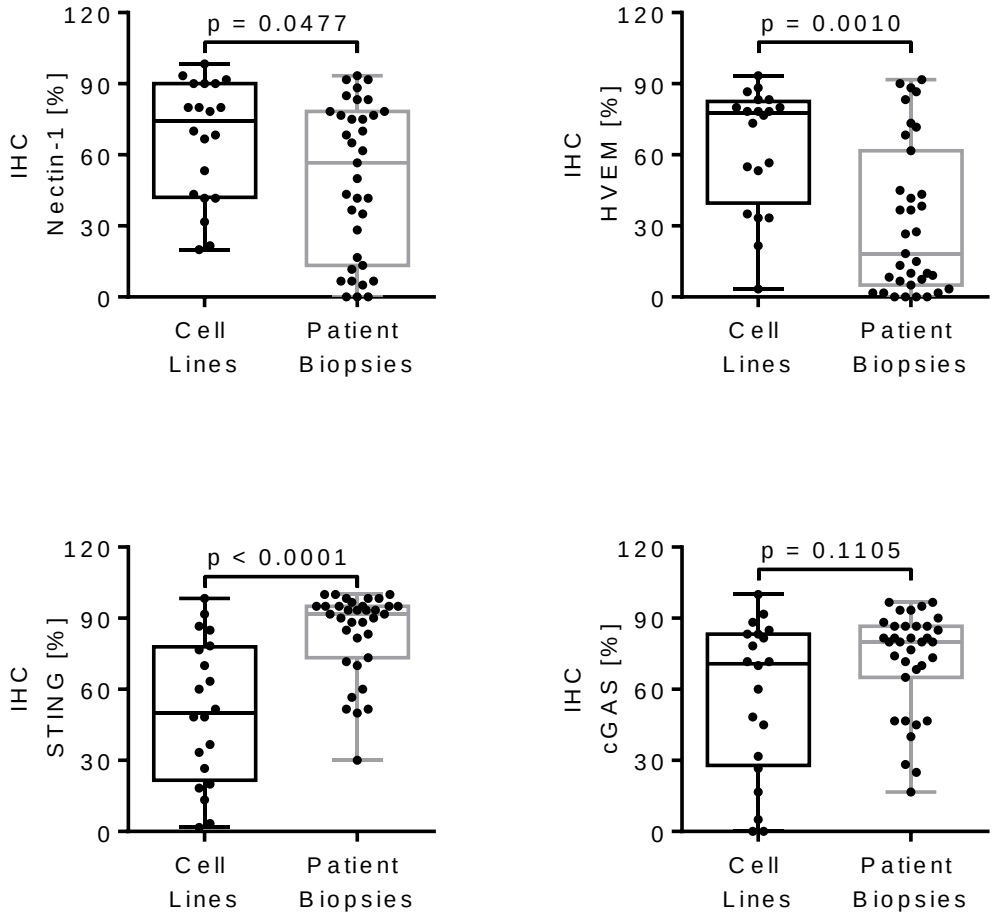

Figure S 6: Comparison of Nectin-1, HVEM, STING, and cGAS expression levels in melanoma cell lines and melanoma metastasis. Range of positivity (%) for the four biomarkers after staining of paraffin-embedded melanoma cell lines and pretreatment biopsies using immunohistochemistry (IHC) as outlined in the Methods section. Box plots show median and interquartile ranges in addition to minimum and maximum values; statistics was calculated using the Mann-Whitney test.

Supplementary Figure S 7

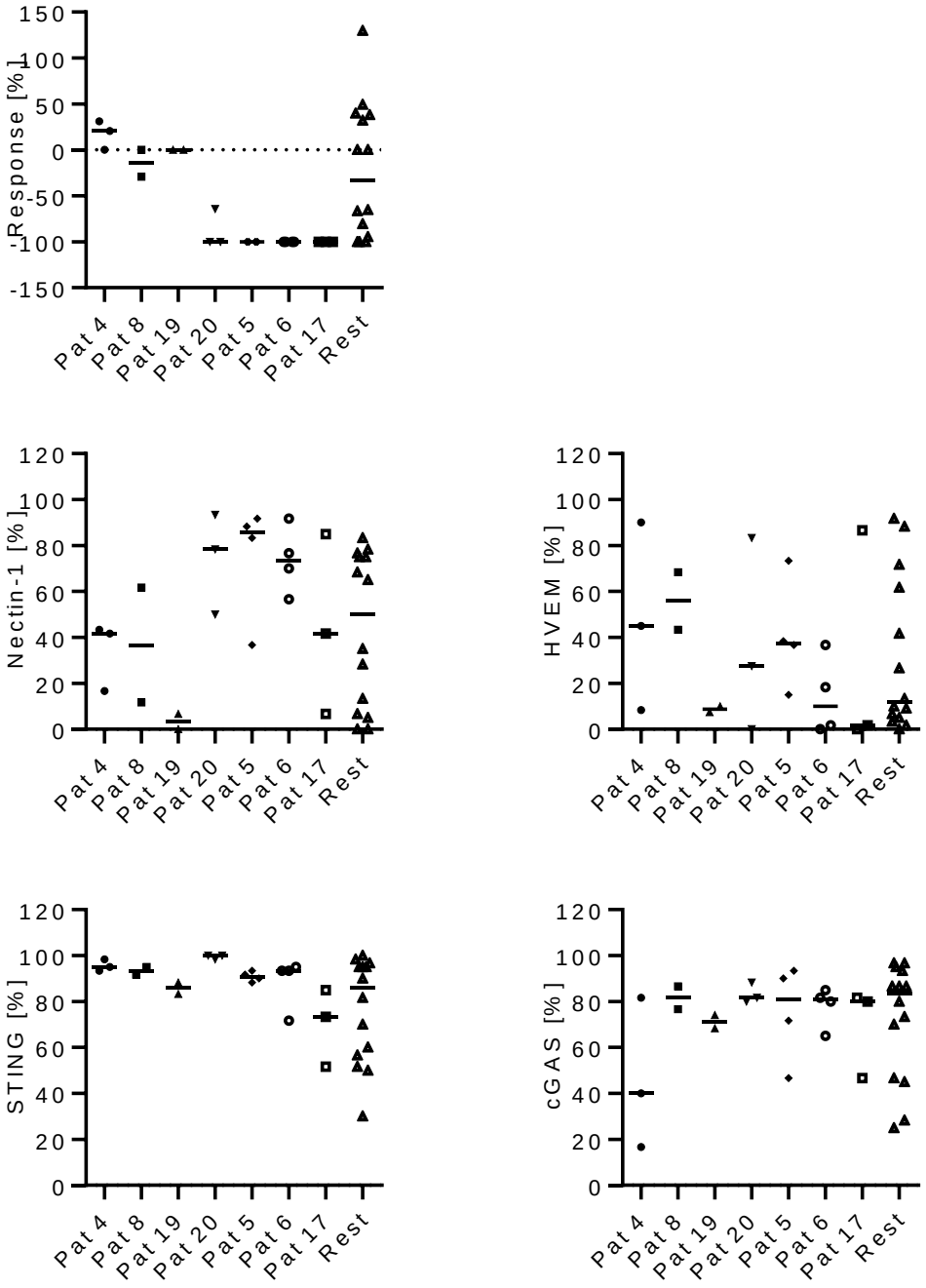

Figure S 7: Clinical response to T-VEC injection and expression levels of biomarkers in patients with two or more biopsies before treatment. The symbols represent metastases of the individual patients, showing the degree of tumor regression upon T-VEC injection and the percentage (%) of cells expressing Nectin-1, HVEM, STING, and cGAS. Horizontal bars represent median values.

2.2 Expression of the plasma membrane citrate carrier (pmCiC) in human cancerous tissues – correlation with tumor aggressiveness

Summary:

The focus of this chapter is the expression of the pmCiC in various human cancer tissues and its correlation with tumor aggressiveness. The study investigates pmCiC levels across different cancer types, emphasizing its potential role as a prognostic marker. Results indicate that higher pmCiC expression correlates with increased tumor aggressiveness and metastatic potential, suggesting that pmCiC could be a valuable marker for predicting cancer progression.

Objective addressed:

Investigation of pmCiC as a prognostic marker for the aggressiveness of various tumor types.

Expression of the plasma membrane citrate carrier (pmCiC) in human cancerous tissues – correlation with tumor aggressiveness

Barbara Schwertner[1,†,*], George Dahdal[1,†], Wolfgang Jagla[2], Luis Grossmann[3], Konstantin Drexler[1], Michael P. Krahn[4], Katja Evert[5], Mark Berneburg[1], Sebastian Haferkamp[1], Christine Ziegler[3], Eric K. Parkinson[6], Grit Zahn[7], Maria E. Mycielska[3, ~] and Andreas Gaumann[2,*]

1: Department of Dermatology, University Hospital Regensburg, Regensburg, Germany.

2: Institute of Pathology Kaufbeuren-Ravensburg, Kaufbeuren, Germany.

3: Department of Structural Biology, Institute of Biophysics and Physical Biochemistry, University of Regensburg, Regensburg, Germany.

4: Medical Cell Biology, Internal Medicine D, University Hospital Münster, Münster, Germany.

5: Institute of Pathology, University of Regensburg, Regensburg, Germany.

6: Centre for Oral Immunobiology and Regenerative Medicine, Institute of Dentistry, Barts and the London School of Medicine and Dentistry, Queen Mary University of London, London E1 2AD, UK.

7: Eternygen GmbH, Berlin, Germany.

~: MetaSMIte, Sp. z o.o. Krakow, Poland (present address).

*: Correspondence: Andreas.Gaumann@pathologie-kaufbeuren.de and

Barbara.schwertner@ukr.de

†: These authors contributed equally to this work and share first authorship

Manuscript information:

Frontiers in Cell and Developmental Biology Cancer Cell Biology. 2024 Jul 03; 12:1308135.

Received 5 October 2023

Accepted 17 June 2024

Doi: 10.3389/fcell.2024.1308135

2.2.1 Abstract

We have recently shown that cancer cells of various origins take up extracellular citrate through the plasma membrane citrate carrier (pmCiC), a specific plasma membrane citrate transporter. Extracellular citrate is required to support cancer cell metabolism, in particular fatty acid synthesis, mitochondrial activity, protein synthesis and histone acetylation. In addition, cancer cells tend to acquire a metastatic phenotype in the presence of extracellular citrate. Our recent study also showed that cancer-associated stromal cells synthesise and release citrate and that this process is controlled by cancer cells. In the present study, we evaluated the expression of pmCiC, fibroblast activation protein-α (FAP) and the angiogenesis marker cluster of differentiation 31 (CD31) in human cancer tissues of different origins. In the cohort studied, we found no correlation between disease stage and the expression of FAP or CD31. However, we have identified a clear correlation between pmCiC expression in cancer cells and cancer-associated stroma with tumour stage. It can be concluded that pmCiC is increased in cancer cells and in cancer-supporting cells in the tumour microenvironment at the later stages of cancer development, particularly at the metastatic sites. Therefore, pmCiC expression has the potential to serve as a prognostic marker, although further studies are needed.

Keywords: biomarker, cancer, citrate, tumour microenvironment, plasma membrane citrate carrier (pmCiC)

2.2.2 Introduction

Cancer cells require increased metabolism to meet the demands of rapid proliferation and metastatic activity (Warburg, 1925; Pascale *et al.,* 2020). In order to do this, these cells need to employ specific metabolic pathways and supply them with appropriate metabolites (Romero-Garcia *et al.,* 2011). One of the key substrates is citrate, which is considered the central metabolite in cancer cells (Icard *et al.,* 2021). Citrate is a Krebs cycle intermediate and the primary substrate for fatty acid synthesis, a hallmark of cancer (Röhrig & Schulze, 2016). Citrate is normally synthesized intracellularly in the mitochondrial cycle in both, cancer and normal cells. However, cancer cells require excess citrate for cytosolic fatty acid synthesis, likely from the reverse Krebs cycle (Parkinson *et al.,* 2021; Metallo *et al.,* 2011). Cancer cells can also take up citrate from the extracellular space via the plasma membrane citrate transporter pmCiC [UniProt: D9HTE9, GenBank accession number: HM037273.1, NCBI Reference Sequences: NP_001243463.1 (protein), NM_001256534.2 (nucleotide)], which belongs to the SLC25 family (Mycielska *et al.,* 2018). The pmCiC is a variant of the mitochondrial citrate carrier (mCiC) with a different start codon (Mazurek *et al.,* 2010). The two transporters have individual first exons, but the rest of the sequence is identical (Mazurek *et al.,* 2010). It already has been shown that pmCiC is expressed in human cancer tissues and that the transporter is increasingly present at the invasion front as well as at metastatic sites (Mycielska *et al.,* 2018; Drexler *et al.,* 2021). Cancer cells can take up extracellular citrate from the blood, but elevated levels are also found in some organs such as the liver, bone or brain (Parkinson *et al.,* 2021). Unfortunately, not much is known about citrate levels in specific human organs other than the prostate and brain, and even less is known about citrate levels in cancerous tissues (Parkinson *et al.,* 2021). Our previous study showed that cancer cells deprived of extracellular citrate increased the expression of pmCiC in cancer-associated fibroblasts and this caused an increase in citrate export from these cells (Drexler *et al.,* 2021). Recently, it has become clear that stromal support is crucial to promote cancer progression and sustain the process of metastasis (Xu *et al.,* 2022; Lee *et al.,* 2023). In particular, the tumour microenvironment has been shown to provide cancer cells with the necessary metabolites through the formation of new blood vessels as well as metabolic substrates released by cancer-associated cells (Eisenberg *et al.,* 2020; Chen *et al.,* 2021). The cancer-associated stroma has also been shown to release growth factors and modulate the immune response (Nishida, 2021; Chen *et al.,* 2023). Tumour-associated macrophages play an important role in the cancer microenvironment. They are known to support tumour progression by establishing infrastructure and increasing the release of inflammatory factors (Zhou *et al.,* 2019; Maller *et al.,* 2021). Citrate uptake by cancer cells has been shown to support their metabolism (Mycielska *et al.,* 2018). In particular, uptake of extracellular citrate decreased mitochondrial activity, reactive oxygen species synthesis and significantly reduced glucose uptake in human prostate cancer cells (Mycielska *et al.,* 2018). Further studies showed that

extracellular citrate enhanced the metastatic properties of cancer cells in vitro and in vivo (Drexler *et al.,* 2022). Consistently, administration of gluconate, a specific blocker of pmCiC, reduced subcutaneous pancreatic tumour growth and metastatic spread in mice, as well as tumour growth and angiogenesis of Merkel cell carcinoma in the chorioallantoic membrane (CAM) assay (Drexler *et al.,* 2021; Drexler *et al.,* 2022). Daily administration of gluconate also reduced stromal transformation and increased tumour immune infiltration in mice (Drexler *et al.,* 2022).

In the present study, we investigated whether pmCiC expression is associated with increased disease aggressiveness of cancer and can serve as a prognostic marker together with pmCiC expression in the stroma and blood vessels.

2.2.3 Materials and Methods

Biopsies

The study included ninety-two patients with human gastrointestinal (20), lung (39), prostate (14) and urothelial (19) cancers. For each primary tumour (stage IV), the associated metastasis, if present, was also examined. This results in a maximum total number of 29 metastases. The tissues were retrospectively analyzed by immunohistochemistry. In some cases, it was not possible to perform and evaluate all the stainings for each biopsy because there was not enough material available. Accordingly, the number of stained sections varies depending on the antibody and the evaluation. One patient biopsy was excluded from the study because of missing information about the entity. The ethical commission of the Faculty for Medicine, University of Regensburg (14-101-0263), approved the study.

Immunohistochemistry (IHC)

Patient biopsies were fixed with buffered formalin and embedded in paraffin according to standard procedures (Canene-Adams, 2013). Samples were cut into 2 µm thick slices. Slices were deparaffinized with xylene (Merck, Darmstadt, Germany) and rehydrated with ethanol (2 × 100% ethanol, 2 × 95% ethanol, 2 × 70% ethanol. Each step 5 min).

Immunohistochemical staining was performed with the primary antibodies anti-pmCiC (Mazurek et al., 2010; GenScript USA Inc., N-Terminal peptide of protein, Antigen Sequence CYDEVVKLLNKVWKTD, Host species: Rabbit, concentration 9.259 mg/mL, dilution for IHC 1:2200), anti-FAP (Abcam, ab240989, Anti-Fibroblast activation protein, alpha antibody [SP325] - BSA and Azide free, clone SP325, host species: rabbit, monoclonal; concentration 1.023 mg/mL, dilution for IHC 1:100, lot number GR3392926-3) and anti-CD31 [Zytomed Systems, MSK091-05 (0.5 mL concentrate), Mouse anti-CD31 (PECAM-1), clone JC70, host species: mouse, monoclonal, concentration 15.3 µg/mL, dilution for IHC 1:300, lot number A0479]. All primary antibodies used were from the same batch. The secondary antibodies used were included in the kits used for IHC (see below).

For pmCiC and FAP staining, the kit ZytoChem Plus HRP-Kit Rabbit (Zytomed/Biozol, Eching, Germany) was used, performing the protocol according to the manufacturer's instructions. Epitope retrieval was performed with HIER Citrate Buffer pH6 (Zytomed) for anti-pmCiC and with HIER TRIS-EDTA Buffer pH 8.0 (Zytomed) for anti-FAP. Both buffers were heated to 90°C before the sections were steamed for 20 min. Sections were stained using AEC+ High-Sensitivity Substrate Chromogen Ready-to-Use (Dako/Agilent Technologies, Hamburg, Germany) and counterstained using hematoxylin (Carl Roth, Karlsruhe, Germany).

For CD31 staining, the kit ZytoChem Plus (AP) Polymer Kit (Zytomed/Biozol) was used, performing the protocol according to the manufacturer's instructions. After the retrieval step sections were rinsed in cold water and PBS buffer. Then primary antibody was applied for 45

min at room temperature (RT). After a washing step, blocking buffer was applied for 30 min at RT. Then another washing step was done before antibody detection was induced applying the AP Polymer for 30 min at RT. Finally, sections were stained with the chromogen substrate alkaline phosphatase for 30 min at RT and counterstained with hematoxylin (Carl Roth).

Evaluation of immunohistochemical staining

All sections were scanned using a slide scanner (Pannoramic Scan from 3DHISTECHTM). Scanning was performed with a × 20 objective (Micrometer/pixel X: 0.242535; Micrometer/pixel Y: 0.242647). The scans were analyzed on the computer using the free software “CaseViewer” from 3DHistech (https://www.3dhistech.com/solutions/caseviewer/). Complete sections were analysed. All samples were scored blindly.

For the CD31 analysis, the areas of highest vascular density (hot spots) were identified on the entire sections by an experienced pathologist and up to five of these hot spots per section were then analysed/quantified. Snapshots were taken at virtual ×20 magnification (corresponding to the ×20 magnification on the microscope) for evaluation. Positive vessels were counted manually according to the international consensus for the evaluation of angiogenesis (Vermeulen *et al.,* 2002). For each CD31 staining, five different sections were evaluated on the microscope at ×20 magnification using the hot spot method. The mean value was then calculated (from the up to five hot spots), providing the CD31 value for further analyses. Staining of pmCiC in blood vessels was analyzed by defining no pmCiC staining in vessels as 0 and detectable staining in vessels as 1.

A semi-quantitative assessment method called “histochemical score” (H-score) was used to evaluate the pmCiC and FAP stainings. We quantified the intensity and the extent of staining within tissue samples. Staining intensity was graded on a scale of 0–3, where 0 indicates no staining, 1 indicates weak staining, 2 indicates moderate staining, and 3 indicates strong staining. The extent of staining was evaluated by determining the percentage of positively stained cells within the sample, represented as a percentage ranging from 0% to 100% (in increments of 10). Intensity of staining and percentage were multiplied to generate the score of 300. A score 300 equal to 300 represents the highest possible score. An experienced pathologist carried out the IHC evaluation.

Statistics

Statistical analyses were performed using GraphPad Prism v. 8.4.2 (GraphPad Software Inc., San Diego, CA, United States). The p values for comparing groups were calculated using the Mann-Whitney test. Box plots show median and interquartile ranges in addition to minimum and maximum values. The line in the middle of the box represents the median. Correlations were evaluated using the Spearman’s rank correlation coefficient analysis. Two-tailed p-values ≤0.05 were considered statistically significant. A simple linear regression line has been

included in the figures showing correlations to provide an additional visual aid to help understand the data. No statistical conclusions can be drawn from these linear regression lines.

2.2.4 Results

2.2.4.1 Expression of pmCiC, CD31, and FAP in primary tumors versus metastasis and their correlation with different tumor stages

We have recently found that pmCiC expression may play a role in the process of metastasis (Drexler *et al.,* 2021), and therefore we wanted to investigate whether the level of pmCiC expression in cancer cells correlates with the tumour stage in human tissues. Indeed, pmCiC expression in tumour cells increased steadily with tumour stage (Figure 12A). With 45% of stage I samples, 40% of stage II samples, 84.6% of stage III samples, and 63.6% of stage IV samples showed pmCiC expression levels above zero. On the other hand, there was no difference in the expression of pmCiC between stage IV of primary tumours and metastatic tissues (Figure 12B). In fact, the distribution of pmCiC expression levels was very similar in both groups. Consistently, there was a clear correlation between the expression of pmCiC in stage IV primary tumours and the expression of pmCiC at the corresponding metastatic sites (Figure 12C). However, the number of tissues expressing pmCiC in cancer cells was higher in metastasis than in primary tissues at stage IV (63.6% and 72.4%, respectively).

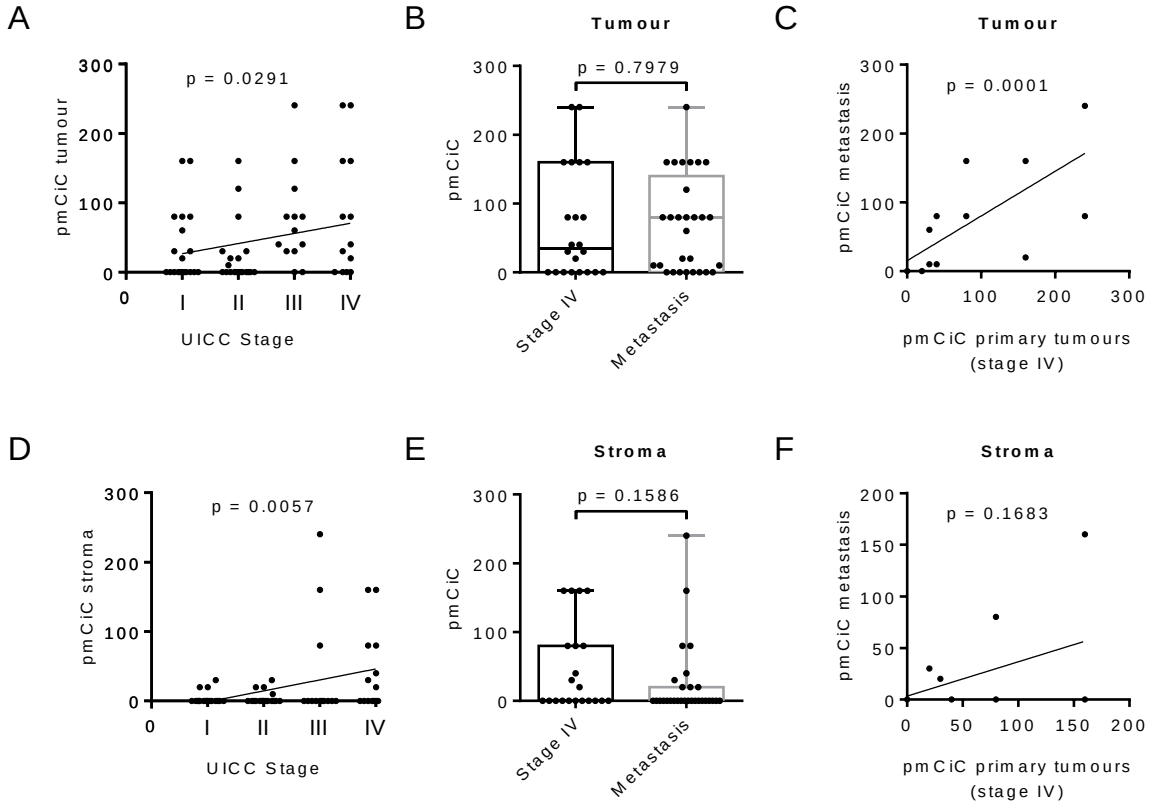

Figure 12: Expression of pmCiC in patient biopsies analysed by immunohistochemistry. (A) Spearman's rank correlation coefficient analysis of pmCiC expression in cancer cells and stage. N = 75 (stage I: 20, stage II: 20, stage III: 13, stage IV: 22). (B) Box plot analysis of pmCiC expression in primary tumours of stage IV compared with metastasis. N = 51 (22 stage IV tumours, 29 metastasis). (C) Spearman's rank correlation coefficient analysis of pmCiC in primary tumours stage IV and the corresponding metastases. (D) Spearman's rank correlation coefficient analysis of pmCiC expression in the stroma surrounding cancer cells and stage. N = 73 (stage I: 20, stage II: 19, stage III: 13, stage

IV: 21). (E) Box plot analysis of pmCiC expression in the stroma of primary tumours of stage IV compared with metastasis. N = 50 (21 stage IV tumours, 29 metastasis). (F) Spearman's rank correlation coefficient analysis of pmCiC in the stroma of primary tumours stage IV and the corresponding metastases. Box plots show median and interquartile ranges in addition to minimum and maximum values. The line in the middle of the box represents the median. p values for box plots were calculated using the Mann-Whitney test. pmCiC expression is presented as Score 300.

Our recent study showed that citrate can be provided to cancer cells by the cancer-associated stroma and released from benign cells via pmCiC (Mycielska *et al.,* 2018; Drexler *et al.,* 2021). Furthermore, extracellular citrate has been shown to induce an invasive or colonising phenotype in cancer cells, so this metabolite exchange may be particularly important in supporting metastatic activity and the process of colonisation of distant organs. Correlating pmCiC expression in the stroma of the primary tumours with the tumour stage, showed an even stronger association than in the cancer cells themselves. The pmCiC expression in the stroma increased steadily with tumour stage (Figure 12D). This is consistent with stroma transformation and citrate supply being a critical element in the development of metastatic tumours. The results of the study indicate that 15% of stage I samples, 21.1% of stage II samples, 23.1% of stage III samples, and 47.6% of stage IV samples showed pmCiC expression levels above zero. Similar to pmCiC in cancer cells, there was no statistically significant difference between pmCiC expression in the stroma of cancer cells in primary stage IV tumour sites and in metastases (Figure 12E). We did not observe a correlation between pmCiC expressed in the stroma of stage IV tissues and metastasis (Figure 12F), however this could be due to the small number of tissues available for analysis. Moreover, there was a small decline in the number of metastatic tissues expressing pmCiC compared to the number of tissues expressing pmCiC in the stroma at stage IV, 47.6% and 31%, respectively.

For successful disease progression and metastasis, cancer cells require support from the surrounding tissue, usually through the formation of new blood vessels and activation of the stroma. We used CD31, a marker of endothelial cells, and FAP, expressed by activated fibroblasts, to study angiogenesis and stroma formation in human cancer tissues. Interestingly, markers of angiogenesis and stromal activation showed no correlation with tumour stage when analysing the expression of CD31 (Figure 13A) or FAP (Figure 13D). In fact, the expression of CD31 and FAP in human cancer tissues showed a fairly even distribution across the different tumour stages, suggesting that their expression is important for tumour development, but does not necessarily need to increase at later stages of tumour progression. There was also no difference between CD31 expression levels in primary stage IV cancer tissues compared to metastases (Figure 13B). Thus, there was no correlation between CD31 expression in the primary tumour and the corresponding metastases Figure 13C). However, noticeably, FAP expression was clearly reduced when comparing metastatic tissues with stage IV primary tumour sites (Figure 13E). No correlation of FAP expression was observed between metastatic tissues and corresponding stage IV primary tumours (Figure 13F).

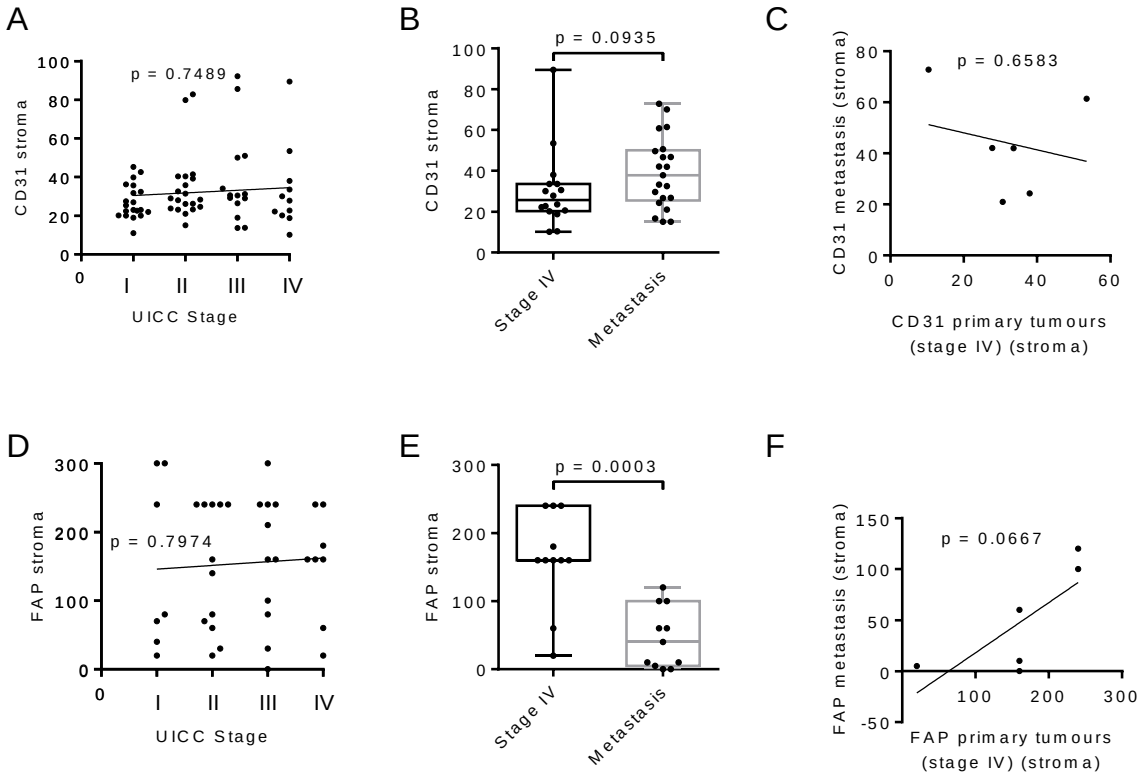

Figure 13: Expression of CD31 and FAP in the stroma surrounding tumour tissue of patient biopsies analysed by immunohistochemistry. (A) Spearman's rank correlation coefficient analysis of CD31 expression and stage. N = 70 (stage I: 20, stage II: 20, stage III: 14, stage IV: 16). (B) Box plot analysis of CD31 expression in the stroma of primary tumours of stage IV compared with metastasis. N = 37 (16 stage IV tumours, 21 metastasis). (C) Spearman's rank correlation coefficient analysis of CD31 in the stroma of primary tumours stage IV and the corresponding metastases. (D) Spearman's rank correlation coefficient analysis of FAP expression and stage. N = 41 (stage I: 7, stage II: 12, stage III: 11, stage IV: 11). (E) Box plot analysis of FAP expression in the stroma of primary tumours of stage IV compared with metastasis. N = 22 (11 stage IV tumours, 11 metastasis). (F) Spearman's rank correlation coefficient analysis of FAP in the stroma of primary tumours stage IV and the corresponding metastases. p values for box plots were calculated using the Mann-Whitney test. Box plots show median and interquartile ranges in addition to minimum and maximum values. The line in the middle of the box represents the median. Expression of CD31 is presented as number of positive vessels (mean value). FAP expression is presented as Score 300.

2.2.4.2 Correlation of the pmCiC expression in the stroma versus cancer cells

Our recent study showed that cancer cells control the release of citrate from their local environment and that the level of citrate release depends on the metabolic needs of the cancer (Drexler *et al.,* 2021). That is why we studied whether the expression of pmCiC in cancer cells correlates with pmCiC in the stroma. Indeed, we observed a correlation between these two markers in primary tumours between pmCiC in cancer cells and pmCiC in the stroma (Figure 14A). These data could confirm that the degree of transformation of the cancer-associated stroma depends on the specific metabolic needs of the cancer cells. In this case, the increased expression of pmCiC in cancer cells suggests a higher demand for extracellular citrate by cancer cells. This correlates with increased pmCiC expression in the surrounding stroma,

which is consistent with increased release of this metabolite. This correlation was not observed when the level of expression of either FAP (Figure 14B) or CD31 (Figure 14C) in the stroma was examined in relation to pmCiC in tumour cells.

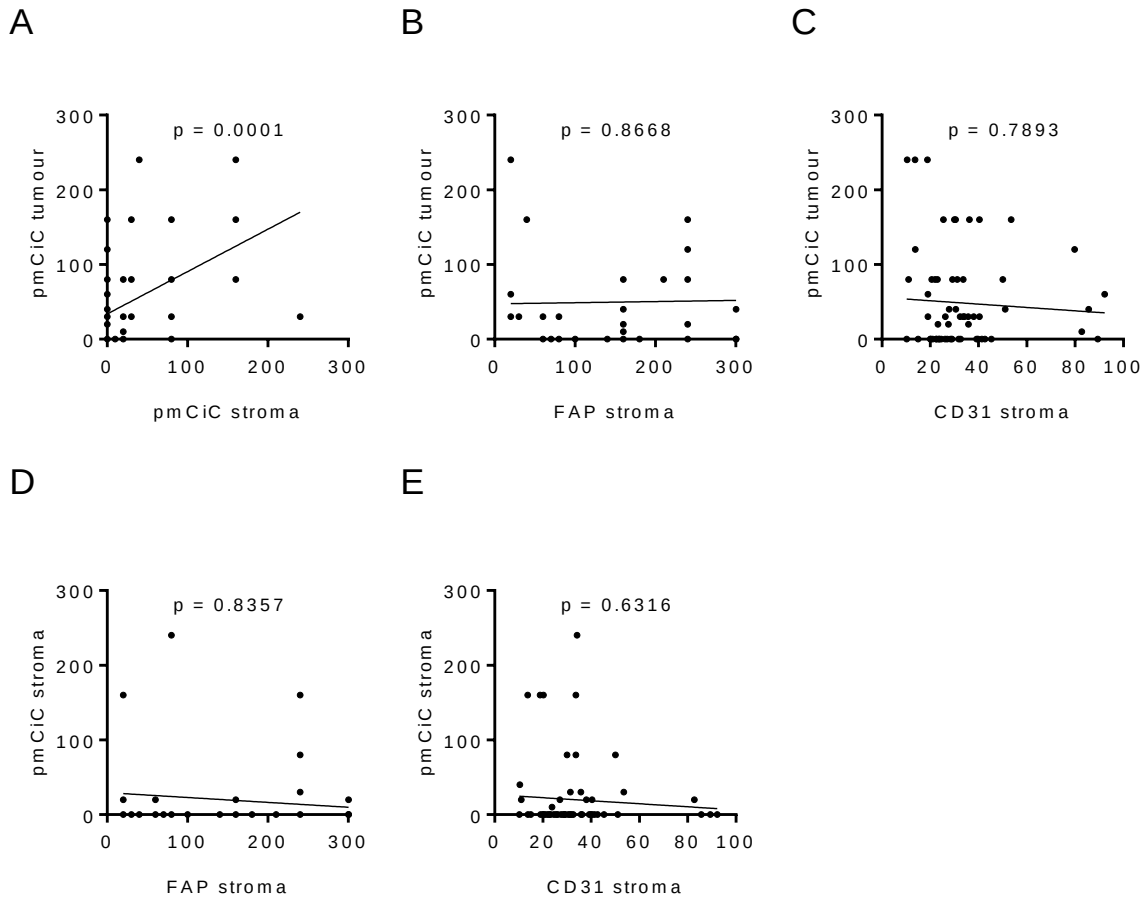

Figure 14: Spearman's rank correlation coefficient analysis of pmCiC expression in cancer cells of primary tumours or in the surrounding tumour stroma, and FAP and CD31 in the surrounding tumour stroma analysed by immunohistochemistry. Correlation of pmCiC expression in cancer cells in tumour tissue and (A) pmCiC expression in the surrounding tumour stroma (N = 73), and (B) FAP expression (N = 40), and (C) CD31 expression (N = 68). Correlation of pmCiC expression in the primary tumour stroma and (D) FAP expression (N = 39), and (E) CD31 expression (N = 67). Expression of pmCiC and FAP is presented as Score 300. Expression of CD31 is presented as number of positive vessels (mean value).

To determine whether the increased activity of the cancer-associated stroma, as indicated by increased citrate release, correlates with FAP and CD31, known markers of stromal formation, we correlated the expression of FAP *versus* pmCiC in the stroma (Figure 14D) and CD31 *versus* pmCiC expression in the stroma (Figure 14E). No correlation was observed with any of the markers tested, suggesting that the expression of pmCiC in the stroma is independent of the classical markers of stromal activation and angiogenesis.

2.2.4.3 Expression of pmCiC in blood vessels

We have previously observed a certain level of pmCiC expression in some of the blood vessels present in human cancer tissue (Drexler *et al.,* 2021; Parkinson *et al.,* 2021). The analysis performed here showed that the presence of pmCiC-stained vessels is increased at later stages of cancer development. There was no statistical significance between pmCiC expression of blood vessels in primary stage IV tumour sites and metastasis (Figure 15A). A steep increase in the occurrence of vessels with pmCiC was observed in stage IV of cancer (Figure 15B).

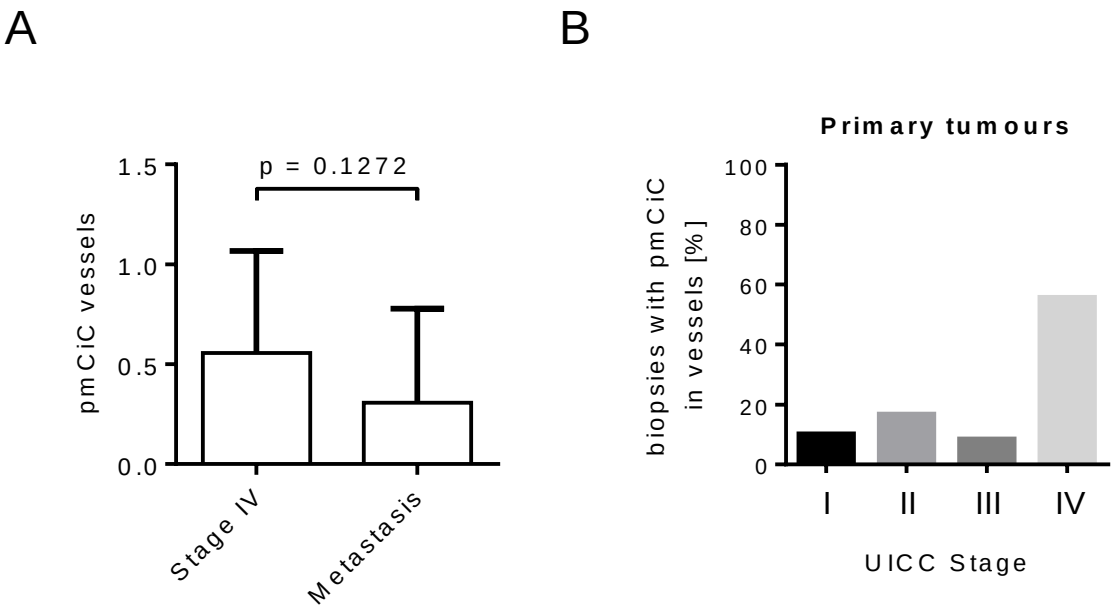

Figure 15: Analysis of pmCiC expression in blood vessels. (A) Analysis of pmCiC expression in vessels of stage IV tumours compared with metastasis. N = 44 (18 stage IV tumours, 26 metastasis). The p value was calculated using the Mann-Whitney test. The graph shows the mean with standard deviation. (B) Percentage of biopsies with pmCiC staining in blood vessels subdivided by tumour stage.

2.2.4.4 Illustration of the data

Figure 16 and Figure 17 summarise the analysis presented above. We chose to compare staining with different markers on consecutive sections of the same tissue. Figure 16 shows two different poorly differentiated urothelial tumours with prominent pmCiC staining in the cancer cells, but also in some vessels and the surrounding stroma. In contrast, Figure 17 shows liver metastases from ductal breast cancer (A1-A3) and prostate cancer (B1-B3).

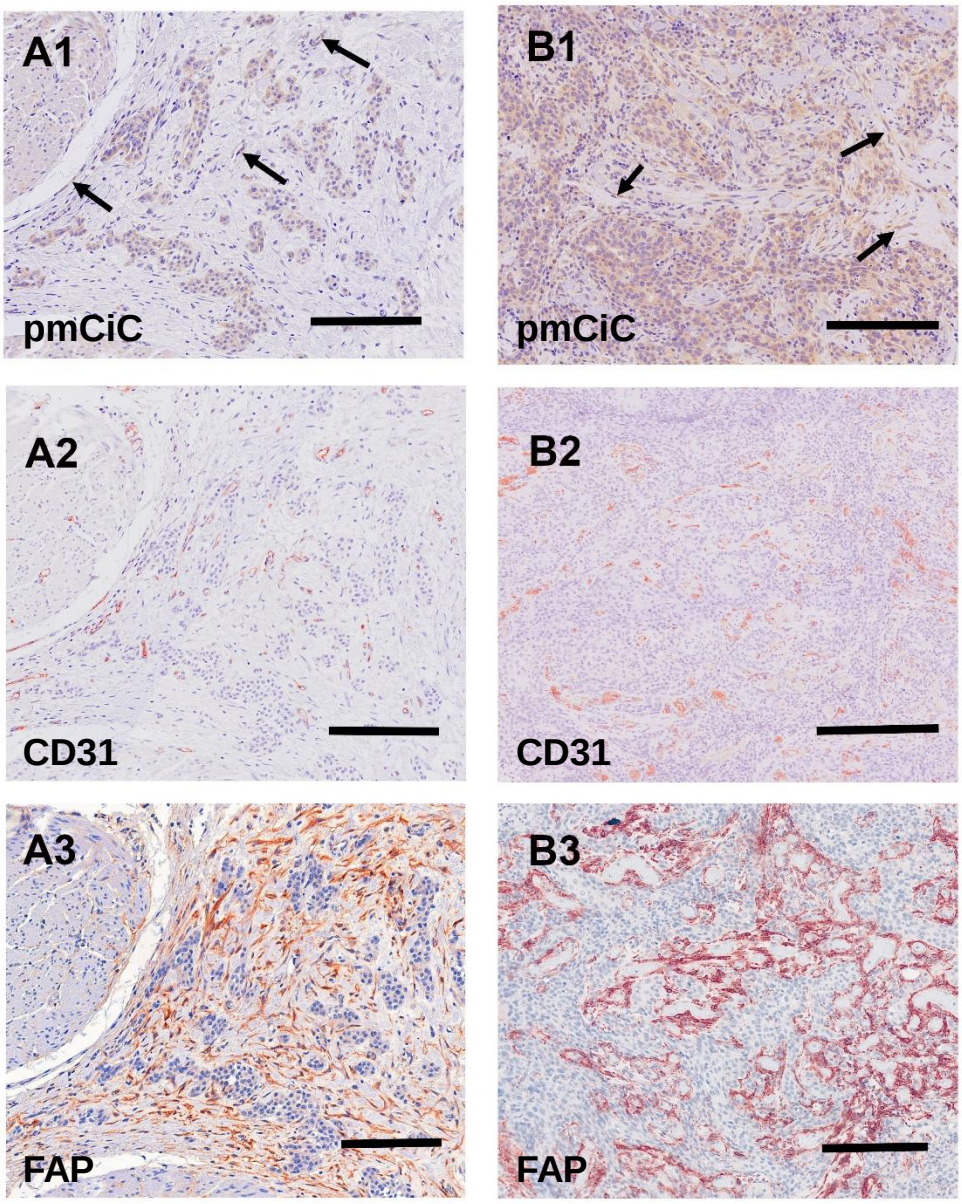

Figure 16: Immunostaining of two urothelial carcinomas. (A1–A3) (scale bar 100 µm) shows a primary muscle-infiltrating urothelial transitional cell carcinoma with positivity for pmCiC in cancer cells (A1) and endothelial cells (A1; →). Serial sections show numerous vessels stained for CD31 (A2) as well as strong stromal reaction with FAP (A3). (B1–B3) (scale bar 100 µm) displays another poorly differentiated urothelial cancer with prominent expression of pmCiC in cancer cells (B1) but also in some vessels (B1; →). Serial section was stained with CD31 ((B2); scale bar 150 µm) to highlight the tumour-associated vasculature. In (B3) there is a strong stromal reaction stained by FAP staining. All samples were counterstained with hematoxylin.

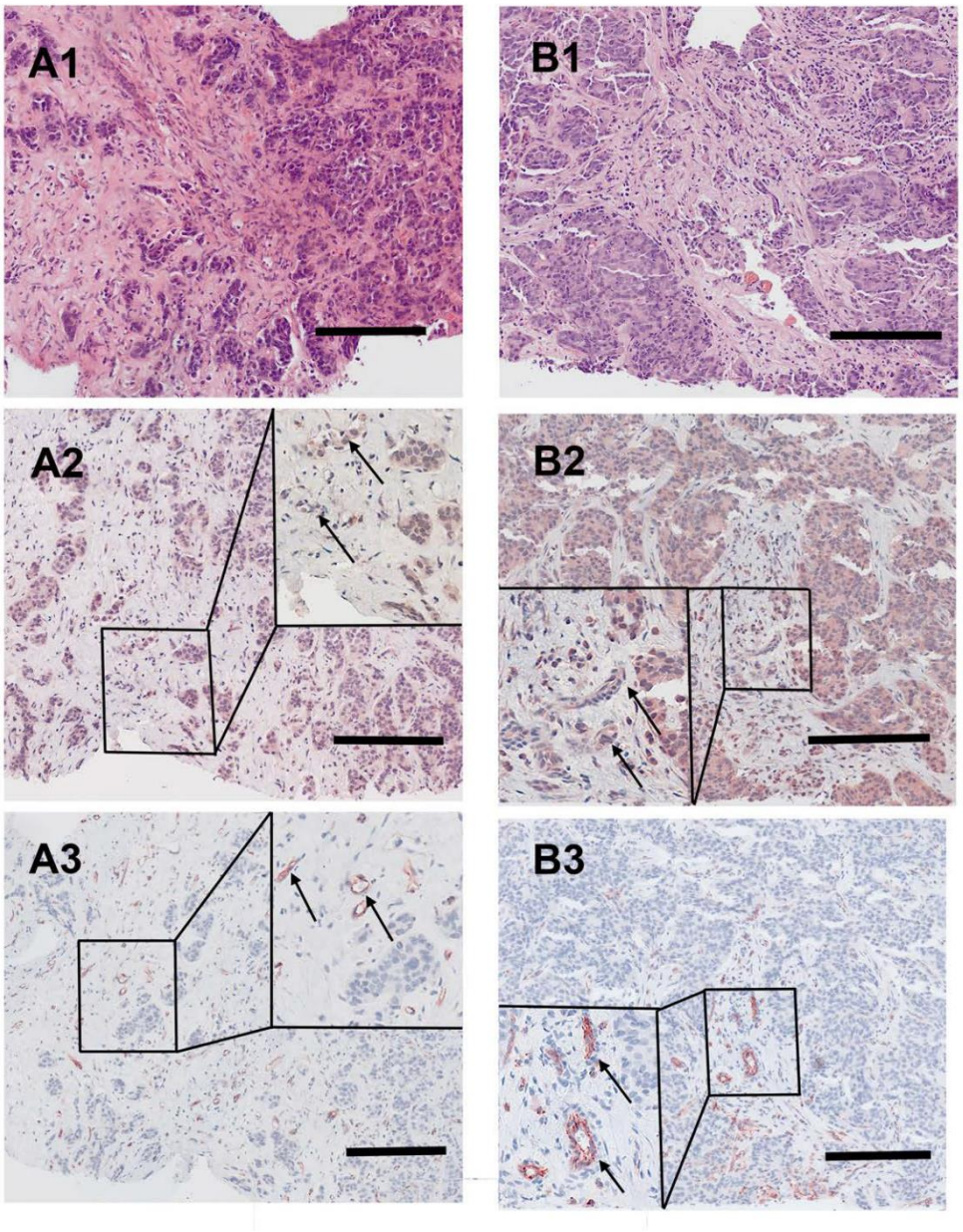

Figure 17: Histological staining of a liver metastasis of a ductal breast cancer and a liver metastasis of a prostate cancer. [(A1–A3); scale bar 100 µm] Liver metastasis of a ductal breast cancer [(A1); HE] shows little nest of atypical infiltrating cancer cells with a desmoplastic stroma expressing pmCiC in tumour cells (A2) as well as some associated small vessels (inset; →; magnification 3 - fold). In (A3) serial section of the metastasis shows tumour associated vessels stained for CD31 (inset; →; magnification 3 - fold). [(B1–B3); scale bar 100 µm] Liver metastasis of a prostate cancer [(B1); HE] displaying a pseudoglandulär atypical cancer with a desmoplastic stroma expressing pmCiC in tumour cells (B2) and few tumour-associated vessels (inset; →; magnification 3 - fold). In (B3) a serial section of the specimen was stained with CD31 to highlight the tumour associated vessels (inset; →; magnification 3 - fold). Images provide an overview and details at higher magnification (inserts; magnification 3 - fold); corresponding size bars are included. Tissues shown in (A2, A3, B2, B3) were counterstained with hematoxylin.

It can be deduced that pmCiC expression is similarly high in poorly differentiated and metastatic cells. Importantly, higher expression of pmCiC in cancer cells correlates with increased levels of stromal cells also expressing pmCiC, particularly in Figure 16(B1). This could be due to increased metastatic activity of the cancer cells or a lack of sufficient citrate at

this site. Interestingly, although the stroma shown in Figure 17 is highly desmoplastic, the level of pmCiC expression in these cells is lower compared to primary urothelial tumours. This may be because citrate is abundant in the liver [reviewed in Parkinson et al. (2021)] and cancer cells have less need for this substrate. Figure 16 and Figure 17 show striking differences in the number and size of blood vessels stained with pmCiC and CD31, suggesting that pmCiC is an earlier marker of angiogenesis than CD31.

2.2.5 Discussion

For the purpose of the present study, we have combined human cancer tissues of different origins and evaluated the expression of pmCiC in cancer and stromal cells to check whether extracellular citrate can be considered as a necessary factor indicating the aggressiveness of the disease. We also put forward our hypothesis that the expression levels of pmCiC in cancer cells versus stroma would correlate with the amount of citrate uptake versus release, respectively. To assess other parameters of the tumour microenvironment, we also used the markers CD31 (Sharma *et al.,* 2013; Bösmüller *et al.,* 2018) and FAP (Ma *et al.,* 2017; Coto-Llerena *et al.,* 2020), which should reflect angiogenesis and fibroblast activation in the tissues studied. It should be noted that the limited number of tissues and the analysis performed without distinguishing for the tumour type might have affected some of the parameters by increasing the variability of the data.

Our study shows for the first time that pmCiC expression in cancer cells in human tissues correlates with tumour stage and is significantly increased at advanced stages of tumour development and metastatic sites, irrespective of tumour origin. This observation supports our recent data suggesting a role for extracellular citrate uptake in the acquisition of a more invasive (epithelial-mesenchymal transition (EMT)) or colonising (mesenchymal-epithelial transition (MET)) character of cancer cells, depending on the duration of citrate presence in the media (Drexler *et al.,* 2021). Therefore, the expression of pmCiC in cancer cells could indicate an increased metastatic potential. In line with this hypothesis, pmCiC expression was less frequent in early stages of tumour development where its expression could indicate an increased likelihood of metastasis formation.

Extracellular citrate is normally present at stable concentrations in the blood and this is one of the sources of citrate for cancer cells, particularly those close to blood vessels. However, this source may not be sufficient as the tumour grows. We have shown that the tumour microenvironment is an additional source of citrate and that the amount of citrate released by cancer-associated fibroblasts depends on the availability of extracellular citrate to cancer cells. Therefore, citrate plays an important role in the communication between cancer cells and the surrounding stroma. Increased or decreased intracellular levels of citrate can be detrimental to cancer cells (Icard *et al.,* 2019; Haferkamp *et al.,* 2020); therefore, this controlled enrichment of the cancer microenvironment with citrate may represent a very interesting and not yet fully understood regulatory mechanism specific to cancer development (Jordan *et al.,* 2022). Not surprisingly, our data from human cancer tissues show a correlation between pmCiC expression in cancer cells and pmCiC expression in the tumour environment, which may indicate a balance between citrate uptake and release and active stromal support of the disease progression. However, due to different levels of extracellular citrate and proximity to blood vessels, the expression of pmCiC in the stroma of primary tumours may also vary from

organ to organ. For these reasons, it is likely that the simultaneous assessment of pmCiC expression in cancer cells and their microenvironment as well as in blood vessels could be a good prognostic marker for disease progression, rather than each of these elements separately. This aspect requires further and more detailed studies.

Some recent studies have shown the involvement of another sodium-dependent citrate transporter, NaCT (encoded by SLC13A5), in the metabolism of liver cancer cells (Li *et al.,* 2017; Kumar *et al.,* 2021). Specifically, citrate uptake in liver cancer cells reduced reductive carboxylation by providing citrate to ATP citrate lyase (ACLY) (Kumar *et al.,* 2021). However, in liver cancer cells, this effect of extracellular citrate on cancer metabolism was particularly pronounced under conditions of reduced extracellular glucose and glutamine. On the other hand, our published study suggests that even under non-starving conditions, extracellular citrate uptake via pmCiC has a significant impact on fatty acid synthesis (Mycielska *et al.,* 2018; Drexler *et al.,* 2021). SLC13A5 also has a very restricted expression pattern. RNA expression data show expression only in liver cancer (Human Protein Atlas, Accessed December 11, 2023). Our very preliminary staining of human liver tissue may suggest that pmCiC may also be expressed in non-differentiated liver cancer cells (data not shown). Therefore, it remains crucial to investigate in the future which citrate transporters (or both) support metastasis.

There are also several groups suggesting that increasing extracellular citrate levels results in increased citrate uptake by cancer cells, leading to their death (LU *et al.,* 2011; Icard *et al.,* 2023). In any case, it is suggested that extracellular citrate and plasma membrane citrate transporters play a significant role either in supporting cancer progression (at physiological levels) or with the potential to destroy cancer (when applied at very high levels).

We also found no correlation between CD31 or FAP expression and tumour stage. There is no agreement regarding the use of CD31 in the field of cancer prognosis. Some studies concluding CD31 to be a prognostic marker (Sandlund *et al.,* 2007; Schmidt *et al.,* 2017; Schlüter *et al.,* 2018), but others failing to confirm this correlation (RASK *et al.,* 2019). Finally, some other studies have found an inverse correlation between CD31 expression and patient survival (VIRMAN *et al.,* 2015; Emmert *et al.,* 2016). In addition, the lack of correlation between CD31 and tumour stage in the present study may be due to the fact that we analysed tumours of different origin together in one group. As different organs have different blood vessel densities, this could affect the overall assessment.

Although we did not find a correlation between CD31 and FAP expression and disease stage, there were increased levels of pmCiC present in the blood vessels of later stage cancers. CD31 is an endothelial cell marker (Bösmüller *et al.,* 2018) and stains all blood vessels at any stage from early to full vascularization. In contrast, we found that pmCiC is only expressed in a small fraction of tiny blood vessels, most likely in the early formation stage, but not in well differentiated vessels. This would be consistent with increased citrate uptake by pmCiC at the

earlier stage of vessel development. Citrate, as the primary substrate for fatty acid synthesis, could contribute to the formation and modification of the plasma membrane necessary for angiogenesis. Blocking fatty acid synthesis has already been shown to affect angiogenesis. In a murine stroke model, the use of cerulenin increased endothelial cell leakage, decreased transcellular electrical resistance and contributed to the breakdown of the blood-brain barrier (BBB) after stroke (Janssen *et al.,* 2021). Knockdown of fatty acid synthase inhibited vessel sprouting by reducing cell proliferation (Bruning *et al.,* 2018). Strikingly, most of the pmCiC-expressing blood vessels were found at stage IV of tumour development. It is possible that these vessels are involved in/facilitate the dissemination of metastatic cells, e.g., due to controlled fatty acid content or other special characteristics. Therefore, the expression of pmCiC in endothelial cells may be a specific feature of early cancer angiogenesis and a different factor to CD31, but this issue remains to be investigated.

The lack of correlation between CD31 and FAP expression in the stroma and cancer stage could be due to several reasons. Firstly, a limited number of tissues examined could certainly play a role in obtaining significant results. In addition, tumours of different origin have different requirements for stromal support (Parkinson *et al.,* 2021). In this case, the combination of all tumour types in one group could further influence the results obtained. In this context, however, it is even more striking that the expression of pmCiC and its correlation with the stage of the tumour were independent of the origin of the tumour and could therefore represent a novel and widely applicable marker of tumour aggressiveness.

We have hypothesised that elevated citrate levels in organs such as the brain, bone or liver facilitate organ colonisation and are therefore the most common sites of secondary tumour growth (Parkinson *et al.,* 2021). In this respect, the variability in the expression of pmCiC in cancer and peritumour tissues, as shown in the present study, could also be caused by different levels of extracellular citrate in the organs from which the tissues were obtained. It is interesting to note that the number of metastatic tissues stained with pmCiC in the stroma is lower than in the primary tumours at stage IV. This observation would be consistent with the fact that the most common organs in which distant metastasis occur, such as the liver, brain, bone or the lung, are rich in citrate (Parkinson *et al.,* 2021). Citrate levels need to be tightly controlled by cancer cells, as its increase was shown to be detrimental to cancer. Since colonising cancer cells in an extracellular citrate-rich environment are less likely to demand additional citrate from the surrounding stroma, it is expected that pmCiC expression will be lower. However, the number of metastatic tissues expressing pmCiC in cancer cells compared to the primary tumours at stage IV increases suggesting an important role of extracellular citrate in organ colonisation.

2.2.6 Conclusion

In conclusion, the expression level of pmCiC in cancer cells from human cancer tissues seem to increase with tumour stage and is particularly elevated at metastatic sites. Importantly, we also found elevated levels of pmCiC in the tumour microenvironment, which may indicate the importance of extracellular citrate in the progression of metastatic disease. However, the exact role of citrate in metastatic progression remains to be elucidated and will be addressed in our next studies. On the other hand, we did not observe significant correlations of other stromal markers, CD31 and FAP, with tumour stage. It is possible that the expression of pmCiC in cancer cells and the supporting stroma may be an early event in the process of metastasis and organ colonization. It is worth noticing that we performed our study on human cancerous tissues of different origins. To our knowledge this is one of the first studies showing a common factor/feature correlating with tumour aggressiveness. Therefore, it should be further investigated in the context of a prognostic marker.

2.3 The role of citrate homeostasis in merkel cell carcinoma pathogenesis

Summary:

This chapter examines the role of citrate homeostasis in the pathogenesis of MCC. The research identifies the expression of pmCiC in MCC cells and tissues, showing that extracellular citrate promotes MCC proliferation. Additionally, it discusses the inhibitory effects of gluconate on MCC growth both *in vitro* and *in vivo*, suggesting a therapeutic potential for targeting citrate metabolism in MCC treatment.

Objective addressed:

To understand how pmCiC expression influences MCC proliferation and to assess the therapeutic effects of targeting citrate metabolism.

The role of citrate homeostasis in merkel cell carcinoma pathogenesis

Konstantin Drexler[1,*], **Barbara Schwertner[1]**, Silke Haerteis[2], Thiha Aung[2,3], Mark Berneburg[1], Edward K. Geissler[4], Maria E. Mycielska[5], and Sebastian Haferkamp[1]

1: Department of Dermatology, University Hospital Regensburg, 93053 Regensburg, Germany

2: Institute for Molecular and Cellular Anatomy, University of Regensburg, 93053 Regensburg, Germany

3: Faculty of Applied Healthcare Science, Deggendorf Institute of Technology, 94469 Deggendorf, Germany

4: Department of Surgery, Section of Experimental Surgery, University Hospital Regensburg, 93053 Regensburg, Germany

5: Department of Structural Biology, Institute of Biophysics and Physical Biochemistry, University of Regensburg, 93053 Regensburg, Germany

*: Correspondence: Konstantin.drexler@ukr.de

Manuscript information:

Cancers (Basel). 2022 Jul 14; 14(14): 3425.

Received 23 May 2022

Accepted 4 July 2022

Doi: 10.3390/cancers14143425

2.3.1 Abstract

Simple summary

Merkel cell carcinoma (MCC) is a rare but highly aggressive skin cancer. Despite important progress, overall understanding of the events that drive MCC carcinogenesis remains incomplete. We discovered that the plasma membrane citrate transporter (pmCiC) is upregulated in Merkel cell carcinoma cell lines. Cancer cells import extracellular citrate via pmCiC to support their metabolism, which is critical to support proliferation and metastatic spread. In this study, we show that inhibition of pmCiC can decrease the growth rate of Merkel cell carcinoma cell lines. Targeting pmCiC and thereby the tumor metabolism should be considered further as a potential anti-cancer therapy.

Abstract

Merkel cell carcinoma (MCC) is a rare but highly aggressive tumor of the skin with a poor prognosis. The factors driving this cancer must be better understood in order to discover novel targets for more effective therapies. In the search for targets, we followed our interest in citrate as a central and critical metabolite linked to fatty acid synthesis in cancer development. A key to citrate uptake in cancer cells is the high expression of the plasma membrane citrate transporter (pmCiC), which is upregulated in the different adenocarcinoma types tested so far. In this study, we show that the pmCiC is also highly expressed in Merkel cell carcinoma cell lines by western blot and human tissues by immunohistochemistry staining. In the presence of extracellular citrate, MCC cells show an increased proliferation rate in vitro; a specific pmCiC inhibitor (Na^+-gluconate) blocks this citrate-induced proliferation. Furthermore, the 3D in vivo Chick Chorioallantoic Membrane (CAM) model showed that the application of Na^+-gluconate also decreases Merkel cell carcinoma growth. Based on our results, we conclude that pmCiC and extracellular citrate uptake should be considered further as a potential novel target for the treatment of Merkel cell carcinoma.

Keywords: cancer, merkel cell carcinoma, citrate, pmCiC, gluconate

2.3.2 Introduction

Merkel cell carcinoma (MCC) is an aggressive tumor of the skin with a rising incidence (Lin *et al.,* 2014) that predominately affects elderly Caucasians (median age at diagnosis is 75–80). Primary tumors have a predilection for sun exposed areas of the skin (Pulitzer, 2017; Becker *et al.,* 2017). In addition to UV-radiation, immune deficiencies are important risk factors for the development of MCCs (Becker *et al.,* 2017); the risk to develop MCC is five-fold greater after organ transplantation and 11-fold greater for patients with AIDS compared to the general population (Lin *et al.,* 2014). Chronic arsenic exposure has also been implicated in the pathogenesis of MCC (Mauzo *et al.,* 2016). Although malignant melanoma is 50-fold more frequent than MCC, the prognosis for patients with MCC is worse (Becker *et al.,* 2017). The five-year survival rate for patients with a localized skin disease is 50–76%, 39% for patients with regional node disease, and 18% for patients with distant metastatic disease (Pulitzer, 2017). Clinical diagnosis of MCC is often difficult in the differential diagnosis since both basal cell carcinoma or squamous cell carcinoma are more common. MCC can also be mistaken for metastasis of neuroendocrine tumors, melanoma, or lymphoma (Pulitzer, 2017). Microscopic diagnosis can also be challenging. The typical presentations are uniform cells with round or oval nuclei that show expression of cytokeratin 20 (95%) and neuroendocrine markers, such as synaptophysin, chromogranin A, neuron-specific enolase, or CD56. Expression of p63 is found in 60% of MCC patients (Pulitzer, 2017; Jankowski *et al.,* 2014; Fukuhara *et al.,* 2016).

After the diagnosis of MCC, a complete excision (1–2cm margin) and adjuvant radiation is normally performed. Sentinel lymph node mapping and biopsy are recommended together with stage imaging (ultrasonography, computer tomography (CT), or positron emission tomography (PET)) (Mauzo *et al.,* 2016). Around 55% of patients with a distant metastatic MCC respond positively to first line treatment with chemotherapy consisting typically of platinum-based + etoposide. However, because the responses are not durable, tumors often recur by 4–15 months with a median progression-free survival of only 94 days and median overall survival of 9.5 months (Becker *et al.,* 2017; Cassler *et al.,* 2016). Although recent studies have shown some evidence of benefits in the long-term response for patients treated with the PD-L1 specific antibody avelumab (Gaiser *et al.,* 2018), more effective novel therapeutic targets are needed.

Membrane transport proteins are involved in the movement of ions and small molecules across biological membranes. Many different membrane transporters have been shown to facilitate cancer development, progression, and drug resistance (Nazemi & Rainero, 2020). A recent study of Mycielska et al. showed that extracellular citrate is supplied to cancer cells through a plasma membrane-specific variant of the mitochondrial citrate transporter pmCiC, which is a member of the SLC25 mitochondrial transporter family (Mycielska *et al.,* 2018). This transporter enables cancer cells to use extracellular citrate for metabolism and supports cell

proliferation. Citrate is a central metabolite for fatty acid synthesis, which is necessary for tumor growing. A lack of citrate also leads to morphological changes in cancer cells; thus, citrate seems to have a high impact on cancer growth (Drexler *et al.,* 2021). Gluconate has been discovered as a specific and irreversible inhibitor for pmCiC (Mycielska *et al.,* 2018; Mycielska *et al.,* 2015; Mycielska *et al.,* 2019), which opens the possibility for therapeutic intervention.

In this study, we have conducted experiments to explore the hypothesis that pmCiC is important for MCC tumors by first measuring expression in MCC cell lines and human tumor biopsies. We then tested the effects of extracellular citrate on MCC proliferation in vitro and applied gluconate-based pmCiC inhibition to these in vitro and in vivo systems to show whether the tumor promoting effects of citrate can be inhibited.

2.3.3 Materials and Methods

Immunohistochemistry

Paraffin-embedded sections were dewaxed using xylol (Merck, Darmstadt, Germany) and then rehydrated by washing twice with absolute ethanol, twice with 96% ethanol, and twice with 70% ethanol. After blocking endogenous peroxidases using 3% H_2O_2 for 10 min, samples were washed once with bi-distilled water, heated in HIER Citrate Buffer pH6 (Zytomed/Biozol, Eching, Germany) at 90 °C for 20 min, and cooled for 20 min. Samples were blocked using the blocking solution of the ZytoChem Plus HRP-kit Rabbit/Mouse (Zytomed) for 10 min.

Sections were labeled at 4 °C overnight using a rabbit monoclonal antibody against pmCiC (D2P2F, Cell Signaling; dilution for patient samples and for cell lines 1:200) and a rabbit monoclonal antibody against Ki67 (Abcam, Cambridge, UK; dilution for cell lines 1:1000). After washing with DPBS, sections were incubated with biotinylated secondary anti-rabbit (HRP060-RB) antibodies for 30 min, washed in DPBS, and incubated with streptavidin HRP conjugate for 20 min (all from ZytoChem Plus HRP Kit, Zytomed). After washing with DPBS, slides were stained using AEC+ High Sensitivity Substrate Chromogen Ready-to-Use (Dako/Agilent Technologies, Hamburg, Germany), counterstained using hematoxylin (Carl Roth, Karlsruhe, Germany), and mounted using Aquatex (Merck). Tissues were collected from patients of the department of dermatology at the university hospital of Regensburg and correlated with clinical outcome. Ethics permission No. 22-2834-104.

Cell culture

Cell lines from primary Merkel cell carcinoma (PeTa), as well as from metastatic disease (WaGa, MS-1, and MKL-1), were grown in RPMI-1640 medium with 1% penicillin/streptomycin, 1% L-glutamine, and 10% fetal bovine serum. Although cell lines were not further authenticated, they were grown at low passage numbers from original sources and were kept typically in culture for only 2 months. Cells were tested and confirmed to be mycoplasma free. The following chemicals were used: citric acid and Na^+- gluconate (Sigma, St. Louis, MO, USA), and dialyzed serum (PAN Biotech GmbH, Aidenbach, Germany). The following antibodies were used: pmCiC specific antibodies (12; custom-made by GenScript Inc., Piscataway, NJ, USA) and Ki67 (Abcam, Cambridge, UK). Experimental media consisted of glucose free RPMI-1640 (Lonza, Basel, Switzerland), 10% dialyzed serum, 2 mM glutamine, 0.25 g/L glucose, ±200 µM citrate, and ±100 µM Na^+-gluconate, unless otherwise stated. The incubation time varied between 24 h, 48 h, 72 h, and 5 weeks, as specified. Western blots were analyzed by measurement of the pixel density using ImageJ software (Laboratory for Optical and Computational Instrumentation (LOCI), University of Wisconsin, Madison, WI, USA). The CyQUANT Direct Cell Proliferation Assay (Thermo Fisher Scientific, Waltham, MA, USA) was used to measure cell proliferation. Cells were counted with LUNA-FL™ Automated

Fluorescence Cell Counter (Logos Biosystems, Anyang-si, Korea). Western blots were analyzed by measurement of the pixel density using ImageJ software.

Chick chorioallantoic membrane model

The Chick Chorioallantoic Membrane (CAM) model was performed as described before (Drexler *et al.,* 2021; Pion *et al.,* 2021; Kohl *et al.,* 2021). Two days after implantation of 2×10^6 Merkel cell carcinoma cells (WaGa and MKL-1), daily treatment with either Na^+-gluconate (500 mg/kg/d) or NaCl 0.9% was performed (n = 20). Pictures were taken and tumors were removed after 5 days. The size of tumors was measured and the surrounding vessels were counted for all tumors.

Statistics

Statistics were performed using GraphPad by Dotmatics. A t-test was performed and significance was assumed for $p < 0.05$.

2.3.4 Results

2.3.4.1 Expression of pmCiC in merkel cell carcinoma cells and merkel cell carcinoma tissues

We first tested whether characterized MCC cell lines express pmCiC in vitro. All four MCC cell lines (WaGa, PeTa, MKL-1, MS-1) showed high expression of pmCiC by Western blotting (Figure 18A).

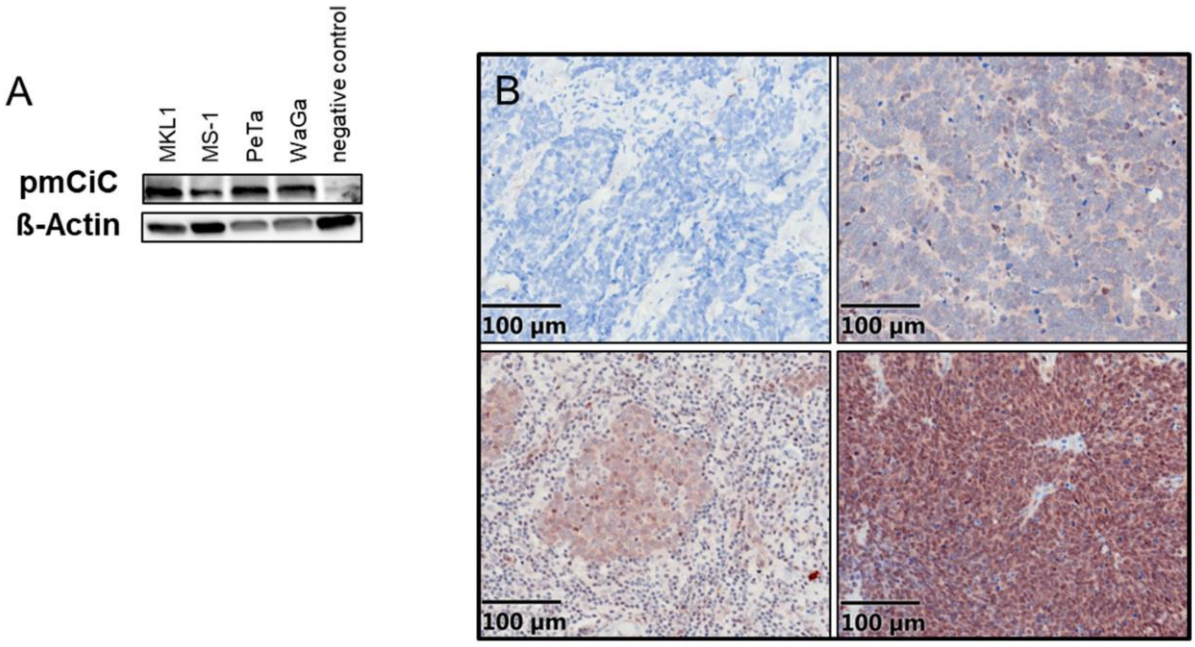

Figure 18: (A) Expression of pmCiC in 4 different cell lines (negative control: melanoma cells known for having no pmCiC). (B) PmCiC expression in Merkel cell carcinoma. Expression was ranked as negative (upper left panel), weak (upper right panel), intermediate (lower left panel), and high (lower right panel)

Next, we utilized immunohistochemical staining to detect pmCiC expression in formalin-fixed and paraffin-embedded primary MCC tissue sections. These results showed that 26 of the 28 samples stained positive for pmCiC (93%), where 2 samples showed no pmCiC expression (−), 9 showed weak/partial expression (+/−), 9 showed high expression (+), and 8 had very high expression (++) (Figure 18B). In total, 13 of the 28 patients had known metastatic disease, while 5 showed no metastases; clinical follow-up data were missing from the remaining 10 patients.

2.3.4.2 Proliferation of MCCs is increased in the presence of extracellular citrate

To investigate the effect of citrate on MCC cells, we used a dialyzed serum that does not contain citrate in experimental cultures of MS-1 cells. For this experiment, one group of cultures was supplemented with 200 µM citrate and the proliferation rate in both groups was measured after 24, 48, and 72 h using the CyQUANT Cell Proliferation Assay. There was a significant difference at 48 and 72 h between cells treated with 200 µM Na+-citrate versus cultures without added citrate, (48 h: $p = 0.00036$; 72 h: $p = 0.00007$; Figure 19A). pH values were measured in these cultures, but no difference was observed in the presence or absence of added citrate (data not shown); therefore, the effect could not be attributed to the pH changes. Similar results were obtained for WaGa cells (data not shown). Another MCC cell line (PeTa) was exposed to similar conditions for 24 and 48 h, with and without added citrate, and cells were directly counted using the LUNA cell counter; direct cell counting was possible with this cell line, since they do not tend to form cell aggregates in culture, unlike the MS-1 cells. A significant difference in number of cells was found after 48 h of incubation with citrate, compared to the cells without citrate (Figure 19B), 12 technical and 3 biological replicates were performed; t-test with citrate 48 h: control $p = 0.0017$; gluconate $p = 0.0008$; citrate + gluconate $p = 0.0007$). After adding 100 µM Na^+-gluconate to inhibit pmCiC-mediated citrate transport into cells, the proliferative effects of citrate were abrogated. Notably, Na^+-gluconate treatment alone had no effect on PeTa MCC cell proliferation (Figure 19B). We also investigated whether a lack of citrate or treatment with Na^+-gluconate might disguise cell proliferation effects via triggering apoptosis. Western blots for caspase 3, 7, 9, and PARP, as well as cleaved caspase 3, 7, 9, and cleaved PARP apoptosis markers did not reveal any evidence that the citrate or Na^+-gluconate effects are related to apoptosis induction (data not shown).

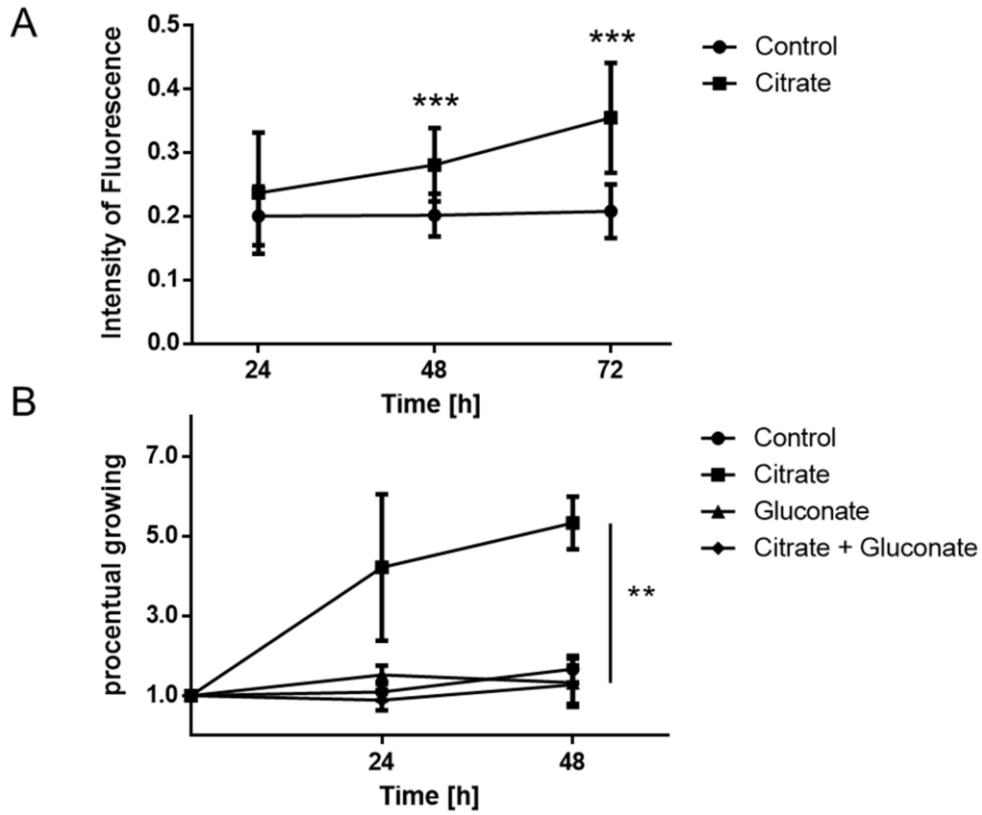

Figure 19: (A) Merkel cell carcinoma cells (MS-1) cultured with or without 200 µM citrate measured after 24 h, 48 h, and 72 h showing a significantly higher proliferation rate when treated with citrate (Method: CyQuant direct cell proliferation assay; t-test 48 h: p = 0.00036; 72 h: p = 0.00007). (B) Merkel cell carcinoma cells (PeTa) showed a higher number of cells after a treatment with 200 µM citrate. After adding 100 µM sodium gluconate, this effect was gone (Method: LUNA-FL™ Automated Fluorescence Cell Counter; t-test with citrate 48 h: control p = 0.0017; gluconate p = 0.0008; citrate + gluconate p = 0.0007; ** means p ≤ 0.01; *** means p ≤ 0.001).

2.3.4.3 Gluconate inhibits growth of merkel cell carcinomas in vivo

Bhat et al. showed that the Chick Chorioallantoic Membrane (CAM) model works well for in vivo testing of MCC tumor cell development (Bhat *et al.,* 2018). In our experiments, the MCC cell lines WaGa and MKL-1 were established for use in this assay, with growing tumors showing high pmCiC expression by Western blotting (Figure 18A). Results from the CAM assay with MCCs WaGa showed significantly (p = 0.01) decreased tumor growth when treated with Na^+-gluconate externally for 5 days compared to tumors treated with NaCl (Figure 20B). Na^+-gluconate (concentration 500 mg/kg/d) or NaCl was applied every 24 h, as previously described (n = 20) (Drexler *et al.,* 2021). Consistent with this observation, Ki67 expression was lower in tumors treated with Na^+-gluconate (Figure 20C) and macroscopic findings showed smaller tumors with gluconate treatment. Immunohistochemistry staining of WaGa tumors showed high expression of the pmCiC, as expected. PmCiC expression was not decreased after gluconate treatment, suggesting that Na^+-gluconate inhibits citrate transport but does not decrease its expression in these tumors. Together, these experiments show that blocking the pmCiC transport of citrate with Na^+-gluconate in vivo results in a reduction in the growth of

MCC tumors. By observing tumor-surrounding vessels, a lower number of vessels could be seen in tumors treated with sodium gluconate compared to the control group (Figure 20D). This effect was observed for MKL-1 (12 vs. 5.25 surrounding vessels, p = 0.03), as well as for WaGa (10 vs. 3.2 surrounding vessels, p = 0.02). These results suggest not only a direct effect of gluconate on proliferation, but also on angiogenesis.

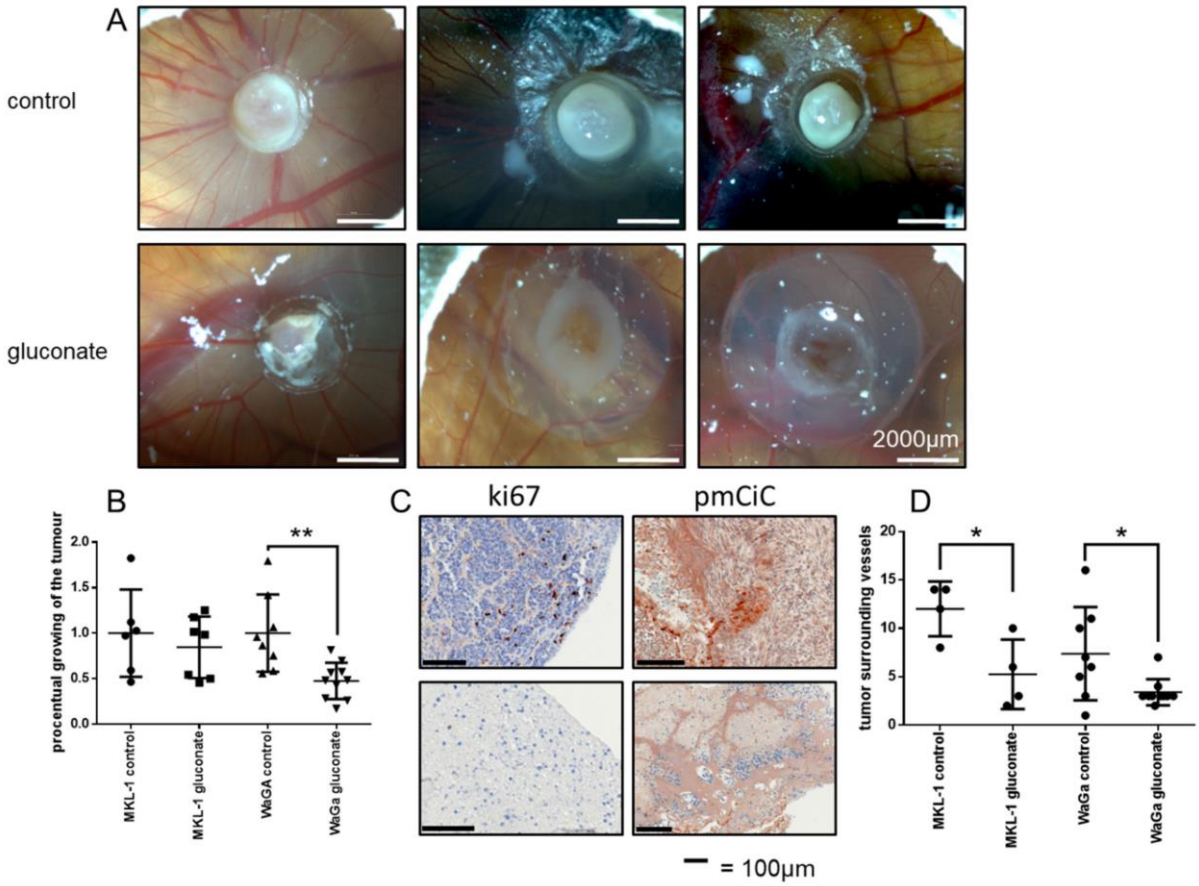

Figure 20: (A) Tumors in CAM-Assay after 5 days of treatment with sodium chloride (control) or sodium gluconate (gluconate; n = 20). (B) Diagrams after measurement of the tumor size showing a statistically significant result for WaGa (t-test MKL-1 p = 0.52; WaGa p = 0.01). (C) Ki67 and pmCiC expression in both groups. Ki67 is downregulated after a 5day treatment with sodium gluconate. (D) Significant differences in the number of tumor-surrounding vessels for WaGa and MKL-1 (t-test MKL-1 p = 0.03; WaGa p = 0.02; * means p ≤ 0.05; ** means p ≤ 0.01).

2.3.5 Discussion

In our present study, we primarily provide evidence that citrate and pmCiC expression may play a role in the biology of human MCC. PmCiC is expressed in 93% of MCC tissue samples and in 4 out of 4 tested cell lines. In vitro, we could detect an effect of extracellular citrate on the proliferation rate of PeTa and MS-1 cell lines. This effect could be blocked in PeTa cells by adding Na^+-gluconate as a specific pmCiC inhibitor. Growth inhibition was most probably due to cell cycle inhibition, rather than induction of apoptosis. We validated these findings using the 3D in vivo CAM model, where Na^+-gluconate lowered MCC proliferation and showed antiangiogenic effects on tumor-surrounding vessels. Therefore, our study supports further research to therapeutically target the pmCiC in human MCC.

PmCiC expression in MCC human tissue was present in most of the specimens studied. Due to the incomplete clinical patient history available, it is difficult to make a firm conclusion about the potential correlation of staining intensity with disease outcome. However, our data strongly suggests that pmCiC is expressed in most patients with metastatic disease, which is consistent with our hypothesis that extracellular citrate uptake plays an important role in supporting metastatic behavior in vivo (Mycielska *et al.,* 2018). From a diagnostic perspective, since the pmCiC was essentially expressed in all aggressive tumor types studied until now, it will not necessarily be useful as a specific marker to facilitate MCC diagnosis; however, its potential to be used as a prognostic marker is worth exploring.

Citrate is the primary substrate in fatty acid synthesis, which is a metabolic hallmark of cancer (Röhrig & Schulze, 2016). By extension, citrate has also logically been considered a central metabolite in cancer cells (Icard *et al.,* 2021). Until recently, it was generally agreed that cancer cells synthesize citrate intracellularly mainly in the process of reverse carboxylation from glutamine (Metallo *et al.,* 2011), and use different metabolic pathways, including the serine pathway (Possemato *et al.,* 2011) and lactate metabolism (Faubert *et al.,* 2017), to secure sufficient amounts of the Krebs cycle intermediates. In this way, cancer cells are able to meet their needs for increased citrate synthesis under changing extracellular conditions, which allows for metabolic flexibility (Haferkamp *et al.,* 2020). A recent study showed that besides intracellular synthesis of citrate, citrate is taken up extracellularly by epithelial-derived cancer cells, such as prostate, gastric, pancreatic, or liver (Kumar *et al.,* 2021). Our present study shows that this is also the case for MCC cells. Since the pmCiC is expressed on many different types of cancer, we speculate that pmCiC-mediated uptake of extracellular citrate is a general mechanism of neoplastic cells to meet their metabolic need (Drexler *et al.,* 2021). In vitro extracellular citrate supported tumor proliferation, but determining the exact mechanism requires further studies. Although in-depth analysis of human tumor pmCiC expression with correlation to metastasis and survival rates was not possible due to insufficient case numbers and an incomplete set of patient data, we plan to undertake these studies in the future.

Blocking of citrate uptake by cancer cells using Na^+-gluconate as a specific pmCiC blocker (Mycielska *et al.,* 2019) reduced subcutaneous tumor growth of human pancreatic L3.6pl cancer cells and changed the tumor's metabolic characteristics (Faubert *et al.,* 2017). The clearly smaller tumor (3D in vivo CAM-model) mass after Na^+-gluconate treatment correlates with the lower MCC tumor cell proliferation rate when deprived of citrate (Schlüter *et al.,* 1993). Gluconate-treated tumors also showed evidence of reduced angiogenesis, which is critical for tumor growth and metastasis (Kohl *et al.,* 2022; Folkman, 1971). Mechanistic studies should be performed to determine if citrate or gluconate has a direct impact on the release of pro-angiogenic factors, such as IL-6, G-CSF, or PGF (Lee *et al.,* 2023).

2.3.6 Conclusion

In conclusion, extracellular citrate uptake via the pmCiC is a potential novel therapeutic target in MCC tumours that highly expresses this critical citrate transporter, especially for cancers that tend to be more aggressive or metastatic. The exact mechanisms that play a role in this effect will require further investigation.

2.4 Cancer-associated cells release citrate to support tumor metastatic progression

Summary:

The final chapter investigates how CAFs release citrate to support tumor metastasis. The study highlights the impact of extracellular citrate on cancer cell metabolism and the induction of invasive phenotypes. It also explores the inhibition of pmCiC with gluconate, demonstrating reduced metastatic spread and stromal transformation *in vivo*. This chapter underscores the critical role of citrate in tumor-stroma interactions and suggests new therapeutic strategies targeting citrate metabolism.

Objective addressed:

To explore the impact of extracellular citrate on cancer cell metabolism and the induction of invasive phenotypes, and to assess the therapeutic potential of inhibiting citrate uptake.

Cancer-associated cells release citrate to support tumor metastatic progression

Konstantin Drexler[1], Katharina M Schmidt[2,*], Katrin Jordan[2], Marianne Federlin[3], Vladimir M Milenkovic[4], Gerhard Liebisch[5], Anna Artati[6], Christian Schmidl[7], Gregor Madej[8], Janina Tokarz[6], Alexander Cecil[6], Wolfgang Jagla[9], Silke Haerteis[10], Thiha Aung[10,11], Christine Wagner[2], Maria Kolodziejczyk[2], Stefanie Heinke[2], Evan H Stanton[2], **Barbara Schwertner[1]**, Dania Riegel[7], Christian H Wetzel[4], Wolfgang Buchalla[3], Martin Proescholdt[12], Christoph A Klein[13], Mark Berneburg[1], Hans J Schlitt[2], Thomas Brabletz[14], Christine Ziegler[8], Eric K Parkinson[15], Andreas Gaumann[9], Edward K Geissler[2], Jerzy Adamski[6,16,17], Sebastian Haferkamp[1,*], Maria E Mycielska[2,*]

1: Department of Dermatology, University Medical Centre, Regensburg, Germany

2: Department of Surgery, University Medical Center, Regensburg, Germany

3: Department of Conservative Dentistry and Periodontology, University Medical Center, Regensburg, Germany

4: Department of Psychiatry and Psychotherapy, University of Regensburg, Regensburg, Germany

5: Institute of Clinical Chemistry and Laboratory Medicine, Regensburg University Hospital, Regensburg, Germany

6: Research Unit Molecular Endocrinology and Metabolism, Helmholtz Zentrum München, German Research Centre for Environmental Health, Neuherberg, Germany

7: Regensburg Center for Interventional Immunology, Regensburg, Germany

8: Department of Structural Biology, Institute of Biophysics and Physical Biochemistry, University of Regensburg, Regensburg, Germany

9: Institute of Pathology, Kaufbeuren-Ravensburg, Kaufbeuren, Germany

10: Institute for Molecular and Cellular Anatomy, University of Regensburg, Regensburg, Germany

11: Center of Plastic, Aesthetic, Hand and Reconstructive Surgery, University of Regensburg, Regensburg, Germany

12: Department of Neurosurgery, University Hospital Regensburg, Regensburg, Germany

13: Experimental Medicine and Therapy Research, University of Regensburg, Regensburg, Germany

14: Department of Experimental Medicine 1, Friedrich-Alexander-University Erlangen, Erlangen, Germany

15: Centre for Immunobiology and Regenerative Medicine, Blizard Institute, Barts and The London School of Medicine and Dentistry, London, UK

16: Lehrstuhl für Experimentelle Genetik, Technische Universität München, Munich, Germany

17: Department of Biochemistry, Yong Loo Lin School of Medicine, National University of Singapore, Singapore

Correspondence: Sebastian.haferkamp@ukr.de, maria.mycielska@ukr.de

*: Contributed equally to this work

Manuscript information:

Life Sci Alliance. 2021 Jun; 4(6): e202000903.

Received 4 May 2020

Accepted 10 Mar 2021

Doi: 10.26508/lsa.202000903

2.4.1 Abstract

Citrate is important for lipid synthesis and epigenetic regulation in addition to ATP production. We have previously reported that cancer cells import extracellular citrate via the pmCiC transporter to support their metabolism. Here, we show for the first time that citrate is supplied to cancer by cancer-associated stroma (CAS) and also that citrate synthesis and release is one of the latter's major metabolic tasks. Citrate release from CAS is controlled by cancer cells through cross-cellular communication. The availability of citrate from CAS regulated the cytokine profile, metabolism and features of cellular invasion. Moreover, citrate released by CAS is involved in inducing cancer progression especially enhancing invasiveness and organ colonisation. In line with the in vitro observations, we show that depriving cancer cells of citrate using gluconate, a specific inhibitor of pmCiC, significantly reduced the growth and metastatic spread of human pancreatic cancer cells in vivo and muted stromal activation and angiogenesis. We conclude that citrate is supplied to tumour cells by CAS and citrate uptake plays a significant role in cancer metastatic progression.

2.4.2 Introduction

Citrate is a central metabolite used by cancer cells for fatty acid synthesis (Wang *et al.,* 2016). One path of citrate synthesis is via the reverse Krebs cycle (Metallo *et al.,* 2011). We have recently discovered that cancer cells can also import extracellular citrate by using a plasma membrane citrate transporter (pmCiC; (Mycielska *et al.,* 2018). This transporter has been cloned from the citrate releasing prostate secretory epithelial cells (Mazurek *et al.,* 2010) and determined to change citrate transport direction, depending on the cell type in which it is expressed (Mazurek *et al.,* 2010; Mycielska *et al.,* 2018). Moreover, extracellular citrate can directly promote cancer proliferation (Petillo *et al.,* 2020) and alter metabolism in vitro (Mycielska *et al.,* 2018). In addition, pmCiC was found to be overexpressed in human cancer cells compared with their benign counterparts in vivo, where it was found to correlate with tumour grade, and was particularly increased at the invasion front and metastatic sites of tumours of different origin (Mycielska *et al.,* 2018). Daily application of a specific pmCiC inhibitor, gluconate, slowed xenograft growth in vivo by incompletely understood mechanisms (Mycielska *et al.,* 2018; Mycielska *et al.,* 2019).

There is now extensive evidence that human cancer cells can induce neighbouring stromal cells to produce proteins and metabolites that aid tumour development, progression, and drug resistance (Nazemi & Rainero, 2020). The metabolites documented include nucleotides, lactate, and amino acids such as serine and glutamine (Nazemi & Rainero, 2020), but the role of citrate in crosstalk between tumour cells and the tumour microenvironment has hitherto not been investigated in this regard. One route of citrate supplied to cancer could be through blood. Citrate blood concentration is around 200 μM (Mycielska *et al.,* 2015). However, blood supply to growing tumours is often restricted and metastatic growth requires new blood vessel formation. Another source of extracellular citrate could be tumour-surrounding tissue known to have elevated citrate levels, for example, benign prostate epithelium (Eidelman *et al.,* 2017) or astrocytes in the brain (reviewed by (Mycielska *et al.,* 2015)).

Cancer-associated fibroblasts (CAFs) have already been shown to support cancer metabolism by releasing several growth factors, enzymes, and metabolites (Sakamoto *et al.,* 2019). The main objective of this study was to determine whether CAFs/cancer-associated stromal cells are the source of extracellular citrate to cancer cells and the effects of extracellular citrate on cancer metastatic progression.

We report evidence that CAFs are a substantial source of citrate for cancer cells and that CAFs release citrate via the pmCiC. Importantly, the metabolic activity of CAFs depends strongly on the availability of citrate to cancer cells suggesting that citrate synthesis and release is one of the main metabolic tasks of CAFs. We also show that extracellular citrate plays a role in the induction of an invasive phenotype and subsequent organ colonisation by cancer cells. Consistent with this observation, daily treatment of mice with gluconate (a specific inhibitor of

pmCiC in cancer cells) significantly reduced cancer spread, stromal transformation, angiogenesis, and increased immune infiltration. Citrate is, therefore, a critical element of the cross-talk between cancer cells and cancer-associated surrounding tissue and the presence of extracellular citrate is crucial for metastatic progression.

2.4.3 Materials and Methods

Cell culture

Cell lines PC-3M, PNT2-C2, and L3.6pl were grown as described previously (Mycielska *et al.,* 2018). Adult human dermal primary fibroblasts were derived from the skin biopsies of healthy donors as described by (Milenkovic *et al.,* 2018). Naive human hepatic stellate cell line hHSC (iX Cells Biotechnologies) and two permanently activated human hepatic stellate cell lines LX2 and HSChTERT (Meyer *et al.,* 2017) were cultured as depicted before (Schmidt *et al.,* 2018). The following chemicals were used: citric acid and Na+-gluconate (Sigma-Aldrich), and dialyzed serum (PAN Biotech GmbH). The following antibodies were used: pmCiC antibodies ((Mazurek *et al.,* 2010); custom-made by GenScript Inc.), SLC25A5, vimentin, Slug, Snail, EGFR, E-cadherin, N-cadherin (Cell Signalling), SLC6A14, Glut1, Ki67, pan cytokeratin (Abcam), TGFβ-RII, PDGFRα (Santa Cruz Biotechnology), and TUNEL (R&D Systems). Experimental media consisted of glucose-free Roswell Park Memorial Institute 1640 medium (RPMI-1640) (Lonza), 5% dialyzed serum, 2 mM glutamine, 0.5 g/l glucose, and ±200 μM citrate, unless otherwise stated. The incubation time varied between 48 h, 2 wk, and over 2 mo, as specified. Western blots were analysed by measurement of the pixel density using ImageJ software (Laboratory for Optical and Computational Instrumentation [LOCI], University of Wisconsin-Madison).

For conditioning, the cells were plated at 1×10^6 (PC-3M) or 2×10^6 (L3.6pl) per T75 flask in regular growth media for 24 h (PC-3M) or 48 h (L3.6pl). After that, they were incubated in RPMI or DMEM, respectively, with 0.5% FBS and 2 mM glutamine for 48 h (Figure S 8). Media were then collected, filtered, and supplemented with 2 g/l (PC-3M) or 4 g/l (L3.6pl) glucose and 2 mM glutamine to avoid starvation. Fibroblasts were grown in conditioned media for 72 h and collected for further analysis. To study the extracellular citrate effect on fibroblast activation, PC-3M cells were preincubated in RPMI media with 5% dialyzed serum, 2 mM glutamine, 0.5 g/l glucose, and with or without 200 μM citrate. After 48 h, media were changed to conditioning media and the procedures were carried out as described above. Hepatic stellate cells were exposed to regular medium (10% FBS), low serum medium (1% FBS), and conditioned medium from PC-3M and L3.6pl for 48 h (LX2, HSChTERT) or 72 h (hHSC); afterwards cells were harvested and pmCIC expression was measured by Western blot.

Seahorse assay

3×10^4 primary dermal fibroblasts cells were grown in XFp eight well miniplates (Agilent Technologies) at 37°C, humidified air, and 5% CO2/95% air. Cartridges were prepared according to the manufacture's recommendations. The XFp Cell Mito Stress Test Kit (Agilent Technologies) contained the mitochondrial stress compounds oligomycin (1 μM), FCCP (2 μM), and rotenone/antimycin A (1 μM). Oxygen consumption rate and extracellular acidification

rate (ECAR) were measured by means of an XFp Seahorse Flux Analyzer (Agilent Technologies) and were normalised by cell number. Directly after measurement, the cells were fixed and stained with Hoechst 33342. The cell number per well were counted using ImageJ software.

Cytokine detection and citrate measurements

To measure the release of cytokines, Human Cytokine Antibody Array from RayBiotech was used. Conditioned media were collected from cancer cells as summarised in Figure S 10. Cytokine values from the unconditioned media used for conditioning were subtracted from the values obtained in the media from cancer cells. Consequently, cytokine levels in the media from cancer cells were subtracted from the values obtained in the media from fibroblasts. The kit was used according to the manufacturer's instructions and analysed using supplied positive and negative controls for all the assays. We used the same control media for all conditions tested, and all the membranes were prepared at the same time. The values between different cell types were not compared, but the trend in cytokines released is presented on separate graphs for all conditions tested.

Citrate in the media from fibroblasts was measured using Citrate assay kit (Sigma-Aldrich) according to the manufacturer instructions.

Inhibition of citrate binding to pmCiC analysed by fluorescence quenching

pmCiC was expressed in Sf9 cells using the Baculo-Virus System. Membranes were prepared by sequential centrifugation and solubilized with 2% vol/vol dodecylmaltoside. pmCiC was purified via His-Tag Ni-NTA chromatography and brought to a final concentration of 0.1 mg/ml for fluorescence quenching titration experiments using a JASCO Cary Eclipse spectrometer. The excitation wavelength was set to 285 nm, and emission was measured in between 200 and 500 nm. Trp quenching was detected at different concentrations of citrate in the absence and presence of gluconate. Relative changes in the fluorescence amplitude at 375 nm was plotted against citrate or gluconate concentration and fitted with Hill equation. The double reciprocal plot of fluorescence change against citrate concentration was fitted with a non-linear model. Kd values were determined from rectangular hyperbolic binding models and plotted against respective gluconate concentrations. Amplitude, that is, the maximal change of fluorescence during citrate titration was plotted against respective gluconate concentrations. A previously constructed homology model of pmCiC with citrate and gluconate docked to it (Mycielska *et al.,* 2018) was investigated by for putative trp quenching radii by sulfur using the program UCSF Chimera (Mycielska *et al.,* 2018).

Non-targeted metabolomics

Non-targeted metabolomics analysis of the cell media was conducted at the Genome Analysis Center, Research Unit Molecular Endocrinology and Metabolism, Helmholtz Zentrum

München. The samples were stored at −80°C before analysis. On the day of extraction, the samples were thawed on ice and were randomized before 100 µl of each sample was pipetted into a well in a 2-ml 96-well plate. In addition to samples from this study, a pool of samples of the study was aliquoted into aliquots of 100 µl. The aliquots were distributed in six wells of the 96-well plate and were extracted as the samples of the study. Besides those samples, 100 µl of human reference plasma sample (Seralab) was also extracted as the samples of the study. These samples served as technical replicates throughout the data set to assess process variability. In addition, 100 µl of water was extracted as samples of the study and placed in six wells of each 96-well plate to serve as process blanks.

Protein was precipitated and the metabolites in the samples were extracted with 475 µl methanol, containing four recovery standard compounds to monitor the extraction efficiency. After centrifugation, the supernatant was split into four aliquots of 100 µl each onto two 96-well microplates. The first two aliquots were used for LC–MS/MS analysis in positive and negative electrospray ionization mode. Two further aliquots on the second plate were kept as a reserve. The samples were dried on a TurboVap 96 (Zymark, Sotax). Before LC–MS/MS in positive ion mode, the samples were reconstituted with 50 µl of 0.1% formic acid and those analysed in negative ion mode with 50 µl of 6.5 mM ammonium bicarbonate, pH 8.0. Reconstitution solvents for both ionization modes contained further internal standards that allowed monitoring of instrument performance and also served as retention reference markers. To minimize human error, liquid handling was performed on a Hamilton Microlab STAR robot (Hamilton Bonaduz AG).

LC–MS/MS analysis was performed on a linear ion trap LTQ XL mass spectrometer (Thermo Fisher Scientific GmbH) coupled with a Waters Acquity UPLC system (Waters GmbH). Two separate columns (2.1 × 100 mm Waters BEH C18 1.7 µm particle) were used for acidic (solvent A: 0.1% formic acid in water, solvent B: 0.1% formic acid in methanol) and for basic (A: 6.5 mM ammonium bicarbonate, pH 8.0, B: 6.5 mM ammonium bicarbonate in 95% methanol) mobile phase conditions, optimized for positive and negative electrospray ionization, respectively. After injection of the sample extracts, the columns were developed in a gradient of 99.5% A to 98% B in 11 min run time at 350 µl/min flow rate. The eluent flow was directly connected to the ESI source of the LTQ XL mass spectrometer. Full-scan mass spectra (80–1,000 m/z) and data-dependent MS/MS scans with dynamic exclusion were recorded in turns. Metabolites were annotated by curation of the LC–MS/MS data against proprietary Metabolon's chemical database library (Metabolon, Inc.) based on retention index, precursor mass, and MS/MS spectra. In this study, 109 metabolites, 63 compounds of known identity (named biochemical), and 46 compounds of unknown structural identity (unnamed biochemical) were identified. The unknown chemicals are indicated by a letter X followed by a

number as the compound identifier. The metabolites were assigned to cellular pathways based on PubChem, KEGG, and the Human Metabolome Database.

Cell collection, homogenization, and targeted metabolomics

The medium was aspirated, the PC-3M cells were quickly washed twice with 2 ml warm PBS, and their metabolism was subsequently quenched by the addition of pre-cooled (dry ice) 300 µl extraction solvent, a 80/20 (vol/vol) methanol/water mixture. Cells were scraped off the culture vessel using rubber tipped cell scrapers (Sarstedt) and together with the solvent collected in pre-cooled micro tubes (0.5 ml; Sarstedt). The culture well was rinsed with another 100 µl extraction solvent, and the liquid was also transferred to the tube. The samples were stored at −80°C until further use.

For homogenization, 80-mg glass beads (0.5 mm, VK-05; PeqLab) were added to the cell samples, which were homogenized using the Precellys24 homogenizer at 0–3°C for two times over 25 s at 3,720g with a 5-s pause interval.

To normalize the obtained metabolomics data from cell homogenates for differences in cell number, the DNA content was determined using a fluorescence-based assay for DNA quantification. The assay was performed as previously described (Muschet *et al.,* 2016). Briefly, the fluorochrome Hoechst 33342 (10 mg/ml in water; Life Technologies, Thermo Fisher Scientific) was diluted in PBS to the final concentration of 20 µg/ml. 80 µl of this dilution was applied to each well of a black 96-well plate (F96, Nunc; Thermo Fisher Scientific). After brief vortexing of the cell homogenates, 20 µl of the sample was added to the Hoechst 33342 dilution to gain 100 µl of total volume per well and mixed by pipetting. Each sample was applied to the plate in four replicates. 20 µl extraction solvent was used for blank measurements. The plate was incubated at room temperature in the dark for 30 min and the fluorescence was read using a GloMax Multi Detection System (Promega) equipped with an UV filter (λEx 365 nm, λEm 410–460 nm; Promega). Subsequently, the samples were centrifuged at 4°C and 11,000g for 5 min, and 10 µl of the supernatant was used for the metabolite quantification.

The targeted metabolomics approach was based on liquid chromatography-electrospray ionization-tandem mass spectrometry (LC-ESI-MS/MS) and flow injection-electrospray ionization-tandem mass spectrometry (FIA-ESI-MS/MS) measurements by AbsoluteIDQ p180 Kit (BIOCRATES Life Sciences AG). The assay allows simultaneous quantification of 188 metabolites out of 10 µl plasma and includes free carnitine, 39 acylcarnitines (Cx:y), 21 amino acids (19 proteinogenic + citrulline + ornithine), 21 biogenic amines, hexoses (sum of hexoses–about 90–95% glucose), 90 glycerophospholipids (14 lysophosphatidylcholines [lysoPC] and 76 phosphatidylcholines [PC]), and 15 sphingolipids (SMx:y). The abbreviations Cx:y are used to describe the total number of carbons and double bonds of all chains, respectively (for more details see (Römisch-Margl *et al.,* 2012). For the LC-part, compound identification and

quantification were based on scheduled multiple reaction monitoring measurements (sMRM). The method of AbsoluteIDQ p180 Kit has been proven to be in conformance with the EMEA-Guideline “Guideline on bioanalytical method validation (21 July, 2011),” which implies proof of reproducibility within a given error range. Sample preparation and LC–MS/MS measurements were performed as described in the manufacturer in manual UM-P180. Analytical specifications for limit of detection (LOD) and evaluated quantification ranges, further LOD for semiquantitative measurements, identities of quantitative and semiquantitative metabolites, specificity, potential interferences, linearity, precision and accuracy, reproducibility, and stability were described in Biocrates manual AS-P180. The LODs were set to three times the values of the zero samples (extraction solvent). The LLOQ and ULOQ were determined experimentally by Biocrates.

The assay procedures of the AbsoluteIDQ p180 Kit as well as the metabolite nomenclature have been described in detail previously (Römisch-Margl *et al.,* 2012; Zukunft *et al.,* 2013).

Sample handling was performed by a Hamilton Microlab STAR robot (Hamilton Bonaduz AG) and an Ultravap nitrogen evaporator (Porvair Sciences), beside standard laboratory equipment. Mass spectrometric analyses were carried out on an API 4000 triple quadrupole system (Sciex Deutschland GmbH) equipped with a 1200 Series HPLC (Agilent Technologies Deutschland GmbH) and a HTC PAL auto sampler (CTC Analytics) controlled by the software Analyst 1.6. Data evaluation for quantification of metabolite concentrations and quality assessment was performed with the software MultiQuant 3.0.1 (Sciex) and the MetIDQ software package, which is an integral part of the AbsoluteIDQ Kit. Metabolite concentrations were calculated using internal standards and reported in micrometres.

In addition to the investigated samples, five aliquots of a pooled reference plasma (Ref_Plasma-Hum_PK3) were analysed on each kit plate. The results of these reference plasma aliquots can be used for calculation of potential batch effects and data normalization (of different studies).

Mitochondrial toxicity test

Mitochondrial ToxGlo Assay by Promega was used. Cells were preincubated with either control medium or medium containing 200 µM citrate for 48 h. The assay was performed according to the manufacturer’s instructions. As recommended, galactose was used instead of glucose. Highest citrate concentrations were set to be at 10 mM, highest gluconate concentrations were set to be at 600 µM.

Immunohistochemistry

Human tissue (use granted by the Ethics Commission of the University of Regensburg, number 14-101-0263) was stained with pmCiC specific antibody, as described before (Mazurek *et al.,* 2010). Expression of the pmCiC in cancer cells and cancer-associated stroma was assessed

by scanning up to 20 high-power fields from one slide (Zeiss Microscope Axiovision). The total number of positive stained tumour cells was counted and depicted in percentage of all tumour cells. The same method was applied for the assessment of stromal cells.

To calculate the relative number of the immune cells in liver metastasis, we have used ImageJ software. Two border and two middle areas of 250 μm by 250 μm were evaluated for each metastasis (four per experimental group). For each area the number of nuclei and immune cells were calculated. The results were expressed as a ratio of the number of immune cells to the total number of nuclei per area.

Scanning electron microscopic imaging

PC-3M cells and fibroblasts were plated on plastic coverslips (Sarstedt) and left to grow in normal media for 24 h. The media were then changed into experimental media as described before. The cells were fixed with 2.5% glutaraldehyde for 4 min and washed with Sörensen buffer (Morphisto). Immediately before HVSEM imaging, the coverslips were washed in aqua millipore and then exposed to ascending series of ethanol (Merck) before critical point drying (Balzers CPD 030). The coverslips were mounted onto aluminium stubs using self-adhesive carbon discs (Baltic Praeperation). Coverslips were platinum sputter–coated (Bal-tec SCD 005; Pt-target: Baltic Praeperation) and introduced into the specimen chamber of the FEI Quanta 400 FEG electron microscope under high vacuum conditions. The angulation of the specimen to the beam was 90°. Images were taken using the Everhart-Thornley detector detector at a working distance of 10 mm and an accelerating voltage of 4 kV at 2,000× original magnification. Cells with round body and a distinct pseudopodium extended in one direction were considered as ameboidal, cells with no contact with other cells or cells with no more than 20% contact with others cells were considered as single.

Lipidomics

Lipids were quantified by direct flow injection electrospray ionization tandem mass spectrometry (ESI-MS/MS) in positive ion mode using the analytical setup and strategy described previously (Liebisch *et al.,* 2004; Liebisch *et al.,* 2006). A fragment ion of m/z 184 was used for phosphatidylcholine (PC), sphingomyelin (SM) (Liebisch *et al.,* 2004) and lysophosphatidylcholine (LPC) (Liebisch *et al.,* 2002). The following neutral losses were applied: phosphatidylethanolamine (PE) 141, phosphatidylserine (PS) 185, phosphatidylglycerol (PG) 189, and phosphatidylinositol (PI) 277 (Matyash *et al.,* 2008). PE-based plasmalogens (PE P) were analysed according to the principles described by Zemski-Berry and Murphy (Zemski Berry & Murphy, 2004). Sphingosine based ceramides (Cer) and hexosylceramides (HexCer) were analysed using a fragment ion of m/z 264 (Liebisch *et al.,* 1999). Free cholesterol and cholesteryl ester were quantified using a fragment ion of m/z 369 after selective derivatization of free cholesterol (Liebisch *et al.,* 2006). Lipid species were

annotated according to the recently published proposal for shorthand notation of lipid structures that are derived from mass spectrometry (Liebisch *et al.,* 2013). Glycerophospholipid species annotation was based on the assumption of even numbered carbon chains only. SM species annotation is based on the assumption that a sphingoid base with two hydroxyl groups is present.

Statistical analysis for non-targeted metabolomics

Statistical analysis was performed using R (version 3.6.1) (R Core Team, 2018). Assay-specific quality control was used to correct for not available (NA) values, by minimum value imputation [min/sqrt(2)] with a random permutation. The randomizing factor was located in the range of 0.75 times to 1.25 times min/sqrt(2).

Metabolites which had to be excluded because of having more than 40% NA (entries for which the measurement did not yield any information as to the peak area) over all samples were 3,4-hydroxyphenyl-lactate, 4-acetamidobutanoate, creatinine, γ-glutamylisoleucine, γ-glutamylleucine, glutathione (oxidized) GSSG, hippurate, N-acetylmethionine, N1-methylguanosine, pro-hydroxy-pro, and pseudouridine as well as the unknown metabolites X-15382, X-15484, X-16266, X-17105, X-17121, and X-18225.

Statistics testing was carried out using Mann–Whitney U test with Bonferroni correction for multiple testing. Normal data distribution could not be detected by Shapiro–Wilk test. Significance was set at the $P < 0.05$ level, additionally a partial least squares-discriminant analysis (PLS-DA) was performed in R.

Statistical analysis for targeted metabolomics

NA (entries for which the measurement did not yield any information as to the concentration) imputation was performed for metabolites with less than 40% missing values. Metabolites with more than 40% missing values were discarded. These excluded metabolites (or metabolite ratios) were found to be as follows:

ADMA, α-AAA, c4-OH-Pro, Carnosine, DOPA, Dopamine, Nitro-Tyr, SDMA, Serotonin, PC ae C42:4, SM (OH) C14:1, SM C26:0, ADMA/Arg, SDMA/Arg, and Serotonin/Trp.

Also, metabolites of the reference samples were checked for coefficients of variation of more than 25% in their respective reference samples. The following metabolites were detected to be in violation of this criterium and subsequently removed:

C5-DC (C6-OH), Histamine, PEA, Spermine, lysoPC a C26:0, lysoPC a C26:1, lysoPC a C28:0, lysoPC a C28:1, PC aa C24:0, PC aa C26:0, and PC ae C30:1.

Statistics testing was carried out using t test with Benjamini–Hochberg correction for multiple testing. Significance was set at the $P < 0.05$ level. Log-normal data distribution was detected by Shapiro-Wilks normality test. In addition, a PLS-DA was performed in R.

In vivo experiments

Mouse experiments were conducted according to the regulations of the State of Bavaria (permission granted by Regierung von Unterfranken, 55.2-2532.1-34/14 for subcutaneous (Mycielska *et al.,* 2018) and AZ 55.2-2532-2-805 intrasplenic model, respectively). In the intrasplenic injection model, L3.6pl cells (1×10^5 cells per animal) were injected into the lower spleen pole of athymic nude mice (13 animals per group; age: 6–8 wk, Crl:NU(NCr)-Foxn1nu, Charles River). To avoid side effects of intrasplenic "primary tumours," the spleen was removed 15 min after tumour cell injection. Treatment started on day 1 after tumour cell injection and comprised daily intraperitoneal injection of sodium gluconate (500 mg/kg/d); the control group was injected with NaCl only. After 24 d the mice were euthanized. Upon necropsy, livers were dissected and processed for further analyses. Hepatic tumour load was evaluated by a macroscopic score (0 = no tumour load; 1 = small singular tumours; 2 = large singular tumours; 3 = confluent tumours in less than half of liver; 4 = confluent tumours in more than half of liver; 5 = tumours in all liver segments).

The 3D in vivo tumour model (CAM, chorioallantoic membrane) was carried out as described in previous publications (Feder *et al.,* 2020; Pion *et al.,* 2021; Troebs *et al.,* 2020). Fertilized chicken eggs were incubated in a ProCon egg incubator (Grumbach) at 37.8°C and 63% humidity under hourly rotation for a 4-d period until a window of ∼1 × 1 cm was cut into the eggshell and sealed again with tape. After 4-d incubation, 2×10^6 human pancreas cancer cells (L3.6pl) suspended in 30 µl Matrigel (Corning) were grafted onto the CAM. After 2 d of tumour growth, tumour was daily treated with gluconate or NaCl (control) for 5 d before tumour excision. Tumour weight was determined and tumour volume was measured using Keyence VHX-7000 microscope (Keyence Germany, Neu-Isenburg (Troebs *et al.,* 2020)).

Statistical analysis

Statistical analysis was performed using unpaired two-sided t test unless otherwise stated. Details of statistical analysis for non- and targeted metabolomics are included in the Supplemental Information.

2.4.4 Results

2.4.4.1 Availability of citrate to cancer cells determines metabolic activity of CAFs

Human fibroblasts grown in control media versus media conditioned by prostate cancer cell line PC-3M (CAFs) exhibited distinctly different metabolic characteristics (Figure S 8, Figure S 9, and Figure 23A). One of the metabolites which was released at a high level by CAFs was citrate. CAFs also released significant amounts of panthotenate, biotin, and proline. All these metabolites are involved in the support of fatty acid synthesis (panthotenate), their metabolism (biotin), or protein synthesis (proline). As observed earlier (Romero *et al.,* 2015), we also found that CAFs released increased amounts of several amino acids. Analysis of conditioned media from cancer cells and unconditioned media showed that neither of them contained citrate (Figure S 8 and Figure S 10A). Therefore, it can be deduced that citrate present in the media from transformed fibroblasts is exclusively due to the synthesis and release from CAFs. Furthermore, the levels of pyruvate which can be used by cells for intracellular citrate synthesis remained the same in the conditioned media from cancer cells and fibroblasts, suggesting that pyruvate does not play a significant role in CAF's support of cancer metabolism.

Release of citrate indicated that this metabolite might play an important role in the crosstalk between cancer cells and CAFs. Therefore, we decided to study the differences in the way stroma is transformed in response to cancer cells preincubated without or with extracellular citrate (CM PC-3M−cit and CM PC-3M+cit, respectively; Figure S 10B and C). Cancer cells were preincubated with, or without citrate for 48 h, and the medium was removed and replaced with the citrate-free media used for conditioning for another 48 h. To determine the effects of extracellular citrate only, under all experimental conditions for cancer cells and fibroblasts and at each step of the experimental procedure, glucose and glutamine were supplied in excess to allow for unlimited intracellular citrate synthesis (Figure S 10). Using the Seahorse instrument, we determined that CAFs transformed with the CM PC-3M−cit media showed a significant increase in their O_2 consumption and glycolytic activity as compared with CAFs transformed with the CM PC-3M+cit media (Figure 21A). Increased O_2 consumption was insensitive to mitochondrial blockers, suggesting non-mitochondrial use of the oxygen. Correspondingly, there was also a significant decrease in mitochondrial ATP synthesis. CAFs transformed by CM PC-3M−cit expressed high level of glycolysis, whereas CAFs transformed with the CM PC-3M+cit media used predominantly OXPHOS to synthesise ATP. Media from fibroblasts grown in either CM PC-3M−cit or CM PC-3M+cit were then examined for citrate content. We found that the level of citrate in media from fibroblasts stimulated with CM PC-3M−cit were significantly higher (~300 μM, Figure 21B) than the concentration of citrate produced by fibroblasts stimulated with CM PC-3M+cit (~200 μM). These data stay in line with the metabolic

changes (Figure 21A) where fibroblasts releasing more citrate showed higher metabolic activity and a shift towards glycolysis.

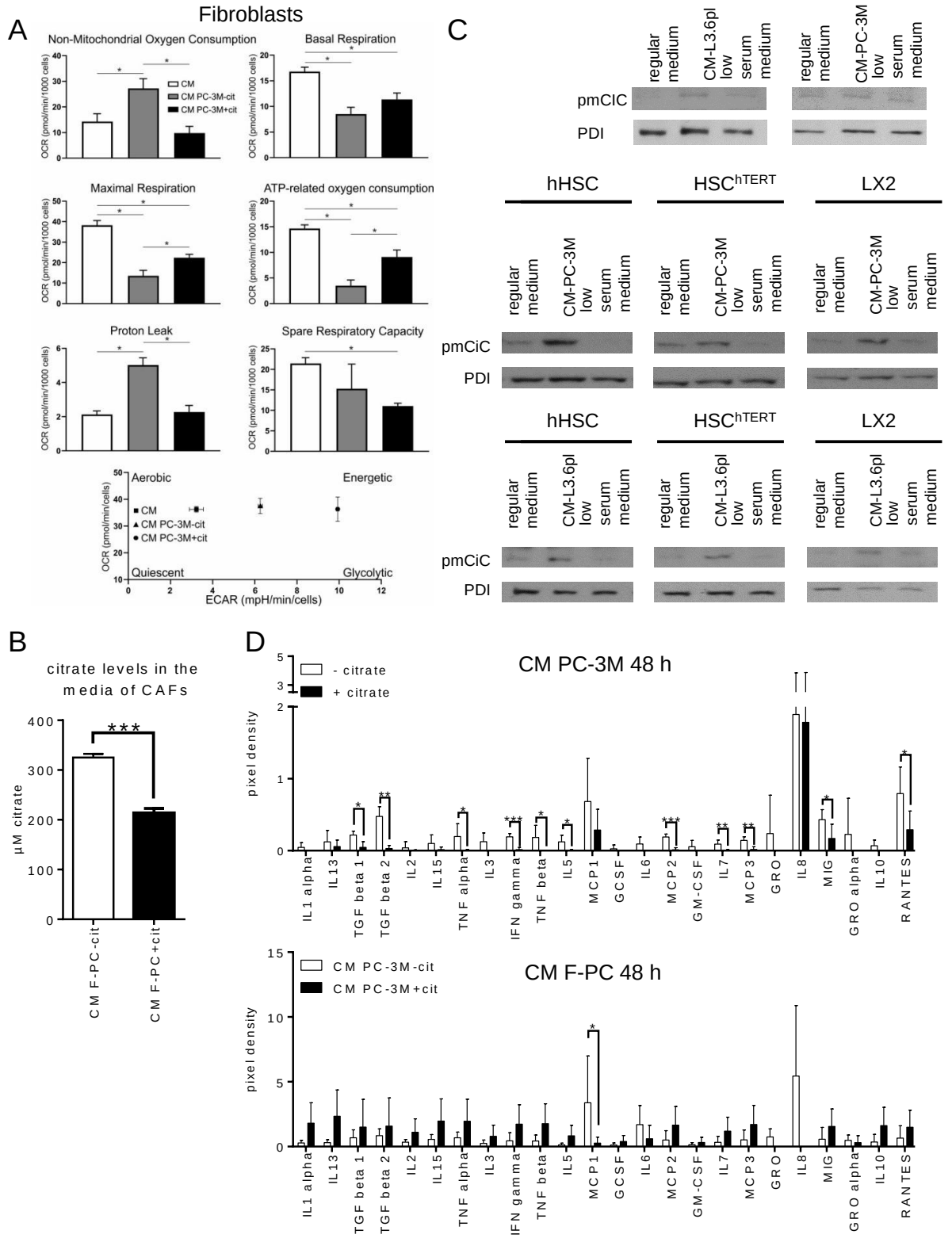

Figure 21: Cancer-associated fibroblasts release citrate through pmCiC. (A) Seahorse analysis of the metabolic characteristics and the energy map of fibroblasts grown in media used for conditioning, CM PC-3M−cit or CM PC-3M+cit (n = 4). The graphs show differences between normal fibroblasts (white), fibroblasts transformed with CM PC-3M−cit (grey), and CM PC-3M+cit (black). (B) The graph depicts citrate levels in the media from fibroblasts stimulated with CM PC-3M−cit (white) and CM PC-3M+cit (black). (C) pmCiC expression in fibroblasts and different hepatic stellate cell lines grown in

regular medium, low serum medium or transformed with conditioned media from PC-3M cells or L3.6pl cells. (D) The graphs show selected cytokines (n = 5) released from PC-3M cancer cells preincubated without or with extracellular citrate for 48 h (CM PC-3M−cit CM PC-3M+cit, respectively; upper panel) and human primary skin fibroblasts transformed by CM PC-3M−cit CM PC-3M+cit (CM F-PC−cit and CM F-PC+cit, respectively; lower panel).

It is important to note that no citrate was present in either of the conditioned media used to transform fibroblasts (Figure S 10); therefore, the obtained results are exclusively due to the presence/absence of extracellular citrate in the preincubation media of cancer cells.

Altogether, these data indicate that one of the crucial metabolites released by CAFs in support of cancer cells is citrate. The amount of citrate released and in consequence CAFs metabolic activity is determined by the availability of citrate to cancer cells.

Transformation of fibroblasts with conditioned media from the PC-3M or L3.6pl (human prostate or pancreatic cancer cells, respectively) resulted in the expression of pmCiC (Figure 21C; able to transport citrate to the extracellular space as shown already in the case of benign prostate epithelial cells; (Mazurek *et al.,* 2010)). Similarly, hepatic stellate cells, known to support metastases to liver (Milette *et al.,* 2017), incubated with conditioned media from human prostate cancer PC-3M or human pancreatic L3.6pl cells showed a significant expression of the pmCiC (Figure 21C). PmCiC expression was very low/negligible in fibroblasts and all hepatic stellate cell lines measured under control conditions (where no conditioned media from cancer cells were present; Figure 21C). It is important to note that although LX2 and $HSCh^{TERT}$ are permanently activated human hepatic stellate cell lines, they only express pmCiC after incubation with conditioned media from cancer cells. Therefore, it can be concluded that citrate synthesis and release from CAFs takes place only when it is induced by cancer cells.

To investigate the functional consequences of these metabolic alterations, we next determined the differential expression of cytokines under the above conditions. Cancer cells grown in the presence of extracellular citrate largely released cytokines known to stimulate tumour metastatic activity like MCP1 (Li *et al.,* 2013), IL-8 (Yuan *et al.,* 2005), and RANTES ((Azenshtein *et al.,* 2002); Figure 21D and Figure S 11). On the other hand, cancer cells deprived of citrate released cytokines largely associated with stromal transformation (Figure 21D and Figure S 11A-H). These included MCP2,3, IL-5, TGFβs, and GROs (although GROs are not statistically different between the groups). These cytokines were either absent in the media from cancer cells preincubated with citrate or expressed at a low level. GRO and MCP2 and 3 are known to transform stroma (Yang *et al.,* 2006; Argyle & Kitamura, 2018; Sun *et al.,* 2018), whereas IL-5 has been shown to modulate tumour environment (Zaynagetdinov *et al.,* 2015). TGFβs act on the tumour microenvironment by stimulating the transformation of fibroblasts into myofibroblasts (Papageorgis & Stylianopoulos, 2015). Release of these cytokines suggests that cancer cells deprived of citrate concentrate their efforts on transforming the surrounding stroma to get metabolic support.

In response to CM PC-3M+cit, fibroblasts released several cytokines (Figure 21D and Figure S 11) known to support cancer cell's metastatic behaviour such as IL13 (known to support cancer cell survival and metastasis; (Suzuki *et al.,* 2015)), MCP2,3 (Zhang *et al.,* 2020), and RANTES (Singh *et al.,* 2018). CM PC-3M−cit also stimulated release of different cytokines from fibroblasts but they tended (although not statistically different) to be at a lower level (Figure 21D and Figure S 11).

Next, we investigated whether citrate induced any changes in PC-3M metabolism that might account for the above phenotypes. PC-3M cells incubated with extracellular citrate showed changes at the metabolite levels. We have focused on the differences between the −citrate versus +citrate groups. In the presence of extracellular citrate, cancer cells decreased intracellular levels of metabolites associated with intracellular citrate synthesis (reviewed by (Haferkamp *et al.,* 2020). In particular, there was a comparatively low level of intracellular glutamate, glutamine, but also glycine and serine (Figure 22A). Consistently, cancer cells grown in the media not supplemented with extracellular citrate showed an increased release of citrate-synthesis related metabolites such as lactate, serine, or acetylcarnitine (Figure S 8). Compared with cancer cells preincubated without citrate, extracellular citrate supply decreased overall intracellular levels of metabolites shown best by total amounts of different metabolic groups and ratios (Figure S 12 and Figure S 13). This observation is consistent with a catabolic switch of cancer cells preincubated with citrate for 48 h associated with increased invasive activity (epithelial-mesenchymal transition [EMT]; (Cha *et al.,* 2015; Luo *et al.,* 2017; Wu *et al.,* 2019)).

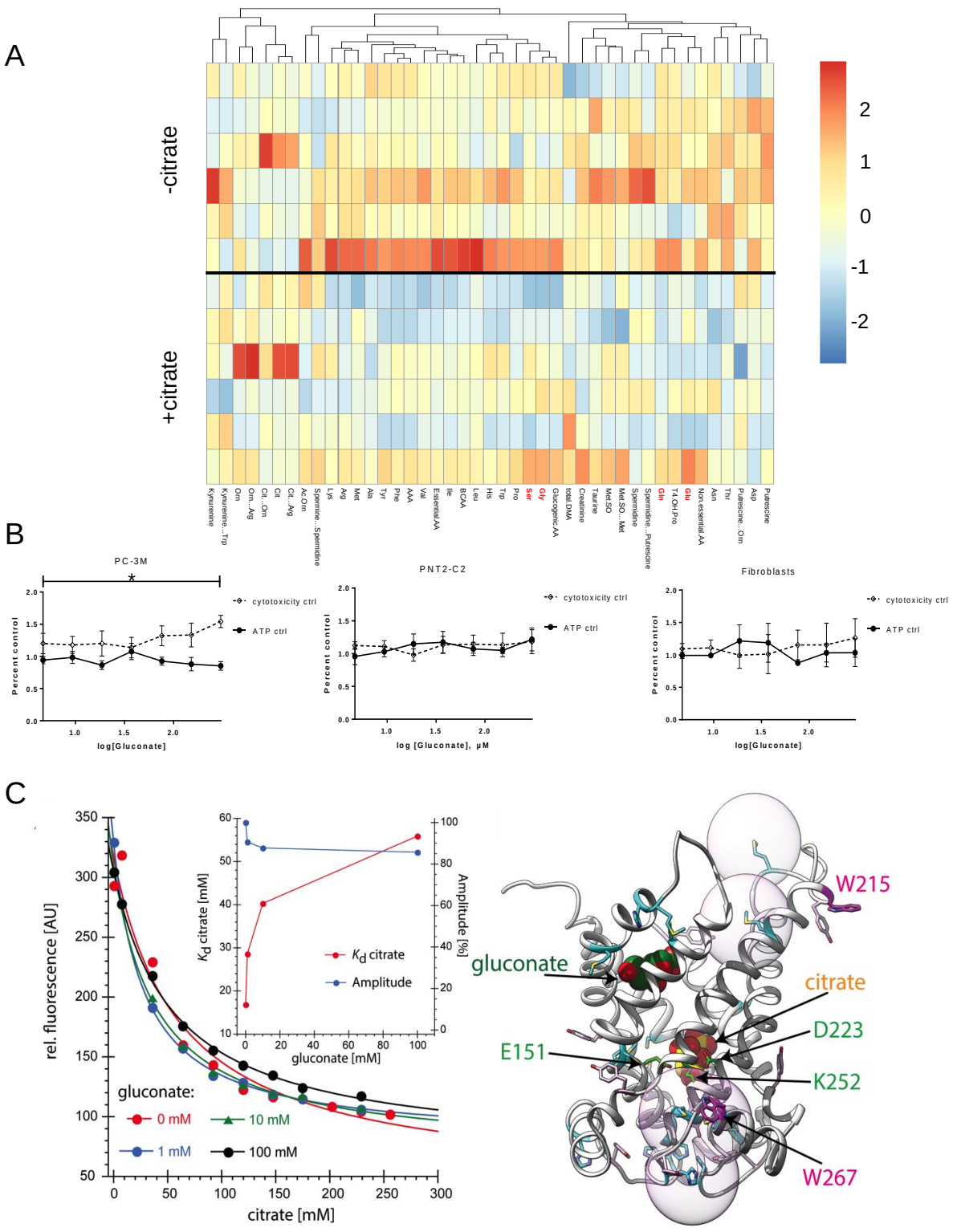

Figure 22: 48 h of preincubation with extracellular citrate induces intracellular metabolite changes. (A) Heat map of the intracellular content of amino acids of PC-3M cells grown for 48 h under control conditions or in the media supplemented with 200 µM citrate. Each row represents a separate repeat. (B) Mitotoxicity assay of different types of cells (PC-3M, PNT2-C2, human skin fibroblasts and fibroblasts transformed with conditioned media from PC-3M cells preincubated under control conditions, with extracellular citrate, with gluconate and citrate or with gluconate alone; Fig S7, n ≥ 3) showed that when applied alone at high concentration, gluconate has a cytotoxic effect on cancer cells. (C) Trp quenching at different concentrations of citrate and gluconate. Inset: Kd values determined from the Trp quenching (red) and fluorescence change amplitudes (blue) in titrations of citrate in the presence of different concentrations of gluconate. Right panel: Possible inhibition of citrate binding by gluconate binding to a

second binding site predicted by a homology model (Mycielska *et al.*, 2018). Spheres indicate Trp quenching radii by sulfur.

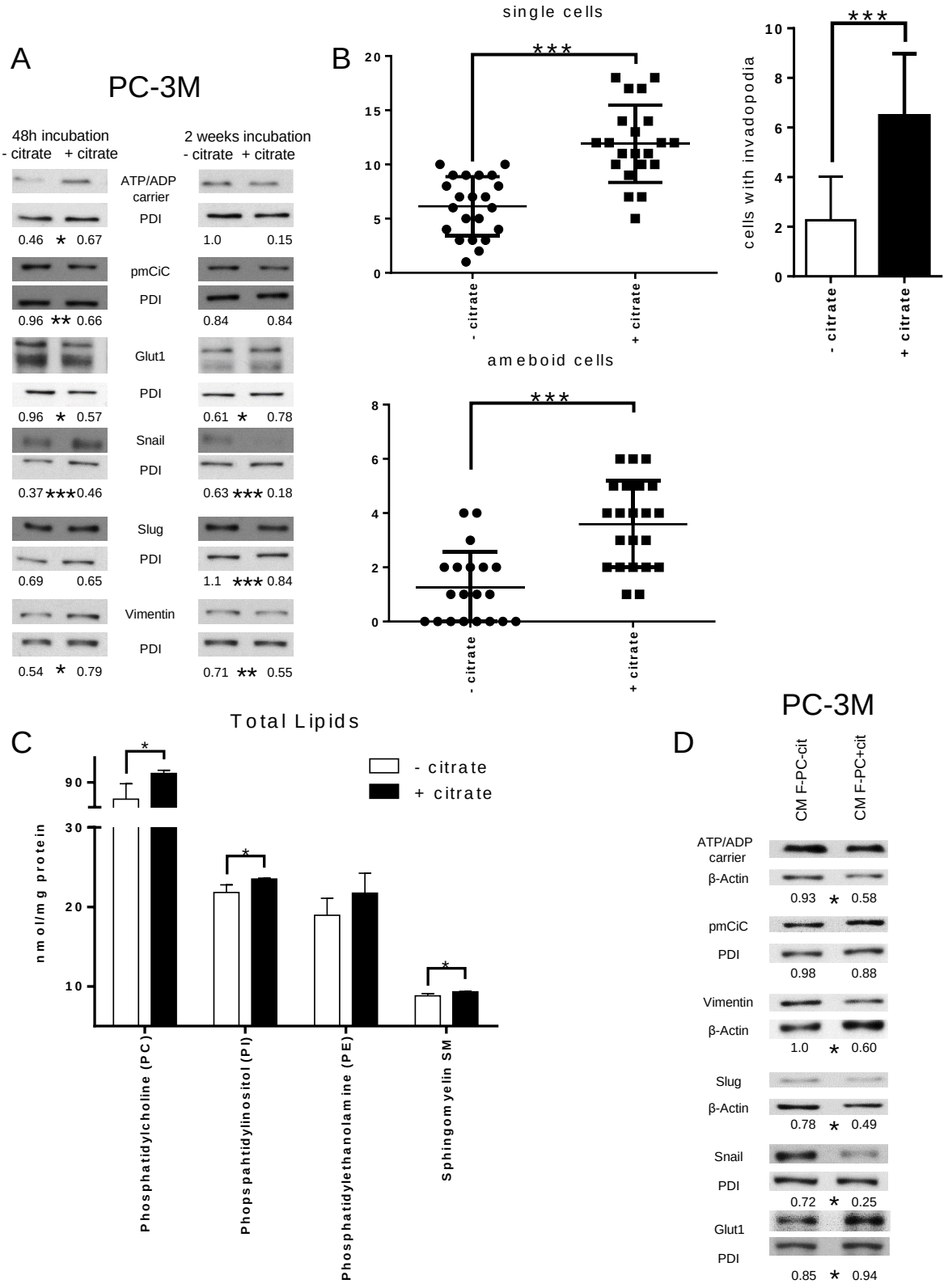

Figure 23: Citrate in the extracellular space induces metabolic changes and contributes to the metastatic status of cancer cells. (A) PC-3M cells were preincubated with or without extracellular citrate for either 48 h (left panel) or 2 wk (right panel). Western blots show typical expression of metabolic transporters and EMT/mesenchymal–epithelial transition related proteins (n ≥ 3). The numbers under

the Western blots show average normalised values obtained using densitometric analysis; stars depict statistical significance. (B) The graphs (left) represent the number of single/ameboid shaped cells in cancer cells preincubated with or without extracellular citrate for 48 h. The graphs on the right hand side show the differences in the number of cells with invadopodia between PC-3M cells grown for 2 wk with or without extracellular citrate. For each condition at least 20 different areas from three repeats were analysed. Pictures were taken with the scanning electron microscope. (C) Measurement of phosphatidylcholine (PC), phopspahtidylinositol (PI), phosphatdylethanolamine (PE), and sphingomyelin (SM) in cells under experimental conditions with or without extracellular citrate for 48 h (n = 4). (D) Western blot analysis of the expression of metabolic transporters and EMT/mesenchymal–epithelial transition–related proteins of PC-3M cells grown for 48 h in the media from fibroblasts transformed with the conditioned media from PC-3M cells preincubated for 48 h with or without extracellular citrate (CM F-PC−cit and CM F-PC+cit, respectively; right panel; n = 3). The numbers under the Western blots show average normalised values obtained using densitometric analysis; stars depict statistical significance.

We have also compared the intracellular metabolite levels of PC-3M cells preincubated without or with extracellular 200 µM citrate, with citrate and 150 µM gluconate and 150 µM gluconate alone (Figure S 14). A detailed statistical analysis confirmed differences between the groups and indicated significant metabolites (derived from the “variables of importance in projection” [VIP], Figure S 14A and B). Significant metabolites included citrate-synthesis related substrates such as glutamine, glutamate, serine as well as total amino acid levels consistent with the catabolic switch.

To check whether pmCiC expressed in cancer cells and in non-cancerous cells differ in the inhibitor profile, we have performed mitotoxicity assay. The mitotoxicity assay indicated that gluconate at the highest concentrations and in the absence of extracellular citrate is a mitochondrial toxin for PC-3M cancer cells (Figure 22B and Figure S 15A). This mitotoxic effect was not observed when gluconate was present in the media of benign cells (PNT2-C2; Figure S 15B, fibroblasts; Figure S 15C, and different groups of CAFs; Figure S 15D-G). The differences in the inhibitor profile between exporting and releasing citrate pmCiC would suggest some alteration in the structure or insertion of the transporter between the two forms of the pmCiC.

We have already established (Mycielska *et al.,* 2018) that cancer cells grown in the presence of extracellular citrate (200 µM) change their metabolism, whereas gluconate is a specific pmCiC blocker. Figure 22C shows that gluconate significantly alters citrate binding to pmCiC. It appears that gluconate binding to pmCiC does not result in a conformational change in pmCiC detectable by Trp fluorescence quenching (Figure S 16A, green curve and blue curve). Citrate on the other hand results in Trp quenching, exhibiting a Kd of 16 mM in the absence of gluconate. Elevated Kd compared with the Km values were reported also for other detergent solubilized transporters (Khafizov *et al.,* 2012). The Kd for citrate increases fourfold in the presence of 100 mM gluconate (Figure 22C). The slope of the citrate/gluconate titration suggests a further, likely allosteric, binding event (Figure S 16B). Docking of citrate and gluconate to the pmCiC model locates gluconate on top of the central citrate binding site (Figure 22C). At this position, gluconate binding would indeed not result in any Trp quenching,

for example, W215 is too far from a sulfur-containing residue such as methionine. Consequently, gluconate might increase the activation threshold while not blocking the citrate binding site during transport in a competitive manner.

2.4.4.2 The presence of extracellular citrate affects cancer cell metabolism and induces invasive phenotypes of cancer cells

We next tested how citrate affects markers known to correlate with EMT, which would be consistent with increased tumour invasiveness (Harner-Foreman *et al.,* 2017) and mesenchymal–epithelial transition (MET) associated with metastatic colonisation (Chao *et al.,* 2010). A 48-h preincubation of cancer cells in extracellular citrate resulted in a decreased Glut1, suggesting reduced glucose uptake. Together with the increased expression of the ATP/ADP carrier, this change is consistent with a switch towards OXPHOS (Figure 23A top left panel) reported to be associated with EMT (Ippolito *et al.,* 2016). 2 wk incubation of cancer cells with extracellular citrate compared with control conditions suggests a metabolic switch towards anaerobic glycolysis consistent with proliferation/colonizing step ((Faubert *et al.,* 2020); as shown by increased Glut1 expression; Figure 23A top right panel).

Consistent with the acquisition of an invasive character as already shown by the metabolomic data and cytokine release, cancer cells preincubated with citrate for 48 h showed an increased expression of Snail and vimentin (Figure 23A left, bottom, panel; (Heldin *et al.,* 2012)). The fact that only some increased EMT features were observed is not surprising as PC-3M was derived from a prostate carcinoma metastasis and likely is already invasive. A longer, 2-wk incubation of cancer cells with extracellular citrate resulted in the opposite effect and a decrease of some EMT markers, suggesting changes consistent with MET and the colonisation stage (Figure 23A, right, bottom panel). Scanning electron micrographs revealed that also cell morphology was citrate dependent (Figure S 17). A 48 h preincubation of cancer cells with citrate resulted in more polarized, highly invasive, spindle-shaped cells with higher number of single and amoeboid cells known to correlate with the EMT phase (Figure 23B and Figure S 17A; (Friedl & Wolf, 2003); (Morley *et al.,* 2014)).

In line with the colonisation step as indicated by the markers (Figure 23A) PC-3M cells preincubated with citrate for 2 wk released mainly cytokines known to support stromal transformation like GROs, IL-8, and IL-3 (Figure S 11F). Cytokines released by PC-3M cells kept under control conditions for 2 wk showed a similar pattern as already seen after 48-h preincubation (compare Figure S 11A with Figure S 11E). This result is consistent with the lack of disease progression/cancer cell reprogramming as already determined by cell morphology and Western blot analysis of cells under control conditions (Figure 23A). Consequently, a similar pattern of cytokine release in CM F-PC−cit after 2 wk and 48 h was also observed (compare Figure S 11C with Figure S 11G). On the other hand, fibroblasts stimulated with CM

PC-3M+cit for 2 wk only released cytokines supporting angiogenesis such as IL-6 and IL-3 (Dentelli *et al.,* 2011; Nagasaki *et al.,* 2014; Masjedi *et al.,* 2018) and metastasis formation/proliferation (MCP1, (Loberg *et al.,* 2006)) correlating with the colonisation process (Figure S 11D and H).

MET occurring under long term incubation of cancer cells with extracellular citrate would also agree with the decreased (but not significantly) expression of the ATP/ADP carrier and increased Glut1 level suggesting an increase in glycolysis (Figure 23A). Increased glycolysis and lactate release could enhance proliferation of the colonizing cells (La Cruz-López *et al.,* 2019). 2-wk preincubation with extracellular citrate resulted in highly spread/flattened cells with long invadopodia, contacting the ECM and other cells consistent with the colonisation step (Figure 23B and Figure S 17B; (Williams *et al.,* 2019)). Importantly, under controlled conditions, cellular morphology remained unchanged at all times. The morphology of cancer cells grown with citrate as depicted with scanning electron microscopy seems also to indicate increased fluidity of their plasma membrane. Consistently, the level of total phosphatidylcholine, phosphatidylinositol, sphingomyelin, and phosphatidylethanolamine (although the last not significant) was increased in cancer cells grown with citrate ((Dawaliby *et al.,* 2016); Figure 23C).

We have already shown that citrate appears only in the media from CAFs and is not present at any significant level in the conditioned media from cancer cells. However, conditioned media from cancer cells contained significant amounts of cytokines, known to support aggressive cancer behaviour. To test whether cancer cell-derived cytokines and potentially other substrates are sufficient to induce changes in cancer cells, we preincubated PC-3M cells with CM PC-3M+cit or CM PC-3M−cit. We did not observe any significant and consistent changes between the two groups of cancer cells (Figure S 18A). However, incubation of PC-3M cells with CM F-PC+cit or CM F-PC−cit resulted in more pronounced differences in cancer cells (Figure 23D). These results indicate that citrate released by CAFs together with other elements might play a crucial role in supporting cancer progression.

The data above show that stromal transformation depends on the metabolic status of cancer cells. CAFs compensate for the lack of metabolites and cytokines in cancer cells to support their invasive and metastatic behaviour. From these data, we proposed that citrate availability is an important requirement for tumour progression and this was investigated further below.

2.4.4.3 Inhibition of pmCiC with gluconate in vivo decreases metastatic spread and stromal transformation

To test the role of extracellular citrate uptake in metastasis, we injected the lower spleen pole of athymic nude mice with human pancreatic cancer L3.6pl cells. To avoid side effects of intrasplenic “primary tumours,” the spleen was removed 15 min after tumour cell injection. Gluconate blockade (daily in vivo injection) of citrate uptake by metastasising human pancreatic cancer cells significantly reduced metastasis rate (Figure 24A). Reduced metastatic spread was accompanied by decreased stromal transformation (αSMA) as shown in Figure 24B. Additional controls showed that gluconate or citrate alone does not induce any changes in the αSMA expression in fibroblasts grown under standard conditions (Figure S 18B). Staining with the anti-fibroblast–activating protein (FAP) antibody showed a pronounced transformation of some stromal cells consistent with hepatic stellate cells in the control group (Figure 24C; (Wang *et al.,* 2005; Kaps & Schuppan, 2020)). This was not observed in the case of gluconate treated mice. Moreover, the size of metastases in the gluconate-treated group was on average smaller with increased immune infiltration (Figure 24D). Although FAP is not a typical immune cell marker, its expression has been previously reported in subpopulations of CD45+/CD45− cells (Jiang *et al.,* 2016).

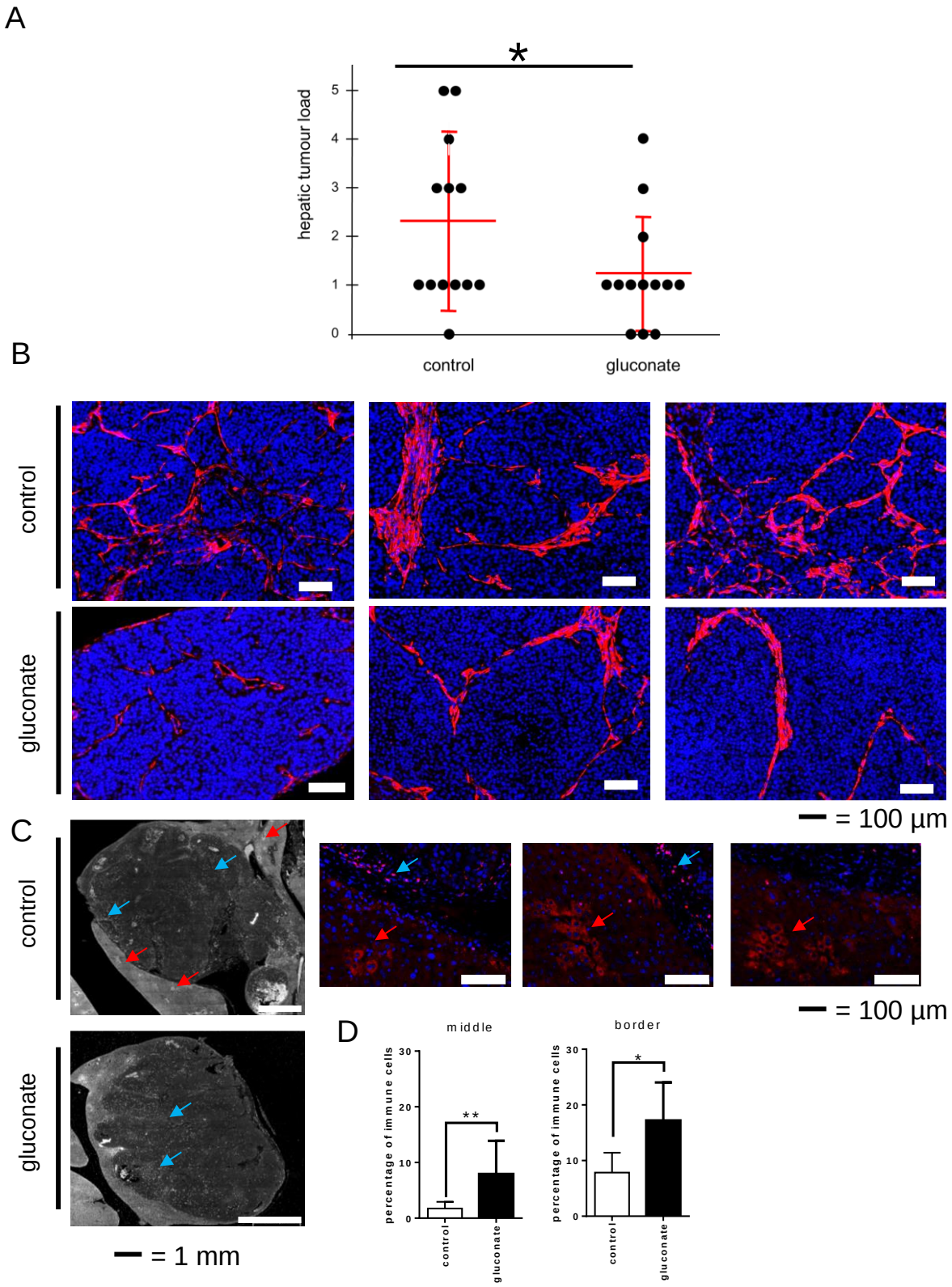

Figure 24: Blocking of citrate uptake by cancer cells decreases metastasis rate in vivo. Human pancreatic cancer L3.6pl cells were injected into the lower spleen pole of immunodeficient mice. 15 min after tumour cell injection, the spleen was removed. Animals were daily intraperitoneally injected with sodium gluconate (500 mg/kg/d), respectively, NaCl. After 24 d, mice were euthanized, and livers and laparotomy wounds were assessed. (A) Liver metastases were evaluated by a macroscopic score (0 = no tumour load; 1 = small singular tumours; 2 = large singular tumours; 3 = confluent tumours in less than half of liver; 4 = confluent tumours in more than half of the liver; 5 = tumours in all liver segments). Hepatic tumour load was significantly decreased (P = 0.046; n = 13 mice per group, one-tailed unpaired t test) in the treatment group (500 mg/kg/d sodium gluconate) compared with control group (NaCl). (B)

Pictures showing differences in the αSMA staining pattern in metastasis in mouse livers treated with gluconate versus control. (C) Liver metastasis were stained with the anti-fibroblast activating protein (FAP) antibody. Red arrows show stained area in the stroma consistent with cancer-associated cells, whereas blue arrows depict immune cells expressing FAP. Enlarged pictures from the control group (on the right) show cells stained with anti-FAP antibody (in red) in the stroma (indicated with red arrows) and immune cells (blue arrows). (D) Graphs showing average number of immune cells per total number of cells in the studied area. For these measurements two border and two central areas were calculated per metastasis. For each experimental group, four different metastases were evaluated.

Treatment of mice injected subcutaneously with human pancreatic L3.6pl cells reduced tumour growth and more importantly changed the metabolic characteristics of cancer tissues (Mycielska *et al.,* 2018). Changes in the tumour tissues were already visible from the beginning of the experiment (Figure 25A, details in (Mycielska *et al.,* 2018)). Experimental tumours in mice treated with gluconate were smaller, rounder, and paler compared to their untreated counterparts. This observation is consistent with decreased angiogenesis (as shown by CD31 staining Figure 25B) accompanied by a significant reduction of stromal transformation (α-SMA; Figure 25B). There was also an increase in apoptosis which was most pronounced at the bottom of the gluconate-treated tissues as determined by TUNEL staining (Figure 25C). In mice treated with gluconate, there was an overall decrease in the expression of PDGFRβ and vimentin (Figure 25D) particularly at the tumour–stroma interface. Decreased levels of PDGFRβ and vimentin in non-cancerous tissue are also consistent with decreased stroma transformation (Figure 25C).

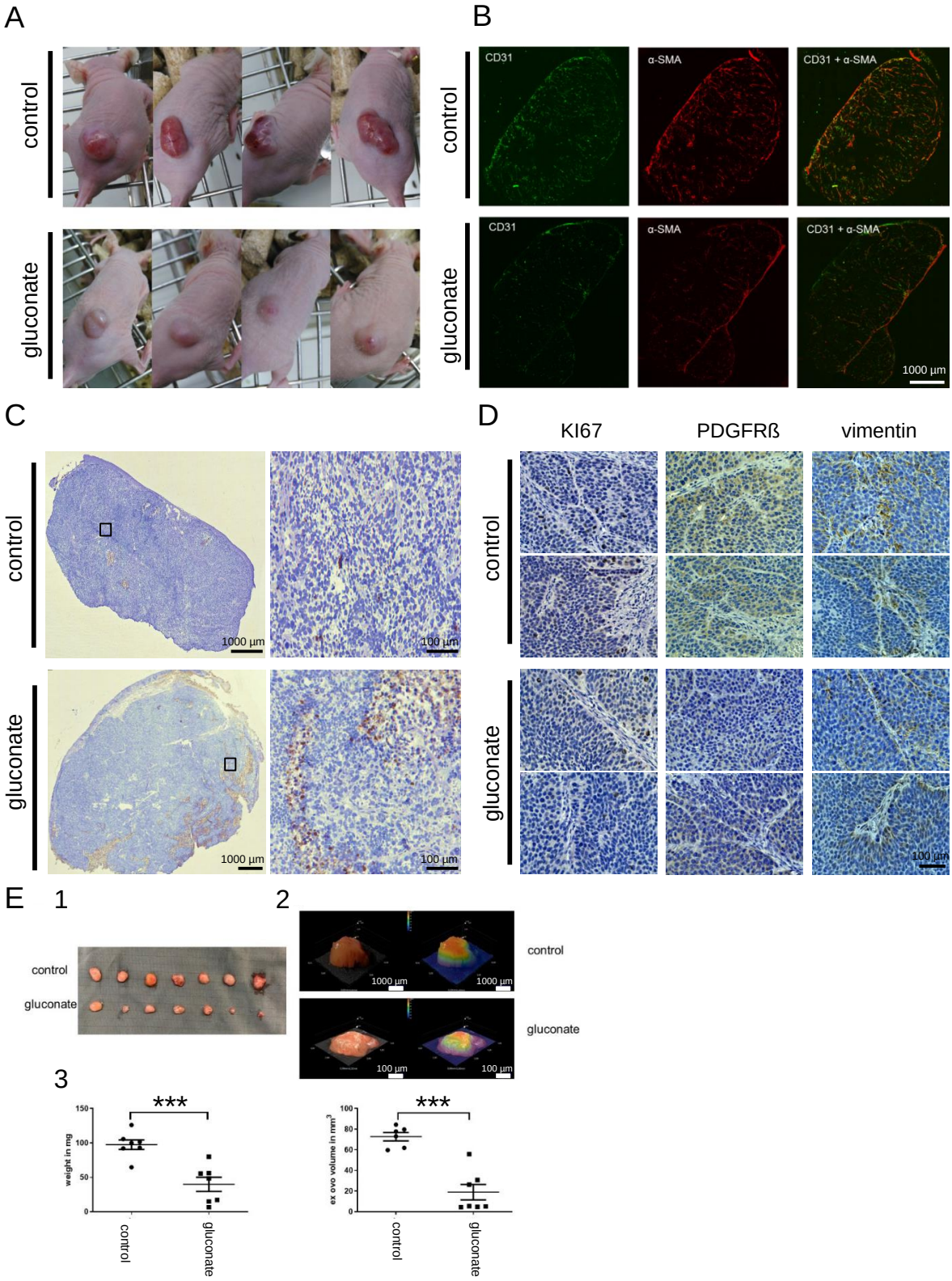

Figure 25: Gluconate treatment in vivo increases apoptosis, decreases angiogenesis, stromal transformation, proliferation and expression of PDGRβ and vimentin in cancerous tissues. Human pancreatic cancer cells L3.6pl were injected subcutaneously in nude mice. Control mice were injected with saline and treated group with Na+-gluconate (as described before, (Mycielska *et al.,* 2018)). (A) Pictures of mice showing qualitative differences between the cancerous growths in treated versus untreated animals. The photos cannot be used to compare tumour size. (B) Angiogenesis (CD31) and stromal transformation (αSMA) were also significantly decreased in the case of treated animals. (C) Staining of the sections of tumours (TUNEL) show increased apoptosis in the treated group. Moreover, apoptotic regions were mainly observed at the lower parts of the tissues. (D) Cancer cells proliferation

in the tissues was decreased (Ki67), as well as PDGFRβ and vimentin expression. (E) The CAM assay was performed using L3.6pl cells. The cells were left to grow for 2 d then NaCl was used in the control group and Na+-gluconate in gluconate group for 5 d. (1) Tumour explants after daily treatment with NaCl (upper) or Na+-gluconate (lower). (2) Examples of tumour volume measurements with the 3D digital microscope (Keyence VHX-7000 microscope). (3) Graphs showing changes in the tumour weight and tumour volume of NaCl versus gluconate treated groups.

We have also performed a CAM assay (chorioallantoic membrane) used as a 3D in vivo tumour model. Treatment of L3.6pl cells with Na^+-gluconate significantly reduced tumour growth and volume (Figure 25E) as compared with the control conditions where equivalent volume of NaCl was used.

To conclude, depriving cancer cells of citrate by applying gluconate in vivo reduced the cancer growth and metastasis rate, angiogenesis, and stromal transformation. Hence, blocking citrate uptake in vivo might result in reduced capability of tumour to progress.

2.4.4.4 pmCiC expression in cancer-associated cells in human cancerous tissues

We next tested whether our in vitro data indicating that CAFs release citrate to support cancer metabolism can be extended to the in vivo environment, by immunostaining analysis of human tissue (Figure 26A-F). Analysis of human pancreatic (Figure 26A and C) and gastric cancer glands (Figure 26B and D) as well as lymph node metastasis (Figure 26E) and lung metastasis (Figure 26F) of gastric cancer confirmed that pmCiC is expressed not only in cancer cells of different organs (Mycielska *et al.,* 2018) but also in some subsets of fibroblasts in the surrounding tumour environment. Moreover, we have also found pmCiC expressed in some of the tumour micro-vessels. This would be consistent with extracellular citrate playing a role in angiogenesis by supporting vessel formation. To complete these studies, we have assessed pmCiC expression in cancer cells and cancer-associated stromal cells of human breast, gastric and pancreatic tissues (Figure 26G). The highest expression of pmCiC in stromal cells was observed in gastric and pancreatic cancers known to intensively produce desmoplastic stroma as compared with other cancer types (Hosein *et al.,* 2020; Oya *et al.,* 2020). Therefore, targeting pmCiC might have an effect not only on cancer cells but also on the tumour's "infrastructure" (supporting cells).

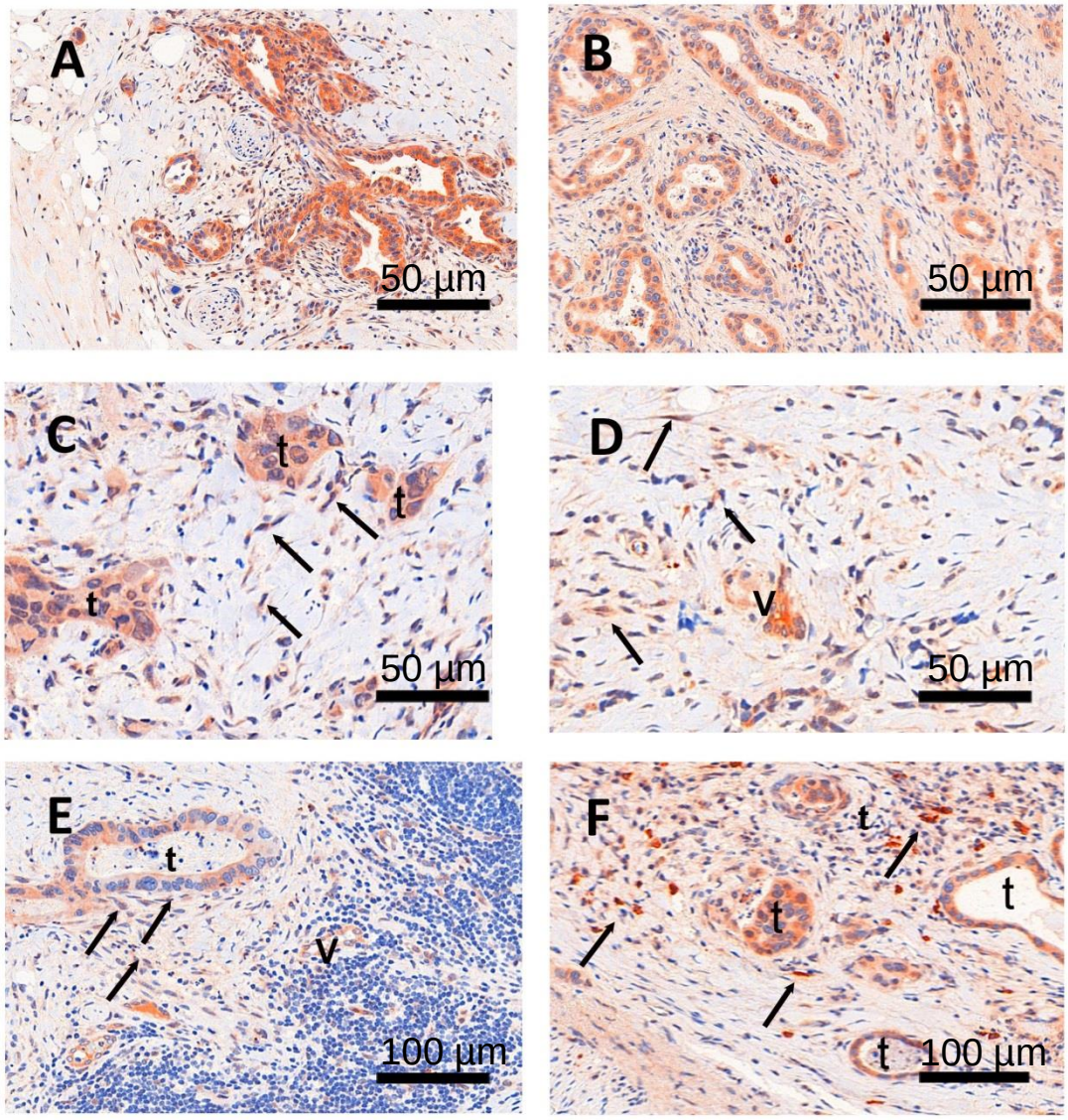

G

	number	pmCIC in tumor cells		pmCIC in stromal cells	
primary tumors:		positive	negative	positive	negative
	N	N (%)	N (%)	N (%)	N (%)
breast cancer	22	12 (55 %)	10 (45 %)	11 (50 %)	11 (50 %)
gastric cancer	11	6 (54 %)	5 (46 %)	11 (100 %)	0 (0%)
pancreas cancer	14	12 (86 %)	2 (14 %)	13 (93 %)	1 (7 %)

Figure 26: pmCiC is expressed in the stroma of human cancerous tissues. (A, B) immunohistochemical staining of pmCIC showed strong expression in human pancreatic (A) and gastric cancer glands (B) (DAB—150 µm). (C, D) In close contact to infiltrating cancer glands, there is also a prominent expression in micro-vessels (v) but also in spindle cells (→) of the tumour microenvironment (TME) in both cancer types (C, D) (DAB, — 50 µm). The latter cell type of the TME could be identified by vimentin as tumour associated fibroblasts (data not shown). (E) Consecutive examination of lymph node metastasis (E) (DAB—50 µm) demonstrate a positive tumour gland but also expression in micro-vessels (v) and fibroblasts. (F) The same was true for a metastatic gastric cancer shown in figure (F) (DAB, — 50 µm). (G) A table showing the number/percentage of human tumour tissues expressing pmCiC in cancer cells and in cancer-associated stroma cells.

2.4.5 Discussion

We have previously shown that cancer cells of different origin take up extracellular citrate through the recently cloned pmCiC (Mycielska *et al.,* 2018). In the present study, we have explored the source of citrate used by cancer cells and, importantly, its potential role in tumour progression.

We have determined that CAFs, together with other cells from the cancer environment such as hepatic stellate cells, express pmCiC with the function of citrate release (summarised in Figure S 19A and B). Increased citrate synthesis by cancer-associated stroma (CAS) is consistent with a recent report showing increased glutamine uptake by cancer-associated cells rather than by cancer cells themselves in vivo (Marin-Valencia *et al.,* 2012).

Our data show that the metabolic activity of CAFs depends on extracellular citrate availability to cancer cells; therefore, it is regulated in the cancer environment. We propose that a lack of extracellular citrate stimulates cancer cells to transform their surroundings to get the necessary substrate. In support of this, we show that cancer cells deprived of extracellular citrate for 48 h release IL-6, which stimulates angiogenesis and GROs involved in stromal transformation/senescence (Nagasaki *et al.,* 2014; Masjedi *et al.,* 2018). Indeed, senescent fibroblasts which are known to be part of the cancer environment (Yang *et al.,* 2006; Mellone *et al.,* 2016), have previously been shown to release high levels of citrate (James *et al.,* 2015). Therefore, cancer cells deprived of citrate may be selected to release factors to stimulate their surroundings to compensate for citrate deficiency. The organ colonisation step, as seen after 2 wk of incubation with extracellular citrate, was accompanied by a release of IL-3, an angiogenesis-stimulating cytokine, complemented by GROs responsible for the stromal transformation. Cancer cells grown long term without citrate released similar cytokines at 48 h and 2 wk, corroborating the hypothesis that citrate is necessary for metastatic reprogramming. Previous studies have shown that other metabolites such as lactate can also play a role in the communication between cancer cells and CAFs (Whitaker-Menezes *et al.,* 2011), but there is no evidence that lactate alone can modify tumour behaviour. Conversely, lactate can also be used for citrate synthesis (reviewed by (Mycielska *et al.,* 2015) and (Haferkamp *et al.,* 2020)).

Persistent and long-term presence of citrate in the media of cancer cells was shown to induce MET associated with growth and colonisation (Brabletz, 2012). This would be consistent with extracellular citrate playing an additional signalling role, where the constant presence of citrate might complete the process of stromal transformation creating a niche ready for the metastatic growth. Previous studies have shown that increased citrate levels precede leptomeningeal carcinomatosis from lung cancer (An *et al.,* 2015), suggesting that cancer cells might transform distant stroma and induce local citrate increase before metastatic processes begins.

The shorter incubation time of cancer cells with extracellular citrate was shown to induce an invasive phenotype with some features consistent with EMT. A similar effect on the protein level was obtained when the cells were incubated with the media from fibroblasts transformed by cancer cells deprived of citrate, therefore induced to supplement this metabolite. This supplementation of citrate by CAS and the induction of an activated fibroblast phenotype could have several implications regarding potential cancer therapies. It is possible that the need for de novo stromal transformation (e.g., after chemotherapy) could induce metastatic processes (EMT and MET) through the local changes of metabolite and cytokine levels and therefore modify the metastatic behaviour of the remaining cancer cells.

Incubation of cancer cells with extracellular citrate decreased an overall level of the metabolites tested. In particular, there was a decrease of intracellular levels of substrates known to be involved in intracellular citrate synthesis, including serine and glycine (Possemato *et al.,* 2011), glutamine and glutamate (Metallo *et al.,* 2011). This would suggest that cancer cells without extracellular citrate supply are forced to use several additional pathways to account for the missing metabolite. Availability of extracellular citrate decreases the levels of several metabolites which can be considered as by-products of increased citrate synthesis (Haferkamp *et al.,* 2020). This metabolic change and more balanced use of metabolic pathways are likely to contribute to the acquisition of a more aggressive phenotype.

Although gluconate had some mitotoxic effects on cancer cells when applied alone, it has to be noted that this effect was observed in the presence of the highest concentrations of gluconate only, much higher than those applied in our in vivo and in vitro experiments. It can be therefore deduced that the effects of gluconate observed in the experiments are due to its specific action on pmCiC and not through some less specific mitochondrial blocking. Moreover, gluconate, till now, has been considered as a physiologically neutral substance and used in medicine as a heavy ion carrier (reviewed by (Mycielska *et al.,* 2019)). It is also used in electrophysiology and transport studies as a Cl^- replacement because it is plasma membrane impermeable (Carini *et al.,* 1997; Bonzanni *et al.,* 2020).

Importantly, we have confirmed that depriving cancer cells of extracellular citrate supply in vivo results in decreased metastatic spread, stromal transformation and angiogenesis. Furthermore, we have observed increased immune cell infiltration of the mouse tumour xenografts treated with gluconate. FAP expressing immune cells have been seen previously (Arnold, James N. *et al.,* 2014; Cremasco *et al.,* 2018) and considered to comprise $CD45^+$ cells, which is consistent with the increased proinflammatory cytokine release by cancer cells deprived of extracellular citrate. Increased release of proinflammatory cytokines has been also associated with citrate uptake by monocytes (Ashbrook *et al.,* 2015), whereas activated macrophages have been determined to accumulate citrate (Jha *et al.,* 2015). This could suggest that preventing cancer cells from taking up extracellular citrate and consequently

increasing local citrate concentration might have a stimulating effect on anti-cancer immune response. Although we found these results particularly interesting, it has to be acknowledged that for this study, immunocompromised mice have been used, and therefore, a more detailed study of immune activity upon gluconate application was not possible.

To conclude, our results demonstrate that citrate is an important metabolite supportive of tumour progression which is synthesized and released by CAS. Moreover, citrate synthesis and release from cancer-associated stroma appears to be one of their major metabolic tasks and is induced and controlled by cancer cells through cross-cellular interactions. We have identified the transporter responsible for citrate release and confirmed its expression in cancer-associated cells in human tissues. Blocking of citrate uptake by cancer cells using gluconate, a specific inhibitor of citrate uptake, reduced cancer spread and decreased stromal transformation and angiogenesis in vivo.

Our novel finding of citrate release by cancer-associated stroma is crucial in understanding the mechanism of tumour environmental support and interactions between cancer cells and the environment. It sheds new light on the mechanism of how stroma stimulates metastatic spread, facilitates organ colonisation and angiogenesis, as well as increases cancer cells' resistance to anti-cancer therapies. Inhibiting citrate release from CAS and/or uptake by cancer cells could offer novel, specific, and readily implemented options for cancer treatment and metastasis prevention.

2.4.6 Supplementary materials

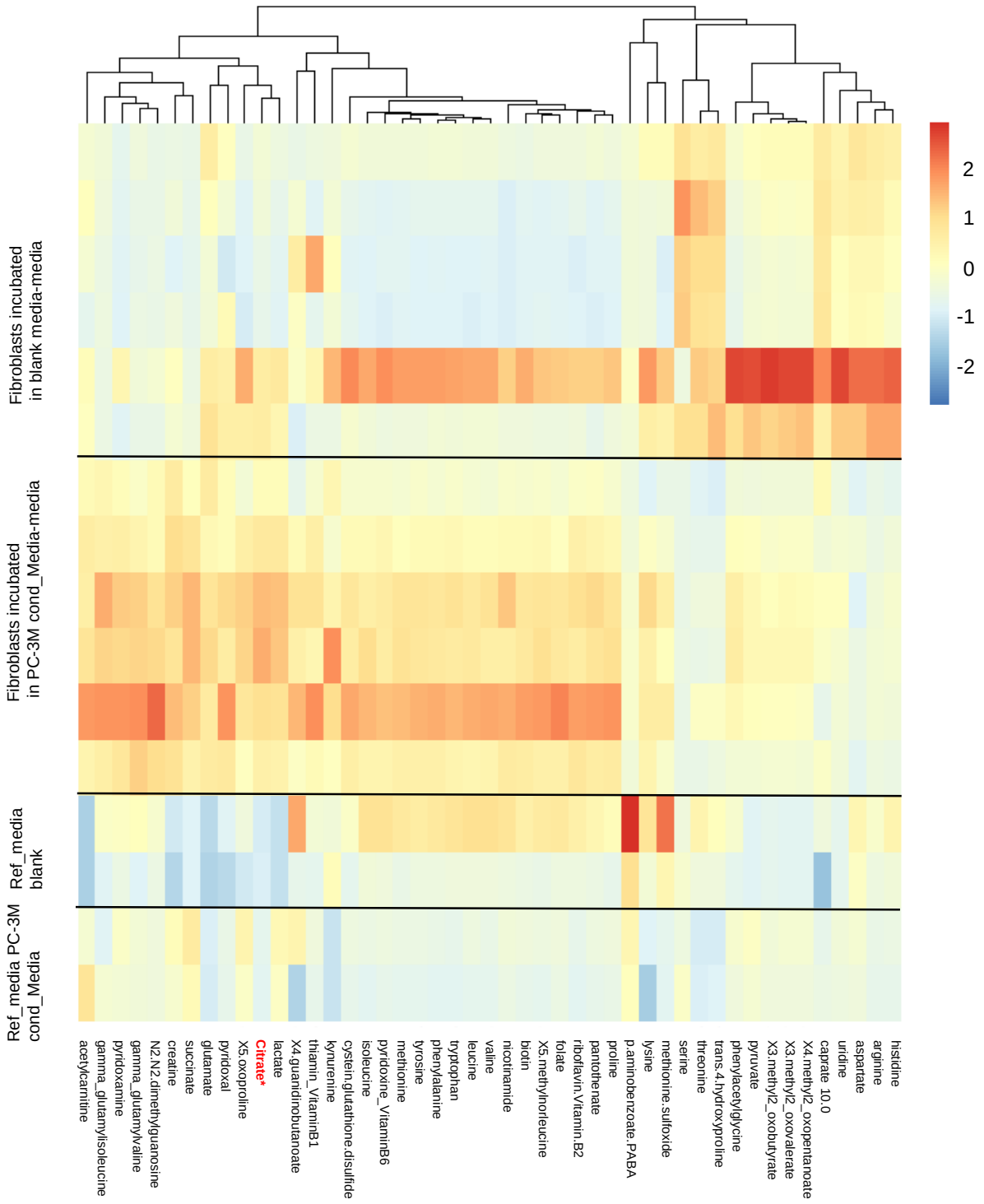

Figure S 8: Cancer-associated fibroblasts release citrate. Metabolomic analysis of supernatants collected from primary cultures of human skin fibroblasts after 72 h incubation in conditioned media from cancer cells or bottle (blank) media (n = 6 per group; Figure S 10A). Reference media show basal level of metabolites in the bottle media (Ref media blank) and conditioned media from PC-3M cells (Ref. media PC-3M; n = 2 per group).

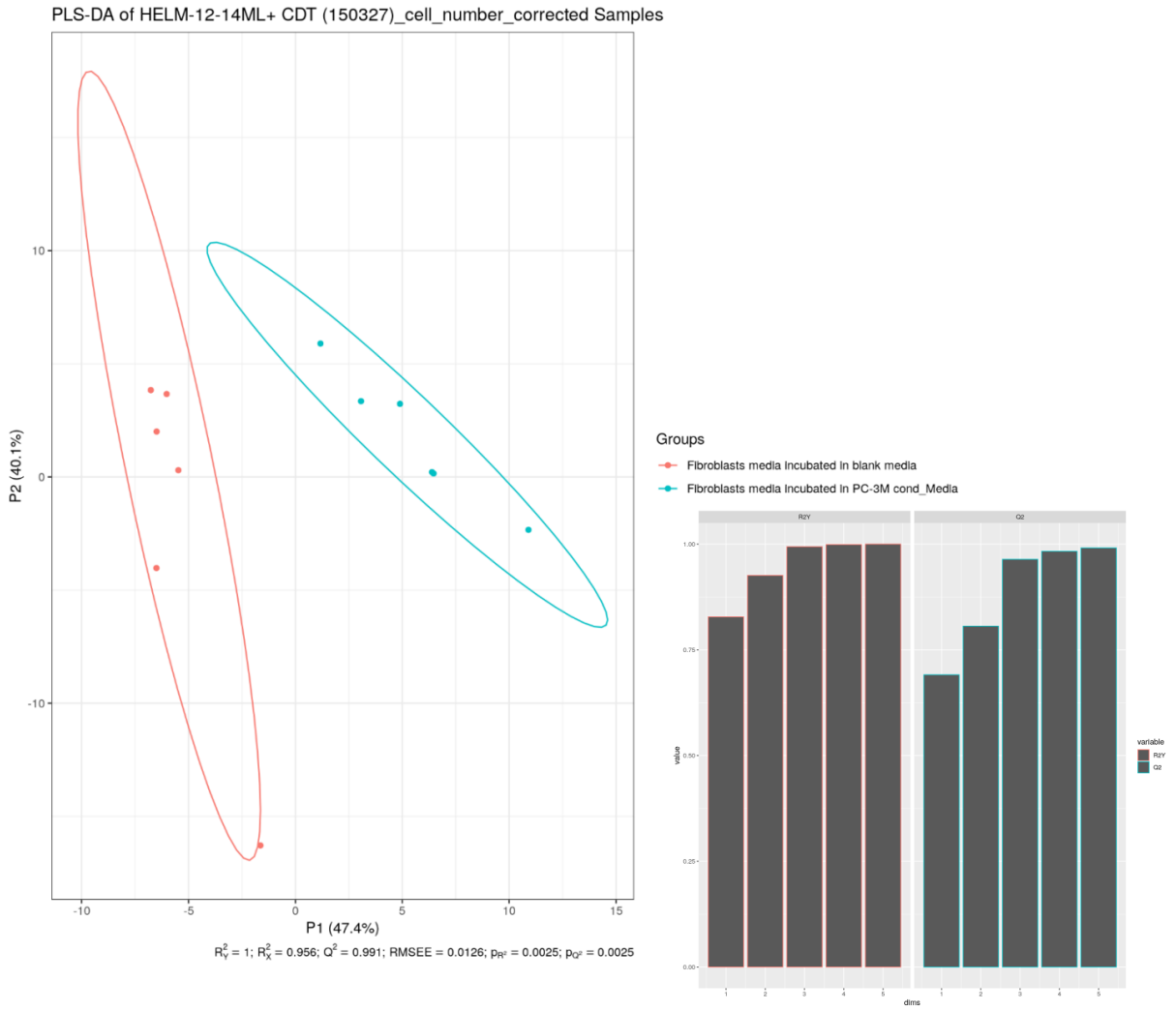

Figure S 9: Statistical analysis of metabolites released by control fibroblasts and cancer-associated fibroblasts. Mann–Whitney U tests showed a total of 27 significantly different metabolites with $P < 0.05$ after Bonferroni correction. The PLS-DA yielded highly significant clustering of the respective groups of fibroblasts grown in media which was conditioned with cancer cells or non-conditioned medium. R2X was calculated to be 0.441, 0.877, 0.919, 0.940, and 0.953. R2Y was calculated to be 0.905, 0.994, 0.999, 0.999, and 1.000. The values given here are listed from first to fifth predictive component for R2X and R2Y, respectively. Q2Y was calculated to be 0.828, 0.979, 0.991, 0.992, and 0.993 (again from first to fifth predictive component), whereas the RMSEE is estimated to be 0.0129. The results were seven times cross-validated and permutation tests were run (i = 2,000). The permutation tests resulted in pR2Y and pQ2Y of 0.0025. As for the VIPs (variables of importance in projection), above the selection threshold (VipScore > 1): 37 metabolites fit this criterion.

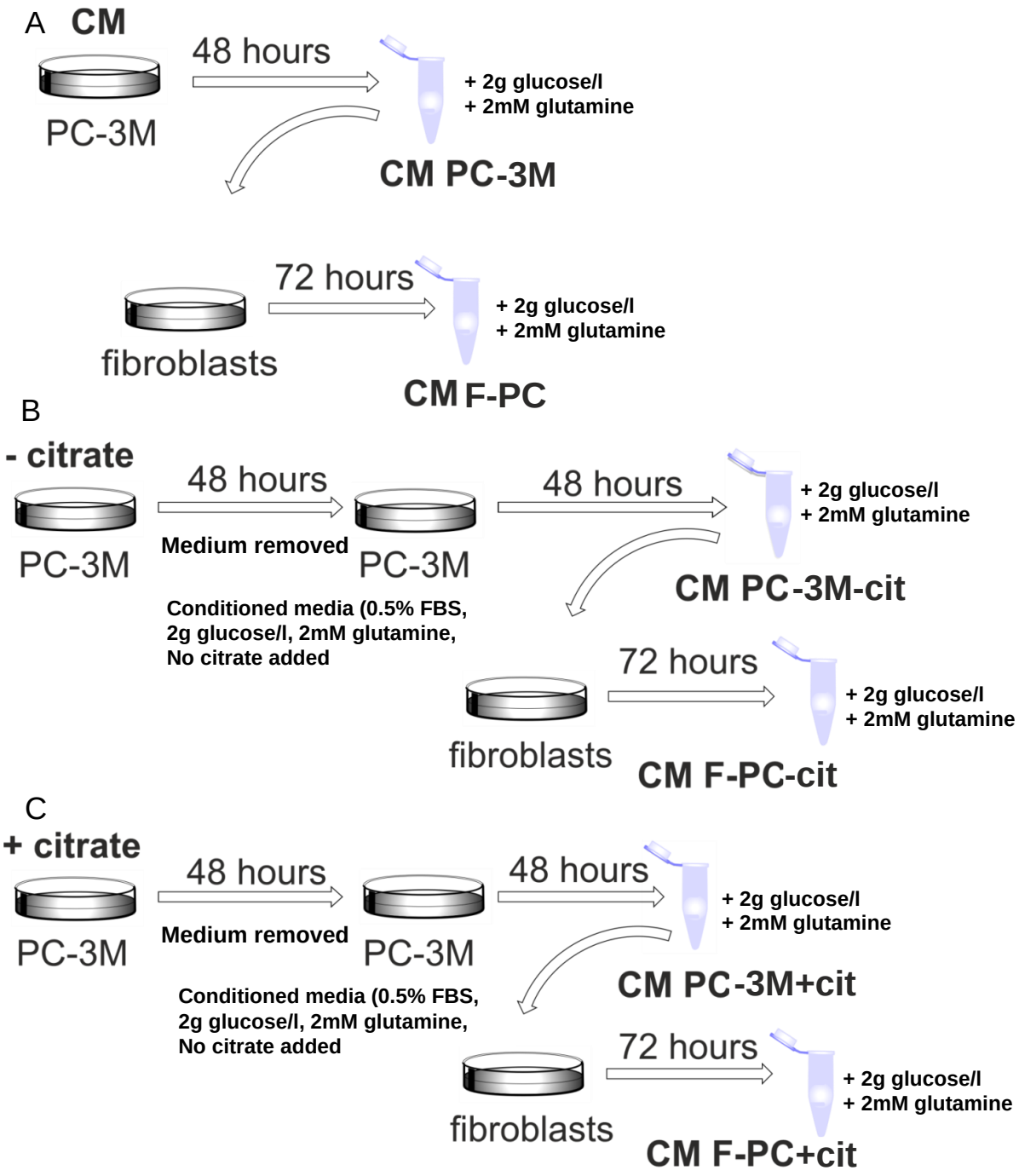

Figure S 10: Experimental procedure scheme. Diagram showing the way in which conditioned media were obtained. (A, B, C) Cancer cells were grown in either (A) normal growth media and then left for conditioning, or before conditioning, the PC-3M cells were incubated in dialyzed serum (B) without or (C) with extracellular citrate for 48 h. The following treatment was the same for all the conditions. Cancer cells were conditioned for 48 h. The collected media were filtered and supplemented with 2 mM glutamine and 2 g/l glucose at every step of the procedure to allow for unlimited intracellular citrate synthesis. Fibroblasts were incubated in similarly prepared media for 72 h.

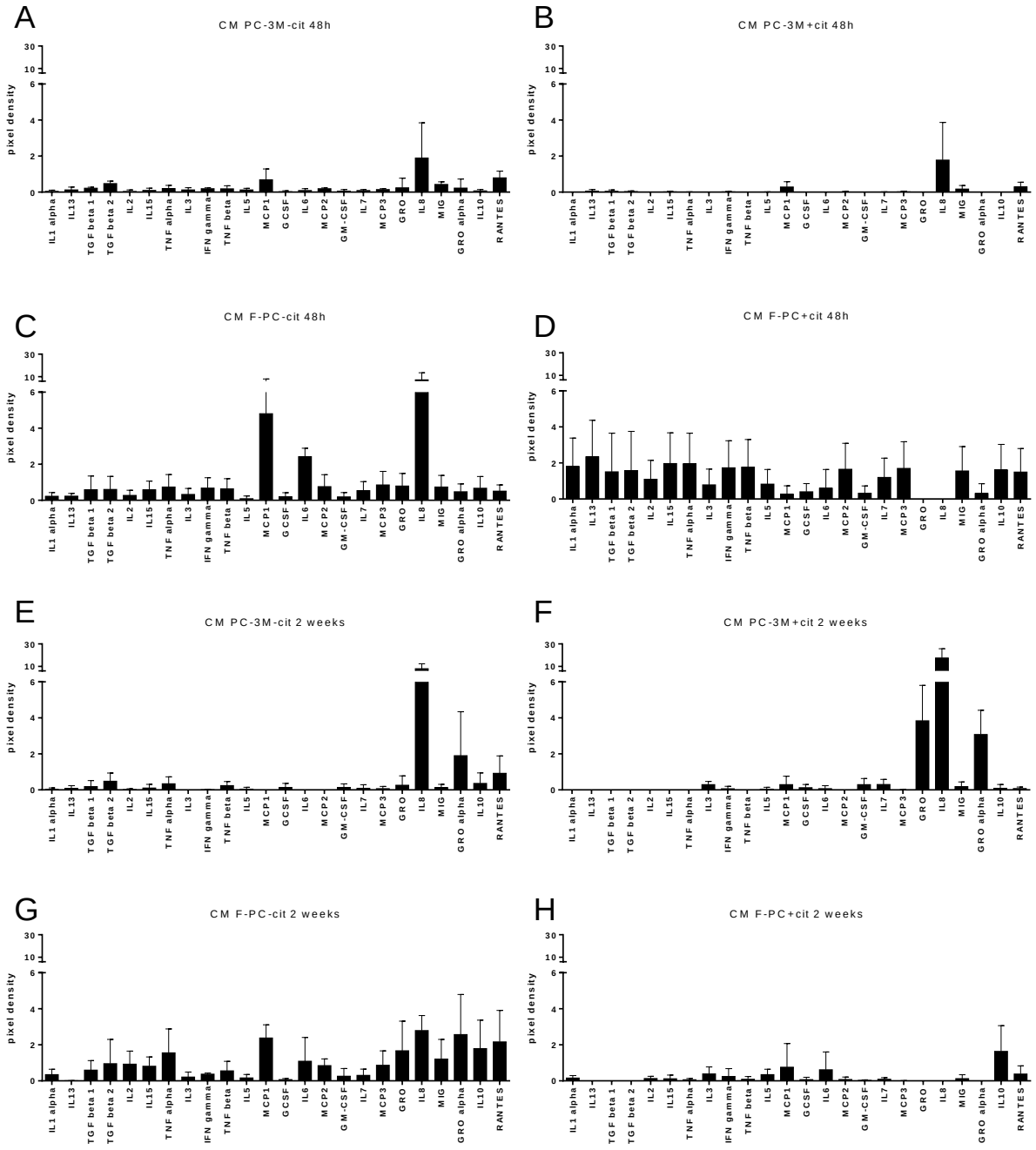

Figure S 11: Cancer cells release different set of cytokines depending on the extracellular citrate availability. (A, B, C, D, E, F, G, H) The graphs show selected cytokines released from cancer cells grown for 48 h (A, B) or 2 wk (E, D) under the following conditions (A) and preincubated without (CM PC-3M−cit) or (B) with extracellular citrate (CM PC-3M+cit) and fibroblasts (C, D and G, H) transformed by the differentially treated cancer cells (C, G) CM F-PC−cit and (D) CM F-PC+cit (F, H) over 48 h or 2 wk, respectively. (A, B, D, E) The values of cytokines released by fibroblasts were obtained by subtracting the values of cytokines measured in conditioned media from cancer cells (A, B and E, D) from the values measured in the media from fibroblasts.

Acylcarnitines (40)			
C0	Carnitine	C10:1	Decenoylcarnitine
C2	Acetylcarnitine	C10:2	Decadienylcarnitine
C3	Propionylcarnitine	C12	Dodecanoylcarnitine
C3:1	Propenoylcarnitine	C12:1	Dodecenoylcarnitine
C3-OH	Hydroxypropionylcarnitine	C12-DC	Dodecanedioylcarnitine
C4	Butyrylcarnitine	C14	Tetradecanoylcarnitine
C4:1	Butenoylcarnitine	C14:1	Tetradecenoylcarnitine
C4-OH (C3-DC)	Hydroxybutyrylcarnitine	C14:1-OH	Hydroxytetradecenoylcarnitine
C5	Valerylcarnitine	C14:2	Tetradecadienylcarnitine
C5:1	Tiglylcarnitine	C14:2-OH	Hydroxytetradecadienylcarnitine
C5:1-DC	Glutaconylcarnitine	C16	Hexadecanoylcarnitine
C5-DC (C6-OH)	Glutarylcarnitine (Hydroxyhexanoylcarnitine)	C16:1	Hexadecenoylcarnitine
C5-M-DC	Methylglutarylcarnitine	C16:1-OH	Hydroxyhexadecenoylcarnitine
C5-OH (C3-DC-M)	Hydroxyvalerylcarnitine (Methylmalonylcarnitine)	C16:2	Hexadecadienylcarnitine
C6 (C4:1-DC)	Hexanoylcarnitine (Fumarylcarnitine)	C16:2-OH	Hydroxyhexadecadienylcarnitine
C6:1	Hexenoylcarnitine	C16-OH	Hydroxyhexadecanoylcarnitine
C7-DC	Pimelylcarnitine	C18	Octadecanoylcarnitine
C8	Octanoylcarnitine	C18:1	Octadecenoylcarnitine
C9	Nonanoylcarnitine	C18:1-OH	Hydroxyoctadecenoylcarnitine
C10	Decanoylcarnitine	C18:2	Octadecadienylcarnitine

Amino Acids (21)			
Ala	Alanine	Lys	Lysine
Arg	Arginine	Met	Methionine
Asn	Asparagine	Orn	Ornithine
Asp	Aspartate	Phe	Phenylalanine
Cit	Citrulline	Pro	Proline
Gln	Glutamine	Ser	Serine
Glu	Glutamate	Thr	Threonine
Gly	Glycine	Trp	Tryptophan
His	Histidine	Tyr	Tyrosine
Ile	Isoleucine	Val	Valine
Leu	Leucine		

Monosaccharides (1)
Sum of Hexoses (including Glucose)

Glycerophospholipids (90)			
lysoPC a C14:0	PC aa C34:1	PC aa C42:0	PC ae C38:2
lysoPC a C16:0	PC aa C34:2	PC aa C42:1	PC ae C38:3
lysoPC a C16:1	PC aa C34:3	PC aa C42:2	PC ae C38:4
lysoPC a C17:0	PC aa C34:4	PC aa C42:4	PC ae C38:5
lysoPC a C18:0	PC aa C36:0	PC aa C42:5	PC ae C38:6
lysoPC a C18:1	PC aa C36:1	PC aa C42:6	PC ae C40:1
lysoPC a C18:2	PC aa C36:2	PC ae C30:0	PC ae C40:2
lysoPC a C20:3	PC aa C36:3	PC ae C30:1	PC ae C40:3
lysoPC a C20:4	PC aa C36:4	PC ae C30:2	PC ae C40:4
lysoPC a C24:0	PC aa C36:5	PC ae C32:1	PC ae C40:5
lysoPC a C26:0	PC aa C36:6	PC ae C32:2	PC ae C40:6
lysoPC a C26:1	PC aa C38:0	PC ae C34:0	PC ae C42:0
lysoPC a C28:0	PC aa C38:1	PC ae C34:1	PC ae C42:1
lysoPC a C28:1	PC aa C38:3	PC ae C34:2	PC ae C42:2
PC aa C24:0	PC aa C38:4	PC ae C34:3	PC ae C42:3
PC aa C26:0	PC aa C38:5	PC ae C36:0	PC ae C42:4
PC aa C28:1	PC aa C38:6	PC ae C36:1	PC ae C42:5
PC aa C30:0	PC aa C40:1	PC ae C36:2	PC ae C44:3
PC aa C30:2	PC aa C40:2	PC ae C36:3	PC ae C44:4
PC aa C32:0	PC aa C40:3	PC ae C36:4	PC ae C44:5
PC aa C32:1	PC aa C40:4	PC ae C36:5	PC ae C44:6
PC aa C32:2	PC aa C40:5	PC ae C38:0	
PC aa C32:3	PC aa C40:6	PC ae C38:1	

Sphingolipids (15)			
SM (OH) C14:1	SM C18:0	SM (OH) C22:1	SM (OH) C24:1
SM C16:0	SM C18:1	SM (OH) C22:2	SM C26:0
SM C16:1	SM C20:2	SM C24:0	SM C26:1
SM (OH) C16:1	SM C22:3	SM C24:1	

Biogenic Amines (21)			
Ac-Orn	Acetylornithine	PEA	Phenylethylamine
ADMA	Asymmetric dimethylarginine	cis-OH-Pro	cis-4-Hydroxyproline
alpha-AAA	alpha-Aminoadipic acid	trans-OH-Pro	trans-4-Hydroxyproline
Carnosine	Carnosine	Putrescine	Putrescine
Creatinine	Creatinine	SDMA	Symmetric dimethylarginine
DOPA	DOPA	Serotonin	Serotonin
Dopamine	Dopamine	Spermidine	Spermidine
Histamine	Histamine	Spermine	Spermine
Kynurenine	Kynurenine	Taurine	Taurine
Met-SO	Methionine sulfoxide	total DMA	Total dimethylarginine
Nitro-Tyr	Nitrotyrosine		

Figure S 12: List of metabolites measured with the AbsoluteIDQ p180 Kit GAC.

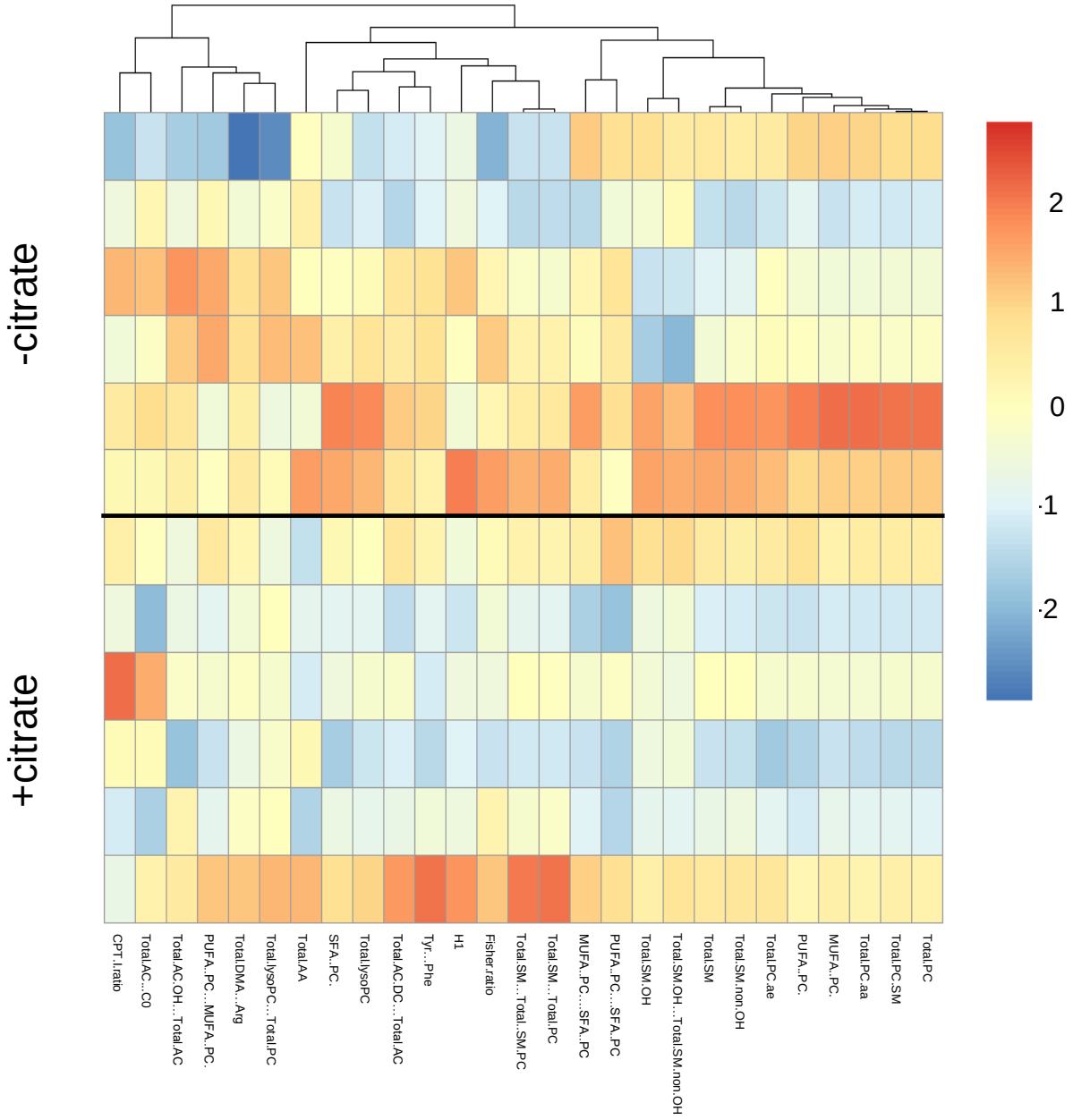

Figure S 13: Extracellular citrate uptake induces changes of the levels of intracellular metabolites. Heat map of ratios and total amounts of different metabolic groups (Figure S 12) of PC-3M cancer cells grown for 48 h under control conditions or in the media supplemented with 200 µM citrate. Each row represents a separate repeat (n = 6).

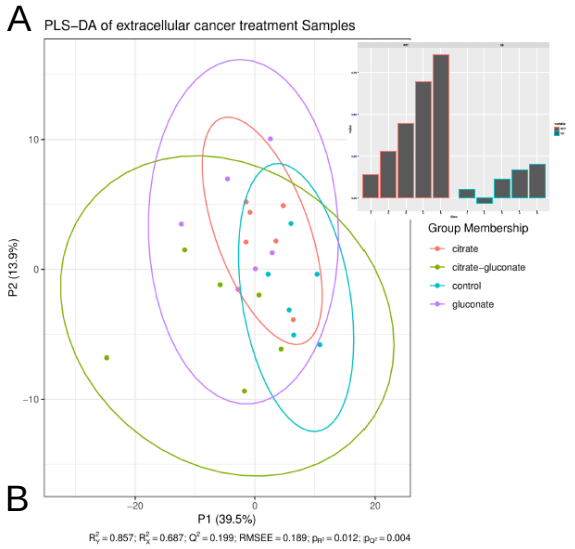

VIP metabolites table

Spermine...Spermidine	C5.1	Arg	Met.SO	PC.aa.C34.4	SM..OH..C22.1	C14	Non.essential.AA	Spermine...Spermidine	C5.1
PC.ae.C42.2	C6.1	C14.1.OH	His	C5	Kynurenine...Trp	C18.1	SM.C26.1	PC.ae.C42.2	C6.1
SM..OH..C24.1	C3.DC..C4.OH.	PC.ae.C44.6	PC.aa.C28.1	Spermidine...Putrescine	AAA	PC.ae.C38.0	Total.AC...C0	SM..OH..C24.1	C3.DC..C4.OH.
C14.1	PC.aa.C40.2	PC.aa.C40.4	Glu	Ala	lysoPC.a.C24.0	Tyr...Phe	Glucogenic.AA	C14.1	PC.aa.C40.2
C4	C10	Total.DMA...Arg	C9	Asn	t4.OH.Pro	Cit...Arg	Fisher.ratio	C4	C10
lysoPC.a.C18.2	Gln	Total.AC.DC...Total.AC	Tyr	Pro	PC.aa.C42.4	Ser	Total.AA	lysoPC.a.C18.2	Gln
C16.1.OH	Putrescine	Thr	Total.SM...Total..SM.PC.	C18	lysoPC.a.C16.0	SM..OH..C16.1	Total.lysoPC...Total.PC	C16.1.OH	Putrescine
lysoPC.a.C17.0	C5.M.DC	C18.2	Total.SM...Total.PC	Ile	C16.1	C12	SM.C22.3	lysoPC.a.C17.0	C5.M.DC
Orn...Arg	Spermidine	PUFA..PC....MUFA..PC.	lysoPC.a.C20.4	PC.aa.C38.1	PC.ae.C42.5	PC.ae.C30.2	C7.DC	Orn...Arg	Spermidine
PC.aa.C42.1	lysoPC.a.C20.3	PC.ae.C44.3	C10.1	Essential.AA	Phe	PC.aa.C36.0	CPT.I.ratio	PC.aa.C42.1	lysoPC.a.C20.3

Figure S 14: Statistical analysis of the intracellular metabolite levels. (A) PLS-DA analysis of pC-3M cancer cells incubated for 48 h under different experimental conditions (control, 200 mM citrate, 200 mM citrate + 150 and 150 mM gluconate). R2Y (cumulative) was calculated to be 0.857. The values given here are not listed from first to fifth predictive component for R2X and R2Y as they never reached near 1.0. Q2Y was calculated to be 0.199, whereas the RMSEE is estimated to be 0.189. This low Q2Y value indicates small differences between the groups. These results were seven times cross-validated and permutation tests were run (i = 2,000). The permutation tests resulted in pR2Y and pQ2Y of 0.012 and 0.004, respectively. (B) For the VIPs (variables of importance in projection) above the selection threshold (VipScore > 1): 80 metabolites fit this criterion.

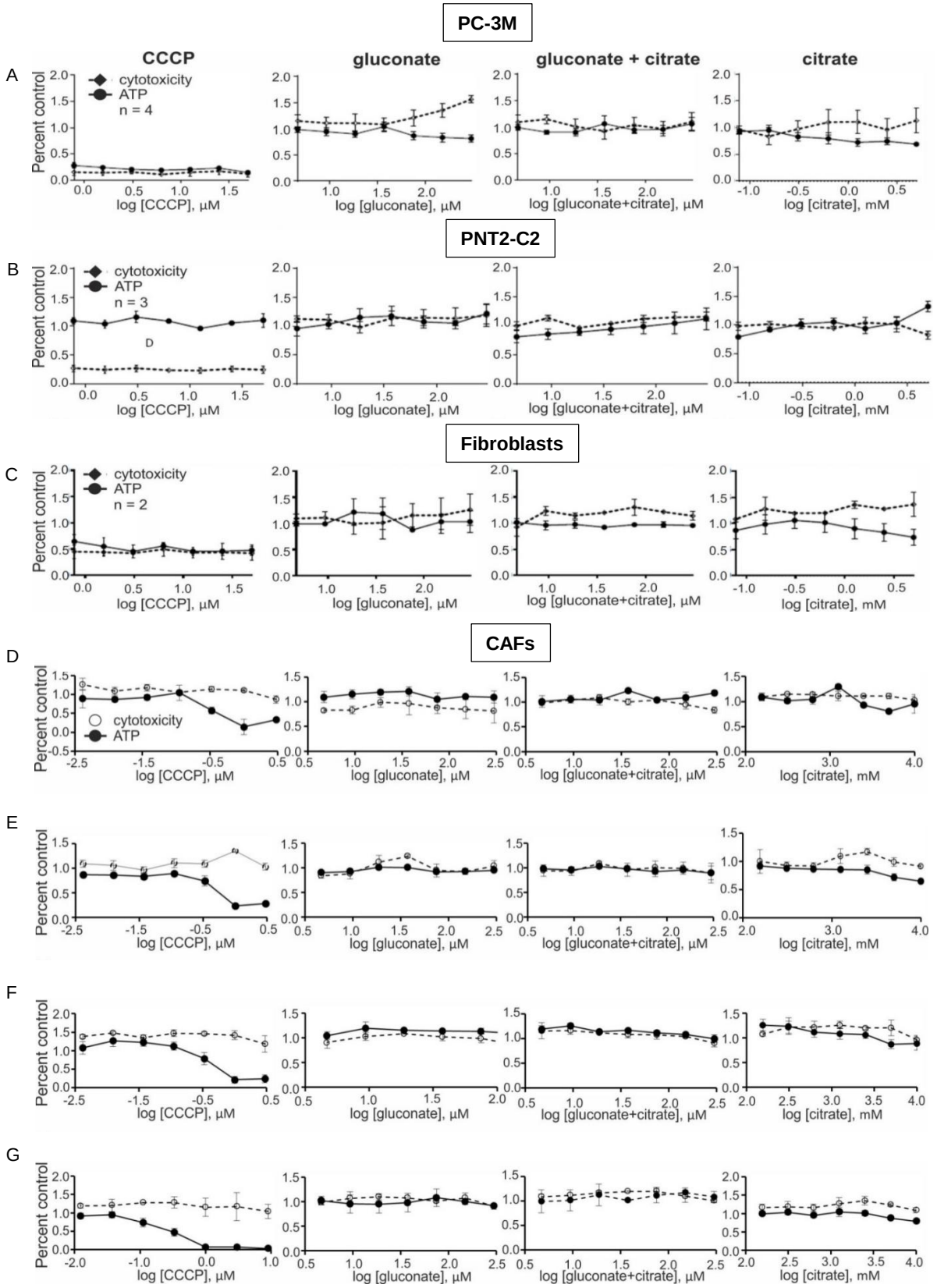

Figure S 15: Study of mitotoxic effects of citrate and gluconate on cancer cells and cancer-associated fibroblasts. (A, B, C) Mitotoxicity assay of different types of cells (cancer (A) versus benign PNT-2C2 cells and untreated fibroblasts (B and C, respectively)) in the presence of ascending concentrations of gluconate, gluconate in the presence of 200 mM citrate and citrate. (D, E, F, G) Fibroblasts transformed with the conditioned media from control (D), preincubated with citrate (E), gluconate (F) and citrate and gluconate (G) cancer cells. The results show mitotoxic activity of the studied compounds by measuring ATP synthesis and cytotoxicity. CCCP stands for carbonyl cyanide m-chlorophenyl hydrazine used as control toxicity test.

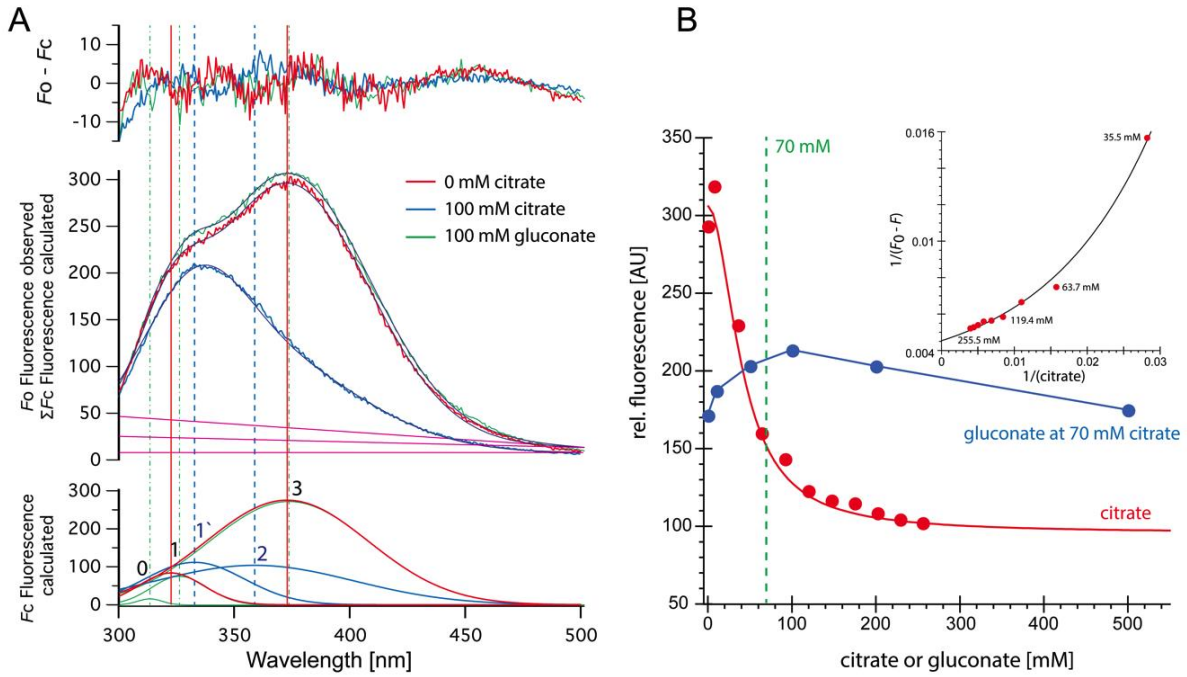

Figure S 16: Trp quenching at different concentrations of citrate. (A) Titration with citrate and gluconate in presence of 70 mM citrate (blue) is shown as raw data and deconvoluted spectra. (B) Changes in relative fluorescence and similar changes depicted in a Benesi–Hildebrand (double reciprocal) plot of citrate data are shown. Similar to the Lineweaver–Burk linearization method, only data that satisfy a 1:1 binding model with a constant Kd result in a linear dependency—the data clearly deviate from this model.

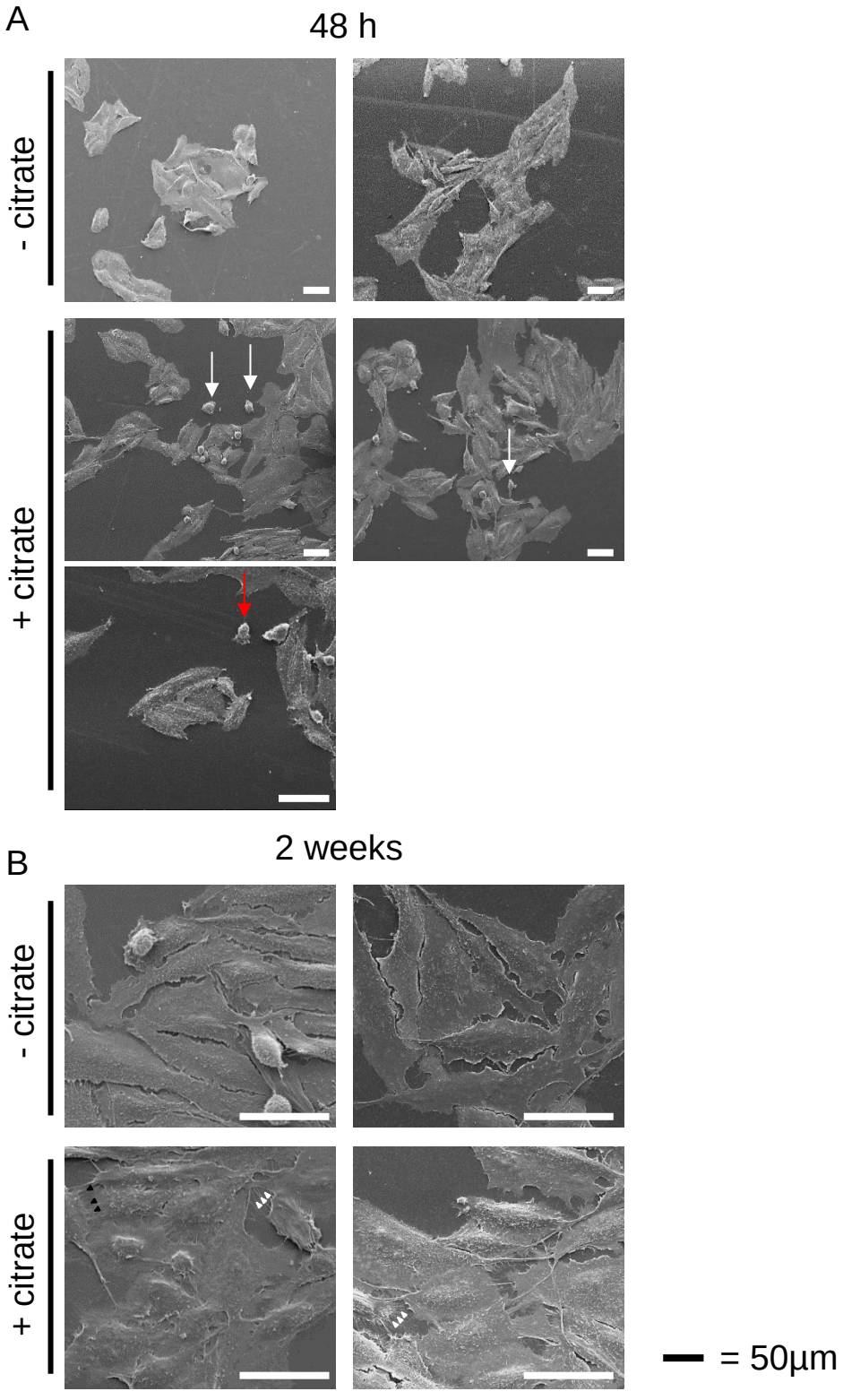

Figure S 17: Extracellular citrate induces changes in cancer cells morphology. (A) Changes in cancer cell morphology influenced by extracellular citrate (A) 48 h of preincubation with extracellular citrate resulted in spindle shape cells with a clear lamelipodium with many relatively short filopodia. There were many single (white arrows) and ameboid shaped (red arrows) cells under conditions with extracellular citrate. (B) On the other hand, long-term preincubation of cancer cells with citrate was consistent with the colonizing phase in which cells are rounder with long invadopodia reaching either ECM (white arrowheads) or each other (black arrowheads). Cells in control conditions (-citrate) showed unchanged morphology regardless of the incubation time. Their plasma membrane seemed to have decreased fluidity with a very small number of filopodia.

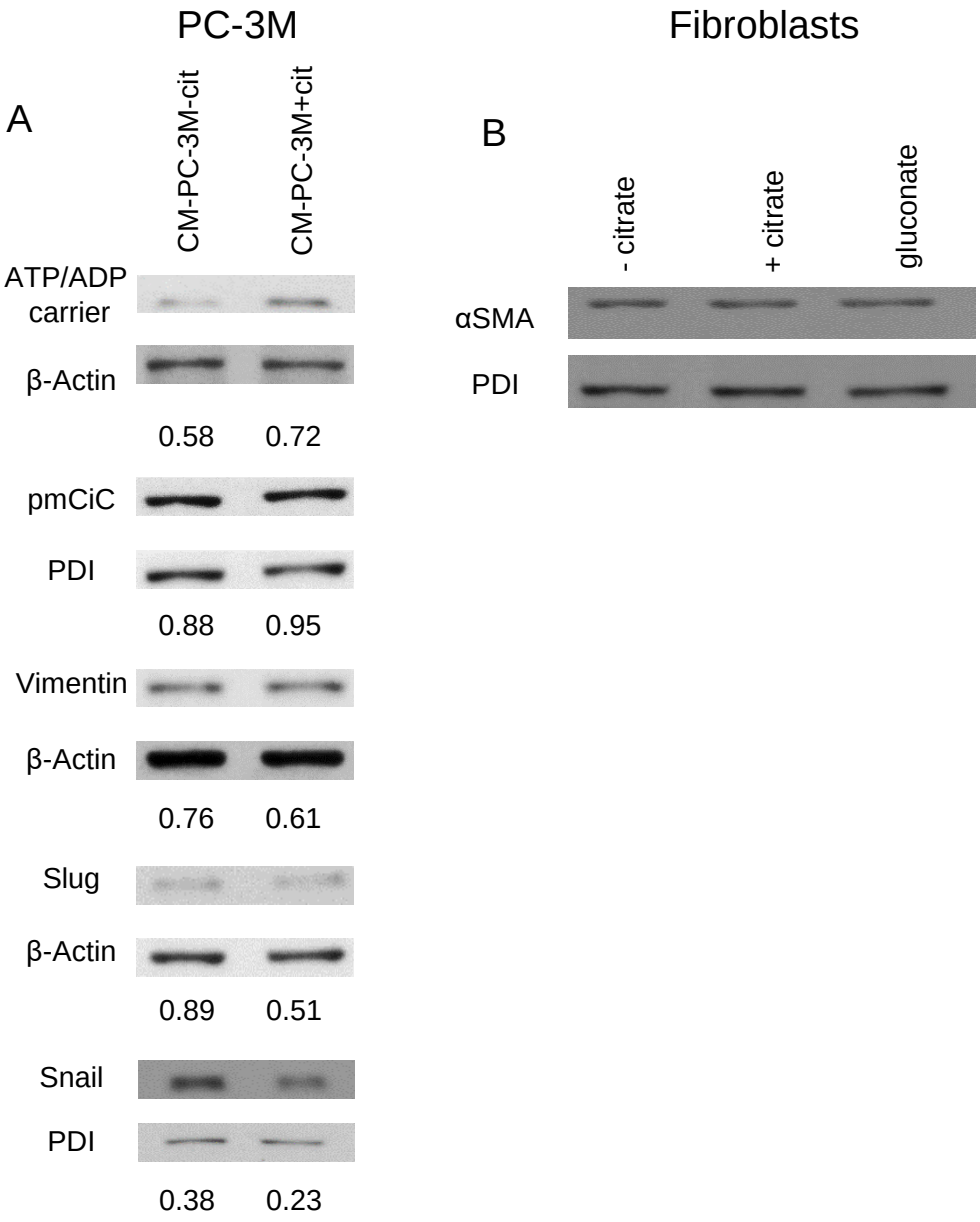

Figure S 18: Conditioned media from cancer cells do not induce significant changes in cancer markers. (A) Western blot analysis of the expression of metabolic transporters and EMT/mesenchymal–epithelial transition–related in fibroblasts grown under standard conditions with added 200 mM citrate or 150 mM gluconate for proteins of PC-3M cells grown for 48 h in conditioned media from PC-3M cells preincubated with or without extracellular citrate (CM PC-3M−cit and CM PC-3M+cit; n = 3). (B) Western blot analysis of the αSMA expression 48 h.

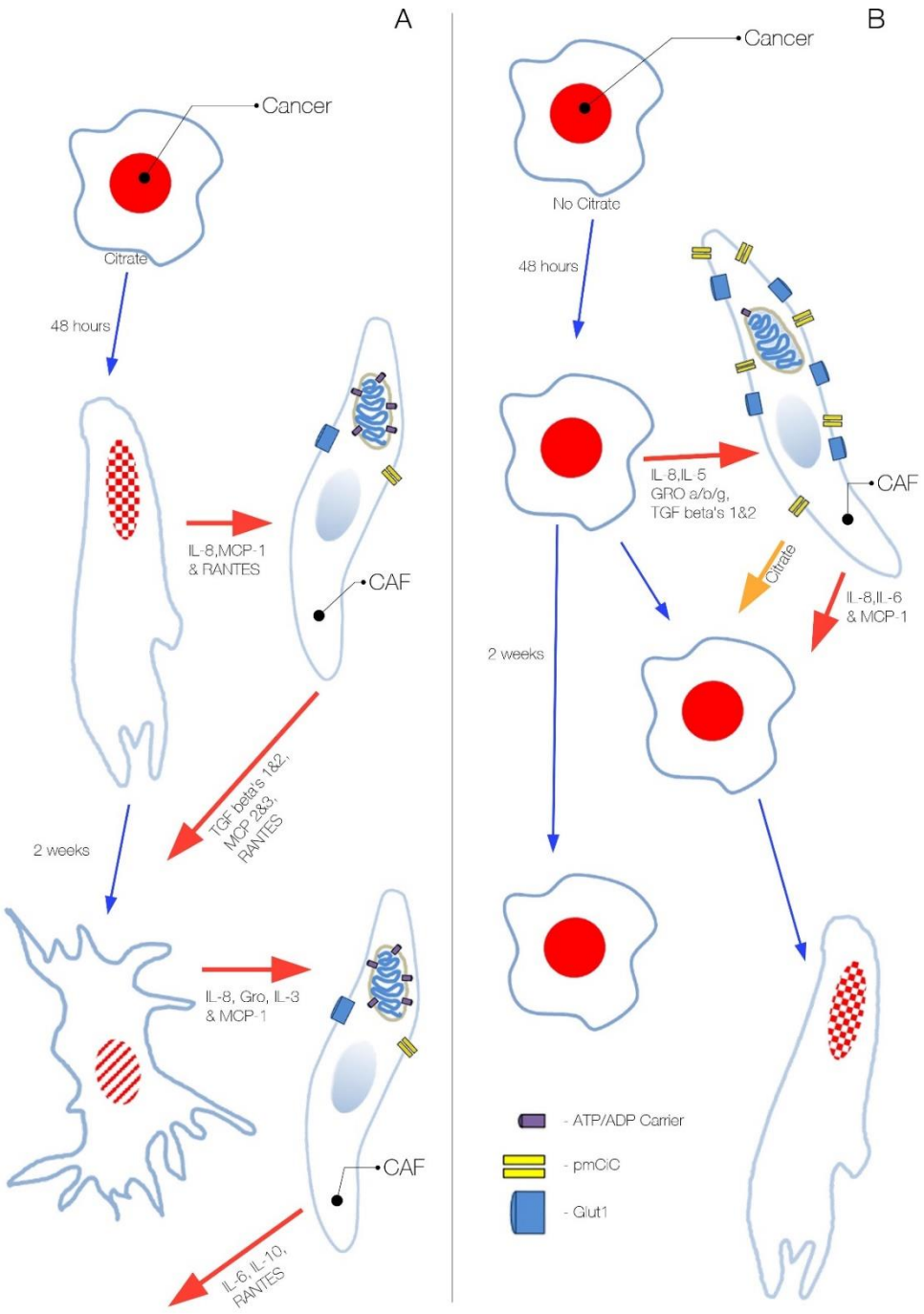

Figure S 19: Cancer cell status and activity depends on the presence of extracellular citrate supplied by cancer-associated cells. (A) In the presence of extracellular citrate cancer cells acquire first an activated EMT-like phenotype, whereas long-term presence of citrate results in the colonizing mesenchymal–epithelial transition–like phenotype. (B) Cancer cells deprived of extracellular citrate release high levels of stroma transforming cytokines and force CASs to release citrate and other necessary elements. Citrate and cytokines supplied by cancer-associated fibroblasts support the acquisition of a metastatic phenotype by cancer cells. Without extracellular citrate the status of cancer cells remains unchanged. The PC-3M cells have red nuclei and the stippling that indicate EMT, whereas the irregular shape and cross lines indicate mesenchymal–epithelial transition and metastatic colonisation.

3 General discussion

3.1 Biomarkers: Key tools in the fight against cancer

Cancer remains a major global health challenge, responsible for millions of deaths annually, with metastatic cancer being particularly lethal (Deyell *et al.,* 2021). The primary goal of cancer treatment is to prevent metastasis and slow down disease progression, but determining the most appropriate treatment approach is often complex. Biomarkers, which are biological indicators reflecting disease status and treatment response, provide valuable insight into clinical decision-making. They facilitate early detection, diagnosis, prognosis, and personalized therapy development, contributing to improved patient outcomes and quality of life. Several biomarkers are already being used in cancer care to aid prognosis, diagnosis, and treatment selection in various types of cancer. Advancing biomarker research is critical to improving early detection, treatment efficacy, and patient survival rates. The introduction and understanding of potential new biomarkers hold great promise for further improving cancer care.

The objective of this thesis was to identify potential new biomarkers. We aimed to identify a biomarker for melanoma patients that predicts the response to oncolytic virus therapy. In addition, we investigated whether pmCiC, a specific plasma membrane citrate transporter, can serve as a prognostic marker for cancer aggressiveness.

3.2 Nectin-1 as a predictor of positive response to T-VEC treatment *in vitro* and *in vivo*

3.2.1 Addressing the need for predictive markers in oncolytic virotherapy

Oncolytic virotherapy represents an innovative approach to the treatment of advanced melanoma. Currently, T-VEC is the only OV approved by the FDA for the treatment of cancer, particularly advanced melanoma (Andtbacka *et al.,* 2015). T-VEC is an attenuated form of the HSV-1. HSV-1 has been genetically modified to contain mutations in the ICP 34.5 and 47 and expresses GM-CSF. The mutations in the ICP 34.5 and 47 lead to the selective replication of the virus in tumour cells and enhance the antigen presentation of HSV-infected cells. Additionally, GM-CSF has been shown to augment the anti-tumour immune response and induce a systemic immune response.

The treatment process using T-VEC can be intense and stressful for patients. Multiple injections are often necessary directly into melanoma lesions, which can cause discomfort and result in local reactions such as pain, swelling, or redness at the injection site. In addition, managing the side effects of T-VEC therapy, such as fever, flu-like symptoms, fatigue, and nausea, as well as potential complications, can increase the overall stress of undergoing

treatment. Although rare, T-VEC may cause more serious side effects, such as immune reactions (including inflammation in various organs of the body such as the liver or lungs), risk of herpes virus infections, and allergic reactions. It is therefore important to carefully consider whether treatment with T-VEC is the optimal and promising course of action.

The objective of this study was to identify predictive markers for melanoma tumour cell response to oncolytic virotherapy. This will aid in the decision-making process for treating patients with this intensive and stressful procedure and optimise treatment results. Nectin-1 is a cell surface adhesion molecule, found on a variety of normal and malignant cells and is involved in the organization of adherens and tight junctions. Nectin-1 has also been shown to promote HSV-1 entry (Krummenacher *et al.,* 2004).

Our study has identified Nectin-1 as a promising biomarker for the treatment of melanoma metastases by intratumoural application of T-VEC. The evaluation included a panel of 20 melanoma cell lines and knockout cells. *In vitro* data were based on MTT metabolic activity and LDH release assays, Western blot, flow cytometry and immunochemistry. In addition, 35 cutaneous melanoma metastases from 21 patients treated with T-VEC were retrospectively analysed for Nectin-1 expression and tumour regression. In both cell lines and melanoma metastases, there was a significant correlation between the level of Nectin-1 expression and tumour cell regression. Oncolytic viral therapy with T-VEC induced pronounced melanoma killing when Nectin-1 expression was high. With our study, we have confirmed the results obtained in thyroid cancers, squamous cell carcinoma, and glioblastoma (Huang *et al.,* 2007; Yu *et al.,* 2007; Friedman *et al.,* 2018). Consequently, our results suggest that Nectin-1 may represent a crucial factor contributing to the efficacy of oncolytic herpes viruses in various tumour types, warranting further investigation in subsequent studies.

3.2.2 Variability in susceptibility to T-VEC-induced oncolysis

Our *in vitro* assays revealed a wide range of susceptibility to T-VEC-induced oncolysis among melanoma cell lines. This reflects what can be seen in trials and studies of real-world T-VEC use (Sun *et al.,* 2020; Kleemann *et al.,* 2021; Andtbacka *et al.,* 2019; Ressler *et al.,* 2021). In a trial (OPTiM trial) of T-VEC versus GM-CSF in unresectable stage III/IV melanoma, 31.5% of patients had an overall response, including 16.9% who had a complete response (Andtbacka *et al.,* 2019). In the GM-CSF group, only 6.4% had an overall response, including one patient who had a complete response. The *in vivo* efficacy and clinical response rates of oncolytic T-VEC therapy are dependent upon a number of factors, including the stage of the disease, the location of the melanoma lesions, and the individual characteristics of the patient. Not all patients respond to treatment the same way and a proportion of patients do not experience favourable outcomes following T-VEC administration. It is important to select an appropriate patient population that is more likely to respond.

3.2.3 The role of Nectin-1 in susceptibility to T-VEC-induced oncolysis

The melanoma cell lines showed a greater susceptibility to T-VEC-mediated oncolysis when Nectin-1 expression was high. In addition, we found that T-VEC entry and oncolytic activity were dependent on the presence of Nectin-1 on the cell surface of the melanoma cell lines. This dependency was more pronounced with the additional knockout of HVEM. HSV-1 enters host cells via receptor-mediated fusion of the viral envelope with a host cell membrane. This requires the binding of the viral envelope glycoprotein gD to one of its receptors, a process which is essential for entry to occur. Nectin-1 and HVEM are two known entry receptors (Krummenacher *et al.,* 2004). Nectin-1 is expressed in human epithelial and neuronal cells, and it has been demonstrated to be the receptor for HSV-1, which enables infection of epithelial cells on mucosal surfaces and spread to cells of the nervous system (Geraghty *et al.,* 1998; Kopp *et al.,* 2009; Karaba *et al.,* 2011). In line with this understanding, our research reveals that knockout cell lines lacking Nectin-1 exhibited notably reduced concentrations of HSV-1 DNA following T-VEC infection compared to control cell lines. These findings highlight the pivotal role of Nectin-1 in the entry of oncolytic HSV-1 into malignant melanoma.

3.2.4 The role of HVEM in susceptibility to T-VEC-induced oncolysis

In contrast to Nectin-1, HVEM was not found to be a predictor of T-VEC-induced melanoma cell death in our *in vitro* and in *vivo* studies. HVEM is a member of the TNF receptor family and was shown to mediate the entry of several wild-type HSV strains into the normally nonpermissive Chinese hamster ovary (CHO) cells and human cells (Montgomery *et al.,* 1996). This also functions through binding of the viral envelope glycoprotein gD to HVEM (Krummenacher *et al.,* 1998). When the receptors Nectin-1 and HVEM are directly compared, Nectin-1 is superior in promoting viral entry compared to HVEM (Krummenacher *et al.,* 2004; Petermann & Rahn *et al.,* 2015; Kopp *et al.,* 2009). This elucidates the findings of our studies. After knocking out HVEM, a significant amount of HSV-1 DNA remained in the cells. However, when Nectin-1 was knocked out, the number of HSV-1 DNA copies was significantly reduced. Nectin-1 appeared to compensate for and mediate the entry of HSV-1 into the melanoma cells.

Interestingly, HVEM-knockout cells were more sensitive to T-VEC-induced cell death compared to the wildtype control. HVEM-expressing cells are normally protected from premature apoptotic death caused by HSV-1 or by the binding of its gD to HVEM (Sciortino *et al.,* 2008). HSV-1 gD activates HVEM and thereby promotes NF-κB activation and cell survival (Cheung *et al.,* 2009). We speculate that this signalling is blocked in HVEM-knockout cells upon T-VEC infection and increased their susceptibility to cell death triggered by T-VEC.

Double knockout of Nectin-1 and HVEM blocked T-VEC entry into IGR-37 cells, as evidenced by reduced HSV-1 copy numbers. Consequently, cells were greatly resistant to T-VEC-

triggered cell death. Under these circumstances, the absence of pro-survival signals from HVEM might be less significant, since cell death does not occur without viral entry.

3.2.5 The role of STING and cGAS in susceptibility to T-VEC-induced oncolysis

In contrast to Nectin-1, there was no correlation observed between the oncolytic efficacy of T-VEC and either STING or cGAS. The cGAS-STING pathway serves as a key element in regulating innate immunity, responding to diverse stimuli such as double-stranded DNA (Ma & Damania, 2016). Its activation is pivotal in defending against viral infections like HSV-1. Upon interaction with dsDNA, cGAS catalyses the synthesis of cGAMP, initiating STING signalling. Activated STING undergoes conformational changes upon cGAMP binding. This results in the phosphorylation of transcription factors such as IRF3 and NF-κB, which in turn leads to the expression of type I interferons, interferon-stimulated genes (ISGs), and various inflammatory mediators, pro-apoptotic genes, and chemokines as part of the body's innate immune response against viruses (Ma & Damania, 2016). The functionality and activity of the cGAS-STING pathway can influence the efficacy of oncolytic tumour therapy.

Bommareddy et al. found that STING expression levels in melanoma cell lines correlated inversely with their sensitivity to T-VEC, with STING knockout cells showing increased susceptibility to T-VEC-induced cell death (Bommareddy *et al.,* 2019). However, there was no observed correlation between T-VEC oncolysis and cGAS expression. Interestingly, melanoma cells exhibiting low STING expression, which were resistant to PD-1 blockade *in vivo*, were sensitive to T-VEC treatment. Additionally, Xia et al. demonstrated that suppression of STING signalling could facilitate immune evasion following DNA damage in melanoma cells, leading to increased susceptibility to HSV-1 (Xia *et al.,* 2016). Taken together, the results indicate that STING expression levels may serve as a predictive biomarker for oncolytic virus activity, which is contrary to the findings of this study. However, several factors must be considered.

Firstly, in our melanoma cell panel, only two cell lines (IGR-39 and LOXIMVI) expressed both, STING and cGAS. The distribution of STING and cGAS could have played a role in minimizing the impact of T-VEC treatment on our cell lines' response. This is because the presence of STING and cGAS in a cell line is fundamental to the functionality of the signalling pathway. Secondly, our melanoma panel did not include cell lines with varying levels of STING in addition to high Nectin-1 expression, which would have allowed effective infection. Consequently, Nectin-1 may have exerted a dominant influence in this context, potentially masking the more subtle role of STING and cGAS. We also tried to analyse different subgroups (Nectin-1-high and Nectin-1-low expressing cell lines), but most likely due to the small number of cell lines in each group, we could not see any correlation. Our data collectively indicate that

STING affects the oncolytic activity in a subset of melanoma cell lines. However, additional mechanisms, independent of STING, may also influence T-VEC-mediated oncolysis.

3.2.6 Consistent findings in flow cytometry, Western blot, and immunohistochemistry analyses

In the clinical setting, immunohistochemistry is the method of choice for the analysis of tumour biopsies, rather than flow cytometry or Western blot. Immunohistochemistry is a well-established method for diagnostic purposes and is widely used for the assessment of biomarkers. Therefore, the melanoma cell panel was embedded into paraffin and we established Nectin-1, HVEM, STING, and cGAS staining. The immunohistochemical analysis revealed a significant correlation between Nectin-1 expression and the oncolytic activity of T-VEC. In contrast, HVEM, STING, and cGAS did not demonstrate this correlation. All in all, the data showed consistency between flow cytometry, Western blot, and immunohistochemistry. The results of the FACS analysis demonstrated a superior correlation between Nectin-1 expression and oncolysis compared to those obtained by IHC. A possible explanation for this discrepancy is that FACS measures surface Nectin-1 expression, which is relevant for viral entry, while IHC also stains the intracellular protein.

3.2.7 T-VEC injection in melanoma metastases: Nectin-1 expression as a predictor of treatment response

A further objective of this study was to correlate *in vitro* data with *in vivo* findings. To this end, we analysed 35 biopsies of melanoma metastasis before injection with T-VEC. We demonstrated that intratumoural T-VEC injection induces a response in 60% of melanoma lesions in patients. In addition, the expression levels of Nectin-1 in pre-treatment biopsies of cutaneous melanoma metastases were a significant predictor of the response to T-VEC-mediated oncolysis.

In contrast to the *in vitro* findings, a correlation was observed between cGAS expression and the response to T-VEC-mediated oncolysis *in vivo*, although this was not statistically significant. This lack of significance may be attributed to environmental factors such as UV exposure and ROS, which can boost DNA immunorecognition, activating the cGAS-STING pathway *in vivo* (Gehrke *et al.,* 2013). In addition, protein expression profiles in immortalized melanoma cell lines may not accurately reflect the complex *in vivo* environment. Melanoma cell lines showed higher Nectin-1 and HVEM expression, while cGAS and STING were more pronounced in melanoma metastases. The abundant presence of these molecules in biopsies may explain why the STING-cGAS pathway did not appear to be a limiting factor in this context. Furthermore, protein expression profiles in immortalized melanoma cell lines may not accurately reflect the complex *in vivo* environment. Melanoma cell lines exhibited higher

Nectin-1 and HVEM expression, while cGAS and STING were more pronounced in melanoma metastases. The abundant presence of these molecules in biopsies may explain why the STING-cGAS pathway did not appear to be a limiting factor in this context.

Taken together Nectin-1 expression levels correlated significantly with tumour cell regression in both cell lines and melanoma metastases. Our results indicate that the baseline expression of Nectin-1 in melanoma metastases is associated with the response to intralesional T-VEC therapy, suggesting its potential as a biomarker. Incorporation of testing for this biomarker into routine laboratory procedures may improve its clinical utility. Improving clinical response prediction may require integrating expression profiles of multiple biomarkers. This could involve utilizing a wider range of cell lines and biopsies from T-VEC-treated patients, which warrants further investigation.

3.3 Expression of pmCiC as a prognostic marker for cancer aggressiveness

3.3.1 Significance of citrate in cancer metastasis: prognostic insights and therapeutic implications

Despite the significant advances that have been made in cancer research and treatment methods, metastatic cancer still represents the most lethal form of the disease (Neophytou *et al.,* 2021). One of the biggest challenges that remains is the development of drugs against resistant cancer cells, which can lead to disease recurrence and the spread of metastases. Cancer is characterized by traits such as unlimited replicative potential, evasion of cell death mechanisms, resistance to growth inhibition signals, stimulation of blood vessel formation (angiogenesis), and promotion of invasion and metastasis (Hanahan & Weinberg, 2011). Cancer cells undergoing proliferation need to produce enough energy for cellular replication while also fulfilling the anabolic demands for biosynthetic macromolecules necessary to construct new cells and to migrate and invade distant organs for metastasis. In order to fulfil these requirements, cancer cells must undergo metabolic alterations which is also a key characteristic of cancer (Hanahan & Weinberg, 2011).

The significance of citrate in tumour biology is underscored by its role as a primary substrate in fatty acid synthesis, a metabolic hallmark of cancer (Wang *et al.,* 2020). It has been shown that cancer cells require constant levels of intracellular citrate to support their metabolism, which can be produced intracellularly or delivered to the cancer cells from the extracellular space (Mycielska *et al.,* 2018). The extracellular uptake of citrate takes place via the pmCiC (Mycielska *et al.,* 2018). This transporter is a variant of the mCiC and belongs to the SLC25 gene family (Mazurek *et al.,* 2010). Histopathological studies have demonstrated that pmCiC

is expressed in tumour cells of various human cancers, and that the transporter is increasingly present at the invasion front as well as at metastatic sites (Mycielska *et al.,* 2018).

The question arises how the citrate is made available to the tumour from the extracellular space. There are several potential routes by which citrate could be delivered to cancer cells. These include the bloodstream, and the supply of citrate from the tumour microenvironment (TME). Recent research underscores the critical role of stromal support in driving cancer progression and facilitating metastasis (Xu *et al.,* 2022; Lee *et al.,* 2023). The TME, through mechanisms such as angiogenesis and metabolic substrate release by cancer-associated cells, provides essential metabolites to cancer cells (Eisenberg *et al.,* 2020; Chen *et al.,* 2021). Additionally, cancer-associated stroma releases growth factors and modulates immune responses (Chen *et al.,* 2023; Nishida, 2021). Tumour-associated macrophages, in particular, contribute significantly to the cancer microenvironment by promoting tumour progression and inflammation (Maller *et al.,* 2021; Zhou *et al.,* 2019). However, the role of citrate in mediating communication between tumour cells and the TME remains uninvestigated in this regard.

The overall aim of the present thesis was to investigate whether cancer-associated stromal cells act as a supplier of extracellular citrate to cancer cells and whether citrate uptake plays a role in cancer metastasis. We also evaluated whether pmCiC expression in cancer and stromal cells is associated with increased cancer aggressiveness and can serve as a prognostic marker.

Our study identified pmCiC as a promising prognostic cancer marker for predicting the progression of metastatic disease. We retrospectively analysed 92 patients with human gastrointestinal (20), lung (39), prostate (14) and urothelial (19) cancers of different tumour stages for pmCiC expression. For each primary tumour (stage IV), the associated metastasis, if present, was also examined. This resulted in a maximum of 29 metastases. Tissues were analysed by immunohistochemistry. We have identified a clear correlation between pmCiC expression in cancer cells and cancer-associated stroma with tumour stage.

In addition, we showed that citrate is supplied to tumour cells by CAS and citrate uptake plays a significant role in cancer metastatic progression (enhancing invasiveness and organ colonisation). Citrate release from CAS is controlled by cancer cells through cross-cellular communication.

In the presence of extracellular citrate there was a general decrease in the levels of metabolites tested in cancer cells. Specifically, intracellular levels of substrates involved in intracellular citrate synthesis, such as serine, glycine, glutamine, and glutamate, were reduced. This suggests that cancer cells lacking extracellular citrate must utilize alternative pathways to compensate. Consistently, the presence of extracellular citrate lowered the levels of several metabolites considered by-products of increased citrate synthesis (Haferkamp *et al.,* 2020).

This metabolic shift likely leads to a more balanced use of metabolic pathways, potentially contributing to a more aggressive cancer phenotype.

Our study suggests that extracellular citrate uptake by cancer cells influences tumour metabolism and microenvironment interactions, potentially contributing to tumour aggressiveness and metastasis formation. From a therapeutic standpoint, targeting citrate metabolism presents promising avenues for cancer treatment. Our findings suggest that blocking citrate uptake or release could inhibit tumour growth, angiogenesis, and metastasis formation. Further research is warranted to elucidate the mechanistic details of citrate-mediated tumour-stroma interactions and translate these findings into effective therapeutic strategies for cancer treatment and metastasis prevention. Our study sheds further light on the complex role of citrate and pmCiC in cancer metabolism, microenvironment interactions and tumour progression.

3.3.2 The metabolic activity of CAFs is regulated by cancer cells

We found that CAFs and other cells of the TME express pmCiC and synthesise increased amounts of citrate. Our findings reveal that the metabolic activity of CAFs depends on the availability of extracellular citrate to cancer cells. We propose that in the absence of extracellular citrate, cancer cells induce changes in their environment to obtain the necessary substrate. This statement was supported by the fact that cancer cells deprived of extracellular citrate for 48 hours release IL-6, which stimulates angiogenesis and growth-regulated oncogenes (GROs) involved in stromal transformation and senescence (Nagasaki *et al.,* 2014; Masjedi *et al.,* 2018). Senescent fibroblasts, known components of the cancer environment, have been shown to release high levels of citrate (James *et al.,* 2015). Thus, cancer cells deprived of citrate induce the release of factors that stimulate their environment to compensate for the citrate deficiency.

3.3.3 Effects of extracellular citrate on tumour progression

We have observed that extracellular citrate played a significant role in EMT-MET transition. During the colonization phase observed after 2 weeks of incubation with extracellular citrate, the release of IL-3, an angiogenesis-stimulating cytokine, and GROs was noted. Cancer cells cultured long-term without citrate released similar cytokines at 48 hours and 2 weeks, indicating the critical role of citrate in metastatic reprogramming. These findings underscore the complex metabolic interplay within the TME and highlight the importance of extracellular citrate in modulating tumour behaviour and metastatic potential.

Continued presence of citrate induces mesenchymal-to-epithelial transition (MET), thereby promoting growth and colonization (Brabletz, 2012). This suggests citrate's signalling role in completing stromal transformation, preparing a niche for metastatic growth. Previous studies

have shown that elevated citrate levels prior to leptomeningeal carcinomatosis in lung cancer suggest that cancer cells may transform distant stroma and induce local citrate elevation prior to metastasis (An *et al.,* 2015).

We also found that shorter exposure to extracellular citrate induces an invasive phenotype akin to epithelial-mesenchymal transition (EMT). This effect was reproduced when cancer cells were exposed to media from fibroblasts transformed by citrate-deprived cancer cells, therefore induced to supplement this metabolite. The process of supplementing citrate by CAS could impact cancer treatment strategies. It raises the possibility that inducing stromal transformation, which may occur as a response to therapies like chemotherapy, could inadvertently promote metastasis. This transformation process, which involves changes in metabolite and cytokine levels in the local environment, may trigger metastatic behaviours such as EMT and MET. The remaining cancer cells may exhibit altered metastatic behaviour, potentially leading to disease progression and treatment resistance.

3.3.4 Impact of citrate deprivation on tumour behaviour

Gluconate, a derivative of glucose, is a salt of gluconic acid. It is typically considered physiologically neutral and is used in medicine as a heavy ion carrier (Mycielska *et al.,* 2019). It also finds utility in electrophysiology and transport research as a substitute for chloride ions due to its inability to cross the plasma membrane (Carini *et al.,* 1997; Bonzanni *et al.,* 2020). Furthermore, gluconate competitively and irreversibly blocks pmCiC (Mycielska *et al.,* 2019).

In our study, we showed that blocking citrate uptake from cancer cells with gluconate significantly reduced the growth and metastasis of human pancreatic cancer cells *in vivo*, while also attenuating stromal activation and angiogenesis. Therefore, preventing citrate uptake *in vivo* could potentially hinder tumour progression. Furthermore, we observed an increase in immune cell infiltration of the gluconate-treated mouse tumour xenografts. This suggests that blocking the uptake of extracellular citrate from cancer cells, which consequently leads to higher citrate levels in the surrounding area, could potentially enhance the anti-cancer immune response. While these findings are intriguing, it is important to note that this study was conducted using immunocompromised mice, which precluded a thorough investigation into the immune response triggered by gluconate application. Therefore, further research is needed to fully understand the impact of gluconate on immune activity in cancer.

For the staining of the immune cells we used FAP, which is not a typical immune cell marker. However, FAP-expressing immune cells have previously been identified and are thought to be CD45+ cells (Arnold, James N. *et al.,* 2014; Cremasco *et al.,* 2018). This observation is consistent with the increased release of pro-inflammatory cytokines by cancer cells when deprived of extracellular citrate. Furthermore, an increased release of pro-inflammatory cytokines has been linked to citrate uptake by monocytes, while activated macrophages have

been observed to accumulate citrate (Ashbrook *et al.,* 2015; Jha *et al.,* 2015). This may suggest that preventing cancer cells from taking up extracellular citrate, and thus increasing the local concentration of citrate, may have a stimulating effect on the immune response against cancer.

We also found that gluconate had mitotoxic effects on cancer cells, but only at very high concentrations, much higher than those used in our experiments. Therefore, the observed effects of gluconate in our experiments were likely due to its specific action on pmCiC rather than non-specific mitochondrial blocking.

3.3.5 Correlation between pmCiC expression and tumour stage

Our study shows that pmCiC expression in cancer cells correlates with tumour stage and significantly increases at advanced stages and metastatic sites, regardless of tumour origin. This supports our hypothesis that extracellular citrate uptake influences cancer cell invasiveness (EMT) or colonisation (MET), with elevated citrate levels in organs such as the brain, bone or liver promoting secondary tumour growth and facilitating organ colonisation (Parkinson *et al.,* 2021; Drexler *et al.,* 2021). However, variable pmCiC expression in cancer and peritumour tissues may also reflect differing extracellular citrate levels in the organs from which the tissues were obtained.

Nevertheless, pmCiC expression was less frequent in the early stages of tumour development. This means that in the initial phases of cancer growth, fewer cancer cells show pmCiC expression. However, as the tumour progresses, pmCiC expression increases. This increase suggests that the presence of pmCiC might be linked to a higher chance of the cancer spreading to other parts of the body (metastasis). The expression of pmCiC in cancer cells could indicate an increased metastatic potential. The correlation between pmCiC expression and metastasis is even stronger when considering the expression of pmCiC in both the cancer cells and the surrounding stromal cells together with the tumour stage. This combined assessment provides a clearer indication of the cancer's potential to metastasise compared to looking at pmCiC expression in cancer cells alone.

Interestingly, the number of metastases with pmCiC staining in the stroma is lower than in primary stage IV tumours. The most common organs in which distant metastasis occur, such as the liver, brain, bone or the lung, are rich in citrate (Parkinson *et al.,* 2021). In this case, the cancer cells need to monitor the citrate level closely, as an elevated citrate level can be harmful. Therefore, colonising cancer cells reduce their demand for additional citrate from the stroma in an extracellular citrate-rich environment. However, the number of metastatic tissues expressing pmCiC in cancer cells increases compared to primary tumours at stage IV. This suggests that extracellular citrate plays a crucial role in the colonization of organs by cancer cells.

The expression of pmCiC in the supportive tissue around the primary tumours (the stroma) can vary depending on the organ. This variation is influenced by two main factors: the levels of extracellular citrate in different organs and how close the tumour is to blood vessels. Different organs have varying amounts of citrate in their environment, and this affects how much pmCiC is expressed in the stroma of tumours located in those organs. Additionally, the proximity to blood vessels can influence the availability of citrate, further affecting pmCiC expression. Assessing pmCiC in cancer cells, their microenvironment, and blood vessels together may provide a better prognostic marker for disease progression than evaluating each element separately. However, this aspect needs more extensive and detailed research.

Our data show a correlation between pmCiC expression in cancer cells and the tumour environment, indicating a balance between citrate uptake and release. Citrate may play a crucial role in communication between cancer cells and the stroma, with the amount of citrate released by cancer-associated fibroblasts depending on extracellular citrate availability (Drexler *et al.,* 2021). Controlled citrate enrichment in the cancer microenvironment may be a unique regulatory mechanism in cancer development because increased or decreased intracellular levels of citrate can be detrimental to cancer cells, as already stated above (Haferkamp *et al.,* 2020; Icard *et al.,* 2019; Jordan *et al.,* 2022).

3.3.6 Lack of correlation between CD31 or FAP expression and tumour stage

We found no correlation between CD31 or FAP expression and tumour stage. The use of CD31 as a prognostic marker in cancer is contentious, with some studies supporting its prognostic value (Schmidt *et al.,* 2017; Sandlund *et al.,* 2007; Schlüter *et al.,* 2018), while others do not (RASK *et al.,* 2019). Additionally, some research even suggests an inverse correlation between CD31 expression and patient survival (Emmert *et al.,* 2016; VIRMAN *et al.,* 2015). The absence of correlation in our study may be attributed to the analysis of tumours from different origins as a single group. Variations in blood vessel density across different organs could impact the overall assessment.

The levels of FAP were significantly lower in the stromal areas of secondary tumour growth compared to primary tumours. Unlike primary tumours, which are often removed through surgery, metastases are usually not removed because they indicate that the cancer has spread extensively and is often incurable. The tissues from metastases from our study might have been obtained at an early stage of their development. At this early stage, the stroma and the cancer-supporting infrastructure might not yet be fully developed.

We also did not find a correlation between CD31 and FAP expression in the stroma and cancer stage. This could be due to a number of factors. Firstly, the number of tissue samples was too small to obtain reliable data. Secondly, analysing tumours of different origins may have

influenced the results (Parkinson *et al.,* 2021). The biological characteristics and stromal interaction requirements of tumours from different organs are different. In addition, each organ has a unique microenvironment that affects how tumours grow and interact with surrounding tissues. These differences can affect the expression of markers such as CD31 and FAP. By grouping tumours from different organs into a single category, it is difficult to draw clear conclusions about the relationship between CD31 and FAP expression and cancer stage.

More strikingly, the consistent correlation of pmCiC with tumour stage, independent of tumour origin, suggests that it may be a novel, broadly applicable and stable marker of tumour aggressiveness.

3.3.7 Increased pmCiC expression in blood vessels of advanced cancer stages

In our study, there was an increase in pmCiC levels in the blood vessels of patients with later-stage cancer. However, pmCiC was observed primarily in a small subset of small blood vessels, indicating its presence during the early stages of vessel formation rather than in fully developed vessels. In contrast, CD31 is an endothelial cell marker and stains all blood vessels at any stage from early to full vascularization (Bösmüller *et al.,* 2018). This observation implies that pmCiC might have a role in facilitating citrate uptake specifically during the initial stages of blood vessel formation, potentially contributing to angiogenesis in early cancer progression.

Citrate, which is a crucial component in fatty acid synthesis, could play a role in shaping and adapting the plasma membrane necessary for angiogenesis, the process of forming new blood vessels. Inhibiting fatty acid synthesis can affect angiogenesis, such as in a murine stroke model where cerulenin caused endothelial cell leakage and disrupted the blood-brain barrier (Janssen *et al.,* 2021).

We found that most blood vessels expressing pmCiC were found in stage IV tumours, suggesting a potential association between pmCiC-expressing blood vessels and the spread of metastatic cells. This implies that pmCiC expression in endothelial cells might be specific to early cancer angiogenesis and could influence metastasis through mechanisms involving controlled fatty acid levels or other unique characteristics. However, further research is needed to fully understand this relationship.

4 Summary and Conclusions

Cancer is a major global health challenge, responsible for millions of deaths each year, particularly from metastatic forms (Deyell *et al.,* 2021). The main goal of treatment is to prevent metastasis and slow disease progression, although choosing the right approach is often challenging. Biomarkers, which are biological indicators of disease status and treatment response, are essential for early detection, diagnosis, prognosis and personalised treatment to improve patient outcomes. Advancing biomarker research is critical for improved detection, treatment success and survival rates. This thesis aimed to discover new potential biomarkers, specifically to predict the response of melanoma patients to oncolytic virus therapy and to assess pmCiC as a marker of cancer aggressiveness.

Oncolytic virotherapy is an innovative treatment for advanced melanoma, with T-VEC being the only FDA-approved OV for this purpose (Andtbacka et al., 2015). T-VEC is a modified HSV-1 virus engineered to selectively replicate in tumour cells and enhance immune response by expressing GM-CSF. Treatment involves multiple injections into melanoma lesions, which can cause local reactions and systemic side effects, such as fever, fatigue, and nausea. Serious complications, though rare, include immune reactions and herpes virus infections. Despite the proven efficacy of oncolytic herpes viruses like T-VEC in treating malignant melanoma, some patients don't benefit from it. This underscores the need for biomarkers that can predict treatment success or failure, especially in advanced cases. Previous research has suggested potential markers like cGAS and STING for recognizing HSV DNA and Nectin-1 as an HSV-1 entry receptor associated with tumour regression. However, these markers haven't been systematically evaluated for T-VEC treatment in melanoma.

This study aimed to identify predictive markers for melanoma response to oncolytic virotherapy to optimize treatment decisions. Nectin-1, a cell surface molecule facilitating HSV-1 entry, was identified as a promising biomarker. Analysis of 20 melanoma cell lines and 35 cutaneous melanoma metastases from 21 patients treated with T-VEC showed a significant correlation between Nectin-1 expression and tumour regression. High Nectin-1 levels were associated with effective melanoma cell killing by T-VEC. These findings suggest that Nectin-1 could be a key factor in the efficacy of oncolytic herpes viruses across various tumour types, meriting further research.

In the second part of the present study, we investigated whether pmCiC expression is associated with increased disease aggressiveness of cancer and can serve as a prognostic marker. Our study sheds light on the complex role of citrate in cancer metabolism and microenvironment interactions. Extracellular citrate emerges as a key player in tumour progression, with potential implications for metastasis and therapeutic interventions. The expression of pmCiC in human cancer tissues appears to increase with tumour stage, and is

particularly elevated at metastatic sites. Additionally, elevated pmCiC levels were also found in the tumour microenvironment. However, the exact role of citrate in metastatic progression requires further investigation in future studies. Conversely, there were no significant correlations observed between the stromal markers CD31 and FAP, and tumour stage. It is plausible that pmCiC expression in cancer cells and surrounding stroma may be an early event in metastasis and organ colonization. Notably, our study included human cancerous tissues from various origins, representing one of the initial investigations revealing a common factor associated with tumour aggressiveness. Therefore, its potential as a prognostic marker warrants further investigation. In addition, we fond CAS as a novel source of extracellular citrate for cancer. We identified the transporter responsible for citrate release and confirmed its expression in human tissues. Blocking citrate uptake by cancer cells using gluconate reduced cancer spread and stromal transformation *in vivo*. Our discovery of citrate release by CAS sheds new light on tumour-stroma interactions, metastasis promotion, and resistance to therapy. Inhibiting citrate release and uptake may offer promising strategies for cancer treatment and metastasis prevention.

In summary, Nectin-1 and pmCiC have the potential to serve as predictive and prognostic biomarkers, with the capacity to assist in the prediction of therapeutic outcomes and the determination of tumour aggressiveness.

Lists of figures

Main figures:

Supplementary figures:

List of tables

References

Ablasser, A., **Goldeck, M.**, **Cavlar, T.**, **Deimling, T.**, **Witte, G.**, **Röhl, I.**, **Hopfner, K.-P.**, **Ludwig, J. & Hornung, V. (2013).** cGAS produces a 2'-5'-linked cyclic dinucleotide second messenger that activates STING. *Nature* **498**, 380–384.

Abou-Alfa, G. K., **Macarulla, T.**, **Javle, M. M.**, **Kelley, R. K.**, **Lubner, S. J.**, **Adeva, J.**, **Cleary, J. M.**, **Catenacci, D. V. & Borad, M. J. & other authors (2020).** Ivosidenib in IDH1-mutant, chemotherapy-refractory cholangiocarcinoma (ClarIDHy): a multicentre, randomised, double-blind, placebo-controlled, phase 3 study. *The Lancet. Oncology* **21**, 796–807.

Akhtar, M. J., **Khan, S. A.**, **Kumar, B.**, **Chawla, P.**, **Bhatia, R. & Singh, K. (2023).** Role of sodium dependent SLC13 transporter inhibitors in various metabolic disorders. *Molecular and cellular biochemistry* **478**, 1669–1687.

Akram, M. (2014). Citric acid cycle and role of its intermediates in metabolism. *Cell biochemistry and biophysics* **68**, 475–478.

Alvarez-Breckenridge, C., **Kaur, B. & Chiocca, E. A. (2009).** Pharmacologic and chemical adjuvants in tumor virotherapy. *Chemical reviews* **109**, 3125–3140.

Alvarez-Breckenridge, C. A., **Yu, J.**, **Price, R.**, **Wojton, J.**, **Pradarelli, J.**, **Mao, H.**, **Wei, M.**, **Wang, Y. & He, S. & other authors (2012).** NK cells impede glioblastoma virotherapy through NKp30 and NKp46 natural cytotoxicity receptors. *Nature medicine* **18**, 1827–1834.

An, Y. J., **Cho, H. R.**, **Kim, T. M.**, **Keam, B.**, **Kim, J. W.**, **Wen, H.**, **Park, C.-K.**, **Lee, S.-H. & Im, S.-A. & other authors (2015).** An NMR metabolomics approach for the diagnosis of leptomeningeal carcinomatosis in lung adenocarcinoma cancer patients. *International journal of cancer* **136**, 162–171.

Andtbacka, R. H. I., **Collichio, F.**, **Harrington, K. J.**, **Middleton, M. R.**, **Downey, G.**, **Öhrling, K. & Kaufman, H. L. (2019).** Final analyses of OPTiM: a randomized phase III trial of talimogene laherparepvec versus granulocyte-macrophage colony-stimulating factor in unresectable stage III-IV melanoma. *Journal for immunotherapy of cancer* **7**, 145.

Andtbacka, R. H. I., **Kaufman, H. L.**, **Collichio, F.**, **Amatruda, T.**, **Senzer, N.**, **Chesney, J.**, **Delman, K. A.**, **Spitler, L. E. & Puzanov, I. & other authors (2015).** Talimogene Laherparepvec Improves Durable Response Rate in Patients With Advanced Melanoma. *Journal of clinical oncology : official journal of the American Society of Clinical Oncology* **33**, 2780–2788.

Annaval, T., **Wild, R.**, **Crétinon, Y.**, **Sadir, R.**, **Vivès, R. R. & Lortat-Jacob, H. (2020).** Heparan Sulfate Proteoglycans Biosynthesis and Post Synthesis Mechanisms Combine Few

Enzymes and Few Core Proteins to Generate Extensive Structural and Functional Diversity. *Molecules (Basel, Switzerland)* **25**.

Argyle, D. & Kitamura, T. (2018). Targeting Macrophage-Recruiting Chemokines as a Novel Therapeutic Strategy to Prevent the Progression of Solid Tumors. *Frontiers in immunology* **9**, 2629.

Arnold, James N., **Magiera**, Lukasz, **Kraman**, Matthew **& Fearon**, Douglas T. **(2014).** Tumoral immune suppression by macrophages expressing fibroblast activation protein-α and heme oxygenase-1. *Cancer immunology research* **2**, 121–126.

Arnold, M., **Holterhues**, C., **Hollestein**, L. M., **Coebergh**, J. W. W., **Nijsten**, T., **Pukkala**, E., **Holleczek**, B., **Tryggvadóttir**, L. **& Comber**, H. **& other authors (2014).** Trends in incidence and predictions of cutaneous melanoma across Europe up to 2015. *Journal of the European Academy of Dermatology and Venereology : JEADV* **28**, 1170–1178.

Arnold, M., **Singh, D.**, **Laversanne, M.**, **Vignat, J.**, **Vaccarella, S.**, **Meheus, F.**, **Cust, A. E.**, **Vries, E.** de, **Whiteman, D. C. & Bray, F. (2022).** Global Burden of Cutaneous Melanoma in 2020 and Projections to 2040. *JAMA dermatology* **158**, 495–503.

Aronson, J. K. & Ferner, R. E. (2017). Biomarkers-A General Review. *Current protocols in pharmacology* **76**, 9.23.1-9.23.17.

Ashbrook, M. J., **McDonough, K. L.**, **Pituch, J. J.**, **Christopherson, P. L.**, **Cornell, T. T.**, **Selewski, D. T.**, **Shanley, T. P. & Blatt, N. B. (2015).** Citrate modulates lipopolysaccharide-induced monocyte inflammatory responses. *Clinical and experimental immunology* **180**, 520–530.

Azenshtein, E., **Luboshits, G.**, **Shina, S.**, **Neumark, E.**, **Shahbazian, D.**, **Weil, M.**, **Wigler, N.**, **Keydar, I. & Ben-Baruch, A. (2002).** The CC Chemokine RANTES in Breast Carcinoma ProgressionRegulation of Expression and Potential Mechanisms of Promalignant Activity. *Cancer Res* **62**, 1093–1102.

Balch, C. M., **Gershenwald, J. E.**, **Soong, S.-J.**, **Thompson, J. F.**, **Atkins, M. B.**, **Byrd, D. R.**, **Buzaid, A. C.**, **Cochran, A. J. & Coit, D. G. & other authors (2009).** Final version of 2009 AJCC melanoma staging and classification. *Journal of clinical oncology : official journal of the American Society of Clinical Oncology* **27**, 6199–6206.

Bartlett, D. L., **Liu, Z.**, **Sathaiah, M.**, **Ravindranathan, R.**, **Guo, Z.**, **He, Y. & Guo, Z. S. (2013).** Oncolytic viruses as therapeutic cancer vaccines. *Molecular cancer* **12**, 103.

Becker, J. C., **Stang, A.**, **DeCaprio, J. A.**, **Cerroni, L.**, **Lebbé, C.**, **Veness, M. & Nghiem, P. (2017).** Merkel cell carcinoma. *Nature reviews. Disease primers* **3**, 17077.

Bedikian, A. Y., **Millward, M.**, **Pehamberger, H.**, **Conry, R.**, **Gore, M.**, **Trefzer, U.**, **Pavlick, A. C.**, **DeConti, R. & Hersh, E. M. & other authors (2006).** Bcl-2 antisense (oblimersen

sodium) plus dacarbazine in patients with advanced melanoma: the Oblimersen Melanoma Study Group. *Journal of clinical oncology : official journal of the American Society of Clinical Oncology* **24**, 4738–4745.

Bell, C. W., **Jiang, W.**, **Reich, C. F. & Pisetsky, D. S. (2006).** The extracellular release of HMGB1 during apoptotic cell death. *American journal of physiology. Cell physiology* **291**, C1318-25.

Berk-Krauss, J., **Stein, J. A.**, **Weber, J.**, **Polsky, D. & Geller, A. C. (2020).** New Systematic Therapies and Trends in Cutaneous Melanoma Deaths Among US Whites, 1986-2016. *American journal of public health* **110**, 731–733.

Bevona, C., **Goggins, W.**, **Quinn, T.**, **Fullerton, J. & Tsao, H. (2003).** Cutaneous melanomas associated with nevi. *Archives of dermatology* **139**, 1620-4; discussion 1624.

Bhat, V. K., **Krump, C.**, **Bernhart, E.**, **Becker, J. C.**, **Sattler, W. & Ghaffari-Tabrizi-Wizsy, N. (2018).** A short-term in vivo model for Merkel Cell Carcinoma. *Experimental dermatology* **27**, 684–687.

Biomarkers Definitions Working Group **(2001).** Biomarkers and surrogate endpoints: preferred definitions and conceptual framework. *Clinical pharmacology and therapeutics* **69**, 89–95.

Bommareddy, P. K., **Patel, A.**, **Hossain, S. & Kaufman, H. L. (2017).** Talimogene Laherparepvec (T-VEC) and Other Oncolytic Viruses for the Treatment of Melanoma. *Am J Clin Dermatol* **18**, 1–15.

Bommareddy, P. K., **Shettigar, M. & Kaufman, H. L. (2018).** Integrating oncolytic viruses in combination cancer immunotherapy. *Nat Rev Immunol* **18**, 498–513.

Bommareddy, P. K., **Zloza, A.**, **Rabkin, S. D. & Kaufman, H. L. (2019).** Oncolytic virus immunotherapy induces immunogenic cell death and overcomes STING deficiency in melanoma. *Oncoimmunology* **8**, 1591875.

Bonzanni, M., **Payne, S. L.**, **Adelfio, M.**, **Kaplan, D. L.**, **Levin, M. & Oudin, M. J. (2020).** Defined extracellular ionic solutions to study and manipulate the cellular resting membrane potential. *Biology open* **9**.

Boscheinen, J. B., **Thomann, S.**, **Knipe, D. M.**, **DeLuca, N.**, **Schuler-Thurner, B.**, **Gross, S.**, **Dörrie, J.**, **Schaft, N. & Bach, C. & other authors (2019).** Generation of an Oncolytic Herpes Simplex Virus 1 Expressing Human MelanA. *Frontiers in immunology* **10**, 2.

Bösmüller, H., **Pfefferle, V.**, **Bittar, Z.**, **Scheble, V.**, **Horger, M.**, **Sipos, B. & Fend, F. (2018).** Microvessel density and angiogenesis in primary hepatic malignancies: Differential expression of CD31 and VEGFR-2 in hepatocellular carcinoma and intrahepatic cholangiocarcinoma. *Pathology, research and practice* **214**, 1136–1141.

Brabletz, T. (2012). EMT and MET in metastasis: where are the cancer stem cells? *Cancer cell* **22**, 699–701.

Bruning, U., **Morales-Rodriguez, F.**, **Kalucka, J.**, **Goveia, J.**, **Taverna, F.**, **Queiroz, K. C. S.**, **Dubois, C.**, **Cantelmo, A. R. & Chen, R. & other authors (2018).** Impairment of Angiogenesis by Fatty Acid Synthase Inhibition Involves mTOR Malonylation. *Cell metabolism* **28**, 866-880.e15.

Brunnström, H., **Johansson, A.**, **Westbom-Fremer, S.**, **Backman, M.**, **Djureinovic, D.**, **Patthey, A.**, **Isaksson-Mettävainio, M.**, **Gulyas, M. & Micke, P. (2017).** PD-L1 immunohistochemistry in clinical diagnostics of lung cancer: inter-pathologist variability is higher than assay variability. *Modern pathology : an official journal of the United States and Canadian Academy of Pathology, Inc* **30**, 1411–1421.

Burotto, M., **Chiou, V. L.**, **Lee, J.-M. & Kohn, E. C. (2014).** The MAPK pathway across different malignancies: a new perspective. *Cancer* **120**, 3446–3456.

Byrne, E. H. & Fisher, D. E. (2017). Immune and molecular correlates in melanoma treated with immune checkpoint blockade. *Cancer* **123**, 2143–2153.

Campadelli-Fiume, G., **Menotti, L.**, **Avitabile, E. & Gianni, T. (2012).** Viral and cellular contributions to herpes simplex virus entry into the cell. *Current opinion in virology* **2**, 28–36.

Canene-Adams, K. (2013). Preparation of Formalin-fixed Paraffin-embedded Tissue for Immunohistochemistry. In *Methods in Enzymology*, pp. 225–233: Elsevier.

Carini, R., **Bellomo, G.**, **Grazia De Cesaris, M. & Albano, E. (1997).** Glycine protects against hepatocyte killing by KCN or hypoxia by preventing intracellular Na+ overload in the rat. *Hepatology (Baltimore, Md.)* **26**, 107–112.

Cassady, K. A., **Gross, M. & Roizman, B. (1998a).** The herpes simplex virus US11 protein effectively compensates for the gamma1(34.5) gene if present before activation of protein kinase R by precluding its phosphorylation and that of the alpha subunit of eukaryotic translation initiation factor 2. *Journal of virology* **72**, 8620–8626.

Cassady, K. A., **Gross, M. & Roizman, B. (1998b).** The second-site mutation in the herpes simplex virus recombinants lacking the gamma134.5 genes precludes shutoff of protein synthesis by blocking the phosphorylation of eIF-2alpha. *Journal of virology* **72**, 7005–7011.

Cassler, N. M., **Merrill, D.**, **Bichakjian, C. K. & Brownell, I. (2016).** Merkel Cell Carcinoma Therapeutic Update. *Current treatment options in oncology* **17**, 36.

Cha, Y. H., **Yook, J.** in, **Kim, H. S. & Kim, N. H. (2015).** Catabolic metabolism during cancer EMT. *Archives of pharmacal research* **38**, 313–320.

Chao, Y. L., **Shepard, C. R. & Wells, A. (2010).** Breast carcinoma cells re-express E-cadherin during mesenchymal to epithelial reverting transition. *Molecular cancer* **9**, 179.

Chapman, P. B., **Hauschild, A.**, **Robert, C.**, **Haanen, J. B.**, **Ascierto, P.**, **Larkin, J.**, **Dummer, R.**, **Garbe, C. & Testori, A. & other authors (2011).** Improved survival with vemurafenib in melanoma with BRAF V600E mutation. *The New England journal of medicine* **364**, 2507–2516.

Chen, Q. Y., **Gao, B.**, **Tong, D. & Huang, C. (2023).** Crosstalk between extracellular vesicles and tumor-associated macrophage in the tumor microenvironment. *Cancer letters* **552**, 215979.

Chen, Y., **McAndrews, K. M. & Kalluri, R. (2021).** Clinical and therapeutic relevance of cancer-associated fibroblasts. *Nat Rev Clin Oncol* **18**, 792–804.

Cheung, T. C., **Steinberg, M. W.**, **Oborne, L. M.**, **Macauley, M. G.**, **Fukuyama, S.**, **Sanjo, H.**, **D'Souza, C.**, **Norris, P. S. & Pfeffer, K. & other authors (2009).** Unconventional ligand activation of herpesvirus entry mediator signals cell survival. *Proceedings of the National Academy of Sciences of the United States of America* **106**, 6244–6249.

Chou, J., **Chen, J. J.**, **Gross, M. & Roizman, B. (1995).** Association of a M(r) 90,000 phosphoprotein with protein kinase PKR in cells exhibiting enhanced phosphorylation of translation initiation factor eIF-2 alpha and premature shutoff of protein synthesis after infection with gamma 134.5- mutants of herpes simplex virus 1. *Proceedings of the National Academy of Sciences of the United States of America* **92**, 10516–10520.

Clemens, M. J. (2004). Targets and mechanisms for the regulation of translation in malignant transformation. *Oncogene* **23**, 3180–3188.

Connolly, S. A., **Jackson, J. O.**, **Jardetzky, T. S. & Longnecker, R. (2011).** Fusing structure and function: a structural view of the herpesvirus entry machinery. *Nature reviews. Microbiology* **9**, 369–381.

Conrad, D. P., **Tsang, J.**, **Maclean, M.**, **Diallo, J.-S.**, **Le Boeuf, F.**, **Lemay, C. G.**, **Falls, T. J.**, **Parato, K. A.**, **Bell, J. C. & Atkins, H. L. (2013).** Leukemia cell-rhabdovirus vaccine: personalized immunotherapy for acute lymphoblastic leukemia. *Clinical cancer research : an official journal of the American Association for Cancer Research* **19**, 3832–3843.

Costa, A., **Kieffer, Y.**, **Scholer-Dahirel, A.**, **Pelon, F.**, **Bourachot, B.**, **Cardon, M.**, **Sirven, P.**, **Magagna, I. & Fuhrmann, L. & other authors (2018).** Fibroblast Heterogeneity and Immunosuppressive Environment in Human Breast Cancer. *Cancer cell* **33**, 463-479.e10.

Coto-Llerena, M., **Ercan, C.**, **Kancherla, V.**, **Taha-Mehlitz, S.**, **Eppenberger-Castori, S.**, **Soysal, S. D.**, **Ng, C. K. Y.**, **Bolli, M. & Flüe, M.** von **& other authors (2020).** High

Expression of FAP in Colorectal Cancer Is Associated With Angiogenesis and Immunoregulation Processes. *Front. Oncol.* **10**, 979.

Cremasco, V., **Astarita, J. L.**, **Grauel, A. L.**, **Keerthivasan, S.**, **MacIsaac, K.**, **Woodruff, M. C.**, **Wu, M.**, **Spel, L. & Santoro, S. & other authors (2018).** FAP Delineates Heterogeneous and Functionally Divergent Stromal Cells in Immune-Excluded Breast Tumors. *Cancer immunology research* **6**, 1472–1485.

Croft, M. (2003). Co-stimulatory members of the TNFR family: keys to effective T-cell immunity? *Nature reviews. Immunology* **3**, 609–620.

Damaghi, M., **West, J.**, **Robertson-Tessi, M.**, **Xu, L.**, **Ferrall-Fairbanks, M. C.**, **Stewart, P. A.**, **Persi, E.**, **Fridley, B. L. & Altrock, P. M. & other authors (2021).** The harsh microenvironment in early breast cancer selects for a Warburg phenotype. *Proceedings of the National Academy of Sciences of the United States of America* **118**.

David M. Knipe **&** Peter M. Howley **(2020).** *Fields virology:* Wolters Kluwer Health/Lippincott Williams & Wilkins.

Dawaliby, R., **Trubbia, C.**, **Delporte, C.**, **Noyon, C.**, **Ruysschaert, J.-M.**, **van Antwerpen, P. & Govaerts, C. (2016).** Phosphatidylethanolamine Is a Key Regulator of Membrane Fluidity in Eukaryotic Cells. *The Journal of biological chemistry* **291**, 3658–3667.

Decout, A., **Katz, J. D.**, **Venkatraman, S. & Ablasser, A. (2021).** The cGAS-STING pathway as a therapeutic target in inflammatory diseases. *Nat Rev Immunol* **21**, 548–569.

Dentelli, P., **Rosso, A.**, **Olgasi, C.**, **Camussi, G. & Brizzi, M. F. (2011).** IL-3 is a novel target to interfere with tumor vasculature. *Oncogene* **30**, 4930–4940.

Deyell, M., **Garris, C. S. & Laughney, A. M. (2021).** Cancer metastasis as a non-healing wound. *British journal of cancer* **124**, 1491–1502.

Drexler, K., **Schmidt, K. M.**, **Jordan, K.**, **Federlin, M.**, **Milenkovic, V. M.**, **Liebisch, G.**, **Artati, A.**, **Schmidl, C. & Madej, G. & other authors (2021).** Cancer-associated cells release citrate to support tumour metastatic progression. *Life science alliance* **4**.

Drexler, K., **Schwertner, B.**, **Haerteis, S.**, **Aung, T.**, **Berneburg, M.**, **Geissler, E. K.**, **Mycielska, M. E. & Haferkamp, S. (2022).** The Role of Citrate Homeostasis in Merkel Cell Carcinoma Pathogenesis. *Cancers* **14**.

Duffy, M. J. (2013). Tumor markers in clinical practice: a review focusing on common solid cancers. *Medical principles and practice : international journal of the Kuwait University, Health Science Centre* **22**, 4–11.

Eck, S. M., **Côté, A. L.**, **Winkelman, W. D. & Brinckerhoff, C. E. (2009).** CXCR4 and matrix metalloproteinase-1 are elevated in breast carcinoma-associated fibroblasts and in normal

mammary fibroblasts exposed to factors secreted by breast cancer cells. *Molecular Cancer Research* **7**, 1033–1044.

Edwards, R. G. & Longnecker, R. (2017). Herpesvirus Entry Mediator and Ocular Herpesvirus Infection: More than Meets the Eye. *Journal of virology* **91**.

Eidelman, E., **Twum-Ampofo, J.**, **Ansari, J. & Siddiqui, M. M. (2017).** The Metabolic Phenotype of Prostate Cancer. *Frontiers in oncology* **7**, 131.

Eisenberg, L., **Eisenberg-Bord, M.**, **Eisenberg-Lerner, A. & Sagi-Eisenberg, R. (2020).** Metabolic alterations in the tumor microenvironment and their role in oncogenesis. *Cancer letters* **484**, 65–71.

Eisenberg, R. J., **Atanasiu, D.**, **Cairns, T. M.**, **Gallagher, J. R.**, **Krummenacher, C. & Cohen, G. H. (2012).** Herpes virus fusion and entry: a story with many characters. *Viruses* **4**, 800–832.

Emmert, A., **Oellerich, A.**, **Füzesi, L.**, **Waldmann-Beushausen, R.**, **Bohnenberger, H.**, **Schöndube, F. A. & Danner, B. C. (2016).** Prognostic Significance of CD31 Expression in Patients with Non-Small-Cell-Lung Cancer. *ALC* **05**, 21–29.

Erdmann, F., **Lortet-Tieulent, J.**, **Schüz, J.**, **Zeeb, H.**, **Greinert, R.**, **Breitbart, E. W. & Bray, F. (2013).** International trends in the incidence of malignant melanoma 1953-2008--are recent generations at higher or lower risk? *International journal of cancer* **132**, 385–400.

Erdogan, B., **Ao, M.**, **White, L. M.**, **Means, A. L.**, **Brewer, B. M.**, **Yang, L.**, **Washington, M. K.**, **Shi, C. & Franco, O. E. & other authors (2017).** Cancer-associated fibroblasts promote directional cancer cell migration by aligning fibronectin. *The Journal of cell biology* **216**, 3799–3816.

Eton, O., **Legha, S. S.**, **Moon, T. E.**, **Buzaid, A. C.**, **Papadopoulos, N. E.**, **Plager, C.**, **Burgess, A. M.**, **Bedikian, A. Y. & Ring, S. & other authors (1998).** Prognostic factors for survival of patients treated systemically for disseminated melanoma. *Journal of clinical oncology : official journal of the American Society of Clinical Oncology* **16**, 1103–1111.

Faubert, B., **Li, K. Y.**, **Cai, L.**, **Hensley, C. T.**, **Kim, J.**, **Zacharias, L. G.**, **Yang, C.**, **Do, Q. N. & Doucette, S. & other authors (2017).** Lactate Metabolism in Human Lung Tumors. *Cell* **171**, 358-371.e9.

Faubert, B., **Solmonson, A. & DeBerardinis, R. J. (2020).** Metabolic reprogramming and cancer progression. *Science* **368**.

Feder, A.-L., **Pion, E.**, **Troebs, J.**, **Lenze, U.**, **Prantl, L.**, **Htwe, M. M.**, **Phyo, A.**, **Haerteis, S. & Aung, T. (2020).** Extended analysis of intratumoral heterogeneity of primary osteosarcoma tissue using 3D-in-vivo-tumor-model. *Clinical hemorheology and microcirculation* **76**, 133–141.

Fink, B. D., **Bai, F.**, **Yu, L.**, **Sheldon, R. D.**, **Sharma, A.**, **Taylor, E. B. & Sivitz, W. I. (2018).** Oxaloacetic acid mediates ADP-dependent inhibition of mitochondrial complex II-driven respiration. *The Journal of biological chemistry* **293**, 19932–19941.

Folkman, J. (1971). Tumor angiogenesis: therapeutic implications. *N Engl J Med* **285**, 1182–1186.

Food and Drug Administration **(1977).** 182.6757 Sodium gluconate. https://www.ecfr.gov/current/title-21/part-182/section-182.6757.

Friedl, P. & Wolf, K. (2003). Tumour-cell invasion and migration: diversity and escape mechanisms. *Nature reviews. Cancer* **3**, 362–374.

Friedman, G. K., **Bernstock, J. D.**, **Chen, D.**, **Nan, L.**, **Moore, B. P.**, **Kelly, V. M.**, **Youngblood, S. L.**, **Langford, C. P. & Han, X. & other authors (2018).** Enhanced Sensitivity of Patient-Derived Pediatric High-Grade Brain Tumor Xenografts to Oncolytic HSV-1 Virotherapy Correlates with Nectin-1 Expression. *Sci Rep* **8**, 13930.

Früh, K., **Ahn, K.**, **Djaballah, H.**, **Sempé, P.**, **van Endert, P. M.**, **Tampé, R.**, **Peterson, P. A. & Yang, Y. (1995).** A viral inhibitor of peptide transporters for antigen presentation. *Nature* **375**, 415–418.

Fu, X., **Chin, R. M.**, **Vergnes, L.**, **Hwang, H.**, **Deng, G.**, **Xing, Y.**, **Pai, M. Y.**, **Li, S. & Ta, L. & other authors (2015).** 2-Hydroxyglutarate Inhibits ATP Synthase and mTOR Signaling. *Cell metabolism* **22**, 508–515.

Fucikova, J., **Kralikova, P.**, **Fialova, A.**, **Brtnicky, T.**, **Rob, L.**, **Bartunkova, J. & Spísek, R. (2011).** Human tumor cells killed by anthracyclines induce a tumor-specific immune response. *Cancer research* **71**, 4821–4833.

Fuertes, M. B., **Kacha, A. K.**, **Kline, J.**, **Woo, S.-R.**, **Kranz, D. M.**, **Murphy, K. M. & Gajewski, T. F. (2011).** Host type I IFN signals are required for antitumor CD8+ T cell responses through CD8{alpha}+ dendritic cells. *The Journal of experimental medicine* **208**, 2005–2016.

Fukuhara, A., **Irie, K.**, **Yamada, A.**, **Katata, T.**, **Honda, T.**, **Shimizu, K.**, **Nakanishi, H. & Takai, Y. (2002).** Role of nectin in organization of tight junctions in epithelial cells. *Genes to cells : devoted to molecular & cellular mechanisms* **7**, 1059–1072.

Fukuhara, M., **Agnarsdóttir, M.**, **Edqvist, P.-H.**, **Coter, A. & Ponten, F. (2016).** SATB2 is expressed in Merkel cell carcinoma. *Archives of dermatological research* **308**, 449–454.

Gaggioli, C., **Hooper, S.**, **Hidalgo-Carcedo, C.**, **Grosse, R.**, **Marshall, J. F.**, **Harrington, K. & Sahai, E. (2007).** Fibroblast-led collective invasion of carcinoma cells with differing roles for RhoGTPases in leading and following cells. *Nature cell biology* **9**, 1392–1400.

Gaiser, M. R., **Bongiorno, M. & Brownell, I. (2018).** PD-L1 inhibition with avelumab for metastatic Merkel cell carcinoma. *Expert review of clinical pharmacology* **11**, 345–359.

Gallo, M., **Sapio, L.**, **Spina, A.**, **Naviglio, D.**, **Calogero, A. & Naviglio, S. (2015).** Lactic dehydrogenase and cancer: an overview. *Frontiers in bioscience (Landmark edition)* **20**, 1234–1249.

Gandini, S., **Sera, F.**, **Cattaruzza, M. S.**, **Pasquini, P.**, **Picconi, O.**, **Boyle, P. & Melchi, C. F. (2005).** Meta-analysis of risk factors for cutaneous melanoma: II. Sun exposure. *European journal of cancer (Oxford, England : 1990)* **41**, 45–60.

Gao, J., **Shi, L. Z.**, **Zhao, H.**, **Chen, J.**, **Xiong, L.**, **He, Q.**, **Chen, T.**, **Roszik, J. & Bernatchez, C. & other authors (2016).** Loss of IFN-γ Pathway Genes in Tumor Cells as a Mechanism of Resistance to Anti-CTLA-4 Therapy. *Cell* **167**, 397-404.e9.

Garg, A. D., **Krysko, D. V.**, **Vandenabeele, P. & Agostinis, P. (2012).** Hypericin-based photodynamic therapy induces surface exposure of damage-associated molecular patterns like HSP70 and calreticulin. *Cancer immunology, immunotherapy : CII* **61**, 215–221.

Garg, A. D., **Krysko, D. V.**, **Verfaillie, T.**, **Kaczmarek, A.**, **Ferreira, G. B.**, **Marysael, T.**, **Rubio, N.**, **Firczuk, M. & Mathieu, C. & other authors (2012).** A novel pathway combining calreticulin exposure and ATP secretion in immunogenic cancer cell death. *The EMBO journal* **31**, 1062–1079.

Gaynor, R., **Herschman, H. R.**, **Irie, R.**, **Jones, P.**, **Morton, D. & Cochran, A. (1981).** S100 protein: a marker for human malignant melanomas? *Lancet (London, England)* **1**, 869–871.

Gaynor, R., **Irie, R.**, **Morton, D. & Herschman, H. R. (1980).** S100 protein is present in cultured human malignant melanomas. *Nature* **286**, 400–401.

Gehrke, N., **Mertens, C.**, **Zillinger, T.**, **Wenzel, J.**, **Bald, T.**, **Zahn, S.**, **Tüting, T.**, **Hartmann, G. & Barchet, W. (2013).** Oxidative damage of DNA confers resistance to cytosolic nuclease TREX1 degradation and potentiates STING-dependent immune sensing. *Immunity* **39**, 482–495.

Geraghty, R. J., **Krummenacher, C.**, **Cohen, G. H.**, **Eisenberg, R. J. & Spear, P. G. (1998).** Entry of alphaherpesviruses mediated by poliovirus receptor-related protein 1 and poliovirus receptor. *Science (New York, N.Y.)* **280**, 1618–1620.

Goldsmith, K., **Chen, W.**, **Johnson, D. C. & Hendricks, R. L. (1998).** Infected cell protein (ICP)47 enhances herpes simplex virus neurovirulence by blocking the CD8+ T cell response. *The Journal of experimental medicine* **187**, 341–348.

Goldstein, A. M., **Chan, M.**, **Harland, M.**, **Hayward, N. K.**, **Demenais, F.**, **Bishop, D. T.**, **Azizi, E.**, **Bergman, W. & Bianchi-Scarra, G. & other authors (2007).** Features associated

with germline CDKN2A mutations: a GenoMEL study of melanoma-prone families from three continents. *J Med Genet* **44**, 99–106.

Gonzalez-Avila, G., **Sommer, B.**, **Mendoza-Posada, D. A.**, **Ramos, C.**, **Garcia-Hernandez, A. A. & Falfan-Valencia, R. (2019).** Matrix metalloproteinases participation in the metastatic process and their diagnostic and therapeutic applications in cancer. *Critical reviews in oncology/hematology* **137**, 57–83.

Guo, Z. S., **Thorne, S. H. & Bartlett, D. L. (2008).** Oncolytic virotherapy: molecular targets in tumor-selective replication and carrier cell-mediated delivery of oncolytic viruses. *Biochimica et biophysica acta* **1785**, 217–231.

Haferkamp, S., **Drexler, K.**, **Federlin, M.**, **Schlitt, H. J.**, **Berneburg, M.**, **Adamski, J.**, **Gaumann, A.**, **Geissler, E. K. & Ganapathy, V. & other authors (2020).** Extracellular Citrate Fuels Cancer Cell Metabolism and Growth. *Frontiers in cell and developmental biology* **8**, 602476.

Hanahan, D. & Weinberg, R. A. (2011). Hallmarks of cancer: the next generation. *Cell* **144**, 646–674.

Hanly, P., **Ortega-Ortega, M. & Soerjomataram, I. (2022).** Cancer Premature Mortality Costs in Europe in 2020: A Comparison of the Human Capital Approach and the Friction Cost Approach. *Current oncology (Toronto, Ont.)* **29**, 3552–3564.

Harner-Foreman, N., **Vadakekolathu, J.**, **Laversin, S. A.**, **Mathieu, M. G.**, **Reeder, S.**, **Pockley, A. G.**, **Rees, R. C. & Boocock, D. J. (2017).** A novel spontaneous model of epithelial-mesenchymal transition (EMT) using a primary prostate cancer derived cell line demonstrating distinct stem-like characteristics. *Sci Rep* **7**, 40633.

He, B., **Chou, J.**, **Brandimarti, R.**, **Mohr, I.**, **Gluzman, Y. & Roizman, B. (1997).** Suppression of the phenotype of gamma(1)34.5- herpes simplex virus 1: failure of activated RNA-dependent protein kinase to shut off protein synthesis is associated with a deletion in the domain of the alpha47 gene. *Journal of virology* **71**, 6049–6054.

He, B., **Gross, M. & Roizman, B. (1997).** The gamma(1)34.5 protein of herpes simplex virus 1 complexes with protein phosphatase 1alpha to dephosphorylate the alpha subunit of the eukaryotic translation initiation factor 2 and preclude the shutoff of protein synthesis by double-stranded RNA-activated protein kinase. *Proceedings of the National Academy of Sciences of the United States of America* **94**, 843–848.

Heldin, C.-H., **Vanlandewijck, M. & Moustakas, A. (2012).** Regulation of EMT by TGFβ in cancer. *FEBS Letters* **586**, 1959–1970.

Heldwein, E. E. & Krummenacher, C. (2008). Entry of herpesviruses into mammalian cells. *Cellular and molecular life sciences : CMLS* **65**, 1653–1668.

Heneberg, P. (2016). Paracrine tumor signaling induces transdifferentiation of surrounding fibroblasts. *Critical reviews in oncology/hematology* **97**, 303–311.

Higuchi, K., **Kopel, J. J.**, **Sivaprakasam, S.**, **Jaramillo-Martinez, V.**, **Sutton, R. B.**, **Urbatsch, I. L. & Ganapathy, V. (2020).** Functional analysis of a species-specific inhibitor selective for human Na+-coupled citrate transporter (NaCT/SLC13A5/mINDY). *The Biochemical journal* **477**, 4149–4165.

Hillar, M., **Lott, V. & Lennox, B. (1975).** Correlation of the effects of citric acid cycle metabolites on succinate oxidation by rat liver mitochondria and submitochondrial particles. *Journal of bioenergetics* **7**, 1–16.

Holly, E. A., **Kelly, J. W.**, **Shpall, S. N. & Chiu, S. H. (1987).** Number of melanocytic nevi as a major risk factor for malignant melanoma. *Journal of the American Academy of Dermatology* **17**, 459–468.

Hosein, A. N., **Brekken, R. A. & Maitra, A. (2020).** Pancreatic cancer stroma: an update on therapeutic targeting strategies. *Nature reviews. Gastroenterology & hepatology* **17**, 487–505.

Houben, R., **Hesbacher, S.**, **Schmid, C. P.**, **Kauczok, C. S.**, **Flohr, U.**, **Haferkamp, S.**, **Müller, C. S. L.**, **Schrama, D.**, **Wischhusen, J. & Becker, J. C. (2011).** High-level expression of wild-type p53 in melanoma cells is frequently associated with inactivity in p53 reporter gene assays. *PLOS ONE* **6**, e22096.

Huang, Y.-Y., **Yu, Z.**, **Lin, S.-F.**, **Li, S.**, **Fong, Y. & Wong, R. J. (2007).** Nectin-1 is a marker of thyroid cancer sensitivity to herpes oncolytic therapy. *The Journal of clinical endocrinology and metabolism* **92**, 1965–1970.

Human Protein Atlas **(Accessed December 11, 2023).** SCL13A5. https://www.proteinatlas.org/ENSG00000141485-SLC13A5/pathology.

Iacobazzi, V., **Infantino, V. & Palmieri, F. (2013).** Transcriptional Regulation of the Mitochondrial Citrate and Carnitine/Acylcarnitine Transporters: Two Genes Involved in Fatty Acid Biosynthesis and β-oxidation. *Biology* **2**, 284–303.

Icard, P., **Alifano, M. & Simula, L. (2023).** The potential for citrate to reinforce epigenetic therapy by promoting apoptosis. *Trends in Endocrinology & Metabolism* **34**, 586–589.

Icard, P., **Coquerel, A.**, **Wu, Z.**, **Gligorov, J.**, **Fuks, D.**, **Fournel, L.**, **Lincet, H. & Simula, L. (2021).** Understanding the Central Role of Citrate in the Metabolism of Cancer Cells and Tumors: An Update. *International journal of molecular sciences* **22**.

Icard, P., **Fournel, L.**, **Coquerel, A.**, **Gligorov, J.**, **Alifano, M. & Lincet, H. (2018).** Citrate targets FBPase and constitutes an emerging novel approach for cancer therapy. *Cancer cell international* **18**, 175.

Icard, P., **Wu, Z.**, **Alifano, M. & Fournel, L. (2019).** Gluconeogenesis of Cancer Cells Is Disrupted by Citrate. *Trends in Cancer* **5**, 265–266.

Inoue, H. & Tani, K. (2014). Multimodal immunogenic cancer cell death as a consequence of anticancer cytotoxic treatments. *Cell death and differentiation* **21**, 39–49.

Ippolito, L., **Marini, A.**, **Cavallini, L.**, **Morandi, A.**, **Pietrovito, L.**, **Pintus, G.**, **Giannoni, E.**, **Schrader, T. & Puhr, M. & other authors (2016).** Metabolic shift toward oxidative phosphorylation in docetaxel resistant prostate cancer cells. *Oncotarget* **7**, 61890–61904.

J. Berg, J. Tymoczko, G. Gatto, L. Stryer **(2019).** *Biochemistry (9th ed.):* W.H. Freeman & Company.

James, E. L., **Michalek, R. D.**, **Pitiyage, G. N.**, **Castro, A. M.** de, **Vignola, K. S.**, **Jones, J.**, **Mohney, R. P.**, **Karoly, E. D.**, **Prime, S. S. & Parkinson, E. K. (2015).** Senescent human fibroblasts show increased glycolysis and redox homeostasis with extracellular metabolomes that overlap with those of irreparable DNA damage, aging, and disease. *Journal of proteome research* **14**, 1854–1871.

Jankowski, M., **Kopinski, P.**, **Schwartz, R. & Czajkowski, R. (2014).** Merkel cell carcinoma: is this a true carcinoma? *Experimental dermatology* **23**, 792–794.

Janssen, L., **Ai, X.**, **Zheng, X.**, **Wei, W.**, **Caglayan, A. B.**, **Kilic, E.**, **Wang, Y.-c.**, **Hermann, D. M. & Venkataramani, V. & other authors (2021).** Inhibition of Fatty Acid Synthesis Aggravates Brain Injury, Reduces Blood-Brain Barrier Integrity and Impairs Neurological Recovery in a Murine Stroke Model. *Front. Cell. Neurosci.* **15**, 733973.

Jha, A. K., **Huang, S. C.-C.**, **Sergushichev, A.**, **Lampropoulou, V.**, **Ivanova, Y.**, **Loginicheva, E.**, **Chmielewski, K.**, **Stewart, K. M. & Ashall, J. & other authors (2015).** Network integration of parallel metabolic and transcriptional data reveals metabolic modules that regulate macrophage polarization. *Immunity* **42**, 419–430.

Jhawar, S. R., **Thandoni, A.**, **Bommareddy, P. K.**, **Hassan, S.**, **Kohlhapp, F. J.**, **Goyal, S.**, **Schenkel, J. M.**, **Silk, A. W. & Zloza, A. (2017).** Oncolytic Viruses-Natural and Genetically Engineered Cancer Immunotherapies. *Frontiers in oncology* **7**, 202.

Jiang, G.-M., **Xu, W.**, **Du, J.**, **Zhang, K.-S.**, **Zhang, Q.-G.**, **Wang, X.-W.**, **Liu, Z.-G.**, **Liu, S.-Q. & Xie, W.-Y. & other authors (2016).** The application of the fibroblast activation protein α-targeted immunotherapy strategy. *Oncotarget* **7**, 33472–33482.

Jordan, K., Stanton, E. H., Milenkovic, V. M., Federlin, M., Drexler, K., Buchalla, W., Gaumann, A., Adamski, J. & Proescholdt, M. & other authors (2022). *Potential Involvement of Extracellular Citrate in Brain Tumor Progression:* Bentham Science Publishers.

Kaps, L. & Schuppan, D. (2020). Targeting Cancer Associated Fibroblasts in Liver Fibrosis and Liver Cancer Using Nanocarriers. *Cells* **9**.

Karaba, A. H., **Kopp, S. J. & Longnecker, R. (2011).** Herpesvirus entry mediator and nectin-1 mediate herpes simplex virus 1 infection of the murine cornea. *Journal of virology* **85**, 10041–10047.

Kaufman, H. L., **Kim, D. W.**, **DeRaffele, G.**, **Mitcham, J.**, **Coffin, R. S. & Kim-Schulze, S. (2010a).** Local and distant immunity induced by intralesional vaccination with an oncolytic herpes virus encoding GM-CSF in patients with stage IIIc and IV melanoma. *Annals of surgical oncology* **17**, 718–730.

Kaufman, H. L., **Kim, D. W.**, **DeRaffele, G.**, **Mitcham, J.**, **Coffin, R. S. & Kim-Schulze, S. (2010b).** Local and distant immunity induced by intralesional vaccination with an oncolytic herpes virus encoding GM-CSF in patients with stage IIIc and IV melanoma. *Annals of surgical oncology* **17**, 718–730.

Kaufman, H. L., **Kohlhapp, F. J. & Zloza, A. (2015).** Oncolytic viruses: a new class of immunotherapy drugs. *Nat Rev Drug Discov* **14**, 642–662.

Khafizov, K., **Perez, C.**, **Koshy, C.**, **Quick, M.**, **Fendler, K.**, **Ziegler, C. & Forrest, L. R. (2012).** Investigation of the sodium-binding sites in the sodium-coupled betaine transporter BetP. *Proceedings of the National Academy of Sciences of the United States of America* **109**, E3035-44.

Kleemann, J., **Jäger, M.**, **Valesky, E.**, **Kippenberger, S.**, **Kaufmann, R. & Meissner, M. (2021).** Real-World Experience of Talimogene Laherparepvec (T-VEC) in Old and Oldest-Old Patients with Melanoma: A Retrospective Single Center Study. *Cancer management and research* **13**, 5699–5709.

Knebel-Mörsdorf, D. (2016). Nectin-1 and HVEM: cellular receptors for HSV-1 in skin. *Oncotarget* **7**, 19087–19088.

Koh, C. M. (2013). Preparation of Cells for Microscopy using ‘Cell Blocks’. In *Methods in enzymology*, pp. 249–255. Edited by J. Lorsch. Amsterdam, San Diego: Elsevier.

Kohl, C., **Aung, T.**, **Haerteis, S.**, **Ignatov, A.**, **Ortmann, O. & Papathemelis, T. (2022).** The 3D in vivo chorioallantoic membrane model and its role in breast cancer research. *Journal of cancer research and clinical oncology* **148**, 1033–1043.

Kohl, C., **Aung, T.**, **Haerteis, S. & Papathemelis, T. (2021).** Assessment of breast cancer primary tumor material in a 3D in vivo model. *Clinical hemorheology and microcirculation* **79**, 157–166.

Kohlhapp, F. J. & Kaufman, H. L. (2016). Molecular Pathways: Mechanism of Action for Talimogene Laherparepvec, a New Oncolytic Virus Immunotherapy. *Clinical cancer research : an official journal of the American Association for Cancer Research* **22**, 1048–1054.

Kopp, S. J., **Banisadr, G.**, **Glajch, K.**, **Maurer, U. E.**, **Grünewald, K.**, **Miller, R. J.**, **Osten, P. & Spear, P. G. (2009).** Infection of neurons and encephalitis after intracranial inoculation of herpes simplex virus requires the entry receptor nectin-1. *Proceedings of the National Academy of Sciences of the United States of America* **106**, 17916–17920.

Korn, E. L., **Liu, P.-Y.**, **Lee, S. J.**, **Chapman, J.-A. W.**, **Niedzwiecki, D.**, **Suman, V. J.**, **Moon, J.**, **Sondak, V. K. & Atkins, M. B. & other authors (2008).** Meta-analysis of phase II cooperative group trials in metastatic stage IV melanoma to determine progression-free and overall survival benchmarks for future phase II trials. *Journal of clinical oncology : official journal of the American Society of Clinical Oncology* **26**, 527–534.

Krummenacher, C., **Baribaud, F.**, **Ponce de Leon, M.**, **Baribaud, I.**, **Whitbeck, J. C.**, **Xu, R.**, **Cohen, G. H. & Eisenberg, R. J. (2004).** Comparative usage of herpesvirus entry mediator A and nectin-1 by laboratory strains and clinical isolates of herpes simplex virus. *Virology* **322**, 286–299.

Krummenacher, C., **Nicola, A. V.**, **Whitbeck, J. C.**, **Lou, H.**, **Hou, W.**, **Lambris, J. D.**, **Geraghty, R. J.**, **Spear, P. G.**, **Cohen, G. H. & Eisenberg, R. J. (1998).** Herpes simplex virus glycoprotein D can bind to poliovirus receptor-related protein 1 or herpesvirus entry mediator, two structurally unrelated mediators of virus entry. *Journal of virology* **72**, 7064–7074.

Kumar, A., **Cordes, T.**, **Thalacker-Mercer, A. E.**, **Pajor, A. M.**, **Murphy, A. N. & Metallo, C. M. (2021).** NaCT/SLC13A5 facilitates citrate import and metabolism under nutrient-limited conditions. *Cell reports* **36**, 109701.

Kurose, K., **Hoshaw-Woodard, S.**, **Adeyinka, A.**, **Lemeshow, S.**, **Watson, P. H. & Eng, C. (2001).** Genetic model of multi-step breast carcinogenesis involving the epithelium and stroma: clues to tumour-microenvironment interactions. *Hum Mol Genet* **10**, 1907–1913.

La Cruz-López, K. G. de, **Castro-Muñoz, L. J.**, **Reyes-Hernández, D. O.**, **García-Carrancá, A. & Manzo-Merino, J. (2019).** Lactate in the Regulation of Tumor Microenvironment and Therapeutic Approaches. *Frontiers in oncology* **9**, 1143.

Lee, J. V., **Shah, S. A. & Wellen, K. E. (2013).** Obesity, cancer, and acetyl-CoA metabolism. *Drug discovery today. Disease mechanisms* **10**, e55-e61.

Lee, T.-L., **Chen, T.-H.**, **Kuo, Y.-J.**, **Lan, H.-Y.**, **Yang, M.-H. & Chu, P.-Y. (2023).** Tumor-associated tissue eosinophilia promotes angiogenesis and metastasis in head and neck squamous cell carcinoma. *Neoplasia* **35**, 100855.

Li, M., **Knight, D. A.**, **A Snyder, L.**, **Smyth, M. J. & Stewart, T. J. (2013).** A role for CCL2 in both tumor progression and immunosurveillance. *Oncoimmunology* **2**, e25474.

Li, Shichao, **Yang**, Xiaorong, **Yang**, Jinmei, **Zhen**, Jiesheng **& Zhang**, Dechun **(2016).** Serum microRNA-21 as a potential diagnostic biomarker for breast cancer: a systematic review and meta-analysis. *Clinical and experimental medicine* **16**, 29–35.

Li, Tao, **Zheng**, Yuanting, **Sun**, Hong, **Zhuang**, Rongyuan, **Liu**, Jing, **Liu**, Tianshu **& Cai**, Weimin **(2016).** K-Ras mutation detection in liquid biopsy and tumor tissue as prognostic biomarker in patients with pancreatic cancer: a systematic review with meta-analysis. *Medical oncology (Northwood, London, England)* **33**, 61.

Li, Z., **Li, D.**, **Choi, E. Y.**, **Lapidus, R.**, **Zhang, L.**, **Huang, S.-M.**, **Shapiro, P. & Wang, H. (2017).** Silencing of solute carrier family 13 member 5 disrupts energy homeostasis and inhibits proliferation of human hepatocarcinoma cells. *Journal of Biological Chemistry* **292**, 13890–13901.

Liebisch, G., **Binder, M.**, **Schifferer, R.**, **Langmann, T.**, **Schulz, B. & Schmitz, G. (2006).** High throughput quantification of cholesterol and cholesteryl ester by electrospray ionization tandem mass spectrometry (ESI-MS/MS). *Biochimica et biophysica acta* **1761**, 121–128.

Liebisch, G., **Drobnik, W.**, **Lieser, B. & Schmitz, G. (2002).** High-Throughput Quantification of Lysophosphatidylcholine by Electrospray Ionization Tandem Mass Spectrometry. *Clinical Chemistry* **48**, 2217–2224.

Liebisch, G., **Drobnik, W.**, **Reil, M.**, **Trümbach, B.**, **Arnecke, R.**, **Olgemöller, B.**, **Roscher, A. & Schmitz, G. (1999).** Quantitative measurement of different ceramide species from crude cellular extracts by electrospray ionization tandem mass spectrometry (ESI-MS/MS). *Journal of Lipid Research* **40**, 1539–1546.

Liebisch, G., **Lieser, B.**, **Rathenberg, J.**, **Drobnik, W. & Schmitz, G. (2004).** High-throughput quantification of phosphatidylcholine and sphingomyelin by electrospray ionization tandem mass spectrometry coupled with isotope correction algorithm. *Biochimica et biophysica acta* **1686**, 108–117.

Liebisch, G., **Vizcaíno, J. A.**, **Köfeler, H.**, **Trötzmüller, M.**, **Griffiths, W. J.**, **Schmitz, G.**, **Spener, F. & Wakelam, M. J. O. (2013).** Shorthand notation for lipid structures derived from mass spectrometry. *Journal of Lipid Research* **54**, 1523–1530.

Lin, Z., **McDermott, A.**, **Shao, L.**, **Kannan, A.**, **Morgan, M.**, **Stack, B. C.**, **Moreno, M.**, **Davis, D. A.**, **Cornelius, L. A. & Gao, L. (2014).** Chronic mTOR activation promotes cell survival in Merkel cell carcinoma. *Cancer letters* **344**, 272–281.

Lindahl, U., **Kusche-Gullberg, M. & Kjellén, L. (1998).** Regulated diversity of heparan sulfate. *Journal of Biological Chemistry* **273**, 24979–24982.

Liu, B. L., **Robinson, M.**, **Han, Z.-Q.**, **Branston, R. H.**, **English, C.**, **Reay, P.**, **McGrath, Y.**, **Thomas, S. K. & Thornton, M. & other authors (2003a).** ICP34.5 deleted herpes simplex virus with enhanced oncolytic, immune stimulating, and anti-tumour properties. *Gene therapy* **10**, 292–303.

Liu, B. L., **Robinson, M.**, **Han, Z.-Q.**, **Branston, R. H.**, **English, C.**, **Reay, P.**, **McGrath, Y.**, **Thomas, S. K. & Thornton, M. & other authors (2003b).** ICP34.5 deleted herpes simplex virus with enhanced oncolytic, immune stimulating, and anti-tumour properties. *Gene therapy* **10**, 292–303.

Loberg, R. D., **Day, L. L.**, **Harwood, J.**, **Ying, C.**, **St John, L. N.**, **Giles, R.**, **Neeley, C. K. & Pienta, K. J. (2006).** CCL2 is a potent regulator of prostate cancer cell migration and proliferation. *Neoplasia (New York, N.Y.)* **8**, 578–586.

LU, Y., **ZHANG, X.**, **ZHANG, H.**, **LAN, J.**, **HUANG, G.**, **VARIN, E.**, **Lincet, H.**, **Poulain, L. & Icard, P. (2011).** Citrate induces apoptotic cell death: a promising way to treat gastric carcinoma? *Anticancer Research* **31**, 797–805.

Lugowska, I., **Teterycz, P. & Rutkowski, P. (2018).** Immunotherapy of melanoma. *Contemporary oncology (Poznan, Poland)* **22**, 61–67.

Luo, X., **Cheng, C.**, **Tan, Z.**, **Li, N.**, **Tang, M.**, **Yang, L. & Cao, Y. (2017).** Emerging roles of lipid metabolism in cancer metastasis. *Molecular cancer* **16**, 76.

Ma, T. H., **Gao, C. C.**, **Xie, R.**, **Yang, X. Z.**, **Dai, W. J.**, **Zhang, J. L.**, **Yan, W. & Wu, S. N. (2017).** Predictive values of FAP and HGF for tumor angiogenesis and metastasis in colorectal cancer. *neo* **64**, 880–886.

Ma, Z. & Damania, B. (2016). The cGAS-STING Defense Pathway and Its Counteraction by Viruses. *Cell host & microbe* **19**, 150–158.

Maller, O., **Drain, A. P.**, **Barrett, A. S.**, **Borgquist, S.**, **Ruffell, B.**, **Zakharevich, I.**, **Pham, T. T.**, **Gruosso, T. & Kuasne, H. & other authors (2021).** Tumour-associated macrophages drive stromal cell-dependent collagen crosslinking and stiffening to promote breast cancer aggression. *Nat. Mater.* **20**, 548–559.

Marin-Valencia, I., **Yang, C.**, **Mashimo, T.**, **Cho, S.**, **Baek, H.**, **Yang, X.-L.**, **Rajagopalan, K. N.**, **Maddie, M. & Vemireddy, V. & other authors (2012).** Analysis of tumor metabolism reveals mitochondrial glucose oxidation in genetically diverse human glioblastomas in the mouse brain in vivo. *Cell metabolism* **15**, 827–837.

Markovic, S. N., **Erickson, L. A.**, **Rao, R. D.**, **Weenig, R. H.**, **Pockaj, B. A.**, **Bardia, A.**, **Vachon, C. M.**, **Schild, S. E. & McWilliams, R. R. & other authors (2007).** Malignant melanoma in the 21st century, part 1: epidemiology, risk factors, screening, prevention, and diagnosis. *Mayo Clinic proceedings* **82**, 364–380.

Martins, I., **Tesniere, A.**, **Kepp, O.**, **Michaud, M.**, **Schlemmer, F.**, **Senovilla, L.**, **Séror, C.**, **Métivier, D. & Perfettini, J.-L. & other authors (2009).** Chemotherapy induces ATP release from tumor cells. *Cell cycle (Georgetown, Tex.)* **8**, 3723–3728.

Mashal, R. D., **Koontz, J. & Sklar, J. (1995).** Detection of mutations by cleavage of DNA heteroduplexes with bacteriophage resolvases. *Nature genetics* **9**, 177–183.

Masjedi, A., **Hashemi, V.**, **Hojjat-Farsangi, M.**, **Ghalamfarsa, G.**, **Azizi, G.**, **Yousefi, M. & Jadidi-Niaragh, F. (2018).** The significant role of interleukin-6 and its signaling pathway in the immunopathogenesis and treatment of breast cancer. *Biomedicine & pharmacotherapy = Biomedecine & pharmacotherapie* **108**, 1415–1424.

Mason, R., **Au, L.**, **Ingles Garces, A. & Larkin, J. (2019).** Current and emerging systemic therapies for cutaneous metastatic melanoma. *Expert opinion on pharmacotherapy* **20**, 1135–1152.

Matyash, V., **Liebisch, G.**, **Kurzchalia, T. V.**, **Shevchenko, A. & Schwudke, D. (2008).** Lipid extraction by methyl-tert-butyl ether for high-throughput lipidomics. *Journal of lipid research* **49**, 1137–1146.

Mauzo, S. H., **Ferrarotto, R.**, **Bell, D.**, **Torres-Cabala, C. A.**, **Tetzlaff, M. T.**, **Prieto, V. G. & Aung, P. P. (2016).** Molecular characteristics and potential therapeutic targets in Merkel cell carcinoma. *Journal of clinical pathology* **69**, 382–390.

Mazurek, M. P., **Prasad, P. D.**, **Gopal, E.**, **Fraser, S. P.**, **Bolt, L.**, **Rizaner, N.**, **Palmer, C. P.**, **Foster, C. S. & Palmieri, F. & other authors (2010).** Molecular origin of plasma membrane citrate transporter in human prostate epithelial cells. *EMBO reports* **11**, 431–437.

McGarry, J. D., **Takabayashi, Y. & Foster, D. W. (1978).** The role of malonyl-coa in the coordination of fatty acid synthesis and oxidation in isolated rat hepatocytes. *Journal of Biological Chemistry* **253**, 8294–8300.

Medrano, A., **Fernández-Novell, J. M.**, **Ramió, L.**, **Alvarez, J.**, **Goldberg, E.**, **Montserrat Rivera, M.**, **Guinovart, J. J.**, **Rigau, T. & Rodríguez-Gil, J. E. (2006).** Utilization of citrate and lactate through a lactate dehydrogenase and ATP-regulated pathway in boar spermatozoa. *Molecular reproduction and development* **73**, 369–378.

Mellone, M., **Hanley, C. J.**, **Thirdborough, S.**, **Mellows, T.**, **Garcia, E.**, **Woo, J.**, **Tod, J.**, **Frampton, S. & Jenei, V. & other authors (2016).** Induction of fibroblast senescence generates a non-fibrogenic myofibroblast phenotype that differentially impacts on cancer prognosis. *Aging* **9**, 114–132.

Metallo, C. M., **Gameiro, P. A.**, **Bell, E. L.**, **Mattaini, K. R.**, **Yang, J.**, **Hiller, K.**, **Jewell, C. M.**, **Johnson, Z. R. & Irvine, D. J. & other authors (2011).** Reductive glutamine metabolism by IDH1 mediates lipogenesis under hypoxia. *Nature* **481**, 380–384.

Meyer, T., **Koch, A.**, **Ebert, E.-V.**, **Czech, B.**, **Mueller, M.**, **Bosserhoff, A.**, **Lang, S. A. & Hellerbrand, C. (2017).** Effect of melanoma cells on proliferation and migration of activated hepatic stellate cells in vitro. *Pathology, research and practice* **213**, 400–404.

Middleton, M. R., **Grob, J. J.**, **Aaronson, N.**, **Fierlbeck, G.**, **Tilgen, W.**, **Seiter, S.**, **Gore, M.**, **Aamdal, S. & Cebon, J. & other authors (2000).** Randomized phase III study of temozolomide versus dacarbazine in the treatment of patients with advanced metastatic malignant melanoma. *Journal of clinical oncology : official journal of the American Society of Clinical Oncology* **18**, 158–166.

Milenkovic, V. M., **Bader, S.**, **Sudria-Lopez, D.**, **Siebert, R.**, **Brandl, C.**, **Nothdurfter, C.**, **Weber, B. H. F.**, **Rupprecht, R. & Wetzel, C. H. (2018).** Effects of genetic variants in the TSPO gene on protein structure and stability. *PLOS ONE* **13**, e0195627.

Milette, S., **Sicklick, J. K.**, **Lowy, A. M. & Brodt, P. (2017).** Molecular Pathways: Targeting the Microenvironment of Liver Metastases. *Clinical cancer research : an official journal of the American Association for Cancer Research* **23**, 6390–6399.

Mohr, I. & Gluzman, Y. (1996). A herpesvirus genetic element which affects translation in the absence of the viral GADD34 function. *The EMBO journal* **15**, 4759–4766.

Montgomery, R. I., **Warner, M. S.**, **Lum, B. J. & Spear, P. G. (1996).** Herpes Simplex Virus-1 Entry into Cells Mediated by a Novel Member of the TNF/NGF Receptor Family. *Cell* **87**, 427–436.

Morley, S., **Hager, M. H.**, **Pollan, S. G.**, **Knudsen, B.**, **Di Vizio, D. & Freeman, M. R. (2014).** Trading in your spindles for blebs: the amoeboid tumor cell phenotype in prostate cancer. *Asian journal of andrology* **16**, 530–535.

Mullen, J. T. & Tanabe, K. K. (2002). Viral oncolysis. *The oncologist* **7**, 106–119.

Mulvey, M., **Poppers, J.**, **Ladd, A. & Mohr, I. (1999).** A herpesvirus ribosome-associated, RNA-binding protein confers a growth advantage upon mutants deficient in a GADD34-related function. *Journal of virology* **73**, 3375–3385.

Murphy, G. & Nagase, H. (2008). Progress in matrix metalloproteinase research. *Molecular aspects of medicine* **29**, 290–308.

Muschet, C., **Möller, G.**, **Prehn, C.**, **Angelis, M. H.** de, **Adamski, J. & Tokarz, J. (2016).** Removing the bottlenecks of cell culture metabolomics: fast normalization procedure, correlation of metabolites to cell number, and impact of the cell harvesting method. *Metabolomics : Official journal of the Metabolomic Society* **12**, 151.

Mycielska, M. E., **Dettmer, K.**, **Rümmele, P.**, **Schmidt, K.**, **Prehn, C.**, **Milenkovic, V. M.**, **Jagla, W.**, **Madej, G. M. & Lantow, M. & other authors (2018).** Extracellular Citrate Affects

Critical Elements of Cancer Cell Metabolism and Supports Cancer Development In Vivo. *Cancer research* **78**, 2513–2523.

Mycielska, M. E., **James, E. N. & Parkinson, E. K. (2022).** Metabolic Alterations in Cellular Senescence: The Role of Citrate in Ageing and Age-Related Disease. *International journal of molecular sciences* **23**.

Mycielska, M. E., **Milenkovic, V. M.**, **Wetzel, C. H.**, **Rümmele, P. & Geissler, E. K. (2015).** Extracellular Citrate in Health and Disease. *Current molecular medicine* **15**, 884–891.

Mycielska, M. E., **Mohr, M. T. J.**, **Schmidt, K.**, **Drexler, K.**, **Rümmele, P.**, **Haferkamp, S.**, **Schlitt, H. J.**, **Gaumann, A.**, **Adamski, J. & Geissler, E. K. (2019).** Potential Use of Gluconate in Cancer Therapy. *Frontiers in oncology* **9**, 522.

Mycielska, M. E., **Palmer, C. P.**, **Brackenbury, W. J. & Djamgoz, M. B. A. (2005).** Expression of Na+-dependent citrate transport in a strongly metastatic human prostate cancer PC-3M cell line: regulation by voltage-gated Na+ channel activity. *The Journal of physiology* **563**, 393–408.

Nagasaki, T., **Hara, M.**, **Nakanishi, H.**, **Takahashi, H.**, **Sato, M. & Takeyama, H. (2014).** Interleukin-6 released by colon cancer-associated fibroblasts is critical for tumour angiogenesis: anti-interleukin-6 receptor antibody suppressed angiogenesis and inhibited tumour-stroma interaction. *British journal of cancer* **110**, 469–478.

Nakajima, T., **Watanabe, S.**, **Sato, Y.**, **Kameya, T.**, **Shimosato, Y. & Ishihara, K. (1982).** Immunohistochemical demonstration of S 100 protein in malignant melanoma and pigmented nevus, and its diagnostic application. *Cancer* **50**, 912–918.

Nazemi, M. & Rainero, E. (2020). Cross-Talk Between the Tumor Microenvironment, Extracellular Matrix, and Cell Metabolism in Cancer. *Frontiers in oncology* **10**, 239.

Nelson, D. L., Cox, M. M. & Lehninger, A. L. (2021). *Lehninger principles of biochemistry*. New York, NY, Houndmills, Basingstoke: W.H. Freeman and Company; Macmillan Higher Education.

Neophytou, C. M., **Panagi, M.**, **Stylianopoulos, T. & Papageorgis, P. (2021).** The Role of Tumor Microenvironment in Cancer Metastasis: Molecular Mechanisms and Therapeutic Opportunities. *Cancers* **13**.

Nguyen, T.-T., **Ramsay, L.**, **Ahanfeshar-Adams, M.**, **Lajoie, M.**, **Schadendorf, D.**, **Alain, T. & Watson, I. R. (2021).** Mutations in the IFNγ-JAK-STAT Pathway Causing Resistance to Immune Checkpoint Inhibitors in Melanoma Increase Sensitivity to Oncolytic Virus Treatment. *Clinical cancer research : an official journal of the American Association for Cancer Research* **27**, 3432–3442.

Nicola, A. V. (2016). Herpesvirus Entry into Host Cells Mediated by Endosomal Low pH. *Traffic (Copenhagen, Denmark)* **17**, 965–975.

Nishida, N. (2021). Role of Oncogenic Pathways on the Cancer Immunosuppressive Microenvironment and Its Clinical Implications in Hepatocellular Carcinoma. *Cancers* **13**, 3666.

Nissler, K., **Petermann, H.**, **Wenz, I. & Brox, D. (1995).** Fructose 2,6-bisphosphate metabolism in Ehrlich ascites tumour cells. *Journal of cancer research and clinical oncology* **121**, 739–745.

Obeid, M., **Tesniere, A.**, **Ghiringhelli, F.**, **Fimia, G. M.**, **Apetoh, L.**, **Perfettini, J.-L.**, **Castedo, M.**, **Mignot, G. & Panaretakis, T. & other authors (2007).** Calreticulin exposure dictates the immunogenicity of cancer cell death. *Nature medicine* **13**, 54–61.

O'Donnell, C. D., **Kovacs, M.**, **Akhtar, J.**, **Valyi-Nagy, T. & Shukla, D. (2010).** Expanding the role of 3-O sulfated heparan sulfate in herpes simplex virus type-1 entry. *Virology* **397**, 389–398.

Oya, Y., **Hayakawa, Y. & Koike, K. (2020).** Tumor microenvironment in gastric cancers. *Cancer science* **111**, 2696–2707.

Pajor, A. M. (2006). Molecular properties of the SLC13 family of dicarboxylate and sulfate transporters. *Pflugers Archiv : European journal of physiology* **451**, 597–605.

Papageorgis, P. & Stylianopoulos, T. (2015). Role of TGFβ in regulation of the tumor microenvironment and drug delivery (review). *International journal of oncology* **46**, 933–943.

Parkinson, E. K., **Adamski, J.**, **Zahn, G.**, **Gaumann, A.**, **Flores-Borja, F.**, **Ziegler, C. & Mycielska, M. E. (2021).** Extracellular citrate and metabolic adaptations of cancer cells. *Cancer Metastasis Reviews* **40**, 1073–1091.

Pascale, R. M., **Calvisi, D. F.**, **Simile, M. M.**, **Feo, C. F. & Feo, F. (2020).** The Warburg Effect 97 Years after Its Discovery. *Cancers* **12**.

Passarelli, A., **Mannavola, F.**, **Stucci, L. S.**, **Tucci, M. & Silvestris, F. (2017).** Immune system and melanoma biology: a balance between immunosurveillance and immune escape. *Oncotarget* **8**, 106132–106142.

Petermann, P., **Rahn, E.**, **Thier, K.**, **Hsu, M.-J.**, **Rixon, F. J.**, **Kopp, S. J. & Knebel-Mörsdorf, D. (2015).** Role of Nectin-1 and Herpesvirus Entry Mediator as Cellular Receptors for Herpes Simplex Virus 1 on Primary Murine Dermal Fibroblasts. *Journal of virology* **89**, 9407–9416.

Petermann, P., **Thier, K.**, **Rahn, E.**, **Rixon, F. J.**, **Bloch, W.**, **Özcelik, S.**, **Krummenacher, C.**, **Barron, M. J. & Dixon, M. J. & other authors (2015).** Entry mechanisms of herpes

simplex virus 1 into murine epidermis: involvement of nectin-1 and herpesvirus entry mediator as cellular receptors. *Journal of virology* **89**, 262–274.

Petillo, A., **Abruzzese, V.**, **Koshal, P.**, **Ostuni, A. & Bisaccia, F. (2020).** Extracellular Citrate Is a Trojan Horse for Cancer Cells. *Frontiers in molecular biosciences* **7**, 593866.

Pion, E., **Asam, C.**, **Feder, A.-L.**, **Felthaus, O.**, **Heidekrueger, P. I.**, **Prantl, L.**, **Haerteis, S. & Aung, T. (2021).** Laser speckle contrast analysis (LASCA) technology for the semiquantitative measurement of angiogenesis in in-ovo-tumor-model. *Microvascular research* **133**, 104072.

Pol, J. G., **Workenhe, S. T.**, **Konda, P.**, **Gujar, S. & Kroemer, G. (2020).** Cytokines in oncolytic virotherapy. *Cytokine & growth factor reviews* **56**, 4–27.

Possemato, R., **Marks, K. M.**, **Shaul, Y. D.**, **Pacold, M. E.**, **Kim, D.**, **Birsoy, K.**, **Sethumadhavan, S.**, **Woo, H.-K. & Jang, H. G. & other authors (2011).** Functional genomics reveal that the serine synthesis pathway is essential in breast cancer. *Nature* **476**, 346–350.

Pracht, M., **Mogha, A.**, **Lespagnol, A.**, **Fautrel, A.**, **Mouchet, N.**, **Le Gall, F.**, **Paumier, V.**, **Lefeuvre-Plesse, C. & Rioux-Leclerc, N. & other authors (2015).** Prognostic and predictive values of oncogenic BRAF, NRAS, c-KIT and MITF in cutaneous and mucous melanoma. *Journal of the European Academy of Dermatology and Venereology : JEADV* **29**, 1530–1538.

Pulitzer, M. (2017). Merkel Cell Carcinoma. *Surgical pathology clinics* **10**, 399–408.

Puré, E. & Blomberg, R. (2018). Pro-tumorigenic roles of fibroblast activation protein in cancer: back to the basics. *Oncogene* **37**, 4343–4357.

Queiroz, N. M. G. P. de, **Xia, T.**, **Konno, H. & Barber, G. N. (2019).** Ovarian Cancer Cells Commonly Exhibit Defective STING Signaling Which Affects Sensitivity to Viral Oncolysis. *Molecular cancer research : MCR* **17**, 974–986.

Räsänen, K. & Vaheri, A. (2010). Activation of fibroblasts in cancer stroma. *Experimental cell research* **316**, 2713–2722.

RASK, L., **HØGDALL, C. K.**, **KJAER, S. K.**, **CHRISTENSEN, L.**, **JENSEN, A.**, **Blaakaer, J.**, **Christensen, I. J. & Høgdall, E. V. S. (2019).** Association of CD31 and p53 With Survival of Ovarian Cancer Patients. *Anticancer Research* **39**, 567–576.

REED, L. J. & MUENCH, H. (1938). A SIMPLE METHOD OF ESTIMATING FIFTY PER CENT ENDPOINTS12. *Am J Epidemiol* **27**, 493–497.

Ressler, J. M., **Karasek, M.**, **Koch, L.**, **Silmbrod, R.**, **Mangana, J.**, **Latifyan, S.**, **Aedo-Lopez, V.**, **Kehrer, H. & Weihsengruber, F. & other authors (2021).** Real-life use of

talimogene laherparepvec (T-VEC) in melanoma patients in centers in Austria, Switzerland and Germany. *Journal for immunotherapy of cancer* **9**.

Ribas, A., **Dummer, R.**, **Puzanov, I.**, **VanderWalde, A.**, **Andtbacka, R. H. I.**, **Michielin, O.**, **Olszanski, A. J.**, **Malvehy, J. & Cebon, J. & other authors (2017).** Oncolytic Virotherapy Promotes Intratumoral T Cell Infiltration and Improves Anti-PD-1 Immunotherapy. *Cell* **170**, 1109-1119.e10.

Robert Koch Institute (ed.) and the Association of Population-based Cancer Registries in Germany (ed.) **(2022).** *Cancer in Germany 2017/2018. 13th edition.*

Röhrig, F. & Schulze, A. (2016). The multifaceted roles of fatty acid synthesis in cancer. *Nat Rev Cancer* **16**, 732–749.

Romero, I. L., **Mukherjee, A.**, **Kenny, H. A.**, **Litchfield, L. M. & Lengyel, E. (2015).** Molecular pathways: trafficking of metabolic resources in the tumor microenvironment. *Clinical cancer research : an official journal of the American Association for Cancer Research* **21**, 680–686.

Romero-Garcia, S., **Lopez-Gonzalez, J. S.**, **Báez-Viveros, J. L.**, **Aguilar-Cazares, D. & Prado-Garcia, H. (2011).** Tumor cell metabolism: an integral view. *Cancer Biology & Therapy* **12**, 939–948.

Römisch-Margl, W., **Prehn, C.**, **Bogumil, R.**, **Röhring, C.**, **Suhre, K. & Adamski, J. (2012).** Procedure for tissue sample preparation and metabolite extraction for high-throughput targeted metabolomics. *Metabolomics : Official journal of the Metabolomic Society* **8**, 133–142.

Russell, S. J. & Peng, K.-W. (2007). Viruses as anticancer drugs. *Trends in pharmacological sciences* **28**, 326–333.

Sakamoto, A., **Kunou, S.**, **Shimada, K.**, **Tsunoda, M.**, **Aoki, T.**, **Iriyama, C.**, **Tomita, A.**, **Nakamura, S.**, **Hayakawa, F. & Kiyoi, H. (2019).** Pyruvate secreted from patient-derived cancer-associated fibroblasts supports survival of primary lymphoma cells. *Cancer science* **110**, 269–278.

SALAS, M. L., **VINUELA, E.**, **SALAS, M. & SOLS, A. (1965).** CITRATE INHIBITION OF PHOSPHOFRUCTOKINASE AND THE PASTEUR EFFECT. *Biochemical and biophysical research communications* **19**, 371–376.

Samanta, D. & Almo, S. C. (2015). Nectin family of cell-adhesion molecules: structural and molecular aspects of function and specificity. *Cellular and molecular life sciences : CMLS* **72**, 645–658.

Sandlund, J., **Hedberg, Y.**, **Bergh, A.**, **Grankvist, K.**, **Ljungberg, B. & Rasmuson, T. (2007).** Evaluation of CD31 (PECAM-1) expression using tissue microarray in patients with renal cell carcinoma. *Tumor Biology* **28**, 158–164.

Scaffidi, P., **Misteli, T. & Bianchi, M. E. (2002).** Release of chromatin protein HMGB1 by necrotic cells triggers inflammation. *Nature* **418**, 191–195.

Schlüter, A., **Weller, P.**, **Kanaan, O.**, **Nel, I.**, **Heusgen, L.**, **Höing, B.**, **Haßkamp, P.**, **Zander, S. & Mandapathil, M. & other authors (2018).** CD31 and VEGF are prognostic biomarkers in early-stage, but not in late-stage, laryngeal squamous cell carcinoma. *BMC Cancer* **18**, 272.

Schlüter, C., **Duchrow, M.**, **Wohlenberg, C.**, **Becker, M. H.**, **Key, G.**, **Flad, H. D. & Gerdes, J. (1993).** The cell proliferation-associated antigen of antibody Ki-67: a very large, ubiquitous nuclear protein with numerous repeated elements, representing a new kind of cell cycle-maintaining proteins. *The Journal of cell biology* **123**, 513–522.

Schmidt, K. M., **Dietrich, P.**, **Hackl, C.**, **Guenzle, J.**, **Bronsert, P.**, **Wagner, C.**, **Fichtner-Feigl, S.**, **Schlitt, H. J. & Geissler, E. K. & other authors (2018).** Inhibition of mTORC2/RICTOR Impairs Melanoma Hepatic Metastasis. *Neoplasia (New York, N.Y.)* **20**, 1198–1208.

Schmidt, L. H., **Brand, C.**, **Stucke-Ring, J.**, **Schliemann, C.**, **Kessler, T.**, **Harrach, S.**, **Mohr, M.**, **Görlich, D. & Marra, A. & other authors (2017).** Potential therapeutic impact of CD13 expression in non-small cell lung cancer. *PLOS ONE* **12**, e0177146.

Schuster, P., **Lindner, G.**, **Thomann, S.**, **Haferkamp, S. & Schmidt, B. (2019).** Prospect of Plasmacytoid Dendritic Cells in Enhancing Anti-Tumor Immunity of Oncolytic Herpes Viruses. *Cancers* **11**, 651.

Schwertner, B., **Dahdal, G.**, **Jagla, W.**, **Grossmann, L.**, **Drexler, K.**, **Krahn, M. P.**, **Evert, K.**, **Berneburg, M. & Haferkamp, S. & other authors (2024).** Expression of the plasma membrane citrate carrier (pmCiC) in human cancerous tissues—correlation with tumour aggressiveness. *Frontiers in cell and developmental biology* **12**.

Schwertner, B., **Lindner, G.**, **Toledo Stauner, C.**, **Klapproth, E.**, **Magnus, C.**, **Rohrhofer, A.**, **Gross, S.**, **Schuler-Thurner, B. & Öttl, V. & other authors (2021).** Nectin-1 Expression Correlates with the Susceptibility of Malignant Melanoma to Oncolytic Herpes Simplex Virus In Vitro and In Vivo. *Cancers* **13**.

Sciortino, M. T., **Medici, M. A.**, **Marino-Merlo, F.**, **Zaccaria, D.**, **Giuffrè-Cuculletto, M.**, **Venuti, A.**, **Grelli, S.**, **Bramanti, P. & Mastino, A. (2008).** Involvement of gD/HVEM interaction in NF-kB-dependent inhibition of apoptosis by HSV-1 gD. *Biochemical Pharmacology* **76**, 1522–1532.

Sharma, B., **Singh, N.**, **Gupta, N.**, **Lal, P.**, **Pande, S. & Chauhan, S. (2013).** Diagnostic Modalities of Precancerous and Cancerous Cervical Lesions with Special Emphasis on CD31 Angiogenesis Factor as a Marker. *Pathology Research International* **2013**, 243168.

Sharma, H. (2018). Development of Novel Therapeutics Targeting Isocitrate Dehydrogenase Mutations in Cancer. *Current topics in medicinal chemistry* **18**, 505–524.

Shi, Y., **Evans, J. E. & Rock, K. L. (2003).** Molecular identification of a danger signal that alerts the immune system to dying cells. *Nature* **425**, 516–521.

Shiga, K., **Hara, M.**, **Nagasaki, T.**, **Sato, T.**, **Takahashi, H. & Takeyama, H. (2015).** Cancer-Associated Fibroblasts: Their Characteristics and Their Roles in Tumor Growth. *Cancers* **7**, 2443–2458.

Shin, D. S., **Zaretsky, J. M.**, **Escuin-Ordinas, H.**, **Garcia-Diaz, A.**, **Hu-Lieskovan, S.**, **Kalbasi, A.**, **Grasso, C. S.**, **Hugo, W. & Sandoval, S. & other authors (2017).** Primary Resistance to PD-1 Blockade Mediated by JAK1/2 Mutations. *Cancer discovery* **7**, 188–201.

Shoemaker, R. H. (2006). The NCI60 human tumour cell line anticancer drug screen. *Nature reviews. Cancer* **6**, 813–823.

Shukla, D., **Liu, J.**, **Blaiklock, P.**, **Shworak, N. W.**, **Bai, X.**, **Esko, J. D.**, **Cohen, G. H.**, **Eisenberg, R. J.**, **Rosenberg, R. D. & Spear, P. G. (1999).** A novel role for 3-O-sulfated heparan sulfate in herpes simplex virus 1 entry. *Cell* **99**, 13–22.

Shukla, D. & Spear, P. G. (2001). Herpesviruses and heparan sulfate: an intimate relationship in aid of viral entry. *The Journal of clinical investigation* **108**, 503–510.

Singh, S. K., **Mishra, M. K.**, **Eltoum, I.-E. A.**, **Bae, S.**, **Lillard, J. W. & Singh, R. (2018).** CCR5/CCL5 axis interaction promotes migratory and invasiveness of pancreatic cancer cells. *Sci Rep* **8**, 1323.

Soengas, M. S. & Lowe, S. W. (2003). Apoptosis and melanoma chemoresistance. *Oncogene* **22**, 3138–3151.

Spisek, R., **Charalambous, A.**, **Mazumder, A.**, **Vesole, D. H.**, **Jagannath, S. & Dhodapkar, M. V. (2007).** Bortezomib enhances dendritic cell (DC)-mediated induction of immunity to human myeloma via exposure of cell surface heat shock protein 90 on dying tumor cells: therapeutic implications. *Blood* **109**, 4839–4845.

Srivastava, P. K., **Udono, H.**, **Blachere, N. E. & Li, Z. (1994).** Heat shock proteins transfer peptides during antigen processing and CTL priming. *Immunogenetics* **39**, 93–98.

Steinberg, M. W., **Cheung, T. C. & Ware, C. F. (2011).** The signaling networks of the herpesvirus entry mediator (TNFRSF14) in immune regulation. *Immunological reviews* **244**, 169–187.

Sun, J., **Gastman, B. R.**, **McCahon, L.**, **Buchbinder, E. I.**, **Puzanov, I.**, **Nanni, M.**, **Lewis, J. M.**, **Carvajal, R. D. & Singh-Kandah, S. & other authors (2020).** Observational study of talimogene laherparepvec use in the anti-PD-1 era for melanoma in the US (COSMUS-2). *Melanoma management* **7**, MMT41.

Sun, L., **Wu, J.**, **Du, F.**, **Chen, X. & Chen, Z. J. (2013).** Cyclic GMP-AMP synthase is a cytosolic DNA sensor that activates the type I interferon pathway. *Science* **339**, 786–791.

Sun, Q., **Zhang, B.**, **Hu, Q.**, **Qin, Y.**, **Xu, W.**, **Liu, W.**, **Yu, X. & Xu, J. (2018).** The impact of cancer-associated fibroblasts on major hallmarks of pancreatic cancer. *Theranostics* **8**, 5072–5087.

Sung, H., **Ferlay, J.**, **Siegel, R. L.**, **Laversanne, M.**, **Soerjomataram, I.**, **Jemal, A. & Bray, F. (2021).** Global Cancer Statistics 2020: GLOBOCAN Estimates of Incidence and Mortality Worldwide for 36 Cancers in 185 Countries. *CA: a cancer journal for clinicians* **71**, 209–249.

Suzuki, A., **Leland, P.**, **Joshi, B. H. & Puri, R. K. (2015).** Targeting of IL-4 and IL-13 receptors for cancer therapy. *Cytokine* **75**, 79–88.

Szeri, F., **Lundkvist, S.**, **Donnelly, S.**, **Engelke, U. F. H.**, **Rhee, K.**, **Williams, C. J.**, **Sundberg, J. P.**, **Wevers, R. A. & Tomlinson, R. E. & other authors (2020).** The membrane protein ANKH is crucial for bone mechanical performance by mediating cellular export of citrate and ATP. *PLoS genetics* **16**, e1008884.

Taneja, S., **MacGregor, J.**, **Markus, S.**, **Ha, S. & Mohr, I. (2001).** Enhanced antitumor efficacy of a herpes simplex virus mutant isolated by genetic selection in cancer cells. *Proceedings of the National Academy of Sciences of the United States of America* **98**, 8804–8808.

Taniuchi, S., **Miyake, M.**, **Tsugawa, K.**, **Oyadomari, M. & Oyadomari, S. (2016).** Integrated stress response of vertebrates is regulated by four eIF2α kinases. *Sci Rep* **6**, 32886.

The International Agency for Research on Cancer Working Group on artificial ultraviolet (UV) light and skin cancer **(2007).** The association of use of sunbeds with cutaneous malignant melanoma and other skin cancers: A systematic review. *International journal of cancer* **120**, 1116–1122.

Thomann, S., **Boscheinen, J. B.**, **Vogel, K.**, **Knipe, D. M.**, **DeLuca, N.**, **Gross, S.**, **Schuler-Thurner, B.**, **Schuster, P. & Schmidt, B. (2015).** Combined cytotoxic activity of an infectious, but non-replicative herpes simplex virus type 1 and plasmacytoid dendritic cells against tumour cells. *Immunology* **146**, 327–338.

Thomas, S., **Kuncheria, L.**, **Roulstone, V.**, **Kyula, J. N.**, **Mansfield, D.**, **Bommareddy, P. K.**, **Smith, H.**, **Kaufman, H. L.**, **Harrington, K. J. & Coffin, R. S. (2019).** Development of a

new fusion-enhanced oncolytic immunotherapy platform based on herpes simplex virus type 1. *Journal for immunotherapy of cancer* **7**, 214.

Tian, W., **Zhang, W.**, **Wang, Y.**, **Jin, R.**, **Wang, Y.**, **Guo, H.**, **Tang, Y. & Yao, X. (2022).** Recent advances of IDH1 mutant inhibitor in cancer therapy. *Frontiers in pharmacology* **13**, 982424.

Titus-Ernstoff, L., **Perry, A. E.**, **Spencer, S. K.**, **Gibson, J. J.**, **Cole, B. F. & Ernstoff, M. S. (2005).** Pigmentary characteristics and moles in relation to melanoma risk. *International journal of cancer* **116**, 144–149.

Tobin, J. D., **Robinson, C. N.**, **Luttrell-Williams, E. S.**, **Landry, G. M.**, **Dwyer, D. & McMartin, K. E. (2022).** Role of Plasma Membrane Dicarboxylate Transporters in the Uptake and Toxicity of Diglycolic Acid, a Metabolite of Diethylene Glycol, in Human Proximal Tubule Cells. *Toxicological sciences : an official journal of the Society of Toxicology* **190**, 1–12.

Troebs, J., **Asam, C.**, **Pion, E.**, **Prantl, L.**, **Aung, T. & Haerteis, S. (2020).** 3D monitoring of tumor volume in an in vivo model. *Clinical hemorheology and microcirculation* **76**, 123–131.

Uchida, H., **Marzulli, M.**, **Nakano, K.**, **Goins, W. F.**, **Chan, J.**, **Hong, C.-S.**, **Mazzacurati, L.**, **Yoo, J. Y. & Haseley, A. & other authors (2013).** Effective treatment of an orthotopic xenograft model of human glioblastoma using an EGFR-retargeted oncolytic herpes simplex virus. *Molecular therapy : the journal of the American Society of Gene Therapy* **21**, 561–569.

Uhlén, M., **Fagerberg, L.**, **Hallström, B. M.**, **Lindskog, C.**, **Oksvold, P.**, **Mardinoglu, A.**, **Sivertsson, Å.**, **Kampf, C. & Sjöstedt, E. & other authors (2015).** Proteomics. Tissue-based map of the human proteome. *Science* **347**, 1260419.

Vaddepally, R. K., **Kharel, P.**, **Pandey, R.**, **Garje, R. & Chandra, A. B. (2020).** Review of Indications of FDA-Approved Immune Checkpoint Inhibitors per NCCN Guidelines with the Level of Evidence. *Cancers* **12**.

Vermeulen, P. B., **Gasparini, G.**, **Fox, S. B.**, **Colpaert, C.**, **Marson, L. P.**, **Gion, M.**, **Beliën, J. A. M.**, **Waal, R. M. W.** de **& van Marck, E. & other authors (2002).** Second international consensus on the methodology and criteria of evaluation of angiogenesis quantification in solid human tumours. *European Journal of Cancer* **38**, 1564–1579.

VIRMAN, J., **BONO, P.**, **LUUKKAALA, T.**, **SUNELA, K.**, **KUJALA, P. & KELLOKUMPU-LEHTINEN, P.-L. (2015).** VEGFR3 and CD31 as prognostic factors in renal cell cancer. *Anticancer Research* **35**, 921–927.

Vouillot, L., **Thélie, A. & Pollet, N. (2015).** Comparison of T7E1 and surveyor mismatch cleavage assays to detect mutations triggered by engineered nucleases. *G3 Genes|Genomes|Genetics* **5**, 407–415.

Wang, M., **Han, J.**, **Xing, H.**, **Zhang, H.**, **Li, Z.**, **Liang, L.**, **Li, C.**, **Dai, S. & Wu, M. & other authors (2016).** Dysregulated fatty acid metabolism in hepatocellular carcinoma. *Hepatic oncology* **3**, 241–251.

Wang, M., **Zhao, J.**, **Zhang, L.**, **Wei, F.**, **Lian, Y.**, **Wu, Y.**, **Gong, Z.**, **Zhang, S. & Zhou, J. & other authors (2017).** Role of tumor microenvironment in tumorigenesis. *Journal of Cancer* **8**, 761–773.

Wang, W., **Bai, L.**, **Li, W. & Cui, J. (2020).** The Lipid Metabolic Landscape of Cancers and New Therapeutic Perspectives. *Frontiers in oncology* **10**, 605154.

Wang, X. M., **Yu, D. M. T.**, **McCaughan, G. W. & Gorrell, M. D. (2005).** Fibroblast activation protein increases apoptosis, cell adhesion, and migration by the LX-2 human stellate cell line. *Hepatology (Baltimore, Md.)* **42**, 935–945.

Warburg, O. (1925). The Metabolism of Carcinoma Cells. *The Journal of Cancer Research* **9**, 148–163.

Weide, B., **Elsässer, M.**, **Büttner, P.**, **Pflugfelder, A.**, **Leiter, U.**, **Eigentler, T. K.**, **Bauer, J.**, **Witte, M.**, **Meier, F. & Garbe, C. (2012).** Serum markers lactate dehydrogenase and S100B predict independently disease outcome in melanoma patients with distant metastasis. *British journal of cancer* **107**, 422–428.

Whitaker-Menezes, D., **Martinez-Outschoorn, U. E.**, **Lin, Z.**, **Ertel, A.**, **Flomenberg, N.**, **Witkiewicz, A. K.**, **Birbe, R. C.**, **Howell, A. & Pavlides, S. & other authors (2011).** Evidence for a stromal-epithelial "lactate shuttle" in human tumors: MCT4 is a marker of oxidative stress in cancer-associated fibroblasts. *Cell cycle (Georgetown, Tex.)* **10**, 1772–1783.

Whiteside, T. L. (2008). The tumor microenvironment and its role in promoting tumor growth. *Oncogene* **27**, 5904–5912.

Williams, K. C., **Cepeda, M. A.**, **Javed, S.**, **Searle, K.**, **Parkins, K. M.**, **Makela, A. V.**, **Hamilton, A. M.**, **Soukhtehzari, S. & Kim, Y. & other authors (2019).** Invadopodia are chemosensing protrusions that guide cancer cell extravasation to promote brain tropism in metastasis. *Oncogene* **38**, 3598–3615.

Wolchok, J. D., **Chiarion-Sileni, V.**, **Gonzalez, R.**, **Grob, J.-J.**, **Rutkowski, P.**, **Lao, C. D.**, **Cowey, C. L.**, **Schadendorf, D. & Wagstaff, J. & other authors (2021).** CheckMate 067: 6.5-year outcomes in patients (pts) with advanced melanoma. *Journal of clinical oncology : official journal of the American Society of Clinical Oncology* **39**, 9506.

Woo, S.-R., **Corrales, L. & Gajewski, T. F. (2015).** The STING pathway and the T cell-inflamed tumor microenvironment. *Trends in immunology* **36**, 250–256.

Woo, S.-R., **Fuertes, M. B.**, **Corrales, L.**, **Spranger, S.**, **Furdyna, M. J.**, **Leung, M. Y. K.**, **Duggan, R.**, **Wang, Y. & Barber, G. N. & other authors (2014).** STING-dependent cytosolic DNA sensing mediates innate immune recognition of immunogenic tumors. *Immunity* **41**, 830–842.

Workenhe, S. T., **Verschoor, M. L. & Mossman, K. L. (2015).** The role of oncolytic virus immunotherapies to subvert cancer immune evasion. *Future oncology (London, England)* **11**, 675–689.

Wu, Y., **Chen, K.**, **Xing, G.**, **Li, L.**, **Ma, B.**, **Hu, Z.**, **Duan, L. & Liu, X. (2019).** Phospholipid remodeling is critical for stem cell pluripotency by facilitating mesenchymal-to-epithelial transition. *Science advances* **5**, eaax7525.

Xia, T., **Konno, H. & Barber, G. N. (2016).** Recurrent Loss of STING Signaling in Melanoma Correlates with Susceptibility to Viral Oncolysis. *Cancer research* **76**, 6747–6759.

Xu, M., **Zhang, T.**, **Xia, R.**, **Wei, Y. & Wei, X. (2022).** Targeting the tumor stroma for cancer therapy. *Mol Cancer* **21**, 208.

Yang, G., **Rosen, D. G.**, **Zhang, Z.**, **Bast, R. C.**, **Mills, G. B.**, **Colacino, J. A.**, **Mercado-Uribe, I. & Liu, J. (2006).** The chemokine growth-regulated oncogene 1 (Gro-1) links RAS signaling to the senescence of stromal fibroblasts and ovarian tumorigenesis. *Proceedings of the National Academy of Sciences of the United States of America* **103**, 16472–16477.

Yodoya, E., **Wada, M.**, **Shimada, A.**, **Katsukawa, H.**, **Okada, N.**, **Yamamoto, A.**, **Ganapathy, V. & Fujita, T. (2006).** Functional and molecular identification of sodium-coupled dicarboxylate transporters in rat primary cultured cerebrocortical astrocytes and neurons. *Journal of neurochemistry* **97**, 162–173.

Yu, X. & He, S. (2016). The interplay between human herpes simplex virus infection and the apoptosis and necroptosis cell death pathways. *Virology journal* **13**, 77.

Yu, Z., **Adusumilli, P. S.**, **Eisenberg, D. P.**, **Darr, E.**, **Ghossein, R. A.**, **Li, S.**, **Liu, S.**, **Singh, B. & Shah, J. P. & other authors (2007).** Nectin-1 expression by squamous cell carcinoma is a predictor of herpes oncolytic sensitivity. *Molecular therapy : the journal of the American Society of Gene Therapy* **15**, 103–113.

Yu, Z., **Chan, M.-K.**, **O-charoenrat, P.**, **Eisenberg, D. P.**, **Shah, J. P.**, **Singh, B.**, **Fong, Y. & Wong, R. J. (2005).** Enhanced nectin-1 expression and herpes oncolytic sensitivity in highly migratory and invasive carcinoma. *Clinical cancer research : an official journal of the American Association for Cancer Research* **11**, 4889–4897.

Yuan, A., **Chen, J. J. W.**, **Yao, P.-L. & Yang, P.-C. (2005).** The role of interleukin-8 in cancer cells and microenvironment interaction. *Frontiers in bioscience : a journal and virtual library* **10**, 853–865.

Zamarin, D. & Postow, M. A. (2015). Immune checkpoint modulation: rational design of combination strategies. *Pharmacology & therapeutics* **150**, 23–32.

Zaretsky, J. M., **Garcia-Diaz, A.**, **Shin, D. S.**, **Escuin-Ordinas, H.**, **Hugo, W.**, **Hu-Lieskovan, S.**, **Torrejon, D. Y.**, **Abril-Rodriguez, G. & Sandoval, S. & other authors (2016).** Mutations Associated with Acquired Resistance to PD-1 Blockade in Melanoma. *The New England journal of medicine* **375**, 819–829.

Zaynagetdinov, R., **Sherrill, T. P.**, **Gleaves, L. A.**, **McLoed, A. G.**, **Saxon, J. A.**, **Habermann, A. C.**, **Connelly, L.**, **Dulek, D. & Peebles, R. S. & other authors (2015).** Interleukin-5 facilitates lung metastasis by modulating the immune microenvironment. *Cancer Res* **75**, 1624–1634.

Zaytseva, Y. Y., **Rychahou, P. G.**, **Le, A.-T.**, **Scott, T. L.**, **Flight, R. M.**, **Kim, J. T.**, **Harris, J.**, **Liu, J. & Wang, C. & other authors (2018).** Preclinical evaluation of novel fatty acid synthase inhibitors in primary colorectal cancer cells and a patient-derived xenograft model of colorectal cancer. *Oncotarget* **9**, 24787–24800.

Zemski Berry, K. A. & Murphy, R. C. (2004). Electrospray ionization tandem mass spectrometry of glycerophosphoethanolamine plasmalogen phospholipids. *Journal of the American Society for Mass Spectrometry* **15**, 1499–1508.

Zha, S., **Ferdinandusse, S.**, **Hicks, J. L.**, **Denis, S.**, **Dunn, T. A.**, **Wanders, R. J.**, **Luo, J.**, **Marzo, A. M.** de **& Isaacs, W. B. (2005).** Peroxisomal branched chain fatty acid beta-oxidation pathway is upregulated in prostate cancer. *The Prostate* **63**, 316–323.

Zhang, L., **Zhang, J.**, **Liu, Y.**, **Zhang, P.**, **Nie, J.**, **Zhao, R.**, **Shi, Q.**, **Sun, H. & Jiao, D. & other authors (2021).** Mitochondrial STAT5A promotes metabolic remodeling and the Warburg effect by inactivating the pyruvate dehydrogenase complex. *Cell death & disease* **12**, 634.

Zhang, X., **Chen, L.**, **Dang, W.-Q.**, **Cao, M.-F.**, **Xiao, J.-F.**, **Lv, S.-Q.**, **Jiang, W.-J.**, **Yao, X.-H. & Lu, H.-M. & other authors (2020).** CCL8 secreted by tumor-associated macrophages promotes invasion and stemness of glioblastoma cells via ERK1/2 signaling. *Laboratory investigation; a journal of technical methods and pathology* **100**, 619–629.

Zhou, J., **Zheng, S.**, **Liu, T.**, **Liu, Q.**, **Chen, Y.**, **Ma, R.**, **Tan, D. & Lu, X. (2019).** Infiltrated M2 tumour-associated macrophages in the stroma promote metastasis and poor survival in oesophageal squamous cell carcinoma. *Histology and histopathology* **34**, 563–572.

Zukunft, S., **Sorgenfrei, M.**, **Prehn, C.**, **Möller, G. & Adamski, J. (2013).** Targeted Metabolomics of Dried Blood Spot Extracts. *Chromatographia* **76**, 1295–1305.